Synthesis and Post-polymerisation Modification of Degradable Polymers Based on Polycarbonates/Polyesters Prepared Using Ring-opening Copolymerisation

Ni Yi

Trinity College

Department of Inorganic Chemistry

University of Oxford

May 2018

A thesis submitted in partial fulfilment of the requirements for the degree of Doctor of Philosophy in Chemistry.

For Grandpa and my dearest family

Declaration

This work described in this thesis was conducted at Imperial College London and University of Oxford between October 2014 and May 2018 and is the work carried out by the author unless otherwise stated.

The copyright of this thesis rests with the author and is made available under a Creative Commons Attribution Non-Commercial No Derivatives licence. Researchers are free to copy, distribute or transmit the thesis on the condition that they attribute it, that they do not use it for commercial purposes and that they do not alter, transform or build upon it. For any reuse or distribution, researchers must make clear to others the licence terms of this work.

Abstract

This thesis describes the synthesis of degradable materials based on functional aliphatic polycarbonates/polyesters synthesised *via* ring-opening copolymerisation (ROCOP) and post-polymerisation modifications.

Chapter 3 details the synthesis of cationic poly(ester-*b*-carbonate-*b*-ester) *via* ring-opening copolymerisation of CO_2 and vinyl-cyclohexene oxide (v-CHO), ring-opening polymerisation (ROP) of *rac*-lactide, and subsequent post-polymerisation modifications of this material through a radical thiol-ene reaction and a quaternisation reaction. These cationic polymers show high surface zeta-potential (> 40 mV) and display effective antibacterial properties with killing efficiencies of > 99.9% against Gram-negative bacteria *Escherichia coli*.

Chapter 4 describes the synthesis of amphiphilic block poly(phosphoester-*b*-carbonate-*b*-phosphoester)s using ROCOP of CO_2 and v-CHO and ROP of ethyl ethylene phosphate (EP). These amphiphilic block polymers self-assemble into either micelles or vesicles, depending on the hydrophobic/hydrophilic block ratio. The potential use of the vesicles in drug delivery is also described, and initial results detailing the enzymatic degradation of these vesicles are presented. In addition, the hydroboration-oxidation is investigated as a new post-polymerisation modification method to functionalise an alkene-containing polycarbonate, poly(vinylcyclohexene carbonate) (^{V}PC). The hydroxyl functionalised polycarbonate shows improved hydrophilicity and cell adhesion, compared to the unfunctionalised precursor. The side chain hydroxyl groups are then tested for making graft poly(carbonate-*g*-phosphoester).

Chapter 5 further investigates the use of the hydroboration-oxidation reaction in functionalising poly(cyclohexadiene carbonate) (^{C}PC) and poly(vinylcyclohexene

maleate) (^{V,M}PE). A selective post-polymerisation modification is also demonstrated on a blend of ^{C}PC and ^{V}PC or ^{V,M}PE featuring both terminal and internal alkene groups using the hydroboration-oxidation method, where the terminal alkene groups are functionalised exclusively. Lastly, an orthogonal post-polymerisation approach is carried out on the unreacted internal alkene groups of hydroxyl-containing ^{V,M}PE *via* thiol-ene reactions to install other functional groups such as carboxyl, amine and methoxy-poly(ethylene glycol).

Acknowledgements

Firstly, I would like to thank my supervisor Professor Charlotte Williams, for offering me the opportunity to work in her group. I would also like to thank her for encouraging, teaching, and supporting. Without her support, I would not have completed my PhD. It has been a great pleasure to work with her.

During my PhD study, I have been helped by many people, and I would like to take this opportunity to express my appreciation to them. In particular, Peter Haycock and Dr Nick Rees for their help with NMR; Dr Ed White, Dr Mahmoud and Tianyi Chen for their help with TEM analyses; Lisa Haigh for her mass spectrometry service; Stephen Boyer, from London Metropolitan University, for elemental analysis. I would also like to express my gratitude to my collaborators: Gi-byoung Hwang, Dr Elaine Allan and Professor Ian Parkin, from University College London for helping me with the antibacterial tests; Dr Andreas and Professor Alexander Bismarck for helping me measure surface zeta potential and Chunching Li, Dr Shaodong Zhang and Professor Molly Stevens, from Imperial College London, for helping me conduct cell tests and letting me use instruments at the Materials Department.

To all the past and current members of the Williams group, I am extremely grateful for your support, company and laughter. The experiences have made me both a better chemist and a better person. Thank you to Alice, Arnaud, Charlie, Gemma, Arron, Tim, Tom, Peck, Shyeni, Dom, Jameel, Greg and Saïd. It has also been a memorable journey to work with all the knowledgeable postdocs: Guun, Charles, Valentin, Jenni, Anish, Andres, Seb, Sumesh, Leti, Chris and Giulia. Especially thanks to Frank, for answering every single question and guiding me in the field of materials.

I would also like to thank all my friends. Thank you for taking me out for meals and trips and listening to my complaints. Simeng and Isabel, thank you for persuading me to do a PhD with you when I was not ready three years ago. Xuan, thank you for coming to Oxford from Switzerland regularly to take me out of the lab. My PhD life was also enriched by Lu and Kan, thank you for all your invaluable support through the toughest moments of my life.

Special thanks go to my boyfriend and my lovely momo. Thank you for being with me and relieving my stress. Extra special gratitude goes to my parents for their endless patience, love and encouragement. Thank you for always believing in me and giving me the confidence to achieve more in my life.

List of Publications

- ***Carbon dioxide capture and utilisation: using dinuclear catalysts to prepare polycarbonates***

  N. Yi, J. Unruangsri, J. Shaw and C. K. Williams, *Faraday Discuss.*, 2015, **183**, 67-82

- ***Poly(rac-lactide)-b-poly(4-vinyl-1-cyclohexene carbonate)-b-poly(rac-lactide): a functionalisable poly(ester-carbonate) designed for antibacterial applications***

  N. Yi, G. B. Hwang, A. Mautner, A. Bismarck, E. Allan, I. P. Parkin and C. K. Williams, *In preparation.*

- ***Selective and sequential post-polymerisation modification of alternating polyester using hydroboration-oxidation and thiol-ene reactions***

  N. Yi, J. Unruangsri, Y. Zhu and C. K. Williams, *In preparation*.

List of Abbreviations

AC	(Meth)Acryloyl Carbonate
A. flavus	*Aspergillus flavus*
α-AL	α-Angelica Lactone
ALP	Alkaline Phosphatase
Amb	Ambrettolide
A. niger	*Aspergillus niger*
APC	Aliphatic Polycarbonate
APE	Aliphatic Polyester
Ar	Aryl
ATRP	Atom Transfer Radical Polymerisation
BDI	β-Diiminate
BPA	Bispheol-A
C. albicans	*Candida albicans*
CHD	*Trans*-cyclohexane-1,2-diol
CHDO	Cyclohexadiene Oxide
CHO	Cyclohexene Oxide
COP	2-Chloro-2-oxo-1,3,2-dioxaphospholane
COSY	Homonuclear Correlation Spectroscopy
CTA	Chain Transfer Agent
Đ	Dispersities
DBU	1,8-Diazabicyclo[5.4.0]undec-7-ene
DCM	Dichloromethane
D_h	Hydrodynamic Diameter
DI	De-ionised

DLE	Drug Loading Efficiency
DLS	Dynamic Light Scattering
DMF	Dimethyl Formamide
DMSO	Dimethyl Sulfoxide
DMPA	2,2-Dimethoxy-2-phenylacetophenone
$\overline{DP}$	Degree of Polymerisation
DSC	Differential Scanning Calorimetry
ε-CL	ε-Caprolactone
E. coli	*Escherichia coli*
ED	1,2-Epoxy-9-decene
EG	Ethylene Glycol
EH	1,2-Epoxy-5-hexene
FDA	Food and Drug Administration
HSQC	Heteronuclear Single Quantum Coherence
L	Ligand
LO	Limonene Oxide
rac-LA	*rac*-Lactide
LCMs	Large Compound Micelles
LS	Light Scattering
M	Molar
MA	Maleic Anhydride
MAC	5-Methyl-5-allyloxycarbonyl-1,3-dioxan-2-one
MALDI	Matrix Assisted Laser Desorption Ionisation
mCPBA	3-Chloroperoxybenzoic acid
MeOH	Methanol

M_n	Number Average Molar Mass
mPEG	Methoxy-poly(ethylene glycol)
MRSA	Methicillin-resistant *Staphylococcus aureus*
MTT	3-(4,5-Dimethylthiazol-2-yl)-2,5-diphenyltetrazolium bromide
M_w	Weight Average Molar Mass
MWCO	Molar Mass Cutoff
NA	Norbornene anhydride
NMR	Nuclear Magnetic Resonance
PA	Phthalic Anhydride
P. aeruginosa	*Pseudomonas aeruginosa*
PBS	Phosphate-Buffered Saline
PC	Poly(cyclohexene carbonate)
^{C}PC	Poly(cyclohexadiene carbonate)
^{V}PC	Poly(vinylcyclohexene carbonate)
PCL	Poly(ε-caprolactone)
PDI	Polydispersity Index
^{V,M}PE	Poly(vinylcyclohexene maleate)
PEP	Poly(ethyl ethylene phosphate)
PLA	Poly(lactide)
PLGA	Poly(lacide-*co*-glycolide)
PLimC	Poly(limonene carbonate)
PMAC	Poly(5-methyl-5-allyloxycarbonyl-trimethylene carbonate)
PMT	Photomultiplier Tube

PO	Propylene Oxide
PPC	Poly(propylene carbonate)
PPE	Poly(phosphoester)
PPNBr	Bis(triphenylphosphine)iminium Bromide
PPNCl	Bis(triphenylphosphine)iminium Chloride
PTMC	Poly(trimethylene carbonate)
PTX	Paclitaxel
PVIC	Poly(2-vinyloxirane carbonate)
ROCOP	Ring Opening Copolymerisation
ROP	Ring Opening Polymerisation
SA	Succinic Anhydride
S. aureus	*Staphylococcus aureus*
SEC	Size Exclusion Chromatography
TBD	1,5,7-Triazabicyclo[4.4.0]dec-5-ene
TCE	1,1,2,2-Tetrachloroethane
TEM	Transmission Electron Microscopy
TFA	Trifluoroacetic Acid
T_g	Glass Transition Temperature
THF	Tetrahydrofuran
ToF	Time of Flight
TOF	Turnover Frequency
TON	Turnover Number
v-CHO	Vinyl Cyclohexene Oxide
X	Co-ligand
ζ-potential	Zeta potential

List of Figures, Schemes and Tables

Chapter 1

Figure 1.1 A possible mechanism of cationic antimicrobial polymers: cationic polymer interacts with and disrupt the membrane, leading to cytoplasm leakage.

Figure 1.2 Common morphologies of self-assembled amphiphilic block copolymers: spherical micelles, cylindrical micelles and vesicles (also known as polymersomes).

Figure 1.3 A schematic representation of vesicle formation.

Figure 1.4 Structures of poly(lactic acid) (PLA), poly(lactic acid-*co*-glycolide) (PLGA), PCL poly(ε-caprolactone) (PCL), poly(trimethylene carbonate) (PTMC) and polyphosphoesters.

Figure 1.5 Diagram illustrating target polymers and applications.

Figure 1.6 Synthesis of amphiphilic block copolymers from PEG and PPC.

Figure 1.7 Synthesis and micelle formation of cationic amphiphilic polycarbonates, (A) cationic amphiphilic polycarbonates (B) and (C) the formation of micelles as simulated by molecular modelling.

Figure 1.8 Synthetic schemes of a) polycarbonates, b) PEG-APC hydrogel and c) hydrogel coating onto silicone rubber surface.

Figure 1.9 The transformation of PLimC into antibacterial PLimC.

Figure 1.10 Top: Structure of P(LA-*co*-MAC-g-Folic acid). Bottom: Microscope images of thin polymer films showing the effect of folic acid conjugation on adhesion and proliferation of Vero cells. Left to right: PLA, P(LA-*co*-MAC), P(LA-*co*-MAC-g-Folic acid).

Figure 1.11 Selected functional epoxides for ROCOP with CO_2.

Scheme 1.1 Coordination-insertion mechanism for ROP of cyclic monomers, using LA as an example.

Scheme 1.2 Transesterification reactions in the ROP of cyclic monomers, using LA as an example.

Scheme 1.3 Illustration of structures of TBD and its ROP mechanism, where E is electrophilic species and B is the Brønsted base, using δ-valerolactone as an example monomer.

Scheme 1.4 Scheme showing the mechanism of ROCOP, with the initiation, propagation, side reactions and chain transfer reaction.

Scheme 1.5 Synthesis of PLA-*b*-PC-*b*-PLA.

Scheme 1.6 Scheme showing tandem synthesis of poly(phosphoester-*b*-carbonate-*b*-phosphoester).

Scheme 1.7 Functionalisation of P(CL-*co*-AC) *via* Michael addition.

Scheme 1.8 Synthetic strategies for the preparation of poly(1,2-glycerol carbonate).

Scheme 1.9 Synthesis of amphiphilic and water-soluble polycarbonate.

Scheme 1.10 Synthesis of graft copolymers using hydroxyl-containing polycarbonates as initiators.

Scheme 1.11 Functionalisation of unsaturated polyester *via* thiol-ene reaction.

Scheme 1.12 Functionalisation of unsaturated polyester *via* the thiol-ene and inverse-electron-demand Diels-Alder reactions.

Scheme 1.13 Functionalisation of unsaturated polyester on epoxide moiety *via* the thiol-ene reaction.

Scheme 1.14 Selective functionalisation on unsaturated triblock polyesters *via* thiol-ene reaction.

Chapter 2

Figure 2.1 Example of ^{1}H NMR spectrum of an aliquot during LA polymerisation.

Figure 2.2 Example of the ^{1}H NMR spectrum of the purified polymer from ROCOP of CO_2/cyclohexene oxide.

Figure 2.3 Example of $^{31}P\{^{1}H\}$ spectrum for end group analysis of polycaprolactone (PCL) with two types of hydroxyl end groups.

Figure 2.4 Example of ^{1}H DOSY spectrum of a mixture of polylactide (PLA) and poly(cyclohexene carbonate) (PC).

Figure 2.5 A) Example of an SEC trace of PC with a bimodal molar mass distribution (deconvoluted) and B) the separation of PC into two fractions of low and high molar mass, according to a preparative separation by elution time using SEC.

Figure 2.6 Example of Overlaid SEC traces of PC and PLA-PC-PLA, showing an increase in molar mass after block formation.

Figure 2.7 Example of a MALDI-ToF spectrum of PC.

Figure 2.8 Example of a DSC chromatogram of PC, obtained from the second heating cycle.

Figure 2.9 The fluorescence spectrum (A) and calibration curve (B) of Rhodamine B in PBS solution (10.0 mM, pH 7.4, λ_{ex} = 510 nm).

Figure 2.10 Example of images of the dead and live MC3T3-E1 cells on PC surfaces.

Figure 2.11 Example of confocal microscopy images of unattached and attached MC3T3-E1 cells.

Scheme 2.1 The reaction between polymer hydroxyl end groups and 2-chloro-4,4,5,5-tetra-methyldioxaphospholane.

Table 2.1 Summary and comparison of 2D NMR spectroscopic techniques used in this thesis.

Chapter 3

Figure 3.1 A) Overlaid ^{1}H NMR spectra of v-CHO monomer and crude ^{V}PC reaction mixture. B) ^{1}H NMR spectrum of isolated ^{V}PC.

Figure 3.2 Overlaid SEC traces of ^{V}PC produced in the presence of diols (Table 3.1 Entries 1-3).

Figure 3.3 MALDI-ToF spectrum of ^{V}PC synthesised with CHD as CTA (5.7 kgmol^{-1}, Đ = 1.17).

Figure 3.4 A) Overlaid SEC traces of PLA-^{V}PC-PLA formed in Table 3.2. B) Plot of molar masses and dispersities vs. [LA]/[^{V}PC]

Figure 3.5 ^{1}H NMR spectrum of ^{V}PC showing ^{V}PC end group and main chain methine protons, and PLA-^{V}PC-PLA showing PLA main chain and end group methine protons.

Figure 3.6 ^{13}C{^{1}H} NMR spectrum showing the carbonyl region of PLA-^{V}PC-PLA (51.8 kgmol^{-1}, Đ = 1.28)

Figure 3.7 ^{1}H DOSY NMR spectra of A) PLA-^{V}PC-PLA (51.8 kgmol^{-1}, Đ=1.28) and B) a mixture of ^{V}PC and PLA (control).

Figure 3.8 Selected region of ^{31}P{^{1}H} NMR spectra of the product of the reactions between the polymer end groups and 2-chloro-4,4,5,5-tetramethyl dioxaphospholane.

Figure 3.9 Stacked ^{1}H NMR spectra of P6 and NP6.

Figure 3.10 Overlaid SEC traces of P6 and NP6 in THF.

Figure 3.11 ^{1}H NMR spectrum of QP6.

Figure 3.12 Number of *E. coli* ATCC 25922 (colony forming units·mL^{-1}, CFU·mL^{-1}) after exposure to P6 (control) and QP6 prepared using different concentrations for 24 h, at 20 °C.

Figure 3.13 Zeta potential of P6 and QP6 prepared using different concentrations as a function of pH.

Figure 3.14 A) Enlarged ^{1}H NMR spectrum of NP6, showing the ratio of methine signals of PLA block to the NP6 backbone. B) Enlarged ^{1}H NMR spectrum of $Q_{0.25}$P6, showing the ratio of the methine signals of PLA block to ammonium aromatic signals.

Figure 3.15 A) Antibacterial activities of P6 (control) and QP6 samples with different degrees of quaternisation against *E. coli.* B) zeta potential as a function of pH of QP6 with different degrees of quaternisation.

Figure 3.16 Photographs showing bacterial attachment and detachment process, on positively charged surfaces: P6(control), QP6$_{1mg}$, QP6$_{2mg}$, QP6$_{3mg}$, QP6$_{5mg,}$ $Q_{0.25}$P6, $Q_{0.40}$P6, $Q_{0.59}$P6 and $Q_{0.78}$P6.

Figure 3.17 Illustration of the attachment and detachment process.

Figure 3.18 Potential polymer precursors for making antibacterial poly(ester-*b*-carbonate-*b*-ester)s.

Scheme 3.1 Structures of polymers targeted in this work.

Scheme 3.2 Shows the chemical structure of catalyst (**C1**), and the ROCOP of CHO/v-CHO and CO_2.

Scheme 3.3 Schematic illustration of the route to NP6 and QP6.

Table 3.1 Polymerisation data obtained from ROCOP of v-CHO and CO_2 with or without the use of CHD as CTA.

Table 3.2 Polymerisation data for triblock PLA-^{V}PC-PLA.

Table 3.3 Data for polymers with different degrees of quaternisation.

Chapter 4

Figure 4.1 ^{1}H NMR and $^{31}P\{^{1}H\}$ NMR spectra of ethyl ethylene phosphate.

Figure 4.2 $^{31}P\{^{1}H\}$ NMR spectrum of PEP-^{V}PC-PEP.

Figure 4.3 A) ^{1}H NMR spectrum of PEP-^{V}PC-PEP and B) ^{1}H-^{1}H COSY NMR spectrum of PEP-^{V}PC-PEP.

Figure 4.4 Stacked ^{1}H NMR spectra of PEP, PEP-^{V}PC-PEP and ^{V}PC.

Figure 4.5 Overlaid SEC traces of **P7**-**P10** (Table 4.1 Entries 2-5).

Figure 4.6 A) Hydrodynamic diameter (D_h) and polydispersity index (PDI) (size distribution by intensity), B) Cumulant fit and C) Correlation functions of DLS studies of the self-assembled nanostructures (1-4 correspond to entries 1-4 in Table 4.2, respectively).

Figure 4.7 TEM images of representative self-assembled nanostructures from PEP-^{V}PC-PEP: A) & B) micelles formed from **P8** and C) & D) vesicles formed from **P10**.

Figure 4.8 Cumulative release profiles of RhB-loaded **P10** at 37 ºC in PBS buffer (10.0 mM, pH 7.4).

Figure 4.9 Hydrodynamic diameter variation of PEP-^{V}PC-PEP in PBS buffer with or without enzymes during the experimental period: A) PBS buffer (10.0 mM, 37 ºC, pH 7.4), B) 200 UmL^{-1} *Rhizopus arrhizus* lipase, C) 200 UmL^{-1} ALP, and D) 200 UmL^{-1} *Rhizopus arrhizus* lipase and 200 UmL^{-1} ALP.

Figure 4.10 Cumulant fit and correlation functions of DLS studies in **Figure 4.9**

Figure 4.11 Hydrodynamic diameter variation of PEP-^{V}PC-PEP at various pH conditions (size distribution by number).

Figure 4.12 Cumulant fit and correlation functions of DLS studies in **Figure 4.11**

Figure 4.13 ALP catalysed biodegradation of PEP-^{V}PC-PEP with different enzyme concentrations at pH 8.8 and 37 ºC, monitored by DLS. A) & B) Hydrodynamic diameter variation and C) Mean count rate variation of the polymer vesicle solutions after 24 h incubation.

Figure 4.14 Hydrodynamic diameter and mean count rate variation of **P10** vesicle solutions with 200 UmL^{-1} ALP at pH 8.8 and 37 °C, as monitored by DLS.

Figure 4.15 SEC traces of the biodegradation products after treating with 200 UmL^{-1} ALP at pH 8.8 and 37 ºC. A) Overlaid SEC traces before and after treating with ALP for 1 h, obtained from SEC in DMF using monodispersed polystyrene as standard and B) Stacked SEC traces of ^{V}PC and the degradation products of PEP-^{V}PC-PEP, obtained from SEC in THF using monodispersed polystyrene as standard.

Figure 4.16 Stacked ^{1}H NMR spectra of PEP-^{V}PC-PEP before and after enzyme degradation for 24 h.

Figure 4.17 A) Viability of MC3T3-E1 cells (%) treated with ^{V}PC extract medium and controls (PVC and PE) after 72 h incubation, determined by Alamar Blue test and B) Cell viability of ^{V}PC (200 $mg \cdot mL^{-1}$) using a Live/Dead staining method after 24 and 72 h incubation with MC3T3-E1 cells.

Figure 4.18 Viability of MC3T3-E1 cells (%) treated with ^{V}PC degradation products after 72 h.

Figure 4.19 ^{1}H NMR spectrum and $^{13}C\{^{1}H\}$ NMR spectrum of **P11** (9-BBN functionalised ^{V}PC).

Figure 4.20 ^{11}B NMR spectrum of the product obtained from the reaction between ^{V}PC and 9-BBN.

Figure 4.21 Photographs of water droplets on different surfaces: A) uncoated glass, B) ^{V}PC and C) **P12**.

Figure 4.22 SEC trace of **P12**.

Figure 4.23 ^{1}H NMR spectrum of polymer **P12**.

Figure 4.24 Overlaid DSC traces of ^{V}PC, **P12** and **P13**.

Figure 4.25 A) The viability of MC3T3-E1 cells (%) treated with **P12** extract medium and controls (PVC and PE) after 72 h incubation, determined by Alamar Blue test and B) Viability of MC3T3-E1 cells (%) treated with **P12** degradation products and controls after 72 h incubation, determined by Alamar Blue test.

Figure 4.26 Confocal microscopy images of MC3T3-E1 cells on A) ^{V}PC and B) **P12** polymer coatings.

Figure 4.27 Stacked ^{1}H NMR spectra **P12** and poly(carbonate-*g*-phosphoester).

Figure 4.28 Overlaid SEC curves of **P12**, **P14**, **P15** and **P16**.

Figure 4.29 DSC curves of **P12**, **P14**, **P15**, **P16** and PEP_{50}.

Figure 4.30 Potential dual-responsive polymers.

Scheme 4.1 Structures of polymers targeted in this Chapter.

Scheme 4.2 Synthetic route of ethyl ethylene phosphate.

Scheme 4.3 Synthetic route of PEP-^{V}PC-PEP using ^{V}PC as the macroinitiator.

Scheme 4.4 Oxidation of Propylene by P450.

Scheme 4.5 Reaction between ^{V}PC and 9-BBN.

Scheme 4.6 Oxidation of polymer **P11**.

Table 4.1 Syntheses of the PEP-^{V}PC-PEP with different compositions.

Table 4.2 DLS analysis of the self-assembled nanostructures of PEP-^{V}PC-PEP, prepared in Table 4.1.

Table 4.3 Thermal properties of polymer **^{V}PC**, **P12** and **P13**.

Table 4.4 Graft copolymerisation of EP onto **P12** backbone.

Chapter 5

Figure 5.1 Stacked ^{1}H NMR spectra of ^{C}PC and the corresponding hydroborated product **P17**.

Figure 5.2 ^{11}B NMR spectrum of the product obtained from the reaction between ^{C}PC and 9-BBN after reacting at 80°C for 24 h.

Figure 5.3 A) ^{1}H NMR spectrum of polymer **P18**. B) A) ^{1}H-^{1}H COSY NMR spectrum of polymer **P18**. C) An enlarged ^{1}H-^{1}H COSY NMR spectrum corresponding to the selected area in B).

Figure 5.4 A) SEC trace of polymer **P18**, B) Photographs of water droplets on **P18** and C) Overlaid DSC traces of ^{C}PC and **P18**.

Figure 5.5 Stacked ^{1}H NMR spectra of ^{V}PC, ^{C}PC and their reaction mixture at different reaction temperatures and times.

Figure 5.6 ^{1}H NMR spectra of reactions between a mixture of ^{V}PC and ^{C}PC and 9-BBN.

Figure 5.7 Conversion of the alkene groups ((A): ^{V}PC and (B): ^{C}PC) versus reaction time.

Figure 5.8 Stacked ^{1}H NMR spectra of PAmb and Amb.

Figure 5.9 SEC trace of PAmb.

Figure 5.10 MALDI-ToF spectrum of **P19** synthesised with CHD as the CTA.

Figure 5.11 A) ^{1}H NMR spectrum of **P19**, B) ^{1}H-^{1}H COSY NMR spectrum of **P19** and C) Enlarged ^{1}H-^{1}H COSY NMR spectra corresponding to the selected area in B).

Figure 5.12 ^{13}C NMR spectrum of **P19**.

Figure 5.13 SEC trace of **P19** (Table 5.2, Entry 3).

Figure 5.14 Changes in the ^{1}H NMR resonance of the alkene groups during the reaction of **P19** with 9-BBN ($CDCl_3$, with mesitylene as an internal standard).

Figure 5.15 Percentage conversions of the alkene groups (terminal and internal) versus reaction time.

Figure 5.16 Plot of $\ln([C=C]_0/[C=C]_t)$ vs time of terminal alkene groups.

Figure 5.17 ^{1}H NMR spectrum of **P20**.

Figure 5.18 SEC trace of **P20**.

Figure 5.19 A) Photographs of water droplets on **P19** and **P20**. B) Overlaid DSC traces of **P19** and **P20**.

Figure 5.20 ^{1}H NMR spectrum of **P21**.

Figure 5.21 Top: ^{1}H-^{13}C HSQC NMR spectrum of **P21**. Bottom: ^{13}C NMR spectrum of **P21**.

Figure 5.22 Stacked SEC traces of polymers **20-25**.

Figure 5.23 Overlaid DSC traces of polymers **P21-25**.

Figure 5.24 DLS data collected from an aqueous solution of **P21** (10 mg·mL^{-1}).

Figure 5.25 TEM image of the micelles formed from polymer **P21** in aqueous solution (10 mg·mL^{-1}).

Figure 5.26 Photographs of water droplets on polymers (**P20-P25**) coated glass surfaces.

Figure 5.27 Potential alternating polyesters for achieving selective post-polymerisation modification.

Scheme 5.1 Structures of polymers targeted in this work.

Scheme 5.2 ROCOP of CHDO and CO_2 using **C2**. **C2** was applied in combination with a co-catalyst (PPNBr).

Scheme 5.3 Hydroboration of ^{C}PC with 9-BBN.

Scheme 5.4 Oxidation of polymer **P17**.

Scheme 5.5 Ring-opening polymerisation (ROP) of α-angelica lactone (AL) and

ambrettolide (Amb).

Scheme 5.6 ROCOP of MA and v-CHO, and the structure of catalyst investigated for the ROCOP.

Scheme 5.7 Hydroboration-oxidation of **P19**.

Scheme 5.8 Thiol-ene reaction between **P20** and various thiols.

Scheme 5.9 Proposed synthetic route for obtaining amine and boronic acid-containing polymers.

Table 5.1 Polymerisation data for ROP of Amb.

Table 5.2 Polymerisation data for ROCOP of MA and v-CHO.

Table 5.3 Functionalisation of **P20** *via* photo-induced radical thiol-ene reaction.

Chapter 6

Figure 6.1 Schematic representation of the anion exchange reaction and anions to be explored in future studies.

Figure 6.2 Synthetic strategies to make alternating block polyesters for further functionalisation.

Chapter 7

Figure 7.1 ^{1}H NMR spectrum of 4-tert-butyl-2,6-diformylphenol.

Figure 7.2 ^{1}H NMR spectrum of $[H_4L](ClO_4^-)_2$.

Figure 7.3 ^{1}H NMR spectrum of $[H_4L]$.

Figure 7.4 ^{1}H spectrum of **C1**.

Figure 7.5 $^{19}F\{^{1}H\}$ NMR spectrum of **C1**.

Figure 7.6 ^{1}H NMR spectrum of 1,4-cyclohexadiene oxide (CHDO).

Figure 7.7 $^{13}C\{^{1}H\}$NMR spectrum of CHDO.

Figure 7.8 ^{1}H NMR spectrum of tetraethylene glycol monoethylether monotosylate (EG_4-OTs).

Figure 7.9 ^{1}H NMR spectrum of tetraethylene glycol monoethylether thiol (EG_4-SH).

Figure 7.10 ^{1}H NMR spectrum of ^{V}PC.

Figure 7.11 $^{13}C\{^{1}H\}$ NMR spectrum of ^{V}PC.

Figure 7.12 ^{1}H NMR spectrum of ^{C}PC.

Figure 7.13 $^{13}C\{^{1}H\}$ NMR spectrum of ^{C}PC.

Figure 7.14 ^{1}H NMR spectrum of PLA-^{V}PC-PLA.

Figure 7.15 $^{13}C\{^{1}H\}$ NMR spectrum of PLA-^{V}PC-PLA.

Figure 7.16 The fluorescence spectrum (A) and calibration curve (B) of Rhodamine B (RhB) in PBS solution (10.0 mM, pH 7.4). (λ_{ex} = 510 nm).

Scheme 7.1 Synthetic route of **C1**.

Scheme 7.2 Synthetic route of 1,4-cyclohexadiene oxide (CHDO).

Scheme 7.3 Synthetic route of EG_4-OTs and EG_4-SH.

Table 7.1 Relative quantities of reagents used in **Table 3.1**.

Table 7.2 Relative quantities of reagents used for preparing **P1-P6**.

Table 7.3 Relative quantities of reagents used in quaternisation listed in **Table 3.3**.

Table 7.4 Relative quantities of reagents used in **Table 4.1**.

Table 7.5 Relative quantities of reagents used in **Table 4.5**.

Table 7.6 Relative quantities of reagents used in **Table 5.1**.

Table 7.7 Relative quantities of reagents used in **Table 5.2**.

Table 7.8 Relative quantities of reagents used in thiol-ene reactions listed in **Table 5.3**.

Appendices

Figure A1 ^{1}H NMR spectra of P6 (25 wt% of ^{V}PC), $Q_{0.25}$P6.

Figure A2 ^{1}H NMR spectra of $Q_{0.40}$P6, $Q_{0.59}$P6 and $Q_{0.78}$P6.

Figure A3 Overlaid ^{1}H NMR spectra of **P22-P25**, showing the disappearance of the internal alkene signals after the thiol-ene reactions.

Table A1 DLS analyses shown in **Table 4.2**.

Table A2 TEM particle size analysis of self-assembled nanostructures formed from **P8** and **P10**.

Table A3 TEM membrane thickness analysis of self-assembled nanostructures formed from **P10**.

Table A4 Zeta potential analysis of self-assembled nanostructures formed from **P10**.

Table A5 Water contact angle measurements on polymer surfaces (^{V}PC, **P12**).

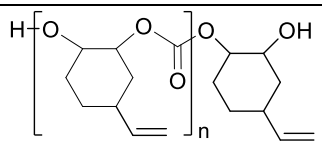
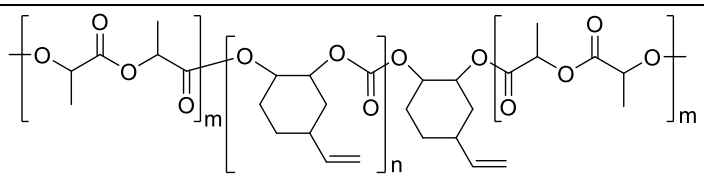
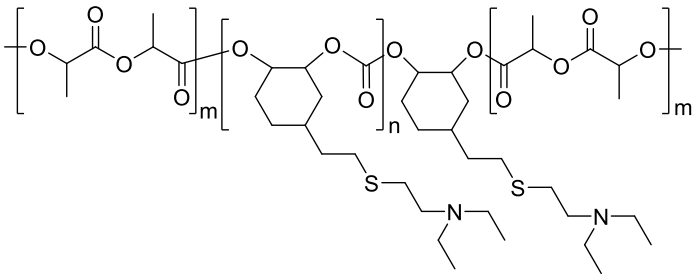
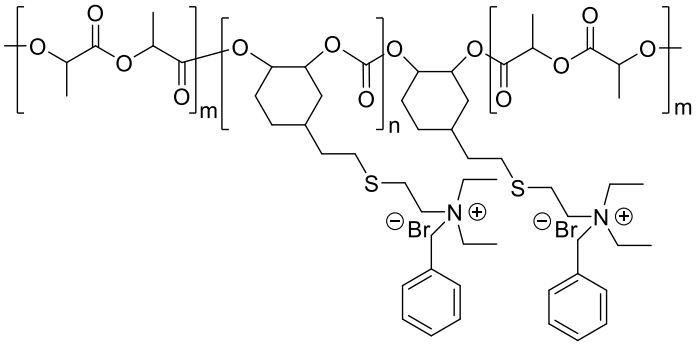
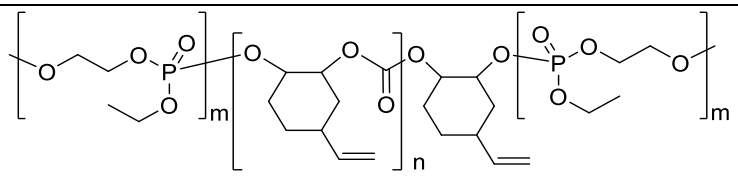
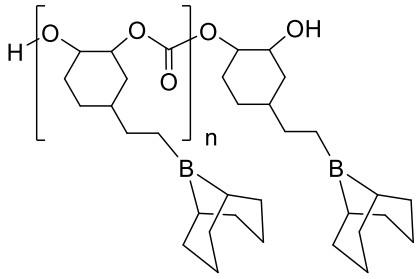
Table A6 Water contact angle measurements on polymer surfaces (**P18**-**P25**).

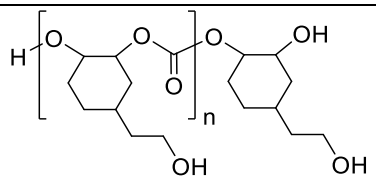
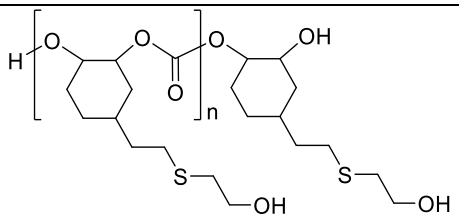
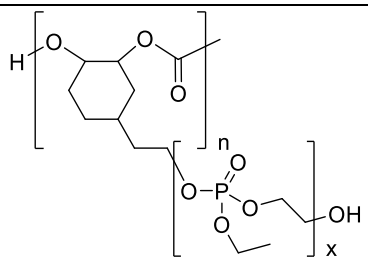
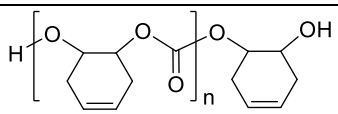
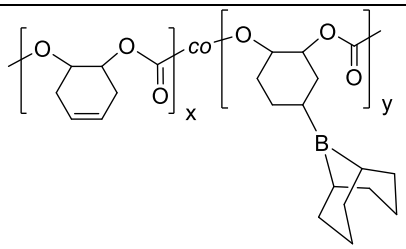
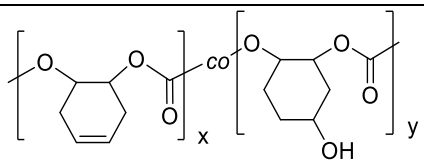
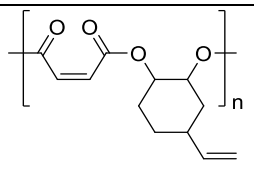
Table A7 DLS analyses of self-assembled nanostructures formed from **P21.**

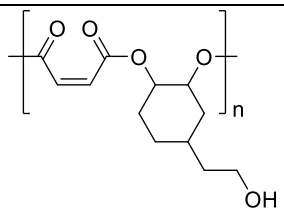
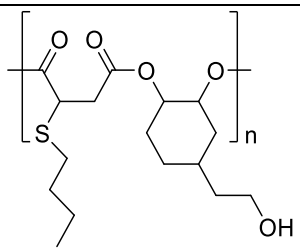
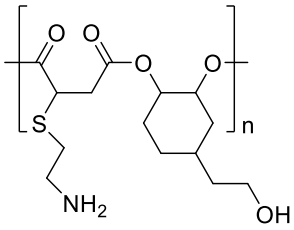
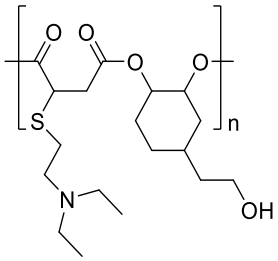
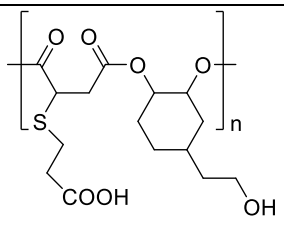
Table A8 Zeta potential analysis of self-assembled nanostructures formed from **P21**.

Table A9 TEM particle size analysis of self-assembled nanostructures formed from **P21**.

List of Polymers

^{V}PC	
PLA-^{V}PC-PLA (P1-P6)	
NP6	
QP6	
PEP-^{V}PC-PEP (P7-P10)	
P11	

P12	
P13	
P14-P16	
^{C}PC	
P17	
P18	
P19	

P20	
P21	
P22	
P23	
P24	

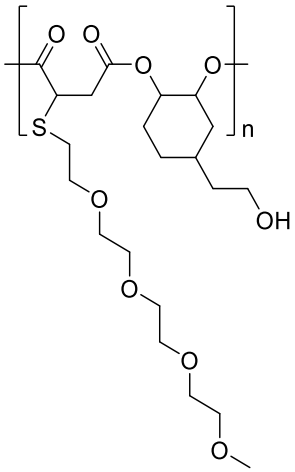
P25	

Table of Contents

Declaration iii

Abstract iv

Acknowledgements vi

List of Publications viii

List of Abbreviations ix

List of Figures, Schemes and Tables xiii

List of Polymers xxiv

Chapter 1 Introduction 1

1.1 Project Motivations 2

1.1.1 Antimicrobial Polymers 2

1.1.2 Evaluation of antimicrobial activity 4

1.1.3 Polymeric self-assembly 5

1.1.4 Preparation methods for polymeric self-assembly 8

1.1.5 Applications in drug delivery and release 9

1.1.6 Degradable polymers 11

1.2 Thesis Aims 13

1.3 Polymerisation techniques 17

1.3.1 Step polymerisations 17

1.3.2 Living/controlled polymerisation 18

1.3.3 Ring-opening polymerisation (ROP) 19

1.3.4 Ring-opening copolymerisation (ROCOP) 22

1.4 Block copolymer formation 26

1.5 Post-polymerisation modifications 28

1.5.1 Functional polycarbonates 30

1.5.2 Functional polyesters 40

1.6 Summary 43

1.7 References 44

Chapter 2 Characterisation Techniques 57

2.1 Polymer Characterisations 58

2.1.1 Nuclear Magnetic Resonance (NMR) Spectroscopy 58

2.1.2 Size Exclusion Chromatography (SEC) 64

2.1.3 Matrix-assisted laser desorption/ionization time-of-flight (MALDI-ToF) mass spectrometry 67

2.1.4 Thermal Analyses....68
2.1.5 Water Contact Angle Measurements....70
2.2 Antibacterial polymers....71
2.2.1 Viable Colony Counting Technique....71
2.2.2 Surface Charge Measurements....73
2.3 Self-assembled Nanostructures....74
2.3.1 Dynamic Light Scattering (DLS)....74
2.3.2 Zeta potential....75
2.3.3 Transmission Electron Microscope (TEM)....75
2.3.4 Fluorescence Spectroscopy....76
2.4 Cell studies....78
2.4.1 Cytotoxicity/Cell Viability Tests....78
2.4.2 Cell Attachment Tests....80
2.5 References....80

Chapter 3 Syntheses and Functionalisations of Poly(ester-*b*-carbonate-*b*-ester) for Antibacterial Applications....83
3.1 Background and Aims....84
3.2 Results and Discussion....86
3.2.1 The ROCOP of carbon dioxide and vinyl cyclohexene oxide (v-CHO)....86
3.2.2 Syntheses of Block Copolymers PLA-^{V}PC-PLA....89
3.2.3 Post-polymerisation Modifications....98
3.2.4 Assessment of antibacterial activities....102
3.2.5 Discussion....112
3.3 Summary and Conclusion....113
3.3.1 Summary....113
3.3.2 Outlook....114
3.4 References....115

Chapter 4 Poly(phosphoester-carbonate) as Potential Platform Materials That Are Capable of Full Degradation....118
4.1 Background and Aims....119
4.2 Results and Discussions....121
4.2.1 Synthesis of cyclic phospholane monomer....121
4.2.2 Syntheses of block poly(phosphoester-*b*-carbonate-*b*-phosphoester)s with different block ratios....122

4.2.3 Self-assembly of the amphiphilic block poly(phosphoester-*b*-carbonate-*b*-phosphoester) 128
4.2.4 TEM characterisation 120
4.2.5 Model Drug Release Experiments 132
4.2.6 *In vitro* Degradation Study of PEP-^{V}PC-PEP 134
4.2.7 Hydroboration-oxidation 148
4.2.8 Syntheses of brush poly(carbonate-*g*-phosphoester) 159
4.3 Conclusions 163
4.3.1 Summary 163
4.3.2 Outlook 164
4.4 References 165

Chapter 5 Selective Post-polymerisation Modifications in Functionalising Unsaturated Polycarbonates and Polyesters 170

5.1 Background and Aims 171
5.2 Results and Discussion 173
5.2.1 Hydroboration-oxidation of poly(cyclohexadiene oxide) (^{C}PC) 173
5.2.2 Selective post-polymerisation modification on a mixture of ^{V}PC and ^{C}PC 179
5.2.3 Syntheses of unsaturated polyesters 182
5.2.4 The syntheses of unsaturated alternating polyesters 186
5.2.5 Selective hydroboration of ^{V,M}PE (P19) 191
5.2.6 Thiol-ene reaction with P20 197
5.3 Summary and Outlook 206
5.3.1 Summary 206
5.3.2 Outlook 206
5.4 References 208

Chapter 6 Conclusions and Outlook 211

6.1 Conclusions 212
6.2 Outlook 212
6.2.1 Antibacterial poly(ester-*b*-carbonate-*b*-ester) polymers 212
6.2.2 Poly(phosphoester-carbonate)s 214
6.2.3 Hydroboration-oxidation and selective post-polymerisation modifications 216
6.3 References 218

Chapter 7 Experimental Section.....220
7.1 General Procedures.....221
7.1.1 Materials.....221
7.1.2 Measurements.....222
7.1.3 Synthesis of C1.....229
7.1.4 Syntheses of monomers/compounds.....236
7.2 Copolymerisation of CO_2 and epoxides.....241
7.2.1 CO_2/v-CHO copolymerisation at 1 bar of CO_2 (^{V}PC).....241
7.2.2 CO_2/v-CHO copolymerisation at 1 bar of CO_2 in the presence of CTA (^{V}PC).....243
7.2.3 CO_2/CHDO copolymerisation at 20 bar of CO_2 (^{C}PC).....243
7.3 Synthesis of antibacterial poly(ester-*b*-carbonate-*b*-ester).....245
7.3.1 Block copolymerisation of ^{V}PC and *rac*-LA.....245
7.3.2 UV-mediated thiol-ene reaction between P6 and 2-(diethylamino)ethanethiol hydrochloride.....248
7.3.3 Quaternisation of NP6 with benzyl bromide (QP6).....249
7.4 Synthesis of amphiphilic poly(phosphoester-*b*-carbonate-*b*-phosphoester).....250
7.4.1 Block copolymerisation of ^{V}PC and EP (PEP-^{V}PC-PEP, P7-P10).....250
7.5 Preparation and evaluation of PEP-^{V}PC-PEP self-assembly.....251
7.5.1 The colloidal self-assembly protocol.....251
7.5.2 Procedure for making the calibration curve of RhB in PBS solution.....252
7.5.3 Colloidal self-assembly drug-loading procedure and in vitro release.....253
7.5.4 In vitro release in the presence of enzymes.....254
7.5.5 Stability of P10 vesicles.....254
7.5.6 Enzymatic biodegradation of P10 vesicles.....254
7.6 Synthesis of brush poly(carbonate-*g*-phosphoester).....255
7.6.1 Hydroboration-oxidation of ^{V}PC (P12).....255
7.6.2 Brush copolymerisation of P12 and EP (P14-P16).....256
7.7 Synthesis and post-polymerisation modification of unsaturated polycarbonates/polyesters.....257
7.7.1 Hydroboration-oxidation of ^{C}PC.....257
7.7.2 Initial NMR reaction between ^{V}PC, ^{C}PC and 9-BBN.....257
7.7.3 NMR reaction between ^{V}PC, ^{C}PC and 9-BBN in the presence of an internal standard.....257
7.7.4 Ring-opening polymerisation of α-AL.....258
7.7.5 Ring-opening polymerisation of Amb.....258

7.7.6 Copolymerisation of v-CHO and MA (^{V,M}PE, P19) 259
7.7.7 NMR reaction between P19 and 9-BBN 260
7.7.8 Hydroboration-oxidation of P19 (P20).....260
7.7.9 Thiol-ene reactions between P20 and thiols 261
7.7.10 Self-assembly protocol 262
7.8 References 262

Appendices.....263
Appendix A – Experimental Data 264
A1. Chapter 3.....264
A2. Chapter 4.....266
A3. Chapter 5.....267
Appendix B – Permissions.....269

Chapter 1

Introduction

1.1 Project Motivations

Polymers are ubiquitous in everyday life, with applications ranging from packaging materials and coatings to adhesives.[1] Development of polymerisation techniques and analytical methods over the last century has vastly improved the control of polymer molar mass, architecture, composition, functionality, and even the exact sequence of polymer chains, leading to the possibility of higher-added-value and more sophisticated applications.[2-4] This thesis targets the development of amphiphilic block copolymers for use in self-assembly to form nanostructures for drug delivery and the synthesis of cationic polymers for antimicrobial applications.

1.1.1 Antimicrobial Polymers

The development of synthetic polymers as antimicrobial materials for reducing bacterial colonisation and biofilm formation, particularly in hospital surfaces/furniture, water purification systems, food packaging and wound healing applications has attracted increasing interest over the past fifty years.[5-7] Two main types of polymeric antimicrobial agents have been developed: polymers combined with small antimicrobial agents and those with inherent antimicrobial activities.[5] The former category of agents operates by releasing conventional antibiotics.[7] However, the use of the conventional antibiotics may lead to the development of antibacterial resistance due to microbial mutation.[8] In contrast, polymers with inherent antimicrobial activities (antimicrobial polymers) are able to slow or prevent the development of drug resistance because they work by disrupting the microbial membranes, which immediately kills microbes.[8-10]

Two key features are often required for a polymer to display antimicrobial activity. First, the majority of antimicrobial polymers are cationic, which enhances adsorption to the

negatively charged microbial membranes through electrostatic interactions.[6, 11] Secondly, hydrophobic groups on the polymers can insert into the cell membrane, causing cytoplasm leakage and promoting cell lysis.[8, 11] One beneficial outcome of this mechanism is that bacterial resistance is less likely to develop since specific molecular pathways are not implicated.[8]

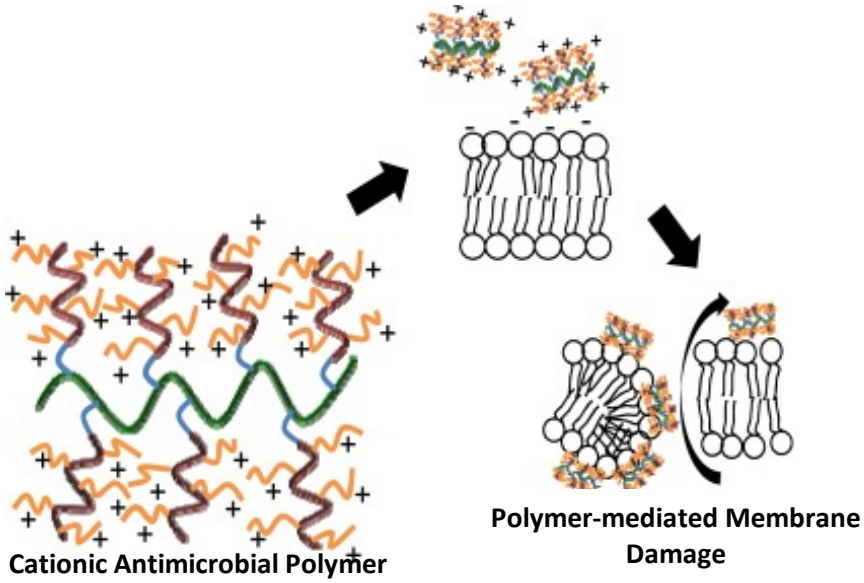


Figure 1.1 A possible mechanism of cationic antimicrobial polymers: cationic polymer interacts with and disrupt the membrane, leading to cytoplasm leakage.[12] Reproduced with permission.

Common target structures are block copolymers containing a hydrophilic block bearing cationic charges and a hydrocarbon hydrophobic block, or random copolymers formed from hydrophobic and hydrophilic comonomers with the latter usually bearing a cationic functional group.[9] A wide range of the cationic groups have been applied, including quaternary ammonium, phosphonium, tertiary sulfonium and guanidinium salts.[5, 11, 13, 14] The antimicrobial activity of cationic polymers usually relates to the charge density of the cationic groups.[6] Quaternary ammonium groups are most widely applied due to their ease of synthesis and intrinsic positive charges that are less strongly pH dependent.[15, 16] The majority of cationic antimicrobial polymers apply linear alkyl

groups as the hydrophobic parts.[14, 17] However, the optimal alkyl chain length needs to be optimised for each polymer structure.[9, 11, 18]

1.1.2 Evaluation of antimicrobial activity

A common group of microorganisms is usually selected for analysing antimicrobial activities and these include Gram-negative, Gram-positive bacteria, as well as some fungi. The commonly applied Gram-negative bacteria are *Escherichia coli* (*E. coli*) and *Pseudomonas aeruginosa (P. aeruginosa)*; the most commonly applied Gram-positive bacterium is *Staphylococcus aureus (S. aureus)*.[19] Representative fungi are *Aspergillus niger (A. niger)*, *Aspergillus flavus (A. flavus)* and *Candida albicans (C. albicans)*.[19] With regards to terminology, the term 'antimicrobial' is used to describe an agent that is both bactericidal and fungicidal, where the term 'antibacterial' applies only to agents that are bactericidal.[19]

The antimicrobial activity is evaluated by measuring the inhibition effect against bacterial growth, as well as any bactericidal effect. There are a number of classical microbiological procedures, adapted by the Clinical & Laboratory Standards Institute (CSLI) into standardised forms, to evaluate the antimicrobial activity.[20] The commonly used plate counting method determines the number of bacterial or fungal cells able to grow in a specific growth medium, and this is reported as colony forming units (CFU).[21] Additionally, the microbial cell morphology is also observed by microscopy (optical or electron) and relates to the physical state of the cell (damaged or not).

For leaching antimicrobial agents, the minimum inhibitory concentration (MIC) assay is usually carried out to determine the lowest concentration of a particular agent needed to inhibit bacterial growth.[20, 22] In the assay, successive dilutions of the antimicrobial under examination are performed and dispensed in equal amounts of a standardised suspension of microbes. Samples are evaluated, after incubation for bacterial growth, to determine the MIC. For non-leaching antimicrobial agents, such as antimicrobial surfaces, the standard method is carried out in shaking flasks (shaking-flask method), where the surfaces are incubated with microbes, and the CFU is determined afterwards.[23]

1.1.3 Polymeric self-assembly

The research into polymeric self-assembly has experienced exponential growth recently due to the wide range of applications.[24, 25] While self-assemblies of small-molecule surfactants are widely applied in cleaning products and cosmetics, their low stability limits use.[25] In contrast, polymeric self-assembly may exhibit greater stability by virtue of the covalent linkages within the hydrophobic parts, restricting the dynamic exchange of amphiphiles between the dissolved and self-assembled phases.[26-28] As such, polymeric self-assemblies are investigated for uses in drug delivery[29-31], as nanoparticle imaging agents[32, 33] and even as catalytic nanoreactors.[34, 35]

The main type of polymers investigated are linear amphiphilic block copolymers, *i.e.* consisting of a hydrophilic and hydrophobic block. Amphiphilic block copolymers form self-assembly, in a particular medium, to minimise unfavourable hydrophilic/hydrophobic interactions between the polymer chains and the surrounding phase. They can adopt various morphologies including spherical micelles, cylindrical micelles, lamellae and vesicles (polymersomes).[26, 27] The structures are determined by

the inherent molecular curvature which relates to a dimensionless packing parameter, p, defined by:

$$p = \frac{v}{a_0 l_c}$$

[v is the volume of the hydrophobic block, a_0 is the optimal interfacial area per molecule and l_c is the length of the hydrophobic block]

As a general rule, spherical micelles are formed when $p \leq 1/3$, cylindrical micelles when $1/2 \leq p \leq 1/3$ and enclosed membrane structures when $1/2 \leq p \leq 1$.

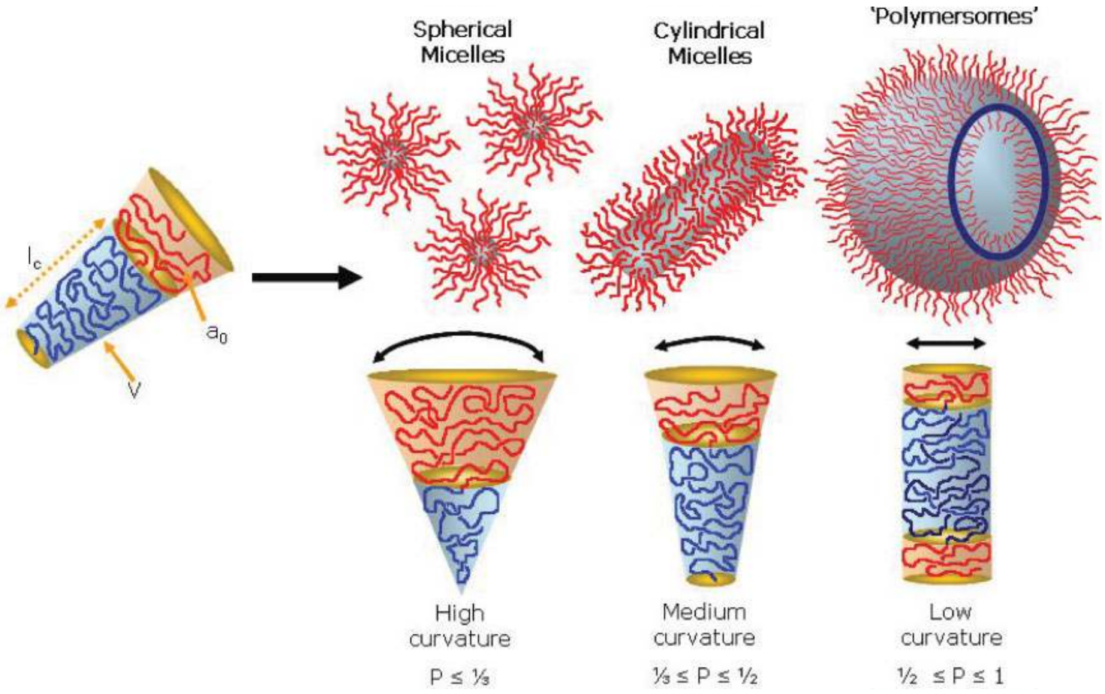


Figure 1.2 Common morphologies of self-assembled amphiphilic block copolymers: spherical micelles, cylindrical micelles and vesicles (also known as polymersomes).[26] Reproduced with permission.

Polymer micelles are core-shell nanostructures, where the hydrophobic block forms the core and the hydrophilic block forms the corona (Figure 1.2).[25, 36, 37] The hydrophilic coronas afford water solubility, while the hydrophobic cores provides a region suitable for encapsulation of hydrophobic drugs, fluorescence probes, and some hydrophobic biomolecules such as genes or proteins.[25, 38-40]

Polymer vesicles or polymersomes are nanoscale hollow spheres featuring a hydrophobic bilayer membrane and hydrophilic internal and external coronas (Figure 1.2).[26] This hollow structure is more complex than a micellar arrangement, and conventionally, their formation is considered to involve two steps.[41] The first is the formation of a membrane bilayer, followed by subsequent bending to form a closed hollow structure. Vesicles can encapsulate hydrophobic molecules within their membrane, but unlike micelles, they are also capable of encapsulating hydrophilic drugs, biomolecules and even smaller nanoparticles within their lumen.[42]

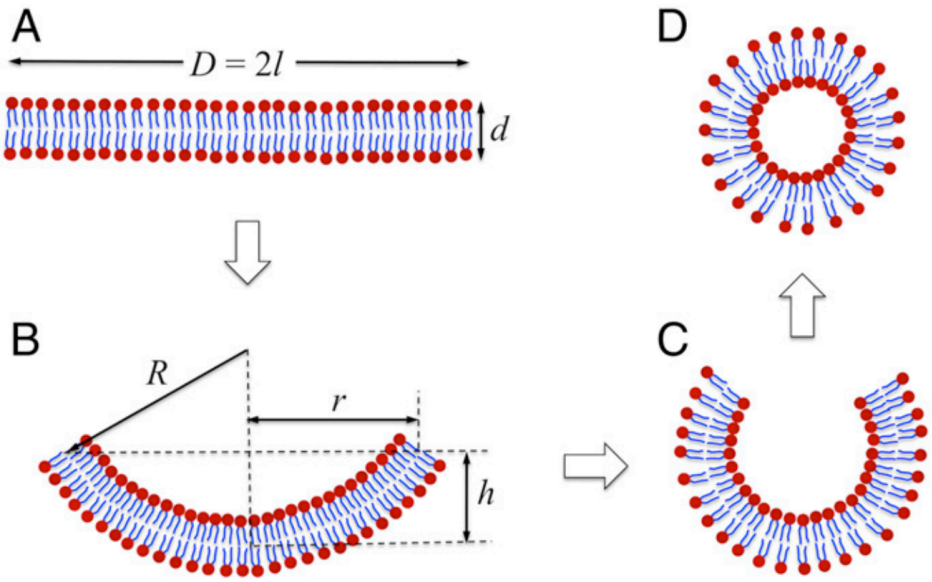


Figure 1.3 A Schematic representation of vesicle formation.[43] A membrane bilayer (A) curves (B and C) and eventually closes to form a vesicle (D).

Amphiphilic alternating copolymers and homopolymers have also been explored for the preparation of polymer self-assemblies.[44-46] These alternating structures show less clearly defined boundaries between hydrophilic and hydrophobic regions and thus, the self-assembly process is thought to be driven by other factors, such as chain end groups, hydrogen bonding and anion-dipole interactions.[44-46]

1.1.4 Preparation methods for polymeric self-assembly

There are several methods for preparing polymeric self-assembly. The 'solvent switch' method has been widely used for non-water soluble polymers.[47-50] Initially, a polar organic solvent (*e.g.* N,N-dimethylformamide (DMF) or tetrahydrofuran (THF)) is required to dissolve the polymer. A second solvent (usually water) is subsequently added to induce self-assembly, where the hydrophilic blocks are solvated to form the corona and the hydrophobic part associate together to core/membrane. It is worth mentioning that the exact organic solvent/water ratio can significantly affect the resultant morphology and the permeability of any vesicle membrane. This technique often necessitates the removal of the organic solvent, for example by dialysis, and thus can be time-consuming and certainly be economically unfavourable to apply on a large-scale.

Another method, which is organic solvent-free, involves the rehydration of the polymer in water, achieved by either a film or bulk swelling step. In the film swelling step, polymers are firstly dissolved in an organic solvent (*e.g.* chloroform), followed by evaporation of the organic solvent to afford a thin film. The subsequent addition of water or aqueous buffer solutions hydrates the thin film to form self-assemblies.[51] In the bulk swelling approach, the polymer is directly dissolved in water to form nanostructures.[52, 53] Longer and more vigorous agitation is usually required to hydrate the polymer fully, and this may lead to structural defects and broad particle size

distributions.[51] Nonetheless, as the self-assemblies are prepared in the absence of organic solvents they can be used without further purifications.

In this thesis, both bulk swelling and 'solvent-switch' methods have been employed. Usually, the bulk swelling method is preferred, as dialysis process is obviated. The 'solvent-switch' method is only employed when the self-assemblies formed by the above method show broad particle size distributions (polydispersity > 0.30).

1.1.5 Applications in drug delivery and release

The delivery and release of hydrophobic drugs such as those used for the treatment of cancer (paclitaxel), female birth control (levonorgestrel) and anti-inflammatory care/pain relief (morphine) are often impeded by their limited water solubility, poor oral bioavailability and/or short half-lives.[54-56] In this respect, polymeric self-assemblies are of interest as they have the potential to overcome some of the challenges.[54, 55, 57-59] For instance, entrapment of the drugs in the micelle core or the vesicle membrane allows them to be delivered at concentrations that exceed their intrinsic water solubility.[54, 55, 57] Additionally, the hydrophilic corona can resist protein adsorption and cellular adhesion, protecting the hydrophobic drug against hydrolysis and enzymatic degradation. Water-soluble drugs, such as the antibiotic gentamicin, can also be entrapped within the interior of vesicles which has shown to improve the permeability through the plasma membrane and avoid rapid clearance from the body.[58, 59]

Polymer self-assemblies that respond to an external stimulus are considered to be 'smart'.[51] Stimuli-responsiveness can be introduced by incorporating various functional groups into the backbone or as side chains. These groups may alter solubility or molecular conformation in response to the external stimuli, thereby triggering

nanostructures disassembly or a morphology transition.[25] Examples of external stimuli triggers include pH,[60] temperature,[61] oxidation/reduction reactions,[62] light,[63] electrical field,[64] magnetic field,[60] sugar,[65] gases[66, 67] or ultrasound.[68] Attempts have also been made to modify the corona of polymer vesicles so as to enable them to cross the blood-brain barrier or to penetrate a cell membrane.[69-71] Such functionalisation reactions involve conjugation to oligopeptides or brain targeting ligands such as Lactoferrin. Similar strategies were also employed to target tumour cells, where the surface of vesicles/micelles was functionalised with ligands such as folic acid or an antibody that bind specifically to proteins such as the transferrin receptor, only present on the surface of tumour cells.[3, 72]

The criteria for designing polymeric self-assembly for drug delivery depend highly on the therapeutic agent and the targeted site of application. Nonetheless, there are general requirements common to all therapies.[55, 73, 74] First, the polymer should be constructed from biocompatible blocks or monomers. Second, it should exhibit a high drug loading capacity, which reduces the need for multiple injections/treatments. Third, it should circulate in the bloodstream for extended periods of time and also shield the therapeutics from degradation in the bloodstream so as to facilitate release at the appropriate site of action. Finally, it should be biodegradable to avoid any accumulation in the body, and the degradation products should also be non-toxic and be able to be completely eliminated from the body by metabolic pathways, with minimal side effects.[55]

1.1.6 Degradable polymers

Synthetic biodegradable polymers generally contain hydrolytically cleavable bonds such as ester, thioesters, amides, carbonates, anhydrides, acetals, phosphonates.[75]

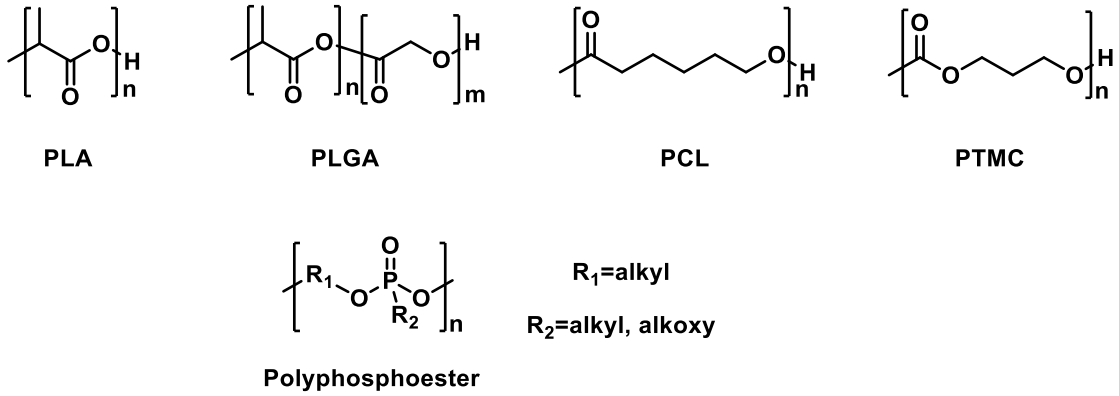


Figure 1.4 Structures of poly(lactic acid) (PLA), poly(lactic acid-*co*-glycolide) (PLGA), PCL poly(ε-caprolactone) (PCL), poly(trimethylene carbonate) (PTMC) and polyphosphoesters.

Currently, aliphatic polyesters, in particular, polylactide (PLA), polycaprolactone (PCL) and poly(lactide-*co*-glycolide) (PLGA) are widely explored as medical materials.[75-78] For example, PLGA has been used in commercially sutures since the 1970s.[75] PCL is used for the fabrication of tissue repair patches and as a filling agent for non-load bearing bone defects.[78] For loading-bearing applications, PLA is mostly used due to its higher mechanical strength (57 MPa compression and 3500 MPa tensile modulus).[78-81] As such, PLA is used in various medical fixation devices, such as screws, plates, pins and rods to support the remodelling of broken bones.[78] For drug delivery applications, a formulation (Genexol-PM) comprising a block copolymer of PLA and poly(ethylene glycol) (PEG) with 16 wt% paclitaxel (PTX) has been clinically approved and is commercially available.[82] However, there are still shortcomings in the properties of PLA that need to be addressed: 1) It is hydrophobic which hampers cell interactions and slows healing; 2) Its degradation results in increased acidity in the surrounding

tissues, which may cause an immune response and can lead to issues of rejection.[75, 79, 83]

Degradable aliphatic polycarbonates do not generate acidic by-products during degradation and are thus investigated as an alternative to PLGA/PLA.[75, 84, 85] They can reduce the risk of inflammation and even rejection for *in vivo* applications, *i.e.* implants.[75] For instance, coatings of poly(trimethylene carbonate) (PTMC) has been shown to improve the compatibility of implants.[75, 84, 86] Since PTMC is an amorphous polymer with a low glass transition temperature (T_g of *ca.* -20 ºC) and low Young's modulus, PTMC-based devices have been limited to copolymers, generally with glycolides, for applications such as flexible sutures, tissue fixation and orthopaedic screws.[85, 87, 88] Additionally, due to its hydrophobic nature, it has been explored as a hydrophobic segment in poly(trimethylene carbonate)-poly(ethylene glycol) (PTMC-PEG) copolymers for the sustained release of Corticosteroids.[89]

More recently, polyphosphoesters (PPE) have emerged as another alternative to aliphatic polyesters.[90-92] They have structures that are somewhat similar to common biopolymers, DNA and RNA, and the phosphorus atom provides higher structural flexibility.[93, 94] Therefore, their physical and chemical properties, such as hydrophilicity and thermal properties, can be quite easily adjusted to the application requirements. For example, the use of short ether substituents confers hydrophilicity to the PPE, which is in marked contrast to the hydrophobicity of polycarbonates.[95, 96] Self-assembled nanoparticles formed from amphiphilic block copolymers comprising aliphatic polyesters (PCL, PLA) and PPE, as the hydrophilic block, were used for drug delivery.[95, 97, 98] The PPE backbone is degraded by a range of enzymes, such as alkaline phosphatases and phosphodiesterases, both of which can be produced in bone and liver cells, under physiological conditions.[90, 95, 99] More interestingly, these enzymes can also

be produced by active bacteria (both Gram positive and Gram negative ones) and PPE's biodegradability can be utilised to trigger antibiotic release.[100-102] In a previous study, a PPE based drug delivery system was developed for targeted Vancomycin delivery to *S. aureus* bacterial infection sites, where the bacterial enzyme degraded the polyphosphoester core and triggered drug release.[100] While PPEs show great academic promise, further research is required in order to realise their potential and their use is not at the same stage of development as aliphatic polyesters.

1.2 Thesis Aims

The majority of biomedical studies, using polyesters, polycarbonates and polyphosphoesters, focus on polymers prepared by ring-opening polymerisation (ROP). This thesis applies alternating polymers (*i.e*. alternating polycarbonates and polyesters), prepared by the ring-opening copolymerisation (ROCOP) of epoxides and CO_2/anhydrides, to target antibacterial materials and drug delivery vehicles. There are two major synthetic strategies to the target materials: 1) copolymerisation to synthesise block copolymers and 2) post-polymerisation modification to introduce groups relevant to the applications. The use of alternating polycarbonates and polyesters (obtained by ROCOP) in biomedical applications is under-explored, but they offer interesting alternative structures to polymers prepared by ROP. Due to the much larger range of available (functionalised) monomers, ROCOP may offer new properties such as sequential patterning with different side chains or two sites for degradation reactions. In addition, alternating polycarbonates and polyesters show a wider range of thermal properties, with glass transition temperature (T_g) values ranging from -60 to 140 ºC, which may allow for a wider processing and operating temperature window.[103] At the same time, alternating polyesters and polycarbonates are expected to be fully degradable and should be able to be designed to be non-toxic and biocompatible. This

thesis aims to modify the material properties of unsaturated alternating polycarbonates/polyesters prepared from a commercially available epoxide (v-CHO), both through copolymerisation and post-polymerisation modifications. The broad objective can be summed up as follows:

1. To prepare antibacterial coating materials using alternating polycarbonates. As both cationic and hydrophobic properties have shown precedent in delivering antibacterial activity, block poly(ester-*b*-carbonate-*b*-ester) polymers are targeted, where the ester block is hydrophobic and the carbonate block delivers the cationic properties. These block copolymers will be synthesised by v-CHO and CO_2 ROCOP, followed by copolymerisation with lactide. Cationic quaternary ammonium groups will be introduced through a series of post-polymerisation modifications to the polycarbonate. PLA has been widely used for packaging and wound healing applications;[104] incorporating cationic alternating polycarbonates into PLA may confer antibacterial properties to materials suitable for these applications.

2. To synthesise amphiphilic polymers and to prepare self-assembled structures for testing in drug delivery applications. Alternating copolymerisation will be used to deliver hydrophobic polycarbonate blocks (from ROCOP of v-CHO and CO_2) and ROP of cyclic phospholane ethyl ethylene phosphate (EP) will deliver the hydrophilic block. EP is selected because its copolymer with PLA has been used to prepare microspheres (PACLIMER®) and loaded with 10 wt% paclitaxel (PTX), to treat cancer; the material is currently in a phase I clinical trial.[105] The self-assembly behaviour of the amphiphilic block copolymer will be studied and it is proposed that different morphologies will be obtained through varying the hydrophobic/hydrophilic block ratio. In particular, vesicles are targeted to encapsulate hydrophobic drugs within their membrane and/or hydrophilic drugs in the interior.

3. To develop post-polymerisation modifications to selectively functionalise alkene-containing polymers. Selective chemical reactions orthogonal to biological systems have become important tools in the field of chemical biology, including protein engineering and remodelling of cell surfaces.[106, 107] However, the application of similar concepts to polymer synthesis remains in its infancy. Here, the first target is to develop means to add hydroxyl functional groups at selective sites along the polymer backbone. This is expected to increase hydrophilicity, and thereby improve biocompatibility and cell adhesion. As a second goal, orthogonal functionalisation reactions will be used to target polymers featuring alternating, different side chain substituents.

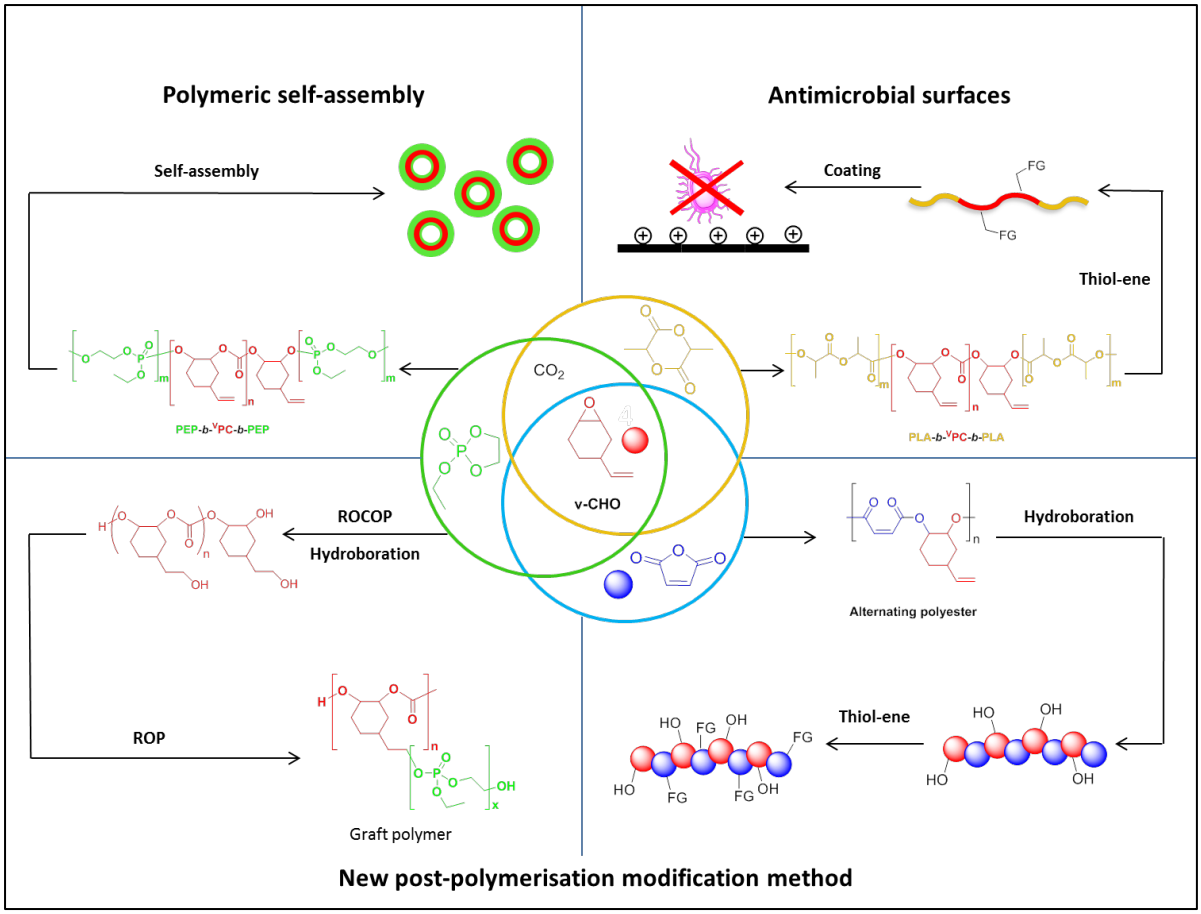


Figure 1.5 Diagram illustrating target polymers and applications.

1.3 Polymerisation techniques

There are two major routes to prepare aliphatic polycarbonates, polyesters and polyphosphoesters: by step polymerisation and by controlled polymerisation, which includes ring-opening polymerisation (ROP) and alternating ring-opening copolymerisation (ROCOP).[79, 84, 93]

1.3.1 Step polymerisations

Aliphatic polyesters can be synthesised by step polymerisation, *i.e.* the reaction between a diol and a dicarboxylic acid (AA + BB) or the condensation of a hydroxy-acid (AB).[79] The major drawback of step polymerisation is the need to achieve very high conversions to produce high molar mass polymers. The synthesis can be extremely challenging, particularly for esterification reactions, which are equilibrium processes. The esterification equilibrium can be driven to high conversions only by removal of the condensate (*i.e.* water) and various techniques have been used to achieve this, *e.g.* application of high vacuum, high temperature, high pressure of inert gas or absorbents such as molecular sieves.[79] Another disadvantage of step polymerisation is that it is typically an uncontrolled process resulting in the formation of ill-defined polymers with unpredictable molar masses, broad dispersities and is limited to simple architectures. In the context of this work, the lack of functional chain-ends prevents step polymerisation being used for further block copolymer synthesis. Conversely, a living/controlled polymerisation affords well-defined polymers with predictable and tuneable molar masses, compositions, architectures, end-group functionalities and narrow molar mass distributions.[108-118] Narrow molar mass distributions are useful in biomedical applications, as individual molar mass fractions of a polydispersed system are expected to exhibit distinct pharmacological activities.[8] Moreover, block copolymers are

explicitly targeted to broaden the range of materials properties and enable self-assembly to particular nanostructures.

1.3.2 Living/controlled polymerisation

According to the IUPAC definition, a living polymerisation is a chain polymerisation from which chain transfer and chain termination reactions are absent. In practice, living polymerisation shows a rate of chain initiation that is fast compared with the rate of chain propagation, so that the number of growing chains remains constant throughout the polymerisation.[119] As a result, the resulting polymers show a high fidelity of end groups, predictable molar mass and narrow dispersity.[119] There are seven criteria, by which a living polymerisation is assessed practically:[120]

1) The polymerisation proceeds until all the monomers have been consumed.

2) The number-average molar mass, M_n, of the polymer has a linear relationship with the monomer conversion.

3) By varying the ratio of initiator/monomer, the molar masses of the polymers can be controlled.

4) The number of polymer chains is constant and independent of the conversion throughout the reaction.

5) The resulting polymer has a narrow dispersity.

6) Block copolymers can be produced by sequential addition of other monomers.

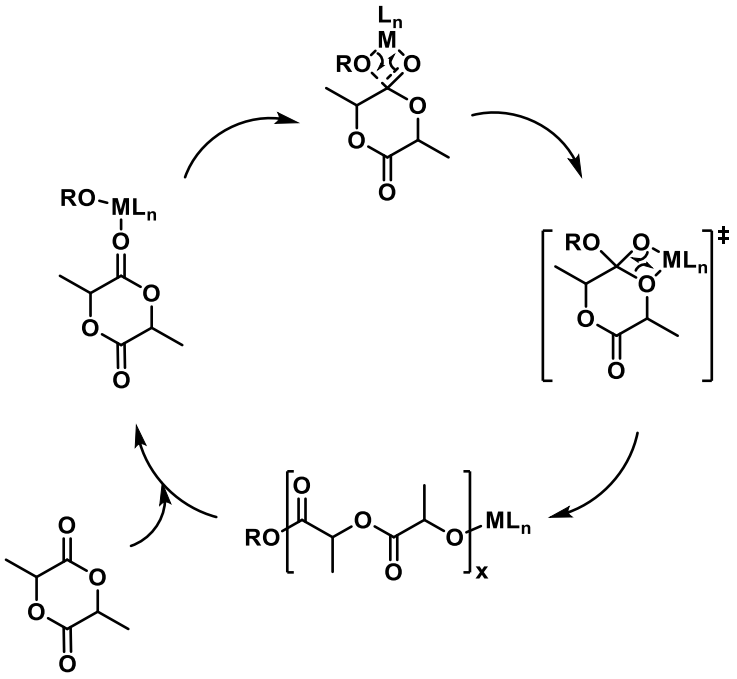
7) Polymers with chain-end functionalities can be produced in quantitative yield.

Here, the term controlled polymerisation is applied, and it refers to a reaction in which chain termination and chain transfer reactions are significantly slower than propagation; thus by control of reaction time, features of living polymerisation are observed.[121]

1.3.3 Ring-opening polymerisation (ROP)

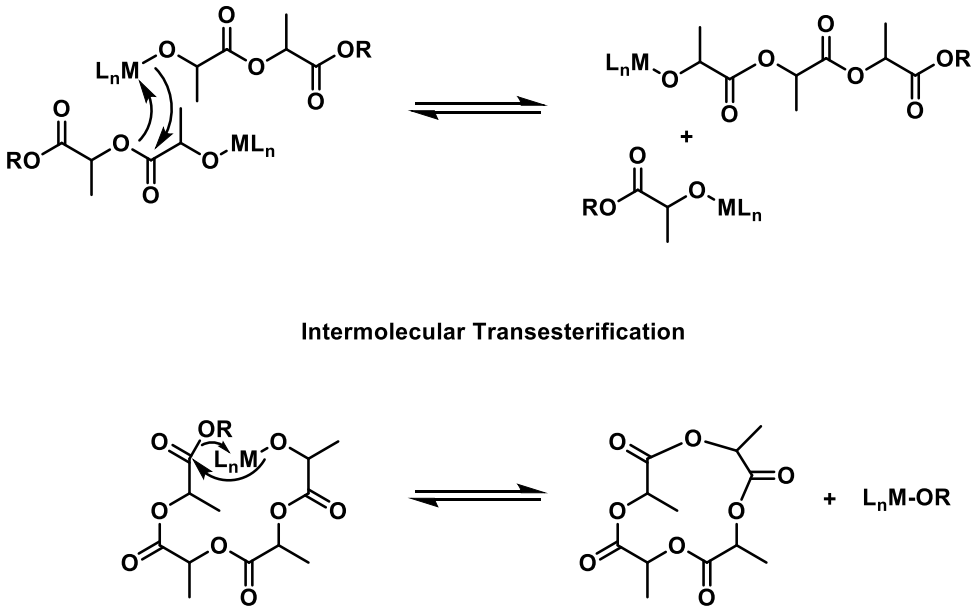
The ring-opening polymerisation (ROP), a type of controlled polymerisation, is often employed to polymerise cyclic lactones, carbonates and phospholanes to afford aliphatic polyesters, polycarbonates and polyphosphoesters. This method allows excellent control over molar mass, with high molar masses achievable while maintaining low to moderate dispersities (< 1.4).[79, 84, 86, 93]

Ring-opening polymerisation only occurs spontaneously if the Gibbs free energy of polymerisation is negative or zero. In general, polymerisation reactions result in a decrease in entropy as the total number of molecules in the system decreases. Consequently, the thermodynamic driving force for the ROP is usually a negative enthalpy of polymerisation which enables the entropy, unfavourable in most polymerisations, to be overcome. A negative enthalpy of polymerisation is usually caused by ring strain. The generally accepted mechanism for ROP involves initiation by either an anionic, cationic, coordination-insertion or an activated monomer mechanism.[79] The coordination-insertion mechanism is commonly used as it enables access to high molar mass polymers (M_n > 10 kgmol^{-1}, Scheme 1.1).[122-124]



Scheme 1.1 Coordination-insertion mechanism for ROP of cyclic monomers, using LA as an example.

The mechanism operates *via* the coordination of the monomer to a Lewis acidic metal alkoxide complex, which activates and attacks the monomer at the carbonyl carbon. Acyl bond cleavage results in ring opening and the generation of a new metal alkoxide species, thus propagating the reaction. However, side reactions, *i.e.* inter- and intramolecular transesterification reactions can also occur (Scheme 1.2). The former occurs when the catalyst coordinates to a carbonyl in the growing polymer chain instead of the carbonyl of the monomer, resulting in chain scrambling. Intramolecular transesterifications proceed similarly, but the catalyst is coordinating to the carbonyl within the same polymer chain, leading to the formation of cyclic by-products.

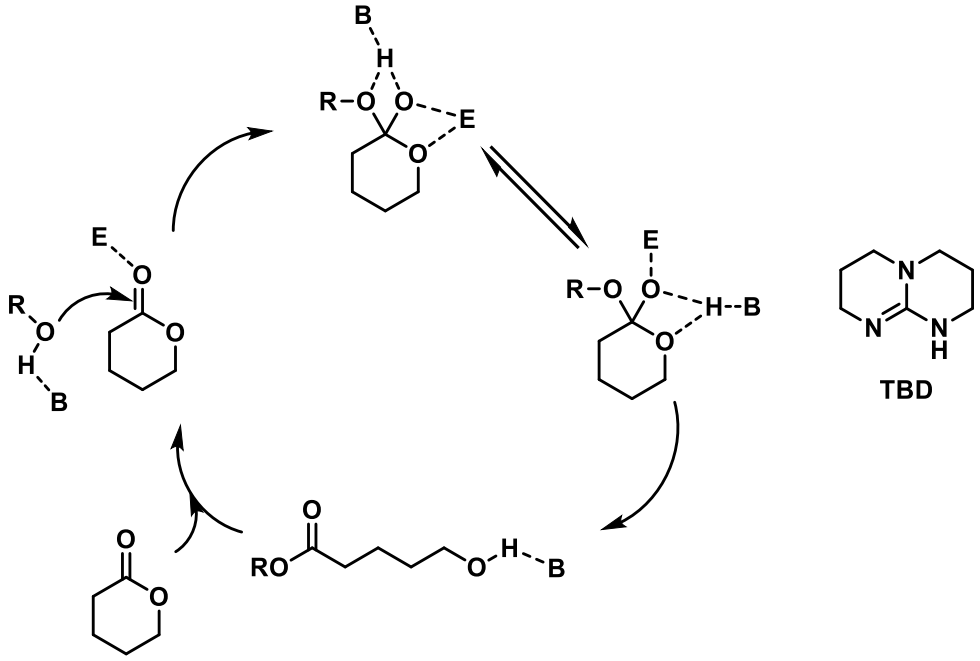


Scheme 1.2 Transesterification reactions in the ROP of cyclic monomers, using LA as an example.

There are many possible metal complex initiators for ROP; detailed reviews provide a comprehensive description of them.[125-127] An examination of the many different metal initiators is beyond the scope of this thesis. A very commonly used initiator for the ROP is tin(II) alkoxide, generated *in situ* by the reaction of tin(II) 2-ethyl hexanoate ($Sn(Oct)_2$) and an intentionally added alcohol.[122, 128, 129] This initiating system has been used in this thesis because it is commercially available and FDA approved for use in medical and food applications.[130]

Organocatalysts have also been widely applied to the ROP of cyclic monomers.[131-135] For example, a guanidine catalyst, 1,5,7,-triazabicyclo[4.4.0]dec-5-ene (TBD), is particularly effective.[131, 136] The polymerisation proceeds *via* an activated monomer mechanism (Scheme 1.3). TBD has also been used in this thesis because it is among the most active organocatalyst in the literature.[136] For example, the ROP of lactide with

0.1% TBD in THF exhibits a turnover frequency (TOF) of 80 s^{-1} at 25 ºC, which is much more active than $Sn(Oct)_2$ (15.3×10^{-5} s^{-1}, 0.1 wt% bulk, 110 ºC). The cytotoxicity of TBD was also assessed using on the fetal human epithelial cell line (FHs74Int) and differentiated human hepatocellular carcinoma cells (HepaRG), where a 100% cell viability at concentrations of over 110 μM (much higher than the residual levels in the polymer) was observed.[137]



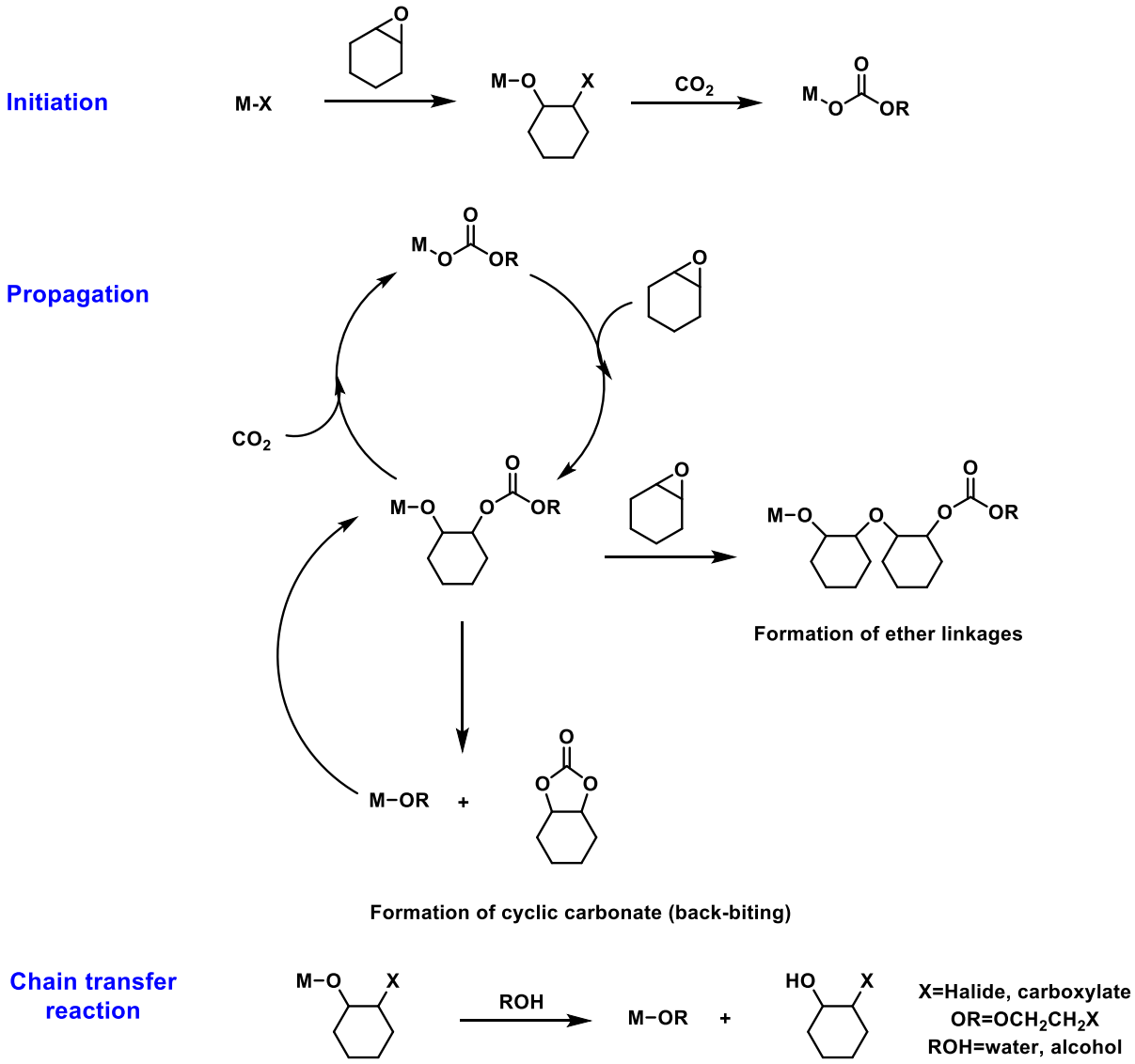
Scheme 1.3 Illustration of structures of TBD and its ROP mechanism, where E is electrophilic species and B is the Brønsted base, using δ-valerolactone as an example monomer.

1.3.4 Ring-opening copolymerisation (ROCOP)

While the ROP is a well-developed polymerisation route, the range of polymer products is limited by the range of cyclic monomers and by their ring strain.[138] Notably, the synthesis of functionalised cyclic esters is very challenging, and substituted 6-membered rings suffer from reduced ring strain and hence reduced polymerisability (*i.e.* the thermodynamic driving force to polymerisation is limited).[79, 138] The ring-opening

copolymerisation (ROCOP) of epoxides and anhydrides/carbon dioxide can overcome these thermodynamic limitations and it represents an alternative controlled polymerisation route in yielding aliphatic polyesters and polycarbonates.[138, 139] One appealing aspect of epoxide/anhydride copolymerisation is the greater diversity of the resulting polymer structures, facilitated by the use of two types of monomers. To date, more than 400 possible polymer structures have been reported by simply changing the epoxide and anhydride pairings.[139] Naturally such a large number of structures leads to a diverse set of material properties, including thermal/mechanical properties and amphiphilicity.[140-143] It is important to emphasise that as both epoxide and anhydride have a high ring strain, so the thermodynamic parameters strongly favour polymerisation, even using substituted monomers.[144, 145]

ROCOP is catalysed by a range of metal complexes with those of Zn(II), Co(III) and Cr(III) being most common.[146-153] While catalyst development is out of the scope of this thesis, the recent intense focus and development of ROCOP catalysts has led to a myriad of comprehensive reviews of catalysts for both CO_2/epoxide ROCOP[108, 147, 151-160] and anhydride/epoxide ROCOP.[103, 139] ROCOP catalysts are usually Lewis acidic metal complexes of the form LMX, where L is the ligand, M is the metal, and X is the initiating group.



Scheme 1.4 Scheme showing the mechanism of ROCOP, with the initiation, propagation, side reactions and chain transfer reaction.

For the ROCOP of CO_2/epoxides, the polymerisation is initiated by the insertion of an epoxide into the MX bond to generate the metal alkoxide intermediates. Carbon dioxide can then insert into the metal alkoxide bond. The initiating group is commonly a carboxylate, alkoxide or halide group. During the polymerisation, this group becomes the chain end group (Scheme 1.4, top). Propagation through the cycle involves the sequential ring-opening of epoxides and insertion of CO_2, leading to the subsequent formation of metal alkoxide and carboxylate intermediates (Scheme 1.4, middle). The

polymerisation is usually terminated by the depletion of monomers or addition of a quenching reagent.

Some catalysts show near perfect alternation and form polymers with 100% carbonate linkages. However, side reactions can occur, with a common one being the reaction of metal alkoxide and epoxide to form ether linkages. The presence of aliphatic ether linkages not only reduces glass transition temperature and viscosity which can be beneficial but also decreases degradability, which may be a disbenefit.[161] The growing polymer chain can also undergo backbiting or depolymerisation reactions to form five-membered cyclic carbonates. These cyclic carbonates are the thermodynamic products of the reaction between CO_2 and epoxides, so they are typically formed under forcing conditions (*e.g.* higher temperatures). The extent of their formation depends on the catalyst and the epoxide being used; reactions with bicyclic epoxides are less likely to give cyclic carbonates.[162]

When polymerisations are carried out with an excess of protic compounds (chain transfer agent, CTA), chain transfer reactions can occur.[108, 163, 164] The protic compounds react with the growing polymer chain, resulting in new metal alkoxide species and hydroxyl terminated polymer chains. The chain transfer reactions are typically proposed to occur more rapidly than propagation, as evidenced by high control and narrow dispersity throughout reactions. Therefore, the addition of CTA can be used to control the polymer molar mass without affecting the catalytic activity. The CTA ends up as a chain end group or chain extender, and the use of polymeric CTAs (or macroinitiators) results in the formation of block copolymers. If the macroinitiator is monofunctional, then AB type block copolymers form, whereas a bifunctional initiator would lead to ABA type block copolymers.

1.4 Block copolymer formation

The preparation of block polymers is an obvious way to alter the material properties, *i.e.* hydrophilicity, thermal and mechanical properties.[165-167] The use of macroinitiators in ROCOP enables straightforward access to various block polymers, including those featuring hydrophilic polymers such as PEG.[163, 168] In 2010, an extensive study of CO_2/propylene oxide (PO) ROCOP was carried out, using cobalt salen catalysts, in the presence of various macromolecular chain transfer agents, such as polyether (*i.e.* polyethylene glycol, PEG), polyester (*i.e.* polycaprolactone, PCL) and polycarbonate (*i.e.* polyhexamethylene carbonate).[163] The different polyols had a wide variety of effects on the properties when compared to the poly(propylene carbonate) (PPC) produced from PO/CO_2 ROCOP. For example, the block copolymer PPC-PEG-PPC was significantly less brittle than PPC, as determined by tensile tests, showing an increase in the strain from less than 0.02 to 7.7.[163]

A series of amphiphilic block polymers comprising a hydrophilic PEG and hydrophobic PPC were prepared using CO_2/PO ROCOP, with PEG as macroinitiators (Figure 1.6).[168] Subsequently, self-assembly was inferred from the critical micelle concentration (CMC) measurements, and NMR spectroscopy was used to confirm the formation of micelles, with the PPC signals disappearing when using D_2O as the solvent.

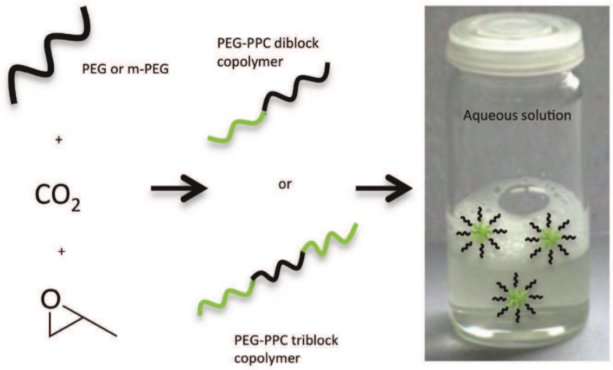
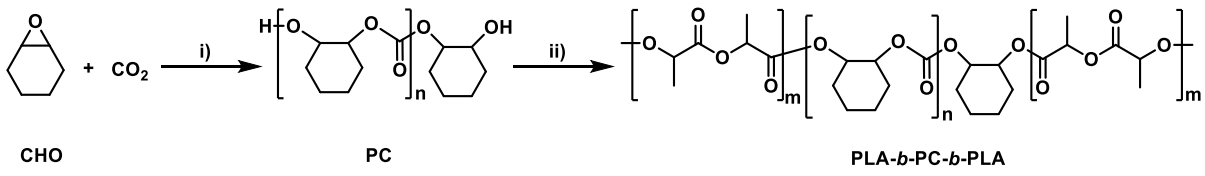


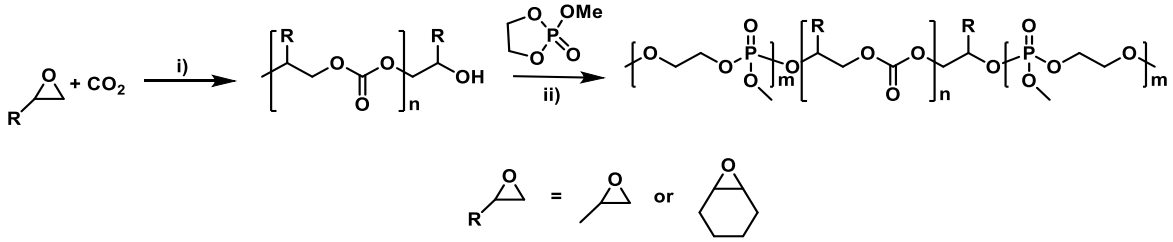
Figure 1.6 Synthesis of amphiphilic block copolymers from PEG and PPC.[168] Reproduced with permission.

Alternatively, polycarbonate macroinitiators have been applied in the ROP of lactones and cyclic phospholanes.[169-172] The synthesis of poly(ester-*b*-carbonate-*b*-ester) was achieved by ROCOP of cyclohexene oxide (CHO) and CO_2, followed by the subsequent ROP of lactide (LA) using the isolated dihydroxyl end-capped poly(cyclohexene carbonate) (PC) as the macroinitiator (Scheme 1.5).[172] The reaction was successful using PC blocks of various molar masses (2.0-10.0 $kgmol^{-1}$) and a range of lactide loadings (100-400 equivalents). In all cases, a T_g was observed at 60 ºC, corresponding to the polylactide (PLA) blocks. In the ABA block copolymers with longer PC, a second T_g was observed at 80-95 ºC, indicating phase separation.



Scheme 1.5 Synthesis of PLA-*b*-PC-*b*-PLA.[172] i) $[LZn_2(CF_3COO)_2]$ (0.1 mol%), 80 ºC, 1 bar CO_2, 24 h. ii) [PC]/[Yttrium catalyst]/[LA]=1/2/100-400, THF, 25 ºC, 5 min.

A similar approach was carried out in the production of poly(phosphoester-*b*-carbonate-*b*-phosphoester)s (Scheme 1.6).[170, 171] The block poly(phosphoester-*b*-carbonate-*b*-phosphoester) (M_n = 13.0-31.0 kgmol^{-1}) are amphiphilic and formed self-assembled structures using a bulk swelling method.[171] The morphology of the self-assembled nanostructures was studied, where micelles (180 ± 15 nm) and rod-shaped micelles (35 ± 10 nm) were observed by SEM. As both the polycarbonate and the polyphosphoester (PPE) blocks are biodegradable, these block copolymers were proposed as potential drug delivery vehicles. However, in their study, the hydrophilic/hydrophobic block ratios of the polymers used to prepare self-assembly were all larger than 0.5, which is expected to deliver only micelle structures. Moreover, the polymers' biocompatibility and biodegradability were not reported.



Scheme 1.6 Scheme showing tandem synthesis of poly(phosphoester-*b*-carbonate-*b*-phosphoester).[171] Reaction conditions: i)[SalenCoTFA]/PPNTFA/H_2O/epoxide = 1/1/15-20/1000, 3 Bar CO_2, 0.5-3.5 h. ii) 1,8-diazobicyclo[5.4.0]-undec-7-ene (DBU)/2- methoxy-2-oxo-1,3,2-dioxaphospholene = 1/10-50, 0 ºC.

1.5 Post-polymerisation modifications

Polymer functionalisation can serve as another means to change the physical/chemical properties of materials, *e.g.* to enhance hydrophilicity and biodegradability.[173, 174] This strategy can also be used to covalently attach biologically active molecules, such as drug molecules, peptides or proteins.[173, 174] Functional polymers are usually prepared *via* two approaches: 1) the polymerisation of monomers containing particular functional

groups or 2) the post-polymerisation modification at a repeating functional group on the polymer backbone or side-chains.[175]

Traditionally, substituted polyesters and polycarbonates were prepared by ROP of functionalised monomers.[86] However, the range of functional groups is limited, particularly because alcohols, amines and carboxylic acids are chain transfer agents, thus affecting the polymerisation.[4] Moreover, the addition of substituents on the cyclic monomers may decrease the ring-strain and affect their ability to be polymerised.[79] In contrast, post-polymerisation modification of relevant side chain substituents alleviates these challenges and allows incorporation of the above groups.[176-179] For instance, benzyl ether/ester functional polymers may be deprotected by hydrogenolysis to yield hydroxyl and carboxyl functional groups (which may then be further functionalised through esterification with proteins/peptides),[180-182] halide functional polymers may be reacted with amines to yield quaternary ammonium groups that can be potentially used for targeting antimicrobial properties,[8, 183] alkene and alkyne groups can be functionalised into a wide range of functionalities (*e.g.* hydroxyl, carboxyl and amine groups) through reactions such as Michael addition,[184, 185] thiol-ene reactions[177, 186, 187] and azide-alkyne cycloadditions.[177, 188, 189] Additionally, incorporation of multiple different substituents or sequential modification with different groups could be used to access new polymers and to improve bioactivity, *e.g.* to allow for cell or tissue targeting.[107, 177, 190, 191]

The work presented in this thesis is focused on the functionalisation of alternating polycarbonates and polyesters (prepared by ROCOP). In particular, the reaction of alkene groups to incorporate cationic groups or hydroxyl groups so as to deliver antimicrobial properties or prepare amphiphilic materials for controlled release is targeted.

1.5.1 Functional polycarbonates

Cationic polycarbonates are easily produced by a quaternisation reaction between tertiary amine and alkyl halide.[85] Quaternary ammonium-functional PTMC derivatives have been extensively studied as degradable antimicrobial polymers.[8, 183, 191-193] The first reported antimicrobial polycarbonates were triblock polycarbonates synthesised from ROP of a halide-functional cyclic carbonate and TMC, followed by the quaternisation with trimethylamine (M_n = 6.2-9.2 kgmol^{-1}, Đ = 1.2-1.3).[8] These polymers formed micelles after bulk swelling in de-ionised (DI) water. These micelles showed average diameters of 43-198 nm and zeta potentials of 47-65 mV, depending on the TMC block length. They also showed high antimicrobial activities against Gram-positive bacteria, *Bacillus subtilis*, *Enterococcus faecalis*, *Staphylococcus aureus* and methicillin-resistant *S. aureus (MRSA*), and the fungus *Cryptococcus neoformans* (~ 100% of microbes were killed at the concentration ranges corresponding to the polymers' MICs). It was also observed that polycarbonates did not affect the electrolyte balance in the blood 48 h post-injection.

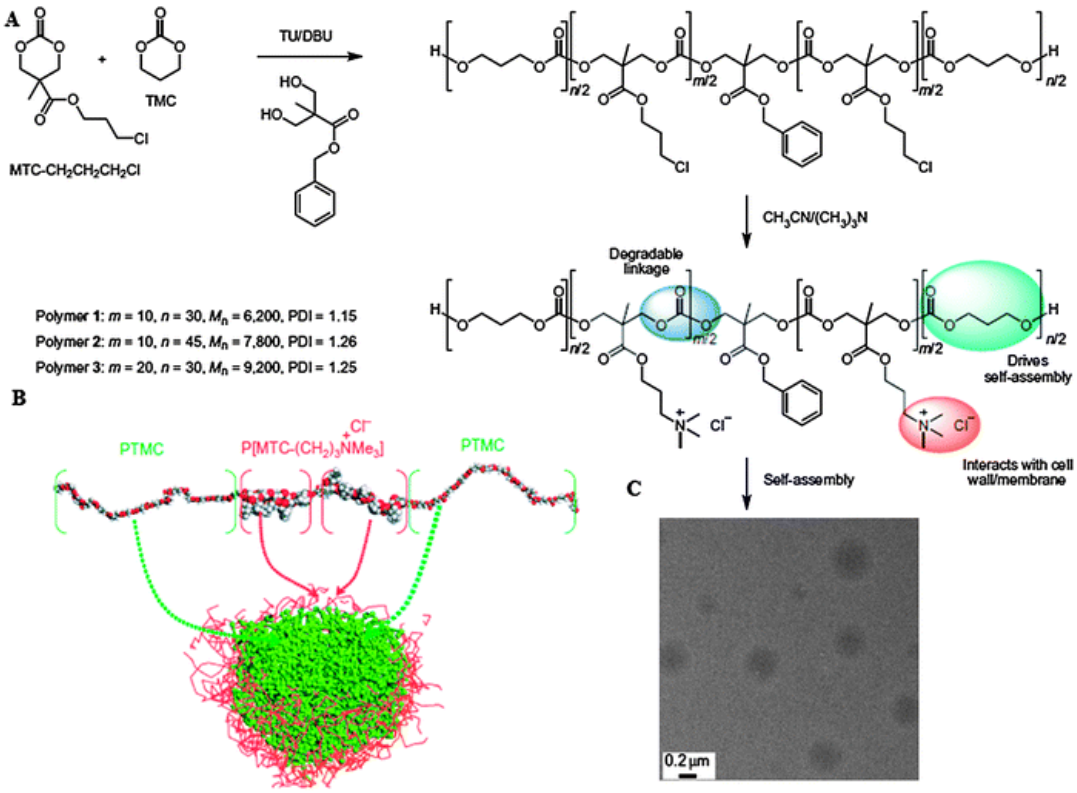


Figure 1.7 Synthesis and micelle formation of cationic amphiphilic polycarbonates, (A) cationic amphiphilic polycarbonates (B) and (C) the formation of micelles as simulated by molecular modelling.[8] Reproduced with permission.

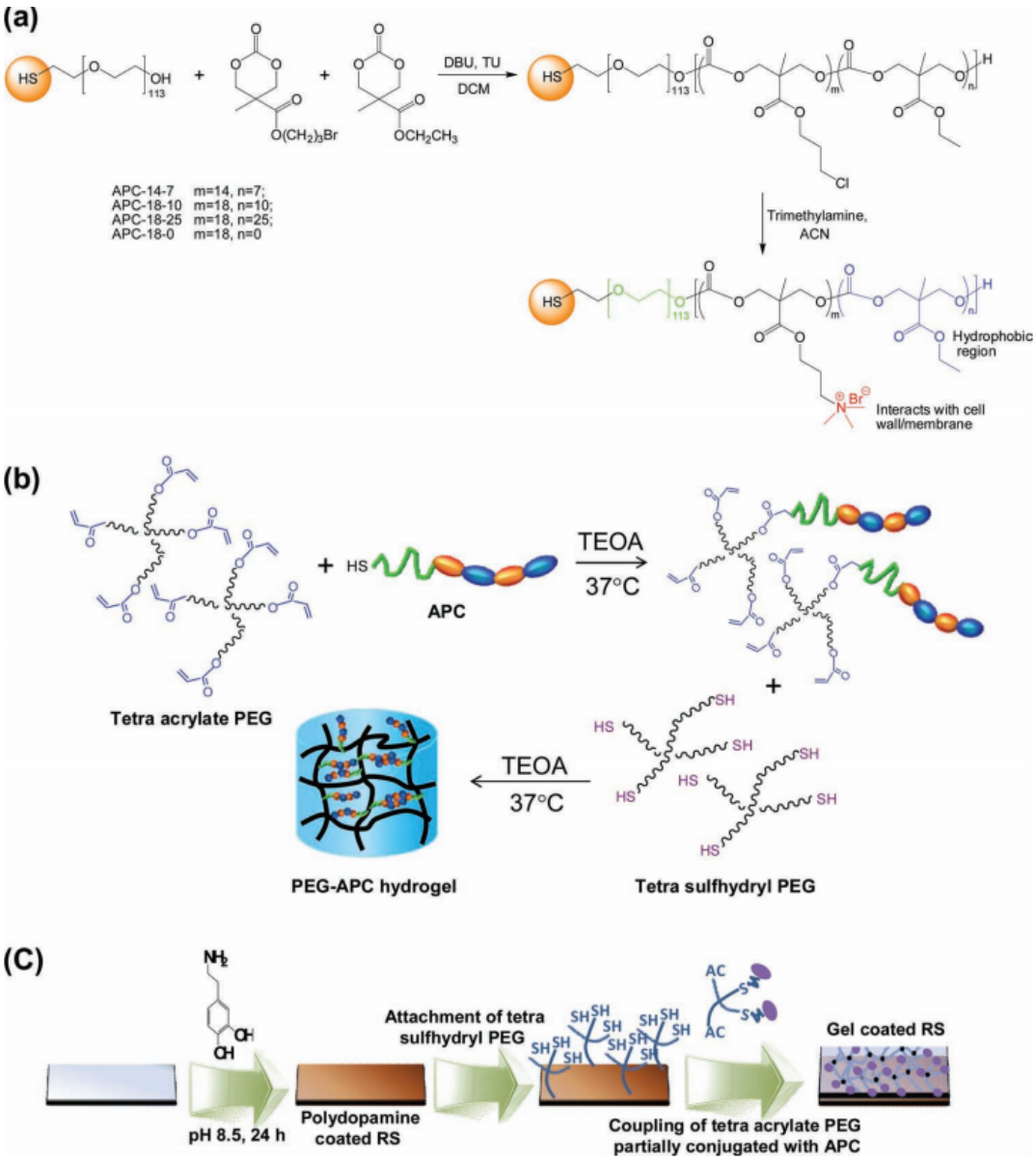


Figure 1.8 Synthetic schemes of a) polycarbonates, b) PEG-APC hydrogel and c) hydrogel coating onto silicone rubber surface.[194] Reproduced with permission.

Effective antimicrobial hydrogels based on cationic polycarbonates have also been reported.[194, 195] The most practical example is a star-shaped polymer (M_n = 10.0 kgmol^{-1}) yielded from the thiol-ene reaction between a tetra-acrylate functional PEG and quaternary ammonium-containing polycarbonate.[194] This polymer underwent gelation within 2 min and the hydrogels (5 × 5 mm^2) possessed strong antimicrobial activity with > 99.9% killing efficiency (~ 10^6 CFU·mL^{-1}) against Gram-positive bacteria *S. aureus*, Gram-negative

bacteria *E. coli* and Fungi *C. albicans*. The hydrogel was also coated onto silicone rubber, a commonly used catheter material, and showed > 99.9% killing efficiency against *S. aureus*. Moreover, no microbes were detected on the surface, by confocal microscopy, indicating antifouling activity, which is likely resulted from the PEG block since it is a well-known antifouling polymer.[196]

Research into cationic alternating polycarbonates is very limited.[197] The first and only example was performed on the ROCOP of CO_2 and limonene oxide (LO), an epoxide derived from D-limonene.[197] In a proof-of-concept work, the vinyl groups of poly(limonene carbonate) (PLimC) (M_n = 54.3 kgmol^{-1}, Đ = 1.13) were transformed to quaternary ammonium functionalities. Polymer films prepared from quaternary ammonium functional PLimC, with 23% amine incorporation and 87% quaternisation degree, showed a killing efficiency of 99.3% (~ 10^5 CFU·mL^{-1}).

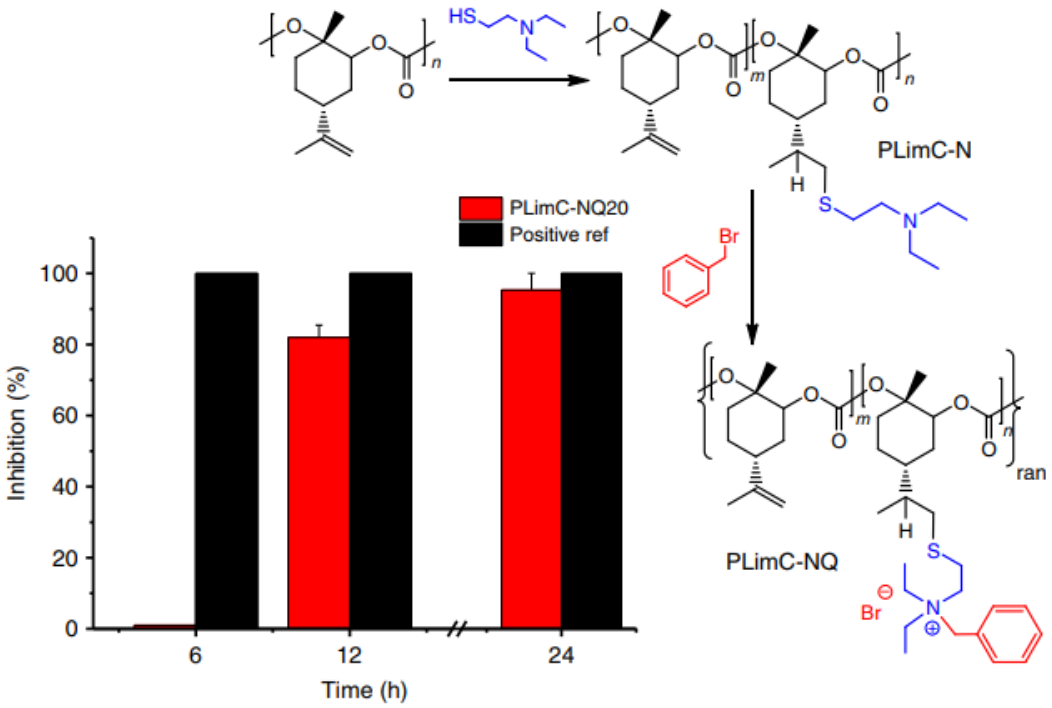


Figure 1.9 The transformation of PLimC into antibacterial PLimC.[197] Reproduced with permission.

Hydroxyl-containing polycarbonates are usually prepared by the homopolymerisation of benzyl-ether or acetal protected cyclic carbonates, followed by deprotection using hydrogenation or hydrolysis under mildly acidic conditions.[84, 86, 198, 199] By copolymerising with other cyclic monomers (*e.g.* LA, ε-CL and TMC), hydroxyl-bearing copolymers can also be obtained.[199, 200] These hydroxyl groups were used for the covalent immobilisation of bioactive molecules such as drugs, peptide and proteins.[198] For example, the tumor-targeting ligand folic acid (FA), lactose and Rhodamine B were conjugated to hydroxyl groups on the polycarbonate block of amphiphilic PEG-*b*-poly(L-lactide-co-2,2-dihydroxymethyl propylene carbonate).[200, 201] These amphiphilic polymers formed micelles *via* a 'solvent-switch' method, with diameters in the range of 60-100 nm. The cellular uptake studies showed an enhanced internalisation of the FA-containing micelles by human ovarian cancer cell lines (SKOV-3) as compared to control materials without FA.[71] In the case of lactose-containing micelles, the *ex vivo* imaging studies showed enriched accumulation in mouse liver as compared to the lactose-free micelles, due to the specific interaction of the lactose moieties with appropriate lactose-receptors.[72]

One common reaction used to install hydroxyl, carboxyl and amine groups is the radical reaction between thiols and alkenes, known as the thiol-ene reaction. Reactions proceed either *via* the free-radical addition of thiols to the alkene groups or *via* the Michael addition of thiols to electron deficient alkene groups.[202] The copolymersation of L-LA and an alkene-containing cyclic carbonate (5-methyl-5-allyloxycarbonyl-1,3-dioxan-2-one, MAC) and the subsequent thiol-ene reaction generated a folic-acid grafted block copolymer.[203, 204] Its cytotoxicity and cell affinity was assessed using Vero cells. Following incubation for 48 h, the folic acid-grafted polymers showed greater cell adhesion and proliferation than either PLA or P(LA-co-MAC), indicating the potential

to limit foreign body reactions typically associated with polymeric soft tissue implants.[203, 204]

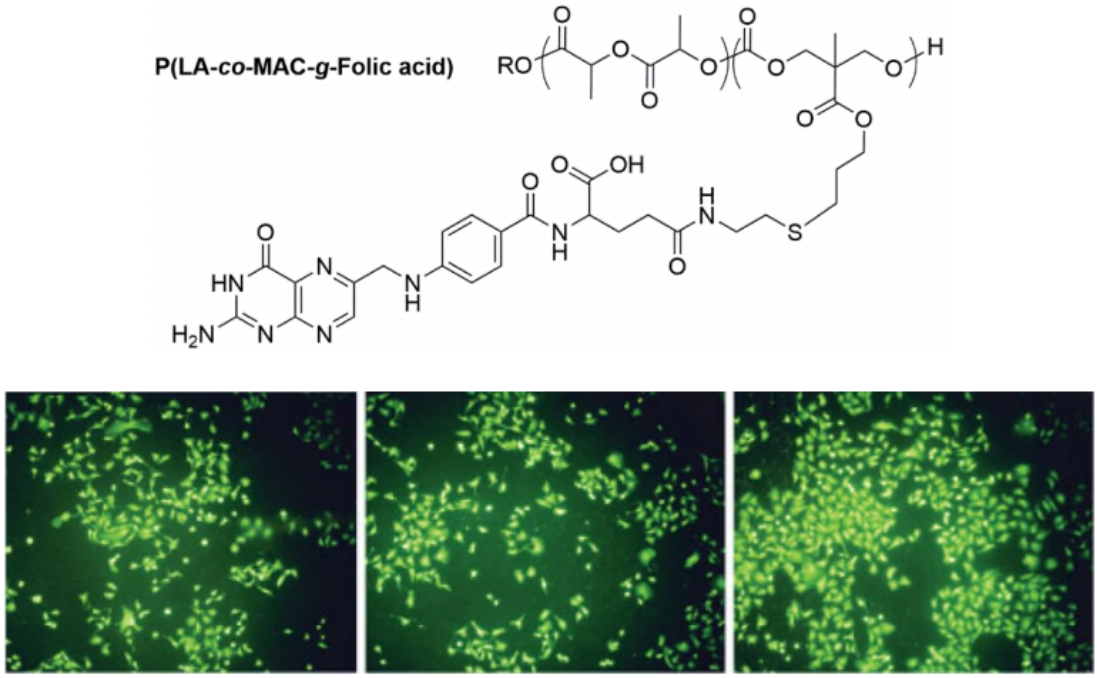
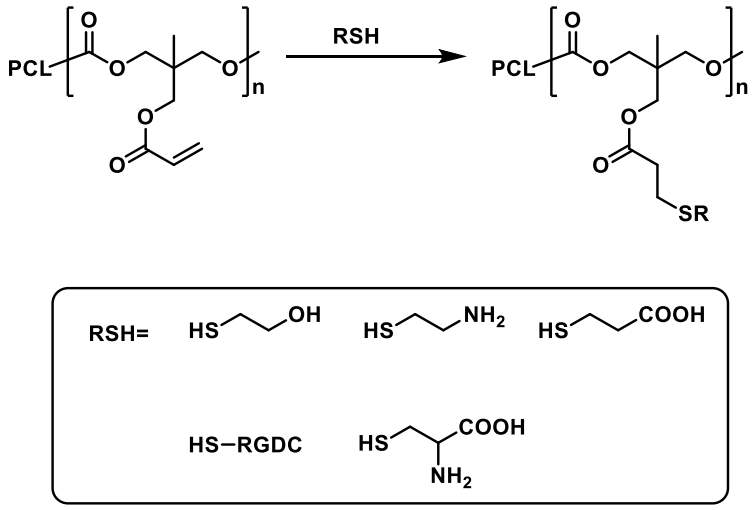


Figure 1.10 Top: Structure of P(LA-*co*-MAC-g-Folic acid). Bottom: Microscope images of thin polymer films showing the effect of folic acid conjugation on adhesion and proliferation of Vero cells. Left to right: PLA, P(LA-*co*-MAC), P(LA-*co*-MAC-g-Folic acid).[203, 204] Reproduced with permission.

A Michael addition reaction was also used to functionalise acryloyl-substituted polycarbonates.[4, 205-209] For example, the copolymerisation of acryloyl carbonate (AC) and CL, and a subsequent Michael addition with hydroxyl-, amine-, carboxyl- and peptide-containing thiols, yielded a range of new functional polymers (M_n ~ 10.0 kgmol^{-1}, Đ ~ 1.4, Scheme 1.7).[205] The hydroxyl-, amine- and peptide-functional polymers all displayed smaller water contact angles (~ 60º) than the parent polymer (~ 70º), indicating increased hydrophilicity. Cell culture studies were performed on thin films of peptide-functional copolymers using L929 fibroblasts. Unlike films of P(CL-*co*-AC), flattened cell morphology was observed for films of peptide functional

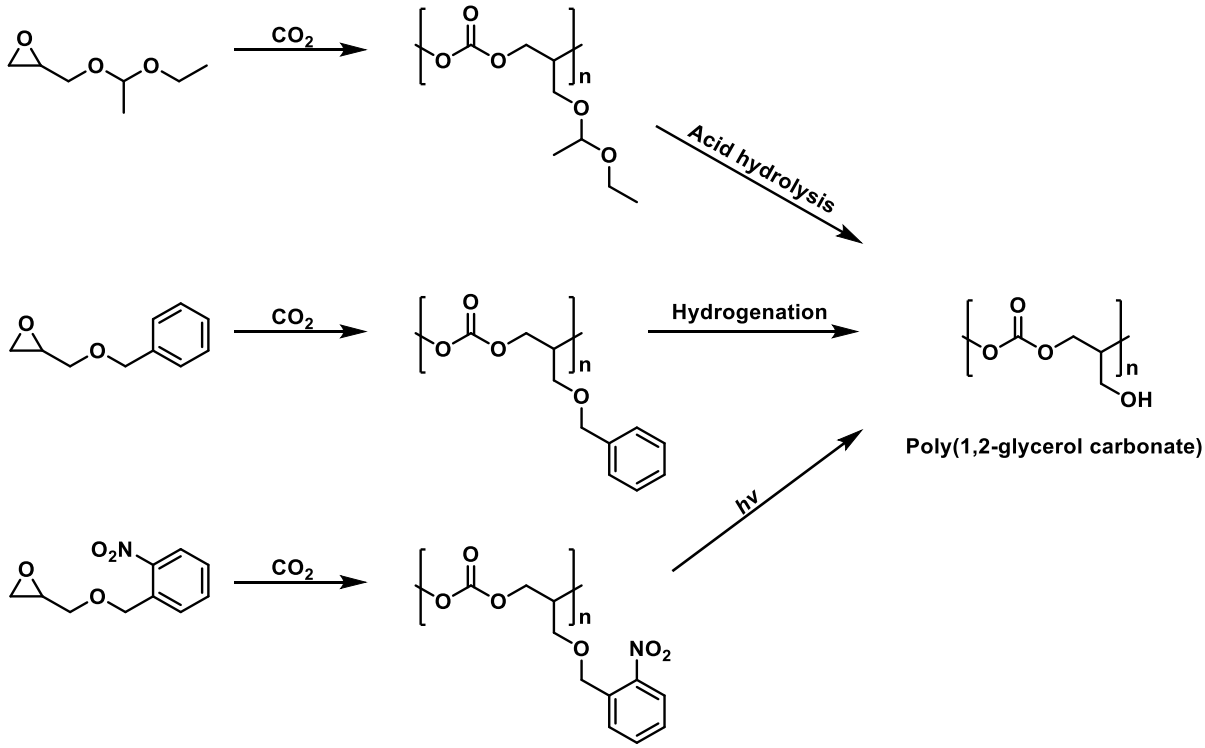
copolymers, indicating an improvement in cell adhesion. Cell counting results showed that *ca.* 63% (relative to tissue culture plate) cells were alive after incubating with the peptide-functional films for 3 days.



Scheme 1.7 Functionalisation of P(CL-*co*-AC) *via* Michael addition.[205]

Glycidyl ethers are also useful in generating alternating functional polycarbonates. Many of these epoxides are commercially available or are conveniently synthesised from epichlorohydrin and the corresponding alcohol. A range of different glycidyl ethers has been copolymerized with CO_2 to give various poly(1,2-glycerol carbonates).[168, 210-225] These polymers were functionalised to produce hydroxyl-functional polycarbonates, for example by the hydrogenation of benzyl ether groups or through acid hydrolysis.[214, 217] Another deprotection strategy applied UV light to a nitrobenzyl ether to yield poly(1,2-glycerol carbonates) without any backbone degradation.[226] Poly(1,2-glycerol carbonate), which is substituted with primary hydroxyl groups, shows a faster degradation ($t_{1/2} \approx 3$ days) compared to poly(1,3-glycerol carbonate), which contains only secondary hydroxyl groups and where no degradation occurs over 4 days.[214] As the hydroxyl groups can be used to further

conjugate with drug molecules such as paclitaxel, these polymers are recommended for the preparation of drug delivery system for cancer treatment.[227]



Scheme 1.8 Synthetic strategies for the preparation of poly(1,2-glycerol carbonate).[214, 217, 226]

Several follow-up studies included the use of isopropylidene (glyceryl glycidyl ether) copolymerised with CO_2 to afford a hydrophilic polyglycerol carbonate, with two hydroxyl groups on each repeat unit after acidic deprotection.[228] Likewise, terpolymers of benzyl glycidyl ether/propylene oxide/CO_2,[229] benzyl glycidyl ether/methyl glycidyl ether/CO_2,[220] propargyl glycidyl ether/methyl glycidyl ether/CO_2,[228] were also assessed. However, these studies were limited to material syntheses and the polymer dispersities were generally very broad (> 2.0).

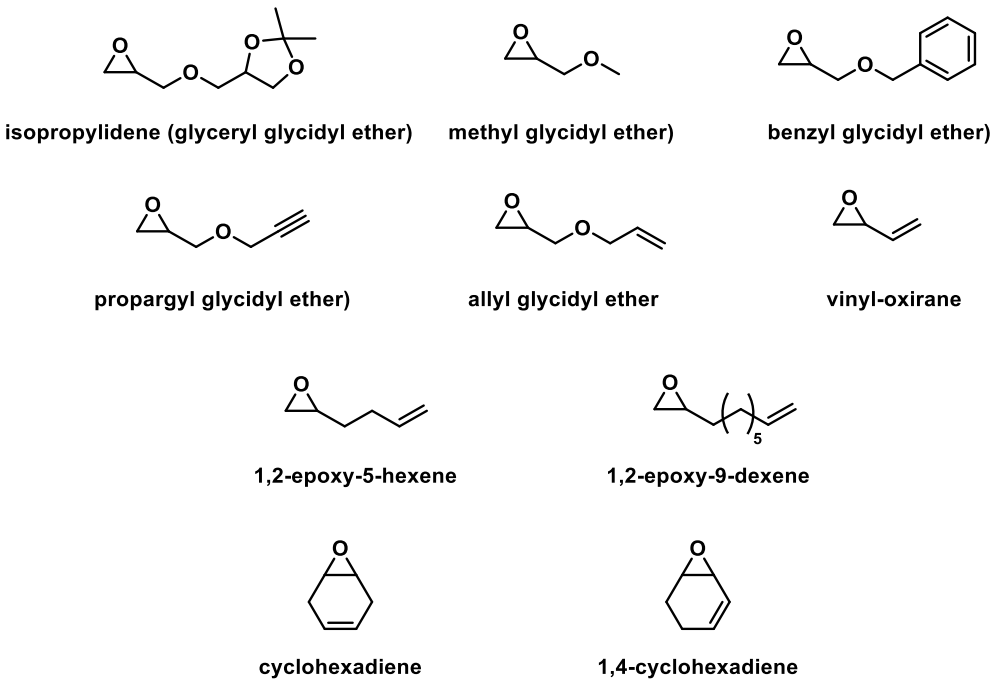
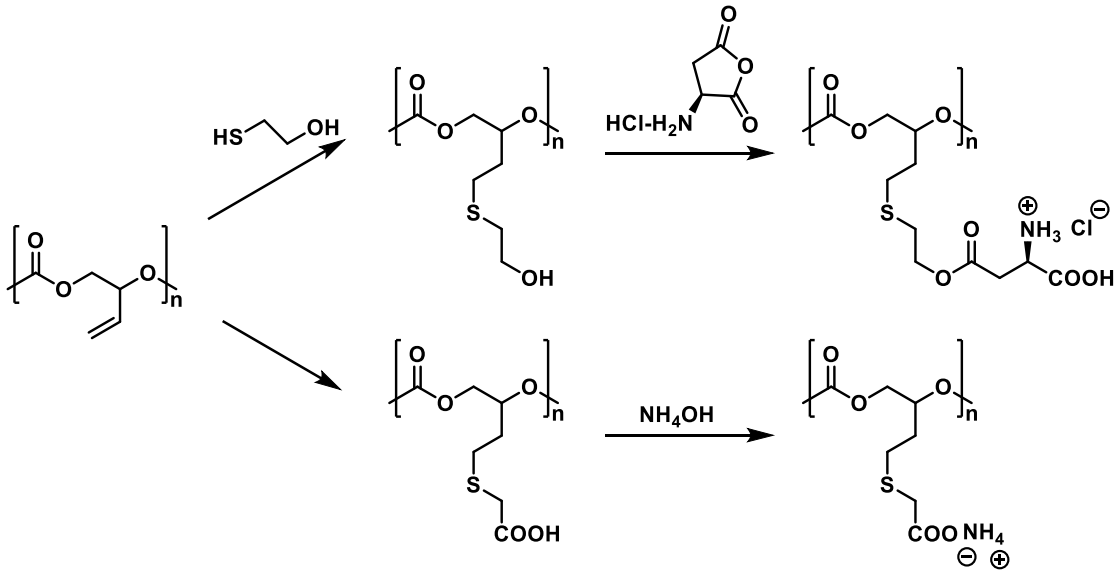


Figure 1.11 Selected functional epoxides for ROCOP with CO_2.

Some alkene-containing epoxides, such as 1,2-epoxy-5-hexene, 1,2-epoxy-9-dexene, cyclohexadiene oxide, 1,4-cyclohexadiene oxide, vinyl-cyclohexene oxide, allyl glycidyl ether have also been employed to generate functional polycarbonates.[230-236]

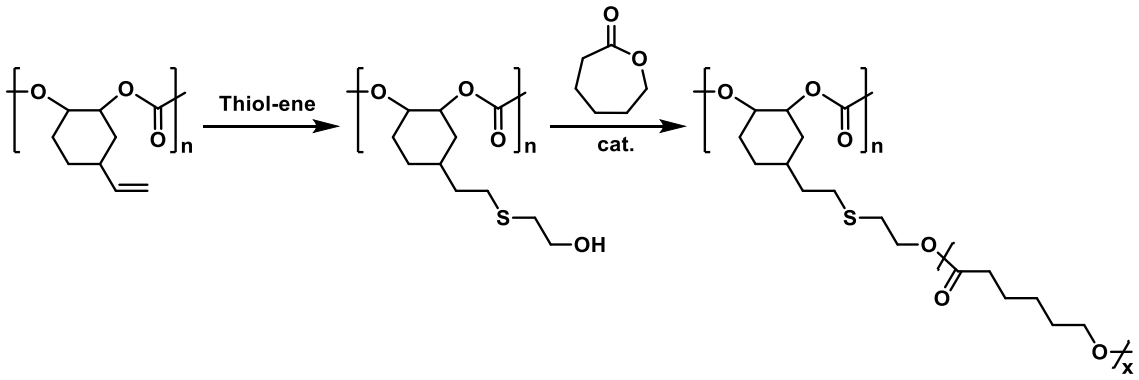
The copolymerisation of vinyl-oxirane, an epoxide possessing a vinyl group, with CO_2 generated an alkene-bearing polycarbonate (M_n = 27.7 kgmol^{-1}, Đ = 1.05, Scheme 1.9).[236] The pendant alkene groups were functionalised, using radical thiol-ene reactions, with hydroxyl and carboxyl groups, which resulted in decreases in T_g values from 18 ºC to -10 and 8 ºC, respectively. The hydroxyl and carboxyl groups were further functionalised, either *via* ring-opening of L-aspartic acid anhydride hydrochloride salt or *via* deprotonation by aqueous ammonium hydroxide, to generate amphiphilic and water-soluble materials. The amphiphilicity was confirmed by the formation of dispersed particles (D_h = 88 ± 49 nm) in water using DLS, where complete dissolution was observed for the water-soluble polymer. Due to intrinsic ionic nature of the

ammonium salt and stronger inter-chain interactions, the T_g values increased to > 45 ºC. Although these materials were significantly more hydrophilic than the unsubstituted polycarbonates, further studies are needed to access the morphology and stability of the nanoparticles in order to target their proposed application as a potential platform for bioconjugation and drug conjugation.



Scheme 1.9 Synthesis of amphiphilic and water-soluble polycarbonate.[236]

The side chain hydroxyl groups, obtained *via* thiol-ene reactions with alkene-functional polycarbonates, were also be used to afford brush polymers.[234, 235] A series of fully degradable brush polymers with ^{V}PC backbone and PCL side chains of different lengths were prepared from ROCOP of v-CHO, CO_2, thiol-ene reaction and subsequent ε-CL ROP (Scheme 1.10). The grafting density of the brush polymer was estimated to be close to 100%, as confirmed by ^{1}H NMR spectroscopy. Depending on the length of the side PCL chain, the crystallisation temperature of the graft polymer can be tuned from -15 to 30 ºC, with degrees of crystallinity ranging from 35 to 47%. The degradation rate is also expected to be impacted since it closely correlates with the degree of crystallinity.[237]



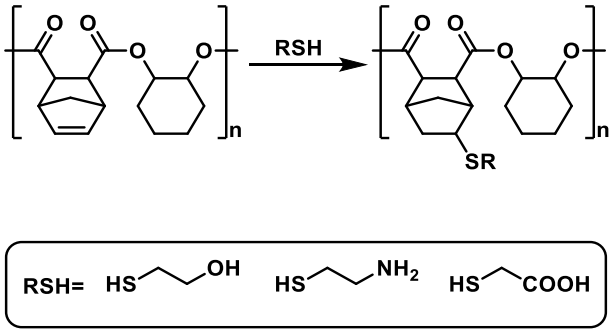
Scheme 1.10 Synthesis of graft copolymers using hydroxyl-containing polycarbonates as initiators.[234]

1.5.2 Functional polyesters

Several examples of functional aliphatic polyesters, synthesised by ROP and incorporating substituents such as benzyl-esters/ethers, acetal-protected alcohols, PEG, alkene and carboxybenzyl-protected amine groups have been reported.[192, 238-241] However, in almost all cases, the degree of polymerisation was limited by issues of low ring-strain and side reactions; moreover, the reactions were also less well controlled.[242]

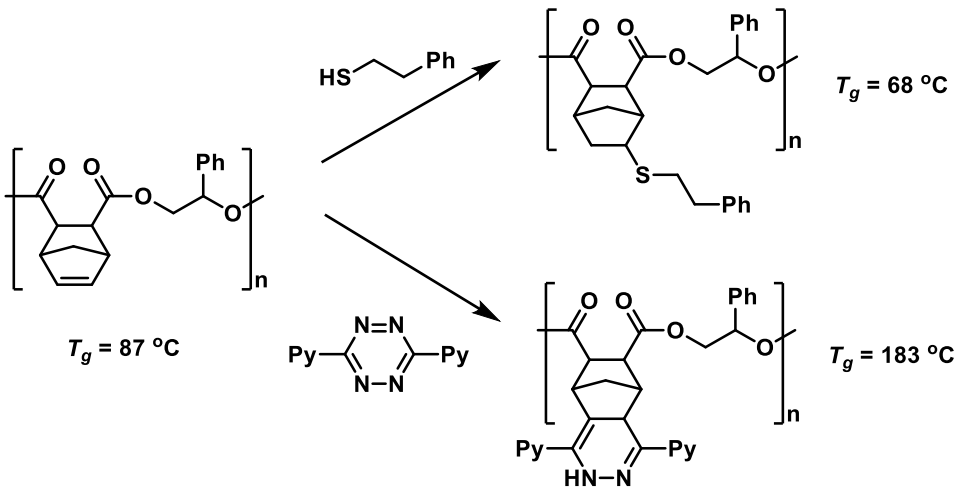
An alternative route to produce functional polyesters is through the alternating polymerisation (*i.e.* ROCOP) of epoxides/anhydrides. While the range of polymerisable lactones is quite narrow, there is a much larger number of epoxides and anhydrides. Further, the incorporation of substituents for post-polymerisation modifications is much easier to achieve and also does not negatively affect the ring strain.[103] The two common functionalisation methods are thiol-ene and inverse-electron-demand Diels-Alder reactions, applying side chain alkene or norbornenyl groups. There are quite a few reports of polymer syntheses, but only limited studies of material properties and applications.[139] Nevertheless, several studies have shown potential in altering polymer thermal properties and solubility.[243, 244]

The thiol-ene reaction was applied to an alternating polyester (M_n = 6.9 kgmol^{-1}, Đ = 1.57), from norbornene anhydride (NA) and CHO, to incorporate hydroxyl, carboxyl and amine groups (Scheme 1.11).[243] The successful functionalisation was confirmed by ^{1}H NMR and IR spectroscopy and by a slight increase in M_n using SEC. Although the thermal properties of the final materials were not assessed, functionalisation with carboxylic acid groups significantly changed the polymer's solubility, with the final polymer being soluble in methanol.[243]



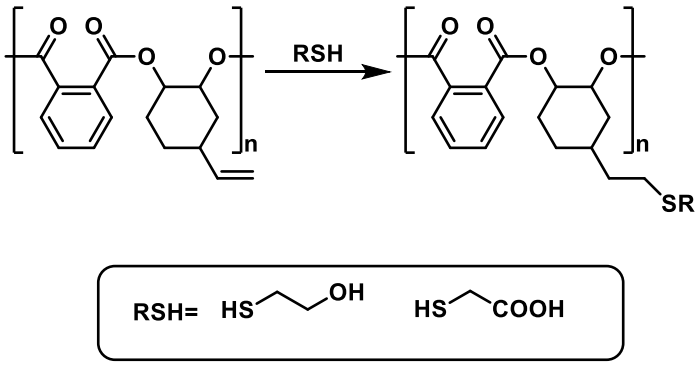
Scheme 1.11 Functionalisation of unsaturated polyester *via* thiol-ene reaction.[243]

Both thiol-ene and inverse-electron-demand Diels-Alder reactions were applied to an alternating polyester, prepared from styrene oxide (SO) and NA (M_n = 3.0 kgmol^{-1}, Đ = 1.12, Scheme 1.12).[244] These reactions reached full conversion, and matrix-assisted laser desorption/ionisation time-of-flight mass spectrometry (MALDI-ToF MS) analysis confirmed that the polymer backbone remained intact. A decrease in T_g from 87 to 68 ºC was observed after incorporation of 2-phenylethanethiol, likely due to increased side-chain flexibility. The addition of rigid, aromatic substituents, through the inverse electron demand Diels-Alder reaction, significantly raised the T_g to 183 ºC.



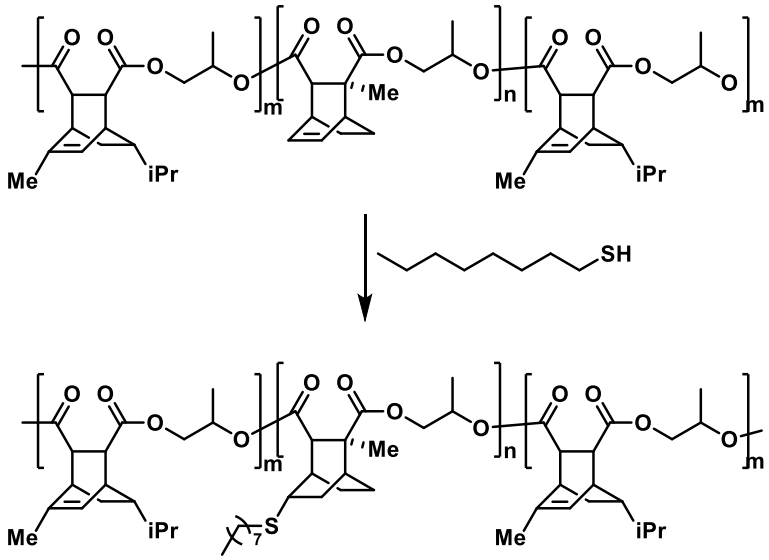
Scheme 1.12 Functionalisation of unsaturated polyester *via* the thiol-ene and inverse-electron-demand Diels-Alder reactions.[244]

Post-polymerisation modifications on the epoxide unit were also investigated using an alternating polyester (M_n = 13.2 kgmol^{-1}, Đ = 1.32) prepared from phthalic anhydride (PA) and v-CHO.[245] Thiol-ene reactions were used to introduce hydroxyl and carboxyl groups via thiol-ene reactions (Scheme 1.13), however, these reactions reached only 86% and 65% conversions, respectively.



Scheme 1.13 Functionalisation of unsaturated polyester on epoxide moiety *via* the thiol-ene reaction.[245]

It is challenging to introduce multiple groups onto a single polymer backbone and to control their positions precisely.[107, 190] Recently, the possibility to selectively and orthogonally functionalise alternating polyesters was also explored.[246] A triblock copolymer (M_n = 13.8 kgmol^{-1}, Đ = 1.04) containing both [2.2.1] and [2.2.2] norbornene structures was synthesised and thiol-ene reactions with 1-octanethiol were conducted. The post-polymerisation modification was selective as demonstrated by the complete consumption of alkene groups on the [2.2.1] structures, while the alkene groups on the [2.2.2] norbornene units remained unreacted (Scheme 1.14). No degradation of the polymers was observed, as confirmed by an increase in M_n to 15.9 kgmol^{-1} after functionalisation. Moreover, the reaction with 1-octanethiol reduced the T_g by 50 ºC.



Scheme 1.14 Selective functionalisation on unsaturated triblock polyesters *via* thiol-ene reaction.[246]

1.6 Summary

While the utilisation of carbon dioxide as a monomer to form polycarbonates is an attractive goal, a considerable amount of work is still required regarding their use and property optimisation. So far, the majority of studies focuses on PO and CHO as epoxide monomers, and so property investigations have been limited. Recently, various

functional epoxides were successfully copolymerised, but so far tailored catalysts have to be used for different epoxide monomers.

The emerging field of functional alternating polycarbonates/polyesters is still in its infancy, and further studies are needed to realise its potential. In particular, the ability to use side-chain substituents to alter chemical properties such as hydrophilicity or to conjugate bioactive molecules necessitates investigations. One attraction of the ROCOP method is the availability of a broad range of functional monomers and its strong thermodynamic feasibility. Another attraction is the access to highly alternating polymer blocks. To date, post-polymerisation modifications have mostly been only demonstrated rather than applied to target particular applications. In particular, the syntheses of materials applications suitable for biomedical uses still requires exploration.

In this thesis, the potential to use ROCOP-derived alternating polymers and their copolymers for preparing antibacterial materials and drug delivery vehicles will be explored. The possibility of carrying out selective functionalisation will also be investigated.

1.7 References

1. R. Mülhaupt, *Angew. Chem., Int. Ed.*, 2004, **43**, 1054-1063.
2. M. P. Lutolf and J. A. Hubbell, *Nat. Biotechnol.*, 2005, **23**, 47.
3. M. W. Tibbitt, C. B. Rodell, J. A. Burdick and K. S. Anseth, *Proc. Natl. Acad. Sci. U. S. A.*, 2015, **112**, 14444-14451.
4. A. W. Thomas and A. P. Dove, *Macromol. Biosci.*, 2016, **16**, 1762-1775.
5. A. Muñoz-Bonilla and M. Fernández-García, *Prog. Polym. Sci.*, 2012, **37**, 281-339.
6. A. C. Engler, N. Wiradharma, Z. Y. Ong, D. J. Coady, J. L. Hedrick and Y.-Y. Yang, *Nano Today*, 2012, **7**, 201-222.

7. E.-R. Kenawy, S. D. Worley and R. Broughton, *Biomacromolecules*, 2007, **8**, 1359-1384.
8. F. Nederberg, Y. Zhang, J. P. K. Tan, K. Xu, H. Wang, C. Yang, S. Gao, X. D. Guo, K. Fukushima, L. Li, J. L. Hedrick and Y.-Y. Yang, *Nat. Chem.*, 2011, **3**, 409.
9. L. Timofeeva and N. Kleshcheva, *Appl. Microbiol. Biotechnol.*, 2011, **89**, 475-492.
10. G. N. Tew, R. W. Scott, M. L. Klein and W. F. DeGrado, *Acc. Chem. Res.*, 2010, **43**, 30-39.
11. M. S. Ganewatta and C. Tang, *Polymer*, 2015, **63**, A1-A29.
12. O. Z. Yuin, C. D. J., T. J. P. K., L. Yan, C. J. M. W., Y. Y. Yan and H. J. L., *J. Polym. Sci., Part A: Polym. Chem.*, 2016, **54**, 1029-1035.
13. B. Gottenbos, D. W. Grijpma, H. C. van der Mei, J. Feijen and H. J. Busscher, *J. Antimicrob. Chemother.*, 2001, **48**, 7-13.
14. A. Jain, L. S. Duvvuri, S. Farah, N. Beyth, A. J. Domb and W. Khan, *Adv. Healthcare Mater.*, 2014, **3**, 1969-1985.
15. A. J. McBain, R. G. Ledder, L. E. Moore, C. E. Catrenich and P. Gilbert, *Appl. Environ. Microbiol.*, 2004, **70**, 3449-3456.
16. M. He and C. C. Chu, *J. Appl. Polym. Sci.*, 2013, **130**, 3736-3745.
17. O Rahn and W. P. V. Eseltine, *Annu. Rev. Microbiol.*, 1947, **1**, 173-192.
18. W. Ren, W. Cheng, G. Wang and Y. Liu, *J. Polym. Sci., Part A: Polym. Chem.*, 2017, **55**, 632-639.
19. M. R. E. Santos, A. C. Fonseca, P. V. Mendonça, R. Branco, A. C. Serra, P. V. Morais and J. F. J. Coelho, *Materials*, 2016, **9**, 599.
20. L. B. Reller, M. Weinstein, J. H. Jorgensen and M. J. Ferraro, *Clin. Infect. Dis.*, 2009, **49**, 1749-1755.
21. L. M. Sanches, D. F. S. Petri, L. D. de Melo Carrasco and A. M. Carmona-Ribeiro, *J. Nanobiotechnol.*, 2015, **13**, 58.
22. I. Wiegand, K. Hilpert and R. E. W. Hancock, *Nat. Protoc.*, 2008, **3**, 163.
23. D. Ochs, *Plastics Additives Handbook*, 2000, 647-680.
24. G. M. Whitesides and B. Grzybowski, *Science*, 2002, **295**, 2418-2421.
25. Y. Mai and A. Eisenberg, *Chem. Soc. Rev.*, 2012, **41**, 5969-5985.
26. A. Blanazs, S. P. Armes and A. J. Ryan, *Macromol. Rapid Commun.*, 2009, **30**, 267-277.

27. G. Riess, *Prog. Polym. Sci.*, 2003, **28**, 1107-1170.
28. A. Blanazs, J. Madsen, G. Battaglia, A. J. Ryan and S. P. Armes, *J. Am. Chem. Soc.*, 2011, **133**, 16581-16587.
29. G. Battaglia, A. J. Ryan and S. Tomas, *Langmuir*, 2006, **22**, 4910-4913.
30. F. Ahmed and D. E. Discher, *J. Controlled Release*, 2004, **96**, 37-53.
31. F. Ahmed, R. I. Pakunlu, A. Brannan, F. Bates, T. Minko and D. E. Discher, *J. Controlled Release*, 2006, **116**, 150-158.
32. P. P. Ghoroghchian, J. J. Lin, A. K. Brannan, P. R. Frail, F. S. Bates, M. J. Therien and D. A. Hammer, *Soft Matter*, 2006, **2**, 973-980.
33. N. A. Christian, M. C. Milone, S. S. Ranka, G. Li, P. R. Frail, K. P. Davis, F. S. Bates, M. J. Therien, P. P. Ghoroghchian, C. H. June and D. A. Hammer, *Bioconjugate Chem.*, 2007, **18**, 31-40.
34. D. M. Vriezema, P. M. L. Garcia, O. N. Sancho, N. S. Hatzakis, S. M. Kuiper, R. J. M. Nolte, A. E. Rowan and J. C. M. van Hest, *Angew. Chem., Int. Ed.*, 2007, **46**, 7378-7382.
35. Z. Wang , M. C. M. van Oers, F. P. J. T. Rutjes and J. C. M. van Hest, *Angew. Chem., Int. Ed.*, 2012, **51**, 10746-10750.
36. L. Zhang and A. Eisenberg, *Science*, 1995, **268**, 1728-1731.
37. T. Smart, H. Lomas, M. Massignani, M. V. Flores-Merino, L. R. Perez and G. Battaglia, *Nano Today*, 2008, **3**, 38-46.
38. A. Harada and K. Kataoka, *Prog. Polym. Sci.*, 2006, **31**, 949-982.
39. A. V. Kabanov, E. V. Batrakova and V. Y. Alakhov, *J. Controlled Release*, 2002, **82**, 189-212.
40. D. Maysinger, J. Lovrić, A. Eisenberg and R. Savić, *Eur. J. Pharm. Biopharm.*, 2007, **65**, 270-281.
41. A. M. and F. S., *Adv. Mater.*, 2003, **15**, 1323-1333.
42. J. D. Robertson, G. Yealland, M. Avila-Olias, L. Chierico, O. Bandmann, S. A. Renshaw and G. Battaglia, *ACS Nano*, 2014, **8**, 4650-4661.
43. C. Huang, D. Quinn, Y. Sadovsky, S. Suresh and K. J. Hsia, *Proc. Natl. Acad. Sci. U. S. A.*, 2017, **114**, 2910-2915.
44. T. T. Liu, W. Tian, Y. Q. Zhu, Y. Bai, H. X. Yan and J. Z. Du, *Polym. Chem.*, 2014, **5**, 5077-5088.
45. Y. Q. Zhu, L. Liu and J. Z. Du, *Macromolecules*, 2013, **46**, 194-203.
46. L.-H. Wang, W. Ting and Y.-Z. You, *Polym. Chem.*, 2015, **6**, 4972-4977.

47. P. L. Soo and A. Eisenberg, *J. Polym. Sci., Part B: Polym. Phys.*, 2004, **42**, 923-938.
48. Q. M. Liu, S. Chen, J. Chen and J. Z. Du, *Macromolecules*, 2015, **48**, 739-749.
49. E. Themistou, G. Battaglia and S. P. Armes, *Polym. Chem.*, 2014, **5**, 1405-1417.
50. M.-T. Popescu, M. Korogiannaki, K. Marikou and C. Tsitsilianis, *Polymer*, 2014, **55**, 2943-2951.
51. J. Z. Du and R. K. O'Reilly, *Soft Matter*, 2009, **5**, 3544-3561.
52. J. Z. Du and S. P. Armes, *Langmuir*, 2009, **25**, 9564-9570.
53. J. Z. Du and S. P. Armes, *Langmuir*, 2008, **24**, 13710-13716.
54. J. H. M. Schellens, M. M. Malingré, C. M. F. Kruijtzer, H. A. Bardelmeijer, O. van Tellingen, A. H. Schinkel and J. H. Beijnen, *Eur. J. Pharm. Sci.*, 2000, **12**, 103-110.
55. M. C. Branco and J. P. Schneider, *Acta Biomater.*, 2009, **5**, 817-831.
56. S. R. Croy and G. S. Kwon, *Curr. Pharm. Des.*, 2006, **12**, 4669-4684.
57. D. E. Discher and A. Eisenberg, *Science*, 2002, **297**, 967-973.
58. W. Huang, C. Shi, Y. Shao, K. S. Lam and J. Luo, *Chem. Commun.*, 2013, **49**, 6674-6676.
59. J. Fang, H. Nakamura and H. Maeda, *Adv. Drug Delivery Rev.*, 2011, **63**, 136-151.
60. S. Louguet, B. Rousseau, R. Epherre, N. Guidolin, G. Goglio, S. Mornet, E. Duguet, S. Lecommandoux and C. Schatz, *Polym. Chem.*, 2012, **3**, 1408-1417.
61. S. H. Qin, Y. Geng, D. E. Discher and S. Yang, *Adv. Mater.*, 2006, **18**, 2905-2909.
62. S. Cerritelli, D. Velluto and J. A. Hubbell, *Biomacromolecules*, 2007, **8**, 1966-1972.
63. J. Babin, M. Pelletier, M. Lepage, J.-F. Allard, D. Morris and Y. Zhao, *Angew. Chem., Int. Ed.*, 2009, **48**, 3329-3332.
64. Q. Yan, J. Yuan, Z. Cai, Y. Xin, Y. Kang and Y. Yin, *J. Am. Chem. Soc.*, 2010, **132**, 9268-9270.
65. H. Kim, Y. J. Kang, S. Kang and K. T. Kim, *J. Am. Chem. Soc.*, 2012, **134**, 4030-4033.
66. Q. Yan, R. Zhou, C. Fu, H. Zhang, Y. Yin and J. Yuan, *Angew. Chem., Int. Ed.*, 2011, **50**, 4923-4927.

67. Q. Yan and Y. Zhao, *J. Am. Chem. Soc.*, 2013, **135**, 16300-16303.
68. W. Chen and J. Du, *Sci. Rep.*, 2013, **3**, 2162.
69. M.-H. Lai, J. H. Jeong, R. J. DeVolder, C. Brockman, C. Schroeder and H. Kong, *Adv. Funct. Mater.*, 2012, **22**, 3239-3246.
70. G. Yasayan, M. Redhead, J. P. Magnusson, S. G. Spain, S. Allen, M. Davies, C. Alexander and F. Fernandez-Trillo, *Polym. Chem.*, 2012, **3**, 2596-2604.
71. Z. Pang, L. Feng, R. Hua, J. Chen, H. Gao, S. Pan, X. Jiang and P. Zhang, *Mol. Pharmaceutics*, 2010, **7**, 1995-2005.
72. M. E. Davis, Z. Chen and D. M. Shin, *Nat. Rev. Drug Discovery*, 2008, **7**, 771.
73. R. Langer and D. A. Tirrell, *Nature*, 2004, **428**, 487.
74. K. Y. Lee and S. H. Yuk, *Prog. Polym. Sci.*, 2007, **32**, 669-697.
75. B. D. Ulery, L. S. Nair and C. T. Laurencin, *J. Polym. Sci., Part B: Polym. Phys.*, 2011, **49**, 832-864.
76. D. J. A. Cameron and M. P. Shaver, *Chem. Soc. Rev.*, 2011, **40**, 1761-1776.
77. J. K. Oh, *Soft Matter*, 2011, **7**, 5096-5108.
78. I. Manavitehrani, A. Fathi, H. Badr, S. Daly, A. Negahi Shirazi and F. Dehghani, *Polymers*, 2016, **8**, 20.
79. C. K. Williams, *Chem. Soc. Rev.*, 2007, **36**, 1573-1580.
80. W.-J. Li and R. S. Tuan, *Macromol. Symp.*, 2005, **227**, 65-76.
81. W.-Y. Yeong, C.-K. Chua, K.-F. Leong and M. Chandrasekaran, *Trends Biotechnol.*, 2004, **22**, 643-652.
82. S. C. Kim, D. W. Kim, Y. H. Shim, J. S. Bang, H. S. Oh, S. W. Kim and M. H. Seo, *J. Controlled Release*, 2001, **72**, 191-202.
83. R. M. Rasal, A. V. Janorkar and D. E. Hirt, *Prog. Polym. Sci.*, 2010, **35**, 338-356.
84. J. Xu, E. Feng and J. Song, *J. Appl. Polym. Sci.*, 2014, **131**, 39822.
85. K. Fukushima, *Biomater. Sci.*, 2016, **4**, 9-24.
86. S. Tempelaar, L. Mespouille, O. Coulembier, P. Dubois and A. P. Dove, *Chem. Soc. Rev.*, 2013, **42**, 1312-1336.
87. K. J. Zhu, R. W. Hendren, K. Jensen and C. G. Pitt, *Macromolecules*, 1991, **24**, 1736-1740.
88. E. Bat, B. H. M. Kothman, G. A. Higuera, C. A. van Blitterswijk, J. Feijen and D. W. Grijpma, *Biomaterials*, 2010, **31**, 8696-8705.

89. R. C. Mundargi, V. R. Babu, V. Rangaswamy, P. Patel and T. M. Aminabhavi, *J. Controlled Release*, 2008, **125**, 193-209.
90. T. Steinbach and F. R. Wurm, *Angew. Chem., Int. Ed.*, 2015, **54**, 6098-6108.
91. G. Lapienis and S. Penczek, *Macromolecules*, 1977, **10**, 1301-1306.
92. P. Klosinski and S. Penczek, *Macromolecules*, 1983, **16**, 316-320.
93. S. Zhang, A. Li, J. Zou, L. Y. Lin and K. L. Wooley, *ACS Macro Lett.*, 2012, **1**, 328-333.
94. J. Liu, Y. Pang, W. Huang, X. Zhai, X. Zhu, Y. Zhou and D. Yan, *Macromolecules*, 2010, **43**, 8416-8423.
95. Z. E. Yilmaz and C. Jérôme, *Macromol. Biosci.*, 2016, **16**, 1745-1761.
96. Y.-C. Wang, Y. Li, X.-Z. Yang, Y.-Y. Yuan, L.-F. Yan and J. Wang, *Macromolecules*, 2009, **42**, 3026-3032.
97. Y.-C. Wang, L.-Y. Tang, T.-M. Sun, C.-H. Li, M.-H. Xiong and J. Wang, *Biomacromolecules*, 2008, **9**, 388-395.
98. Y. H. Lim, G. S. Heo, S. Cho and K. L. Wooley, *ACS Macro Lett.*, 2013, **2**, 785-789.
99. K. N. Bauer, H. T. Tee, M. M. Velencoso and F. R. Wurm, *Prog. Polym. Sci.*, 2017, **73**, 61-122.
100. M. H. Xiong, Y. J. Li, Y. Bao, X. Z. Yang, B. Hu and J. Wang, *Adv. Mater.*, 2012, **24**, 6175-6180.
101. R. W. Titball, *Trends Microbiol.*, 1997, **5**, 265.
102. R. DeVinney, O. Steele-Mortimer and B. B. Finlay, *Trends Microbiol.*, 2000, **8**, 29-33.
103. S. Paul, Y. Zhu, C. Romain, R. Brooks, P. K. Saini and C. K. Williams, *Chem. Commun.*, 2015, **51**, 6459-6479.
104. A. Wendy, A. Allan and T. Brian, *Polym. Int.*, 1998, **47**, 89-144.
105. S. Tobias and W. F. R., *Angew. Chem., Int. Ed.*, 2015, **54**, 6098-6108.
106. N. J. Agard, J. A. Prescher and C. R. Bertozzi, *J. Am. Chem. Soc.*, 2004, **126**, 15046-15047.
107. M. Malkoch, R. J. Thibault, E. Drockenmuller, M. Messerschmidt, B. Voit, T. P. Russell and C. J. Hawker, *J. Am. Chem. Soc.*, 2005, **127**, 14942-14949.
108. S. Inoue, *J. Polym. Sci., Part A: Polym. Chem.*, 2000, **38**, 2861-2871.
109. C. J. Hawker, *Acc. Chem. Res.*, 1997, **30**, 373-382.
110. G. W. Coates, *Chem. Rev.*, 2000, **100**, 1223-1252.

111. M. Okada, *Prog. Polym. Sci.*, 2002, **27**, 87-133.
112. T. P. Lodge, *Macromol. Chem. Phys.*, 2003, **204**, 265-273.
113. N. Hadjichristidis, H. Iatrou, M. Pitsikalis and J. Mays, *Prog. Polym. Sci.*, 2006, **31**, 1068-1132.
114. W. A. Braunecker and K. Matyjaszewski, *Prog. Polym. Sci.*, 2007, **32**, 93-146.
115. G. J. Domski, J. M. Rose, G. W. Coates, A. D. Bolig and M. Brookhart, *Prog. Polym. Sci.*, 2007, **32**, 30-92.
116. N. V. Tsarevsky and K. Matyjaszewski, *Chem. Rev.*, 2007, **107**, 2270-2299.
117. G. Moad, E. Rizzardo and S. H. Thang, *Acc. Chem. Res.*, 2008, **41**, 1133-1142.
118. R. R. Schrock, *Acc. Chem. Res.*, 2014, **47**, 2457-2466.
119. A. F. Halasa, *Rubber Chem. Technol.*, 1981, **54**, 627-640.
120. Q. R. P. and L. Bumjae, *Polym. Int.*, 1992, **27**, 359-367.
121. G. Odian, *Principles of Polymerization*, A John Wiley & Sons, Inc., New Jersey, 4th edn., 2004.
122. A. Kowalski, A. Duda and S. Penczek, *Macromolecules*, 2000, **33**, 7359-7370.
123. J. L. Eguiburu, M. J. Fernandez-Berridi, F. P. Cossío and J. S. Román, *Macromolecules*, 1999, **32**, 8252-8258.
124. H. R. Kricheldorf, M. Berl and N. Scharnagl, *Macromolecules*, 1988, **21**, 286-293.
125. O. Dechy-Cabaret, B. Martin-Vaca and D. Bourissou, *Chem. Rev.*, 2004, **104**, 6147-6176.
126. N. Ajellal, J.-F. Carpentier, C. Guillaume, S. M. Guillaume, M. Helou, V. Poirier, Y. Sarazin and A. Trifonov, *Dalton Trans.*, 2010, **39**, 8363-8376.
127. R. H. Platel, L. M. Hodgson and C. K. Williams, *Polym. Rev.*, 2008, **48**, 11-63.
128. B. Gupta, N. Revagade and J. Hilborn, *Prog. Polym. Sci.*, 2007, **32**, 455-482.
129. S. Penczek, M. Cypryk, A. Duda, P. Kubisa and S. Słomkowski, *Prog. Polym. Sci.*, 2007, **32**, 247-282.
130. K. R. Yoon, K. B. Lee, Y. S. Chi, W. S. Yun, S. W. Joo and I. S. Choi, *Adv. Mater.*, 2003, **15**, 2063-2066.
131. B. G. G. Lohmeijer, R. C. Pratt, F. Leibfarth, J. W. Logan, D. A. Long, A. P. Dove, F. Nederberg, J. Choi, C. Wade, R. M. Waymouth and J. L. Hedrick, *Macromolecules*, 2006, **39**, 8574-8583.

132. L. Mespouille, O. Coulembier, M. Kawalec, A. P. Dove and P. Dubois, *Prog. Polym. Sci.*, 2014, **39**, 1144-1164.
133. P. Olsén, K. Odelius, H. Keul and A.-C. Albertsson, *Macromolecules*, 2015, **48**, 1703-1710.
134. R. C. Pratt, B. G. G. Lohmeijer, D. A. Long, R. M. Waymouth and J. L. Hedrick, *J. Am. Chem. Soc.*, 2006, **128**, 4556-4557.
135. H. Misaka, R. Kakuchi, C. Zhang, R. Sakai, T. Satoh and T. Kakuchi, *Macromolecules*, 2009, **42**, 5091-5096.
136. M. K. Kiesewetter, M. D. Scholten, N. Kirn, R. L. Weber, J. L. Hedrick and R. M. Waymouth, *J. Org. Chem.*, 2009, **74**, 9490-9496.
137. A. Nachtergael, O. Coulembier, P. Dubois, M. Helvenstein, P. Duez, B. Blankert and L. Mespouille, *Biomacromolecules*, 2015, **16**, 507-514.
138. S. Paul, Y. Zhu, C. Romain, R. Brooks, P. K. Saini and C. K. Williams, *Chem. Commun.*, 2015, **51**, 6459-6479.
139. J. M. Longo, M. J. Sanford and G. W. Coates, *Chem. Rev.*, 2016, **116**, 15167-15197.
140. R. C. Jeske, A. M. DiCiccio and G. W. Coates, *J. Am. Chem. Soc.*, 2007, **129**, 11330-11331.
141. E. H. Nejad, A. Paoniasari, C. G. W. van Melis, C. E. Koning and R. Duchateau, *Macromolecules*, 2013, **46**, 631-637.
142. A. M. DiCiccio and G. W. Coates, *J. Am. Chem. Soc.*, 2011, **133**, 10724-10727.
143. L. Feng, Y. Liu, J. Hao, C. Xiong and X. Deng, *J. Polym. Sci., Part A: Polym. Chem.*, 2012, **50**, 1812-1818.
144. K. M. Morgan, J. A. Ellis, J. Lee, A. Fulton, S. L. Wilson, P. S. Dupart and R. Dastoori, *J. Org. Chem.*, 2013, **78**, 4303-4311.
145. S. Huijser, E. HosseiniNejad, R. Sablong, C. de Jong, C. E. Koning and R. Duchateau, *Macromolecules*, 2011, **44**, 1132-1139.
146. D. J. Darensbourg and M. W. Holtcamp, *Coord. Chem. Rev.*, 1996, **153**, 155-174.
147. M. R. Kember, A. Buchard and C. K. Williams, *Chem. Commun.*, 2011, **47**, 141-163.
148. G. Trott, P. K. Saini and C. K. Williams, *Philos. Trans. R. Soc., A*, 2016, **374**.
149. D. J. Darensbourg, *Chem. Rev.*, 2007, **107**, 2388-2410.

150. D. J. Darensbourg and S. J. Wilson, *Green Chem.*, 2012, **14**, 2665-2671.
151. X.-B. Lu, W.-M. Ren and G.-P. Wu, *Acc. Chem. Res.*, 2012, **45**, 1721-1735.
152. S. Klaus, M. W. Lehenmeier, C. E. Anderson and B. Rieger, *Coord. Chem. Rev.*, 2011, **255**, 1460-1479.
153. G. W. Coates and D. R. Moore, *Angew. Chem., Int. Ed.*, 2004, **43**, 6618-6639.
154. D. J. Darensbourg and A. D. Yeung, *Polym. Chem.*, 2014, **5**, 3949-3962.
155. D. J. Darensbourg, *Inorg. Chem.*, 2010, **49**, 10765-10780.
156. E. Brule, J. Guo, G. W. Coates and C. M. Thomas, *Macromol. Rapid Commun.*, 2011, **32**, 169-185.
157. W. Kuran, *Prog. Polym. Sci.*, 1998, **23**, 919-992.
158. H. Sugimoto and S. Inoue, *J. Polym. Sci., Part A: Polym. Chem.*, 2004, **42**, 5561-5573.
159. G. A. Luinstra, *Polym. Rev.*, 2008, **48**, 192-219.
160. R. Korashvili, B. Noernberg, N. Bornholdt, E. Borchardt and G. A. Luinstra, *Chem. Ing. Tech.*, 2013, **85**, 437-446.
161. J. Langanke, A. Wolf, J. Hofmann, K. Bohm, M. A. Subhani, T. E. Muller, W. Leitner and C. Gurtler, *Green Chem.*, 2014, **16**, 1865-1870.
162. D. J. Darensbourg and S.-H. Wei, *Macromolecules*, 2012, **45**, 5916-5922.
163. A. Cyriac, S. H. Lee, J. K. Varghese, E. S. Park, J. H. Park and B. Y. Lee, *Macromolecules*, 2010, **43**, 7398-7401.
164. N. Yi, J. Unruangsri, J. Shaw and C. K. Williams, *Faraday Discuss.*, 2015, **183**, 67-82.
165. N. Andronova and A.-C. Albertsson, *Biomacromolecules*, 2006, **7**, 1489-1495.
166. D. K. Schneiderman, E. M. Hill, M. T. Martello and M. A. Hillmyer, *Polym. Chem.*, 2015, **6**, 3641-3651.
167. H. R. Kricheldorf and S. Rost, *Macromolecules*, 2005, **38**, 8220-8226.
168. J. Hilf, P. Schulze and H. Frey, *Macromol. Chem. Phys.*, 2013, **214**, 2848-2855.
169. G. P. Wu, D. J. Darensbourg and X. B. Lu, *J. Am. Chem. Soc.*, 2012, **134**, 17739-17745.
170. D. J. Darensbourg and G.-P. Wu, *Angew. Chem., Int. Ed.*, 2013, **52**, 10602-10606.
171. G.-P. Wu and D. J. Darensbourg, *Macromolecules*, 2016, **49**, 807-814.

172. M. R. Kember, J. Copley, A. Buchard and C. K. Williams, *Polym. Chem.*, 2012, **3**, 1196-1201.
173. W. Chin, C. Yang, V. W. L. Ng, Y. Huang, J. Cheng, Y. W. Tong, D. J. Coady, W. Fan, J. L. Hedrick and Y. Y. Yang, *Macromolecules*, 2013, **46**, 8797-8807.
174. Y. Zhu, C. Romain and C. K. Williams, *J. Am. Chem. Soc.*, 2015, **137**, 12179-12182.
175. E. Blasco, M. B. Sims, A. S. Goldmann, B. S. Sumerlin and C. Barner-Kowollik, *Macromolecules*, 2017, **50**, 5215-5252.
176. P. L. Golas and K. Matyjaszewski, *Chem. Soc. Rev.*, 2010, **39**, 1338-1354.
177. R. J. Williams, I. A. Barker, R. K. O'Reilly and A. P. Dove, *ACS Macro Lett.*, 2012, **1**, 1285-1290.
178. C. E. Hoyle, A. B. Lowe and C. N. Bowman, *Chem. Soc. Rev.*, 2010, **39**, 1355-1387.
179. M. A. Gauthier, M. I. Gibson and H.-A. Klok, *Angew. Chem., Int. Ed.*, 2009, **48**, 48-58.
180. J. Xu, Z.-L. Liu and R.-X. Zhuo, *J. Appl. Polym. Sci.*, 2006, **101**, 1988-1994.
181. J. Lu and M. S. Shoichet, *Macromolecules*, 2010, **43**, 4943-4953.
182. M. Shi, J. H. Wosnick, K. Ho, A. Keating and M. S. Shoichet, *Angew. Chem., Int. Ed.*, 2007, **46**, 6126-6131.
183. A. C. Engler, J. P. K. Tan, Z. Y. Ong, D. J. Coady, V. W. L. Ng, Y. Y. Yang and J. L. Hedrick, *Biomacromolecules*, 2013, **14**, 4331-4339.
184. D. Xing, L. Ma and C. Gao, *Macromol. Biosci.*, 2014, **14**, 1429-1436.
185. S. Onbulak, S. Tempelaar, R. J. Pounder, O. Gok, R. Sanyal, A. P. Dove and A. Sanyal, *Macromolecules*, 2012, **45**, 1715-1722.
186. D. M. Stevens, A. Rahalkar, B. Spears, K. Gilmore, E. Douglas, M. Muthukumar and E. Harth, *Polym. Chem.*, 2015, **6**, 1096-1102.
187. S. Tempelaar, L. Mespouille, P. Dubois and A. P. Dove, *Macromolecules*, 2011, **44**, 2084-2091.
188. V. Truong, I. Blakey and A. K. Whittaker, *Biomacromolecules*, 2012, **13**, 4012-4021.
189. D. Hu, H. Peng, Y. Niu, Y. Li, Y. Xia, L. Li, J. He, X. Liu, X. Xia, Y. Lu and W. Xu, *J. Polym. Sci., Part A: Polym. Chem.*, 2015, **53**, 750-760.
190. R. Kakuchi and P. Theato, *Polym. Chem.*, 2014, **5**, 2320-2325.

191. Z. X. Voo, M. Khan, K. Narayanan, D. Seah, J. L. Hedrick and Y. Y. Yang, *Macromolecules*, 2015, **48**, 1055-1064.
192. Y. Yu, J. Zou and C. Cheng, *Polym. Chem.*, 2014, **5**, 5854-5872.
193. A. Pascual, J. P. K. Tan, A. Yuen, J. M. W. Chan, D. J. Coady, D. Mecerreyes, J. L. Hedrick, Y. Y. Yang and H. Sardon, *Biomacromolecules*, 2015, **16**, 1169-1178.
194. S. Q. Liu, C. Yang, Y. Huang, X. Ding, Y. Li, W. M. Fan, J. L. Hedrick and Y. Y. Yang, *Adv. Mater.*, 2012, **24**, 6484-6489.
195. A. Y. Yuen, E. Lopez-Martinez, E. Gomez-Bengoa, A. L. Cortajarena, R. H. Aguirresarobe, A. Bossion, D. Mecerreyes, J. L. Hedrick, Y. Y. Yang and H. Sardon, *ACS Biomater. Sci. Eng.*, 2017, **3**, 1567-1575.
196. A. Thomas, S. S. Müller and H. Frey, *Biomacromolecules*, 2014, **15**, 1935-1954.
197. O. Hauenstein, S. Agarwal and A. Greiner, *Nat. Commun.*, 2016, **7**, 11862.
198. W. Chen, F. Meng, R. Cheng, C. Deng, J. Feijen and Z. Zhong, *J. Controlled Release*, 2014, **190**, 398-414.
199. F. Suriano, O. Coulembier, J. L. Hedrick and P. Dubois, *Polym. Chem.*, 2011, **2**, 528-533.
200. X. Hu, S. Liu, Y. Huang, X. Chen and X. Jing, *Biomacromolecules*, 2010, **11**, 2094-2102.
201. P. a. Ma, S. Liu, Y. Huang, X. Chen, L. Zhang and X. Jing, *Biomaterials*, 2010, **31**, 2646-2654.
202. Y. Dai, X. Zhang and F. Xia, *Macromol. Rapid Commun.*, 2017, **38**, 1700357.
203. X. Hu, X. Chen, Z. Xie, S. Liu and X. Jing, *J. Polym. Sci., Part A: Polym. Chem.*, 2007, **45**, 5518-5528.
204. X. Hu, X. Chen, S. Liu, Q. Shi and X. Jing, *J. Polym. Sci., Part A: Polym. Chem.*, 2008, **46**, 1852-1861.
205. W. Chen, H. Yang, R. Wang, R. Cheng, F. Meng, W. Wei and Z. Zhong, *Macromolecules*, 2010, **43**, 201-207.
206. S. Li, F. Meng, Z. Wang, Y. Zhong, M. Zheng, H. Liu and Z. Zhong, *Eur. J. Pharm. Biopharm.*, 2012, **82**, 103-111.
207. B. G. Amsden, A. Sukarto, D. K. Knight and S. N. Shapka, *Biomacromolecules*, 2007, **8**, 3758-3766.

208. Y. Yu, C. Deng, F. Meng, Q. Shi, J. Feijen and Z. Zhong, *J. Biomed. Mater. Res.*, 2011, **99A**, 316-326.
209. B. B. Uysal, U. S. Gunay, G. Hizal and U. Tunca, *J. Polym. Sci., Part A: Polym. Chem.*, 2014, **52**, 1581-1587.
210. M. Takanashi, Y. Nomura, Y. Yoshida and S. Inoue, *Makromol. Chem.*, 1982, **183**, 2085-2092.
211. J. Geschwind and H. Frey, *Macromolecules*, 2013, **46**, 3280-3287.
212. H. Zhang and M. W. Grinstaff, *J. Appl. Polym. Sci.*, 2014, **131**, 39893-39899.
213. D. J. Darensbourg and A. D. Yeung, *Green Chem.*, 2014, **16**, 247-252.
214. H. Zhang and M. W. Grinstaff, *J. Am. Chem. Soc.*, 2013, **135**, 6806-6809.
215. J. Geschwind and H. Frey, *Macromol. Rapid Commun.*, 2013, **34**, 150-155.
216. J. Łukaszczyk, K. Jaszcz, W. Kuran and T. Listos, *Macromol. Rapid Commun.*, 2000, **21**, 754-757.
217. J. Łukaszczyk, K. Jaszcz, W. Kuran and T. Listoś, *Macromol. Biosci.*, 2001, **1**, 282-289.
218. Q. Zhou, L. Gu, Y. Gao, Y. Qin, X. Wang and F. Wang, *J. Polym. Sci., Part A: Polym. Chem.*, 2013, **51**, 1893-1898.
219. L. Gu, Y. S. Qin, Y. G. Gao, X. H. Wang and F. S. Wang, *J. Polym. Sci., Part A: Polym. Chem.*, 2013, **51**, 2834-2840.
220. J. Hilf, A. Phillips and H. Frey, *Polym. Chem.*, 2014, **5**, 814-818.
221. J. Hilf and H. Frey, *Macromol. Rapid Commun.*, 2013, **34**, 1395-1400.
222. J. T. Guo, X. Y. Wang, Y. S. Xu and J. W. Sun, *J. Appl. Polym. Sci.*, 2003, **87**, 2356-2359.
223. Y. Tominaga, T. Shimomura and M. Nakamura, *Polymer*, 2010, **51**, 4295-4298.
224. J. Hilf, P. Schulze, J. Seiwert and H. Frey, *Macromol. Rapid Commun.*, 2014, **35**, 198-203.
225. W.-M. Ren, M.-W. Liang, Y.-C. Xu and X.-B. Lu, *Polym. Chem.*, 2013, **4**, 4425-4433.
226. X. Wu, H. Zhao, B. Nörnberg, P. Theato and G. A. Luinstra, *Macromolecules*, 2014, **47**, 492-497.
227. I. Ekladious, R. Liu, H. Zhang, D. H. Foil, D. A. Todd, T. N. Graf, R. F. Padera, N. H. Oberlies, Y. L. Colson and M. W. Grinstaff, *Chem. Sci.*, 2017, **8**, 8443-8450.

228. H. Jeannette and F. Holger, *Macromol. Rapid Commun.*, 2013, **34**, 1395-1400.
229. Z. Heng and G. M. W., *J. Appl. Polym. Sci.*, 2014, **131**.
230. D. J. Darensbourg, W.-C. Chung, C. J. Arp, F.-T. Tsai and S. J. Kyran, *Macromolecules*, 2014, **47**, 7347-7353.
231. D. J. Darensbourg, W.-C. Chung, A. D. Yeung and M. Luna, *Macromolecules*, 2015, **48**, 1679-1687.
232. R. T. Mathers and G. W. Coates, *Chem. Commun.*, 2004, DOI: 10.1039/B313954A, 422-423.
233. M. Taherimehr, J. P. C. C. Sertã, A. W. Kleij, C. J. Whiteoak and P. P. Pescarmona, *ChemSusChem*, 2015, **8**, 1034-1042.
234. J.-F. Zhang, W.-M. Ren, X.-K. Sun, Y. Meng, B.-Y. Du and X.-H. Zhang, *Macromolecules*, 2011, **44**, 9882-9886.
235. J. Geschwind, F. Wurm and H. Frey, *Macromol. Chem. Phys.*, 2013, **214**, 892-901.
236. D. J. Darensbourg and F.-T. Tsai, *Macromolecules*, 2014, **47**, 3806-3813.
237. J. Li, R. M. Stayshich and T. Y. Meyer, *J. Am. Chem. Soc.*, 2011, **133**, 6910-6913.
238. A.-C. Albertsson and I. K. Varma, *Biomacromolecules*, 2003, **4**, 1466-1486.
239. C. Jérôme and P. Lecomte, *Adv. Drug Delivery Rev.*, 2008, **60**, 1056-1076.
240. R. J. Pounder and A. P. Dove, *Polym. Chem.*, 2010, **1**, 260-271.
241. E. A. Rainbolt, K. E. Washington, M. C. Biewer and M. C. Stefan, *Polym. Chem.*, 2015, **6**, 2369-2381.
242. X. D. Lou, C. Detrembleur and R. Jerome, *Macromol. Rapid Commun.*, 2003, **24**, 161-172.
243. B. Han, L. Zhang, B. Liu, X. Dong, I. Kim, Z. Duan and P. Theato, *Macromolecules*, 2015, **48**, 3431-3437.
244. R. Baumgartner, Z. Song, Y. Zhang and J. Cheng, *Polym. Chem.*, 2015, **6**, 3586-3590.
245. G. Si, L. Zhang, B. Han, Z. Duan, B. Li, J. Dong, X. Li and B. Liu, *Polym. Chem.*, 2015, **6**, 6372-6377.
246. M. J. Sanford, N. J. Van Zee and G. Coates, *Chem. Sci.*, 2018, **9**, 134-142.

Chapter 2

Characterisation Techniques

2.1 Polymer Characterisations

An overview of relevant techniques and data analysis used to characterise the polymers is provided.

2.1.1 Nuclear Magnetic Resonance (NMR) Spectroscopy

One and two-dimensional (2D) NMR spectroscopic techniques were used for the characterisation of polymers throughout this thesis.

When using NMR spectroscopy to characterise polymers, it is usually difficult to identify individual polymer chains because each monomer unit in the chain is similar, leading to signals overlapping and peak broadening. The high molar mass also results in peak broadening due to slow relaxation and tumbling. Nevertheless, NMR is still useful in measuring the polymerisation conversion, analysing the end group and determining the molar mass.

The polymerisation conversion can be determined through relative integration of distinct monomer and polymer resonances. For example, the conversion of *rac*-lactide (*rac*-LA) in the ring-opening polymerisation (ROP) can be calculated from the relative integration of the methine proton in the *rac*-LA (5.00-5.07 ppm) and polymer (5.10-5.24 ppm) (Figure 2.1).

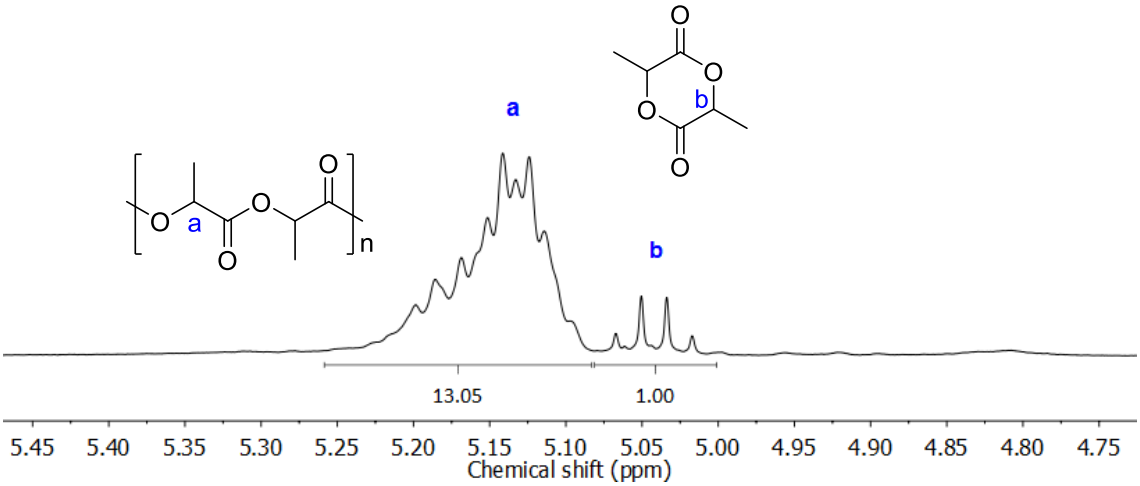


Figure 2.1 Example of ^{1}H NMR spectrum of an aliquot during LA polymerisation ($CDCl_3$, 400 MHz, 298 K). Conversion = 13.05/14.05 = 93%.

The end group of a polymer chain can also be characterised as its chemical shift is often distinct. By comparing the integrals of polymer versus chain end, the degree of polymerisation (DP) can be determined (Figure 2.2).

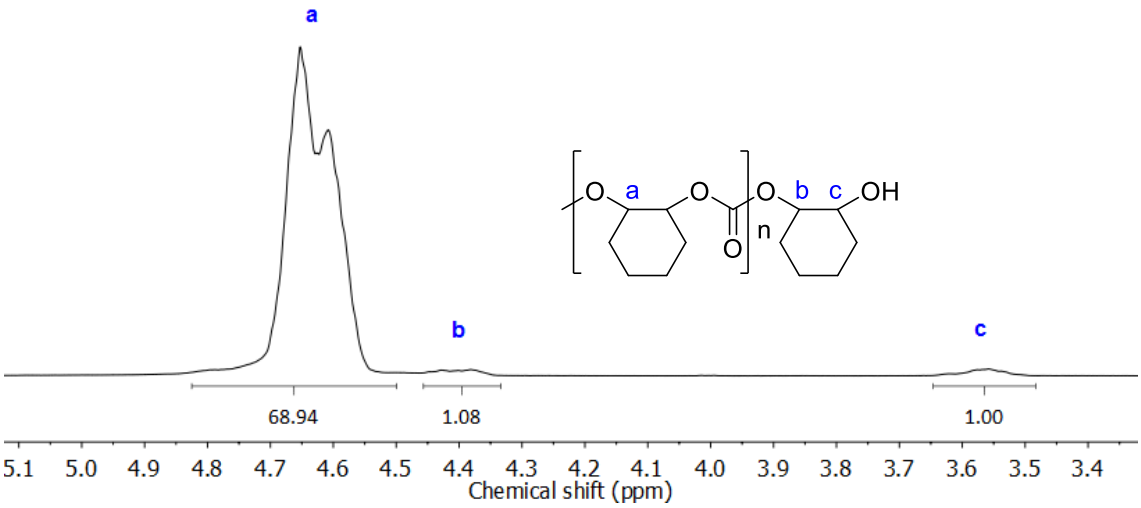
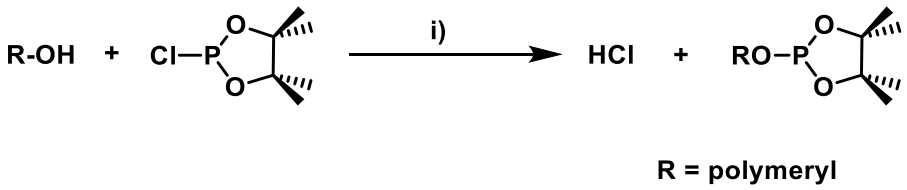


Figure 2.2 Example of the ^{1}H NMR spectrum of the purified polymer from ROCOP of CO_2/cyclohexene oxide. Peak a (4.65 ppm) is assigned to the carbonate linkage, peak H_b (4.45 ppm) and H_c (3.60 ppm) are assigned to the end group methine protons. In this sample, DP is 70, and the estimated molar mass is 142.2 × 70 = 9.9 kgmol^{-1}.

The method of molar mass determination is only reliable when the polymer signals are distinct from the end group, and the end group has a well-resolved signal with a reliable integral (*i.e.* at a low degree of polymerisation). Additionally, for high molar mass polymers, this NMR technique is not recommended due to the low intensity of the end group signals.

2.1.1.1 End group (-OH) determination using ^{31}P NMR spectroscopy

Hydroxyl groups at the polymer chain end are difficult to detect by ^{1}H NMR spectroscopy (due to the rapid proton exchange). A $^{31}P\{^{1}H\}$ NMR spectroscopic analysis method is best employed. This method involves reacting the hydroxyl-terminated polymer sample with a phospholane reagent (2-chloro-4,4,5,5-tetra-methyldioxaphospholane), using bisphenol A as an internal reference. Different hydroxyl groups react with the dioxaphospholane to give phosphinic ester products showing different chemical shifts ($^{31}P\{^{1}H\}$ NMR). The procedure used throughout this thesis was adapted from a previous report by Spyros et al.[1]



Scheme 2.1 The reaction between polymer hydroxyl end groups and 2-chloro-4,4,5,5-tetra-methyldioxaphospholane. i) $Cr(acac)_3$, Bisphenol A (BPA), pyridine, $CDCl_3$, 18 h.

Primary and secondary hydroxyl groups are distinguished by their chemical shifts (146.4-147.8 ppm for primary hydroxyl groups and 146.1-146.2 for secondary hydroxyl groups). Carboxylic acid show signals at *ca.* 135.5-135.7 ppm. The method involves using a stock solution of BPA in pyridine. Excess pyridine is used to scavenge HCl and

to solubilise the BPA standard. Nonetheless, the basicity of the stock solution may result in significant polycarbonate degradation over the timescale of the test, making it unsuitable for the polycarbonate end group analysis.

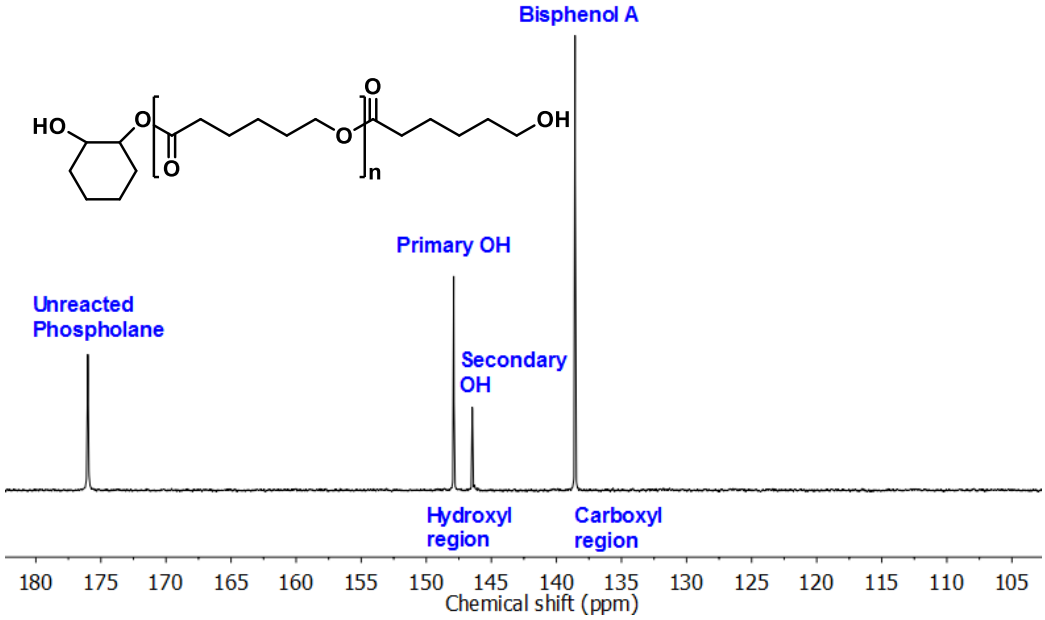


Figure 2.3 Example of $^{31}P\{^{1}H\}$ spectrum for end group analysis of polycaprolactone (PCL) with two types of hydroxyl end groups.

2.1.1.2 2D NMR Spectroscopy

2D NMR spectroscopy was used to gain additional structural data and to assign polymer spectra. Table 2.1 summarises the key techniques used in this thesis, often used simultaneously to assign multiple couplings.

Table 2.1 Summary and comparison of 2D NMR spectroscopic techniques used in this thesis.

	Nucleus	Correlation	Range
COSY	^{1}H-^{1}H	Through-bond	2-4 bonds
HSQC	^{1}H-^{13}C	Through-bond	1 bond
HMBC	^{1}H-^{13}C	Through-bond	2-4 bonds

2.1.1.3 ^{1}H DOSY NMR Spectroscopy

Diffusion-ordered NMR spectroscopy (DOSY) differentiates the NMR signals of different species according to the different diffusion coefficients. DOSY is based on the measurement of translational diffusion coefficients, which depend on a molecule's shape and size. Spin-echo spectra, with different pulsed field gradient strengths, are collected, and the signal decays are analysed. The spin-echo intensity of a spin active nucleus, (I) is related to the diffusion coefficient (D) of the molecule by the following equation:

$$\ln\left(\frac{I}{I_0}\right) = -\gamma^2\delta^2G^2\left(\Delta - \frac{\delta}{3}\right)D$$

[γ is the gyromagnetic ratio, δ is the length of the gradient pulse, G is the gradient strength, Δ is the delay between gradient midpoints, D is the diffusion coefficient and I is the spin-echo intensity]

From the diffusion coefficient of a species, its hydrodynamic radius (R_h) can be calculated using the Stokes-Einstein equation:

$$R_h = \frac{k_B T}{6\pi\eta D}$$

[k_B is the Boltzmann constant, T is the temperature, η is the solvent viscosity at the measured temperature, D is the diffusion coefficient and R_h is the hydrodynamic radius]

For small molecules, ^{1}H DOSY is regularly employed to determine the nuclearity and the presence of aggregation. The molar mass can be estimated if an internal standard of known nuclearity is used. In concept, ^{1}H DOSY technique is similar to SEC, correlating the hydrodynamic radius of the species to its molar mass and therefore having the same limitations. In polymer chemistry, ^{1}H DOSY can be useful to characterise block copolymers. Block copolymers are expected to show a different hydrodynamic radius to the homopolymer (due to the increased molar mass and interactions between blocks). Additionally, all signals from a block copolymer should have the same diffusion coefficient. Any contaminating homopolymers are expected to show different diffusion coefficients (Figure 2.4).

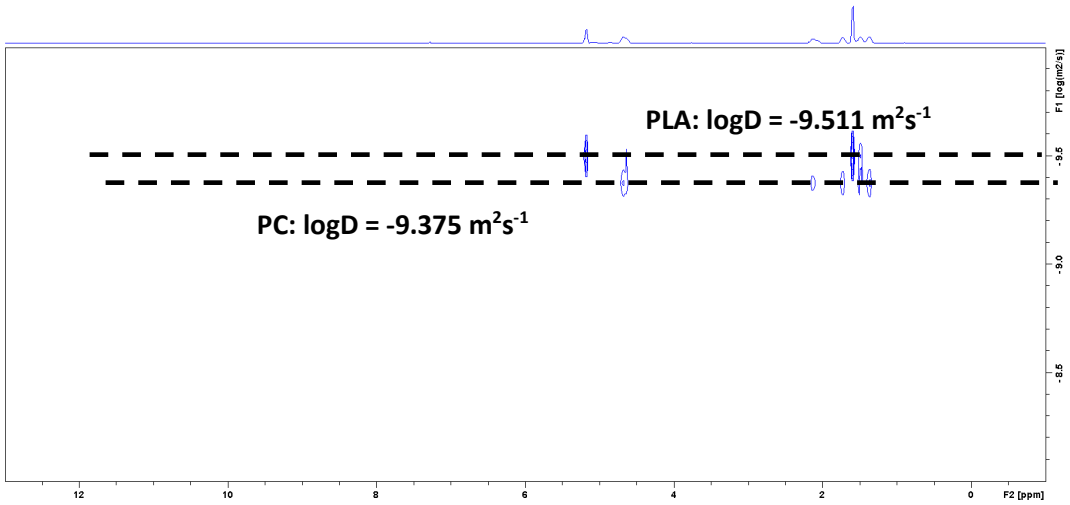


Figure 2.4 Example of ^{1}H DOSY spectrum of a mixture of polylactide (PLA) and poly(cyclohexene carbonate) (PC).

2.1.2 Size Exclusion Chromatography (SEC)

SEC is used to determine the molar mass and dispersity (Đ) of a polymer sample. It separates molecules based on size, or hydrodynamic volume of the sample. Separation is achieved by passing the sample through a column packed by porous beads. When the polymer samples are dissolved in the mobile phase, they are expected to adopt random coil structures. Larger polymer chains cannot enter the pores and it will elute more quickly, and of course smaller chains elute more slowly.

The elution time is directly related to the polymer's hydrodynamic radius, and the relative molar mass of an unknown sample is determined by comparing elution time against a known material. In this work, narrow polystyrene standards (from PSS) were used for calibration.

Polymers show a distribution of chain lengths and the molar mass is reported as the number average molar mass (M_n). The mass average molar mass (M_w) is calculated from the mass fraction distribution of different sized molecules. The ratio of M_w to M_n determines the dispersity (Đ) of the sample, indicating the range of molar mass values.

For polymers chains of similar lengths, the SEC trace is a single, sharp peak with a Gaussian distribution. When two or more polymer chains of differing lengths are present, the SEC trace may appear broad or lopsided.

Bimodal modal molar mass distributions are commonly observed in ROCOP of epoxides and CO_2 and have been observed for a wide range of catalysts in the literature.[2-6] This bimodality is attributed to chains end-capped by both the initiating group (from the catalyst) and di-hydroxyl groups (from 1,2-diols).[7] For example, using the $[LZn_2(OAc)_2]$ for the ROCOP of CHO/CO_2 results in both di-hydroxyl terminated and acetate terminated polymer species.[4] As polymer chains propagate at the same rate from all hydroxyl groups in a well-controlled polymerisation, the molar mass of the di-hydroxyl terminated chains should be double that of chains initiated from the acetate group. As a result, both species are observed in the SEC trace as a bimodal distribution.[7]

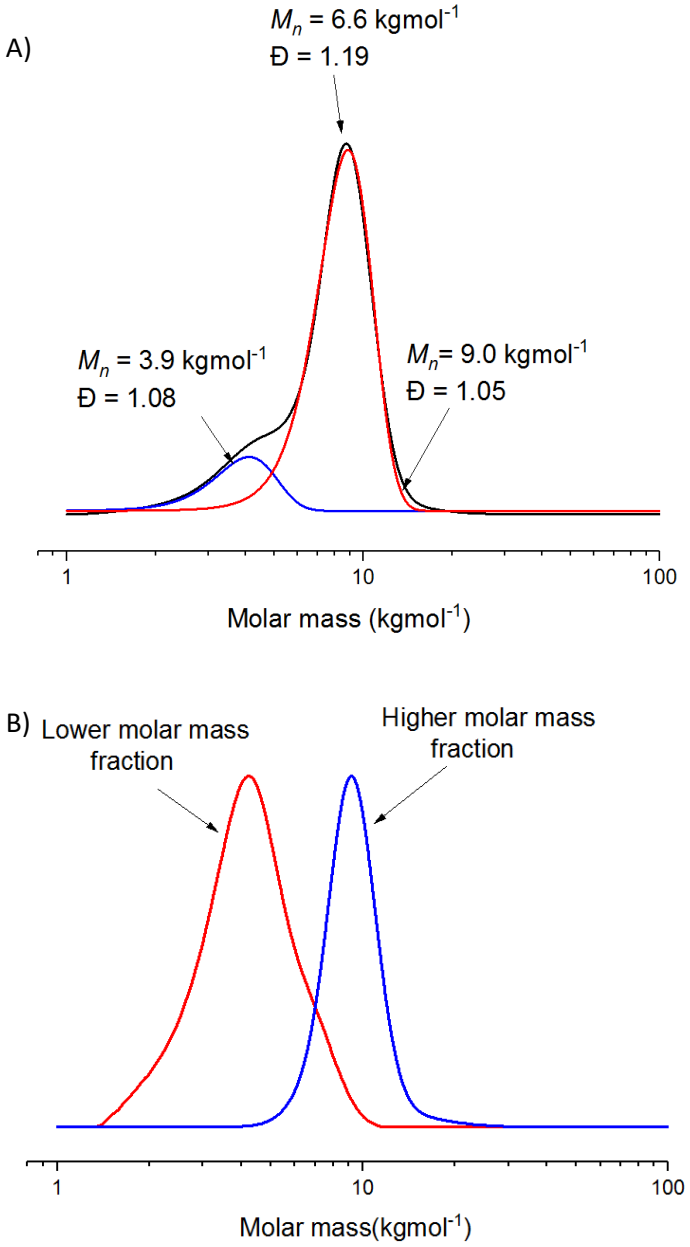


Figure 2.5 A) Example of an SEC trace of PC with a bimodal molar mass distribution (deconvoluted) and B) the separation of PC into two fractions of low and high molar mass, according to a preparative separation by elution time using SEC.

In this thesis, bimodal peaks are reported for both distributions and peak deconvolution (fits to a Gaussian distribution) is applied to ensure accuracy in both M_n and Đ values. SEC is also commonly used to confirm the formation of block copolymers. For example, ABA copolymer synthesis is expected to show a shift to higher molar mass compared to that of the B block (the macro-initiator).

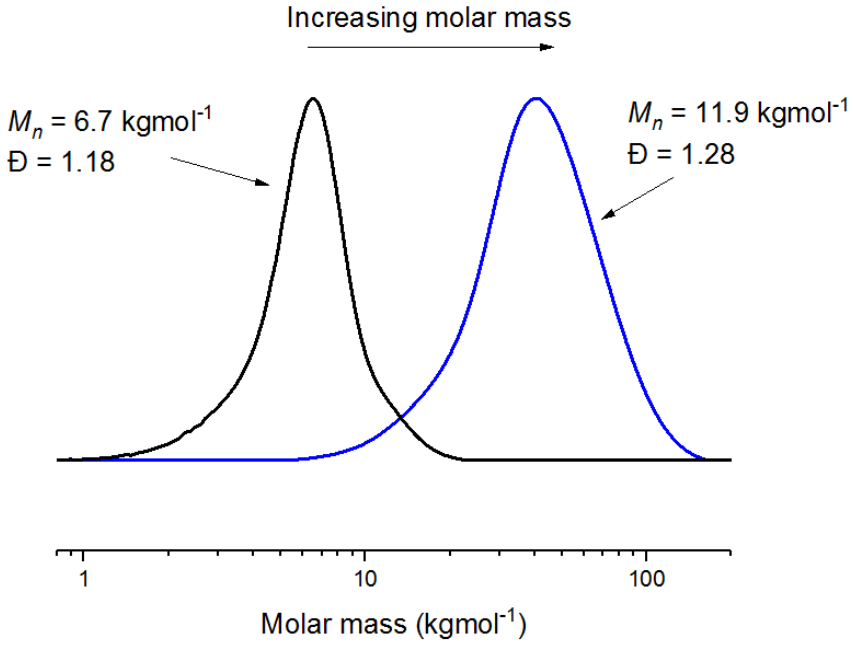


Figure 2.6 Example of Overlaid SEC traces of PC and PLA-PC-PLA, showing an increase in molar mass after block formation.

2.1.3 Matrix-assisted laser desorption/ionization time-of-flight (MALDI-ToF) mass spectrometry

MALDI-ToF is an important soft ionisation technique used to characterise polymers. For polymer analysis, MALDI-ToF is used to determine the molar mass for low M_n samples (Đ < 1.2), regardless of the polymer structure. MALDI-ToF also provides a direct method for assigning the chain end-groups. Each polymer chain of a particular mass gives rise to a separate signal and the difference in *m/z* between two neighbouring signals should be equivalent to the molar mass of the repeat unit. If all chains have the same structure but different chain lengths, usually only one distribution is observed. If there are more than one chain end groups, several distributions will be observed. These distributions are usually separated by the same repeat unit but differ according to the end group mass. The polymer composition is determined by comparison of the theoretical molar masses, with the observed *m/z* values. In this thesis, potassium

ionising agents are used, and the K^+ ion must be taken into account when calculating the theoretical mass. When a polymer has an anionic end group, *e.g.* P-COO_2^-, a salt with the K^+ ion may form and a second K^+ ion is required for ionisation - *i.e.* the structure is P-$2K^+$. Although MALDI-ToF is a powerful method for determining the polymer structure, it is important to emphasise that not all the species are ionised or accelerated in the same way. The intensity of a signal correlates to the volatility of the ionisation products and should not be used to quantify the relative concentration of the polymeric species. In this thesis, potassium trifluoroacetate (KTFA) was used as the ionising agent. For polycarbonates, dithranol was used as the matrix. Trans-2-[3-(4-tert-butylphenyl)-2-methyl-2-propenylidene]malononitrile (DCTB) was used as the matrix for polyesters.

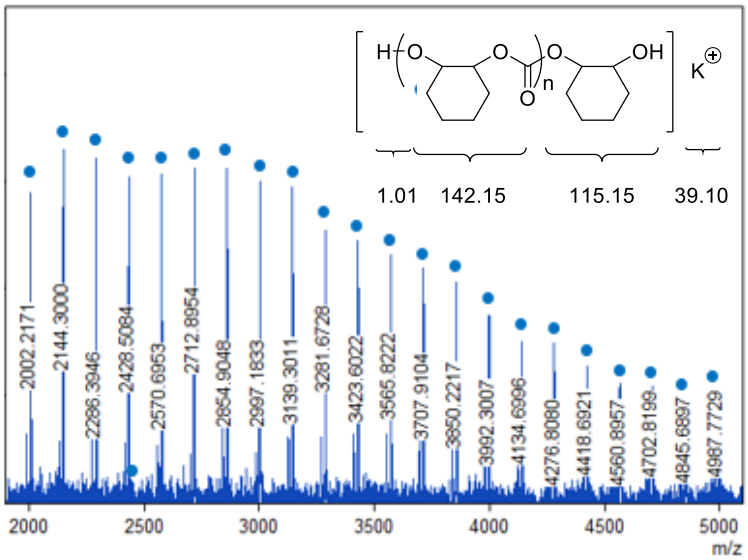


Figure 2.7 Example of a MALDI-ToF spectrum of PC. Each signal is separated by 142 m/z, the molar mass of the repeating unit.

2.1.4 Thermal Analyses

Differential Scanning Calorimetry (DSC) compares the heat required to increase the temperature of a sample against a reference material and is used to characterise the

thermal transitions of polymer samples. Typically, the sample and reference are maintained at the same temperature, and the temperature is increased linearly. The heat required to maintain the sample temperature at the same value as the reference temperature is measured. When the polymer sample undergoes a thermal transition, either endothermic or exothermic, heat flow is detected. Melting is an endothermic process, and crystallisation is an exothermic process. The glass transition is also related to a change in heat capacity, resulting in a baseline shift. The output of a typical DSC experiment is a plot of heat flow (Y-axis) against temperature (X-axis). The enthalpies associated with the thermal transitions can be calculated by integration of a specific transition, given that the mass of the sample is accurately measured.

$$\Delta H = KA$$

[ΔH is the enthalpy of transition, K is the calorimetric constant, and A is the transition area.]

For the semi-crystalline and amorphous polymers studied in this thesis, the main thermal transition is the glass transition temperature (T_g). This is the transition from a 'glassy' state to a viscous or rubbery state. T_g is typically indicated by a step change in the baseline of the DSC chromatogram and is reported here as the mid-point of the transition. The glass transition temperature is dependent on chain mobility and is influenced by the backbone structure, the chain length, the side chain structure and the end group chemistry. Polymers having high T_g (compared to operating temperature) are rigid plastics, whereas polymers having low T_g values (< room temperature) can be used to prepare elastomers.

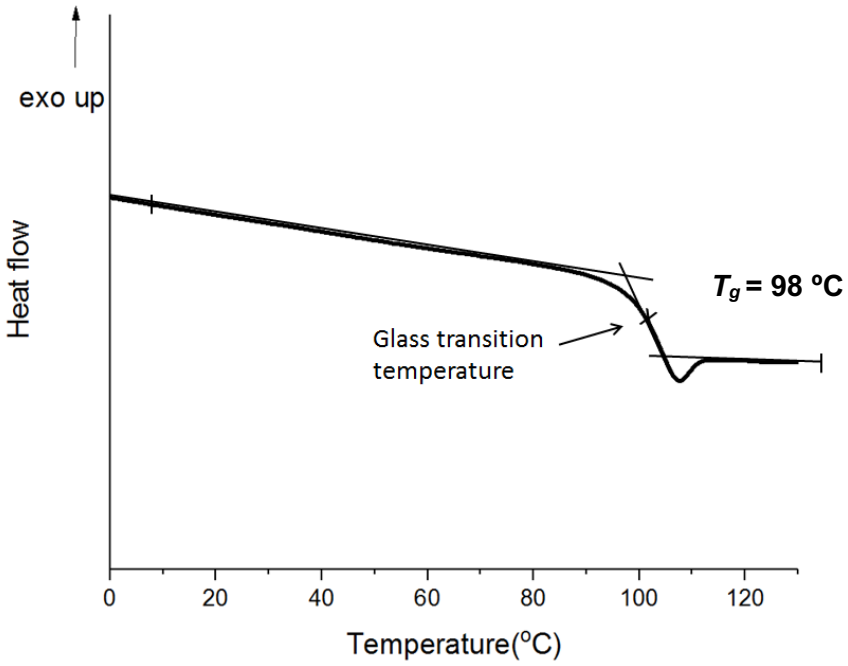


Figure 2.8 Example of a DSC chromatogram of PC, obtained from the second heating cycle.

2.1.5 Water Contact Angle Measurements

Static contact angle measurements are commonly employed to determine surface hydrophilicity. The method quantifies the wettability of a solid surface by a liquid and is based on the Young equation.

$$\sigma_s = \sigma_{sl} + \sigma_l \cos\theta$$

[θ is the contact angle, σ_s is the surface free energy of the solid, σ_l is the surface tension of the liquid and σ_{sl} is the interfacial tension between the liquid and the solid]

A surface is classified as hydrophobic for θ > 90 ° and conversely as hydrophilic when θ is < 90 °. The smaller the water contact angle, the better the wetting and in the case of complete wetting, the contact angle is 0 °.

Drop shape analysis (DSA) is one of the most widely used methods to determine the static water contact angle from the shadow image of a sessile drop. During the measurement, a drop of a pure test liquid is placed onto the solid sample. The drop shape is recorded using a camera, and the contact angle is determined at the intersection between a tangent to the curve and the surface. In this thesis, static water contact angles were measured on three different areas of each sample, and the values are averaged.

2.2 Antibacterial polymers

2.2.1 Viable Colony Counting Technique

The measurements were conducted by Mr Gi-byoung Hwang, working with Prof. Ivan Parkin (University College London) and Dr Elaine Allan (UCL Eastman Dental Institute). All the bacteria analysis was performed using a standard microbiology technique, which is to use serial dilution, followed by a viable colony counting technique, on an agar medium. It is crucial that the number of colony forming units (CFU) is neither too high nor too low. Incubation of an agar plate with a concentration higher than 10^6 CFU·mL^{-1} will cause excessive bacterial growth which reduces the counting accuracy. When the number of colonies is too low, the statistical significance of the estimated colony number will also be low. To avoid these problems, the inoculum of bacterial cell culture needs to be diluted to a suitable concentration. This concentration is usually achieved by carrying out 10-fold dilutions of the solution, with each dilution plated and incubated. After 24 h incubation, at least one plate with a countable number of colonies should be present. The number of colony forming units is then multiplied by the dilution faction to extrapolate the colony count in the undiluted solution.

In this thesis, the bactericidal activity of the samples was tested on *Escherichia coli* (strain ATCC 25922).[8] The counting method was based on a standard dynamic shake flask method.[9] In this method, the samples were placed in direct contact with a bacterial liquid suspension subjected to vigorous shaking to assure the best contact between bacteria and samples. A bacterial liquid suspension with 10^5 $CFU \cdot mL^{-1}$ bacteria was used for incubation with the polymer samples.

Experimental data were subjected to statistical analysis to determine the significance of any decrease in CFU. The statistical analysis used is a non-parametric test known as the Mann Whitney U Test, which is employed to compare two different sets of independent data.[10] The test is non-parametric according to the assumption that the data is not normally distributed.

The null hypothesis is

H_0; *'There is no difference between the antibacterial activity (colony counts) of the test samples and the control samples.'*

And the alternative hypothesis is

H_1; *'There is a difference between the antibacterial activity (colony counts) of the test samples and the control samples.'*

All results were calculated from the data of three independent experiments and analysed using SPSS statistical software package (version 12.0, SPSS, Inc. Chicago, IL, USA). The output gives the P value, which helps to determine the significance of the results against the null hypothesis. A P value < 0.05 is considered significant.[11]

2.2.2 Surface Charge Measurements

Antimicrobial polymers have been designed to kill pathogens via a membrane disruption mechanism, where they directly interact with microbial membranes exploiting electrostatic interactions between cationic polymers and anionic membrane surface. The membrane is disrupted by insertion of hydrophobic components into membrane lipid domains.[12-14] The bacterial adhesion step is particularly important, and the bacteria-polymer electrostatic interactions are strongly dependent on the surface charges, which cannot be measured directly.[15] The polymers' zeta potential relates to its surface charge at a solid/liquid interface and is measured experimentally, *e.g.* using streaming current/potential measurements.[16]

The measurements were conducted by Dr Andreas Maunter (University of Vienna), working with Prof. Alexander Bismarck. In this thesis, the surface zeta potential (ζ-potential) of the antibacterial polymers was determined with a SurPASS electrokinetic analyser from Anton Paar (Graz, Austria) from pH 10 to 2 (as controlled by titrating 0.05 mol·L^{-1} KOH and 0.05 mol·L^{-1}HCl). The ζ-potential was determined from the measured streaming current using the Helmholtz-Smoluchowski equation:

$$\frac{\Delta I_{str}}{\Delta P} = \zeta(I_{str})\frac{\varepsilon_0 \varepsilon_r A_c}{\eta L}$$

[I_{str} is streaming current, P is the applied pressure, ε_0 is vacuum permittivity, ε_r is relative liquid permittivity, η is the electrolyte viscosity, A_c is the cross-section of the streaming channel and L is the length of the streaming channel]

2.3 Self-assembled Nanostructures

Amphiphilic molecules are classified as molecules possessing both solvophobic and solvophilic components (hydrophobic and hydrophilic, if the solvent is water). In the case of an aqueous solvent, only the hydrophilic portion is expected to dissolve. The hydrophobic chains pack together, as favoured entropically.[17] Amphiphilic block polymers can self-assemble into a range of morphologies in solution, including spherical micelles, cylindrical micelles and polymersomes.[18]

2.3.1 Dynamic Light Scattering (DLS)

DLS is a common technique used to determine the size of self-assembled nanostructures formed from amphiphilic polymers. DLS works by measuring the speed at which the particles diffuse by Brownian motion. This is achieved by measuring the rate at which the intensity of the scattered light fluctuates when detected at a specified scattering angle.

In this thesis, DLS was used to determine the hydrodynamic radius (R_h) and polydispersity of the self-assembled nanostructures (*i.e.* micelles and vesicles) formed from an amphiphilic block poly(phosphoester-*b*-carbonate-*b*-phosphoester) or an alternating polyester in aqueous solution. DLS was also used to monitor the enzymatic biodegradation of poly(phosphoester-b-carbonate-b-phosphoester) by monitoring the change in hydrodynamic radius (R_h) and polydispersity. The DLS measurements were conducted using a Zetasizer Nano series instrument (Malvern Instrument). The scattering angle was set at 173^o for analysis. Data processing was carried out using cumulant analysis of the experimental correlation function and analysed *via* the Stokes-Einstein equation.

$$< R_h >= \frac{k_B T}{6\pi\eta D}$$

[k_B is the Boltzmann constant, T is the absolute temperature, η is the viscosity of the solvent and D is the diffusion coefficient]

2.3.2 Zeta potential

Zeta potential provides a way to measure the magnitude of the electrostatic or charge interactions between particles, which could, in turn, describe the stability of particles in emulsions or suspensions. Higher net charge means that there is more strong electrostatic repulsion between the particles, leading to better physical stability. When the charge is low, the particles tend to aggregate.

In this thesis, the physical stability of the vesicles formed from poly(phosphoester-*b*-carbonate-*b*-phosphoester) and the polyester micelles were characterised using a Zetasizer Nano series instrument (Malvern Instruments).

2.3.3 Transmission Electron Microscope (TEM)

In this thesis, conventional TEM is used to study the morphology of the self-assembled nanostructures, using both poly(phosphoester-*b*-carbonate-*b*-phosphoester) and alternating polyesters. The characterisation of vesicles and micelles formed from the poly(phosphoester-*b*-carbonate-*b*-phosphoester) was conducted by Dr Edward R. White (Imperial College London) and Dr Mahmoud Ardakani (Imperial College London) using a JEOL JEM 2100F scanning transmission electron microscope, equipped with an Oxford X-Max 80 SDD EDX detector, at an operating voltage of 200 kV. The characterisation of micelles formed from alternating polyesters was conducted by Miss Tianyi Chen (working with Prof. Peter Nellist at University of Oxford) on a JEOL 3000F scanning transmission electron microscope, equipped with an Oxford X-Max 80 SDD EDX detector. During sample preparation, an electron scattering heavy-

metal compound, uranyl acetate, was used to stain the polymer and to enhance the contrast for visualisation of the nanostructures.

In this thesis, TEM is mainly used to visualise the individual nanostructure so as to define whether micelle or vesicle formation occurs. Polymer vesicles are hollow spheres with a hydrophobic bilayer membrane and hydrophilic internal and external coronas.[18] This hollow structure is different from polymer micelles which consist of a solid hydrophobic core.[18] It is worth mentioning that the TEM images only provide a representative morphology of a very small part of the sample. Any structural hypothesis should be supported by a bulk technique, such as DLS.

2.3.4 Fluorescence Spectroscopy

Of all the methods used to assess drug release from polymeric self-assembled nanostructures, dialysis is the most versatile and popular.[19] In this method, physical separation of the nanostructures is achieved by the use of a dialysis membrane which allows for sampling at periodic intervals. As the encapsulated drug releases from the nanostructures, it diffuses from the dialysis tube, and the concentration of the drug outside the tube continuously increases during the experimental period.

2.3.4.1 Drug loading efficiency

In this thesis, fluorescence experiments were used to evaluate the drug-loading efficiency (DLE) of vesicles formed from poly(phosphoester-*b*-carbonate-*b*-phosphoester). The vesicles were used to encapsulate Rhodamine B (RhB) as a model drug, and its concentration was determined using a pre-obtained calibration curve. The poly(phosphoester-*b*-carbonate-*b*-phosphoester) vesicle solution was incubated with Rhodamine B (RhB) solution at a known concentration. The free drug (not encapsulated) was removed by dialysis, and the vesicle solution was collected and analysed by

fluorescence spectroscopy. Fluorescence wavelengths and intensity values were measured using a Horiba Jobin Yvon FluoroLog-3 spectrophotometer, equipped with a Hamamatsu R928 PMT detector and a double-grating emission monochromator. Emission scan (500-750 nm) mode was used, and λ_{ex} was fixed to be 510 nm. The calibration curve of RhB was obtained by plotting the concentration from 0.02 μg·mL^{-1} to 0.10 μg·mL^{-1} against its respective peak intensities at 591 nm.

The drug loading efficiency (DLE) was calculated using the following equation:

$$\text{DLE}\ (\%) = \frac{M_e}{M_f} \times 100\%$$

[M_e represents the weight of drug encapsulated in vesicles, M_f stands for the starting weight of drug added to the solution]

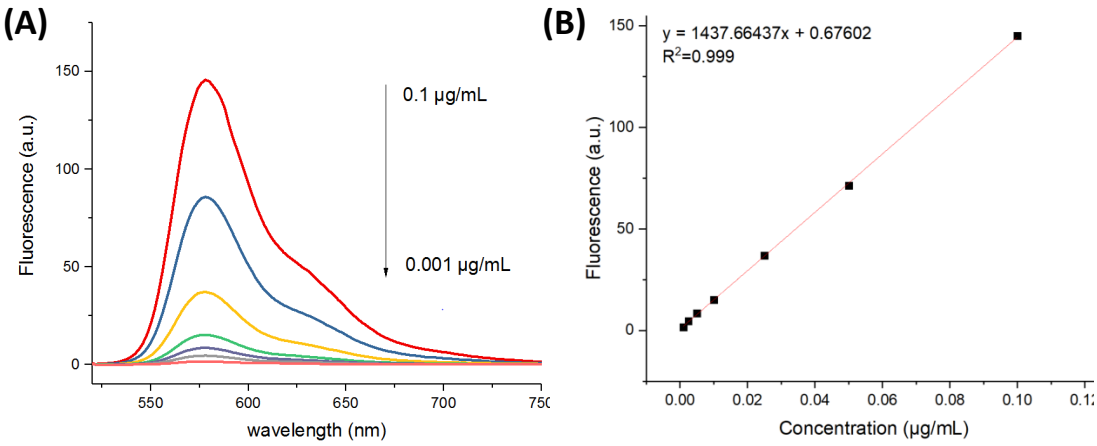


Figure 2.9 The fluorescence spectrum (A) and calibration curve (B) of Rhodamine B (RhB) in PBS solution (10.0 mM, pH 7, λ_{ex} = 510 nm).

2.3.4.2 Drug release

After quantifying the DLE, the RhB loaded vesicle solution was transferred to a clean dialysis tube and dialysed against PBS. Aliquots were taken for fluorescence spectroscopy (λ_{em} = 510 nm) at pre-determined time intervals. The control experiment

uses free RhB delivery without any polymer (*i.e.* a PBS solution containing RhB). The RhB concentration in the control was adjusted to a similar value to that of the RhB loaded vesicle solution, based on the drug loading efficiency.

The percentage release of RhB was calculated according to the equation:

$$\% \text{ cumulative release} = (C_t/C_0) \times 100\%$$

[C_0 is the concentration of encapsulated RhB dye and C_t is the concentration of released RhB dye remaining at time (t)]

2.4 Cell studies

All the cell studies were conducted by Mr Chunching Li (working with Prof. Molly Stevens at Imperial College London) on MC3T3-E1 cells.

2.4.1 Cytotoxicity/Cell Viability Tests

A cytotoxicity test is an important first step in evaluating biocompatibility as it determines cell viability. Reference materials are always included with both a negative (*i.e.* no cytotoxicity response) and positive control (*i.e.* reproducible cytotoxicity) being essential. In this thesis, organo-tin stabilised poly(vinyl chloride) (PVC) is used as the positive control and high-density polyethylene (PE) as the negative control.

2.4.1.1 AlamarBlue™ Reduction Test

The alamarBlue™ reduction test is used to assess cell metabolic activity and establish the reducing power of living cells to infer metabolic activities.[20] The alamarBlue™ contains Resazurin which is reduced to Resorufin by mitochondrial activity. The reduction results in a colour change from non-fluorescent blue to highly fluorescent red. Absorbances at 570 nm and 600 nm were measured using a Perkin Elmer Envision multimode plate reader, and the readings of the wells containing cells

alone and cells incubated with test samples were used to determine the relative levels of metabolic activity.

2.4.1.2 LIVE/DEAD Viability Assay

The LIVE/DEAD viability assay was performed to visualise the ratio of viable and dead cells, after the treatment with the polymer. Calcein-AM, a non-fluorescent dye, is used to assess live cells.[21] Intracellular esterases, result in live cells taking up Calcein-AM and hydrolysing it to its green fluorescent anion, Calcein. Dead cells are stained using ethidium homodimer (EthD-1) which cannot penetrate the cell membrane and thus only enters cells with damaged membranes. Upon binding to nucleic acids, it produces a bright red fluorescence, indicating cell death. It needs to be noted that the background fluorescence levels are relatively low using this technique. The measurement was carried out using an Olympus BX-51 reflected fluorescence microscope (Olympus UK Ltd., London) within 30 min after staining.

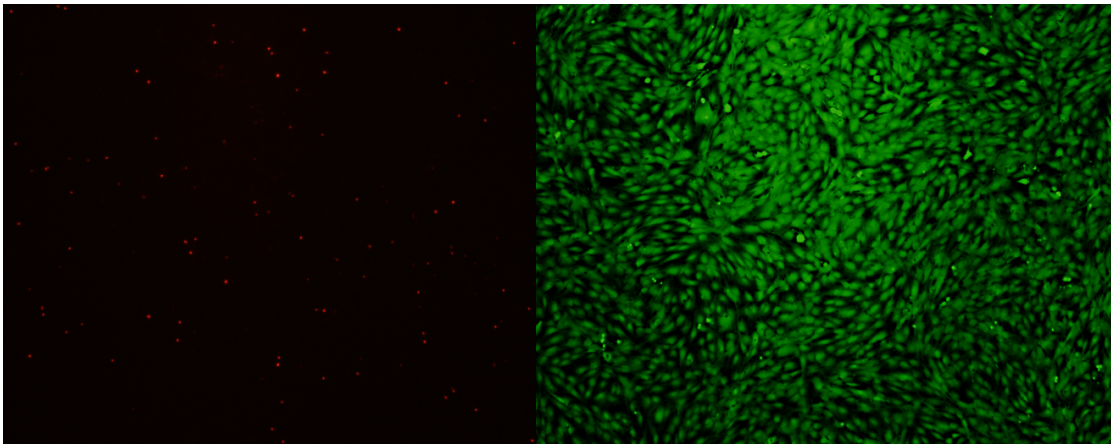


Figure 2.10 Example of images of the dead (red, left) and live (green, right) MC3T3-E1 cells on PC surfaces after 72 h incubation.

2.4.2 Cell Attachment Tests

Most tissue-derived cells need to attach to a solid surface to be viable and to grow. Cell attachment is a crucial precursor to cell spreading, migration and differentiation. Cell attachment to biomaterials is affected by material surface properties such as wettability and chemical functionalities.[22] Direct visualisation of cell attachment was achieved using a Leica SP5 MP/FLIM inverted confocal microscopy. In particular, any changes in cell morphology were used to study cell attachment. If there is a favourable interaction, cells contact the surfaces, form an initial attachment and then exert tension to induce outward movement and acquire a flattened morphology. In contrast, unattached cells tend to be rounded.

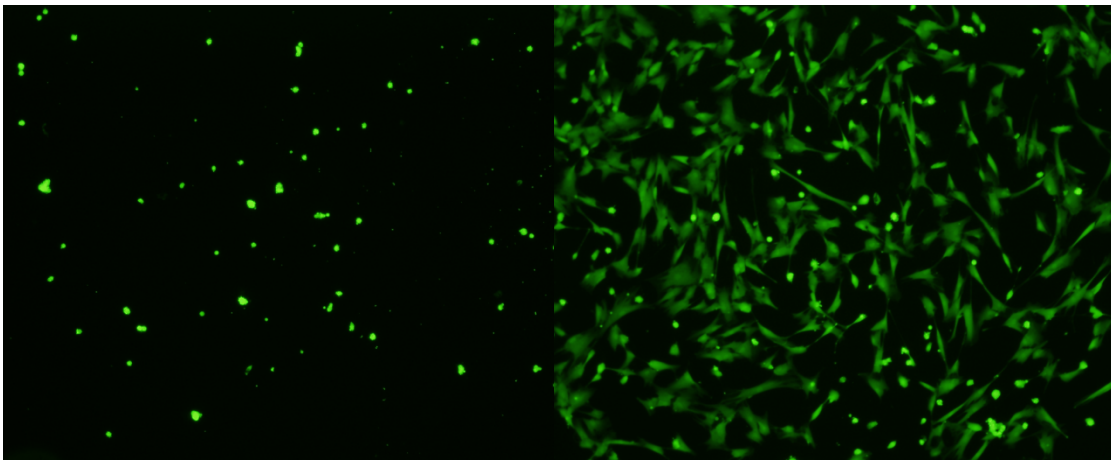


Figure 2.11 Example of confocal microscopy images of unattached (left, non-tissue-treated cell well) and attached (right, tissue-treated cell well) MC3T3-E1 cells.

2.5 References

1. A. Spyros, D. S. Argyropoulos and R. H. Marchessault, *Macromolecules*, 1997, **30**, 327-329.
2. R. K. Dean, L. N. Dawe and C. M. Kozak, *Inorg. Chem.*, 2012, **51**, 9095-9103.
3. K. Nakano, M. Nakamura and K. Nozaki, *Macromolecules*, 2009, **42**, 6972-6980.

4. M. R. Kember and C. K. Williams, *J. Am. Chem. Soc.*, 2012, **134**, 15676-15679.
5. A. Buchard, F. Jutz, M. R. Kember, A. J. P. White, H. S. Rzepa and C. K. Williams, *Macromolecules*, 2012, **45**, 6781-6795.
6. F. Jutz, A. Buchard, M. R. Kember, S. B. Fredrickson and C. K. Williams, *J. Am. Chem. Soc.*, 2011, **133**, 17395–17405.
7. H. Sugimoto and K. Kuroda, *Macromolecules*, 2008, **41**, 312-317.
8. T. D. Minogue, H. A. Daligault, K. W. Davenport, K. A. Bishop-Lilly, S. M. Broomall, D. C. Bruce, P. S. Chain, O. Chertkov, S. R. Coyne, T. Freitas, K. G. Frey, H. S. Gibbons, J. Jaissle, C. L. Redden, C. N. Rosenzweig, Y. Xu and S. L. Johnson, *Genome Announce.*, 2014, **2**, e00969-00914.
9. D. Ochs, *Plastics Additives Handbook*, 2000, 647-680.
10. H. B. Mann and D. R. Whitney, *Ann. Math. Stat.*, 1947, **18**, 50-60.
11. J. D. Storey and R. Tibshirani, *Proc. Natl. Acad. Sci. U. S. A.*, 2003, **100**, 9440-9445.
12. A. C. Engler, J. P. K. Tan, Z. Y. Ong, D. J. Coady, V. W. L. Ng, Y. Y. Yang and J. L. Hedrick, *Biomacromolecules*, 2013, **14**, 4331-4339.
13. Y. Qiao, C. Yang, D. J. Coady, Z. Y. Ong, J. L. Hedrick and Y.-Y. Yang, *Biomaterials*, 2012, **33**, 1146-1153.
14. F. Nederberg, Y. Zhang, J. P. K. Tan, K. Xu, H. Wang, C. Yang, S. Gao, X. D. Guo, K. Fukushima, L. Li, J. L. Hedrick and Y.-Y. Yang, *Nat. Chem.*, 2011, **3**, 409.
15. H. Murata, R. R. Koepsel, K. Matyjaszewski and A. J. Russell, *Biomaterials*, 2007, **28**, 4870-4879.
16. R. J. Hunter, in *Zeta Potential in Colloid Science*, Academic Press, 1981, pp. 179-218.
17. A. Blanazs, S. P. Armes and A. J. Ryan, *Macromol. Rapid Commun.*, 2009, **30**, 267-277.
18. J. Du and R. K. O' Reilly, *Soft Matter*, 2009, **5**, 3544-3561.
19. P. Calvo, J. L. Vila-Jato and M. J. Alonso, *J. Pharm. Sci.*, 1996, **85**, 530-536.
20. J. O'Brien, I. Wilson, T. Orton and F. Pognan, *Eur. J. Biochem.*, 2000, **267**, 5421-5426.
21. M. Berney, F. Hammes, F. Bosshard, H.-U. Weilenmann and T. Egli, *Appl. Environ. Microbiol.*, 2007, **73**, 3283-3290.

22. K. Webb, V. Hlady and P. A. Tresco, *J. Biomed. Mater. Res.*, 1998, **41**, 422-430.

Chapter 3

Syntheses and Functionalisations of Poly(ester-*b*-carbonate-*b*-ester) for Antibacterial Applications

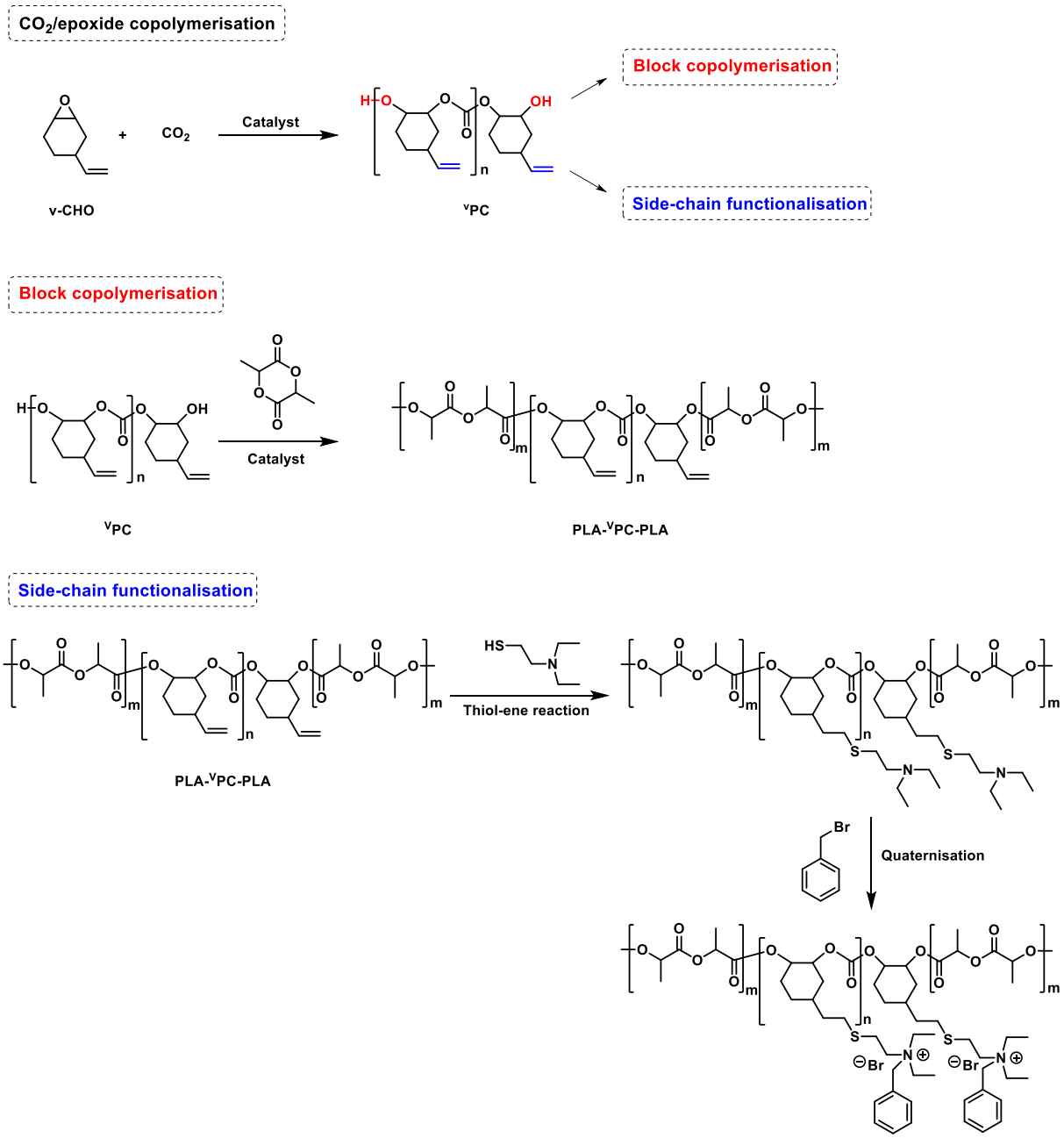
3.1 Background and Aims

Cationic polycarbonates, prepared using ROP, have been investigated as antimicrobial materials.[1-3] However, antimicrobial alternating polycarbonates are much less explored.[4] The goal of this work is to prepare a series of degradable alternating polycarbonates and block polymers to target antibacterial coating materials. In terms of designing antimicrobial polymers, two features are particularly important: cationic substituents and hydrophobic groups.[5, 6] Block poly(ester-*b*-carbonate-*b*-ester) polymers will be targeted, where the carbonate block delivers the antibacterial activity, and the ester block delivers the hydrophobicity. PLA is selected as the polyester block as it is FDA approved and widely applied in packaging and wound healing applications.[7, 8]

The synthesis of ABA block poly(ester-*b*-carbonate-*b*-ester)s, using PLA as the ester block, has been previously reported.[9, 10] However, these polymers were not functionalised and no further application was reported. In this work, the synthesis of an alkene-substituted poly(ester-*b*-carbonate-*b*-ester) is proposed, where the alkene groups offer the potential for post-polymerisation modification to include cationic functionalities to target antibacterial properties.

The proposed synthetic routes are summarised in Scheme 3.1. Firstly, a telechelic, alkene-bearing polycarbonate (^{V}PC) will be synthesised using ring-opening copolymerisation (ROCOP) of CO_2 and vinyl-cyclohexene oxide (v-CHO). This polymer will then be used as a macroinitiator in the ROP of LA to yield PLA-^{V}PC-PLA. The functionalisation of alkene groups will be explored so as to attach cationic groups. Quaternary ammonium groups are targeted as they are positively charged and are not strongly affected by pH, which may allow better interactions with the anionic

bacterial cell wall.[11, 12] Finally, the antibacterial activities of these polymers will be tested in the form of coatings, and the effect of quaternisation degree on antibacterial activities will be studied.

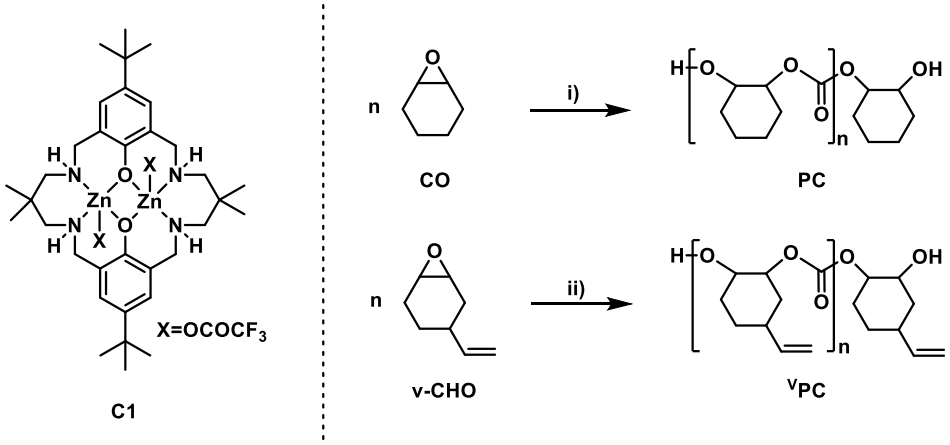


Scheme 3.1 Structures of polymers targeted in this work.

3.2 Results and Discussion

3.2.1 The ROCOP of carbon dioxide and vinyl cyclohexene oxide (v-CHO)

The Williams group have previously reported a di-zinc catalyst, **C1**, which is an effective homogeneous catalyst for the ring-opening copolymerisation (ROCOP) of cyclohexene oxide (CHO) and carbon dioxide.[13-15] It shows a high selectivity in the synthesis for dihydroxyl end-capped polycyclohexene carbonate (PC).[13-15] To further test the catalytic activity in ROCOP of v-CHO and CO_2, **C1** was synthesised according to the reported procedure (See Chapter 7 for more details).



Scheme 3.2 Shows the chemical structure of catalyst (**C1)**, and the ROCOP of CHO/v-CHO and CO_2 to produce poly(cyclohexene carbonate) (PC) and poly(vinyl-cyclohexene carbonate) (^{V}PC). Reaction conditions: i) and ii) [**C1**]/[epoxide]=1/1000, 80 ºC, 1 bar CO_2, 18 h.

C1 showed a good performance using v-CHO, achieving a turnover frequency (TOF) of 24.0 ± 0.8 h^{-1}, at 1 bar CO_2 pressure, which is an activity in-line with previous reports.[15] It should be noted that the activity using v-CHO is more difficult to quantify precisely due to significant overlap of monomer and polymer resonances in the crude ^{1}H NMR spectrum (Figure 3.1). The final polymer shows a very high selectivity for carbonate linkages (≥ 99%), within the detection limit of NMR spectroscopy, *i.e.* they did not show any ether signals at 3.45-3.55 ppm in the ^{1}H NMR spectrum (Figure 3.1).

C1 was also highly selective towards polymer formation (≥ 99%) with negligible formation of cyclic carbonate by-product (≤ 1%), observable by a peak at 4.0 ppm in the ^{1}H NMR spectrum.

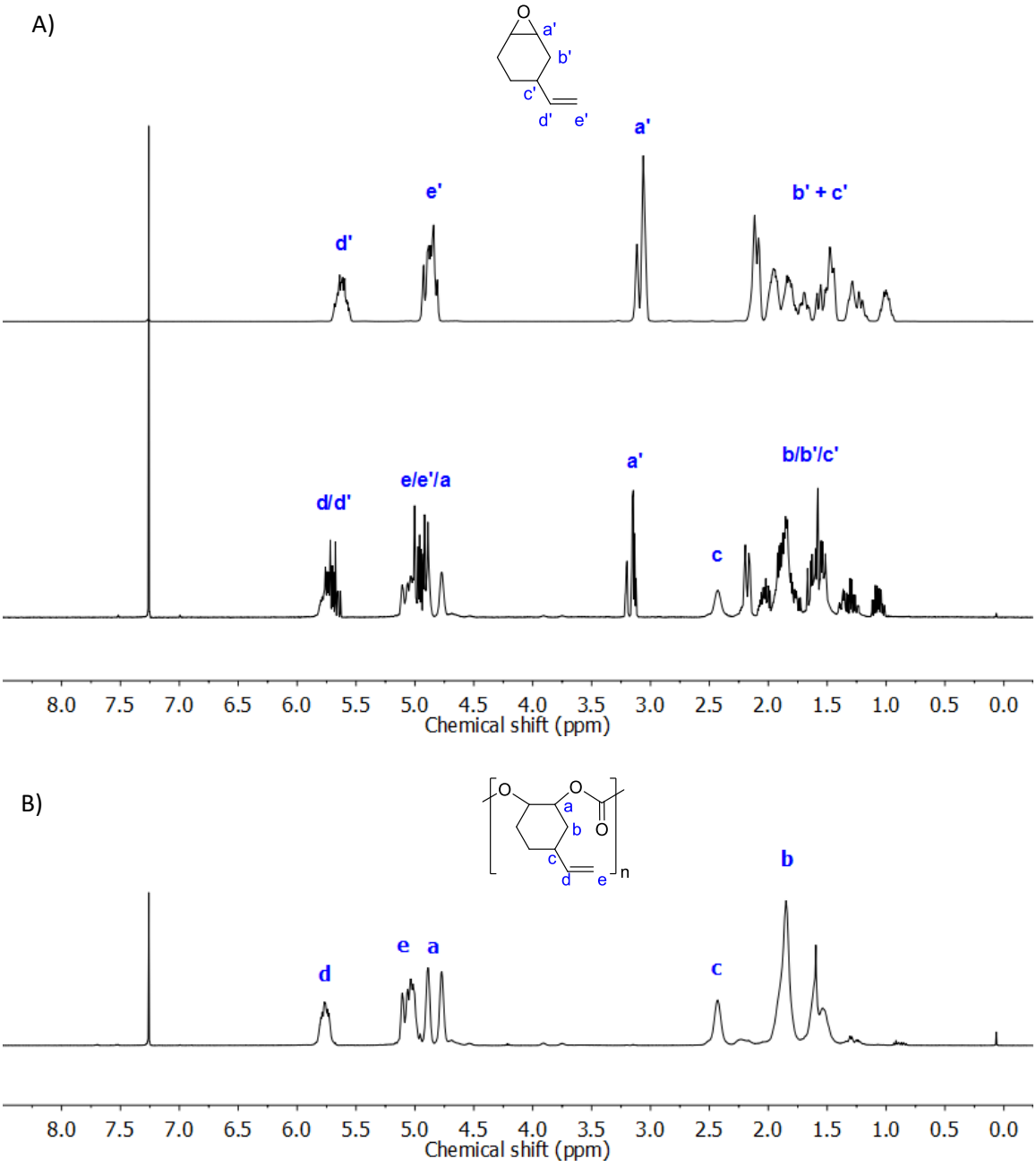


Figure 3.1 A) Overlaid ^{1}H NMR spectra of v-CHO monomer and crude ^{V}PC reaction mixture (400.0 MHz, $CDCl_3$, 25 ºC). The conversion of v-CHO to ^{V}PC was calculated by the ratio of the integrals of peak 'c' to the integrals of peaks d + d'. B) ^{1}H NMR spectrum of isolated ^{V}PC (400.0 MHz, $CDCl_3$, 25 ºC).

The ^{V}PC showed a moderate molar mass (M_n = 6.7 kgmol^{-1}) and a narrow dispersity (Đ = 1.18), as determined by Size Exclusion Chromatography (SEC), calibrated using polystyrene standards. Nonetheless, a bimodal molar mass distribution was observed, which has also been reported for PC using the same catalyst.[13] In the previous study, two fractions of PC containing the higher and lower M_n distributions were separated by preparative SEC. These fractions were analysed by ^{1}H and ^{19}F{^{1}H} NMR spectroscopy, MALDI-ToF and SEC. For both fractions, the ^{1}H NMR spectra were identical, indicating PC end-capped with hydroxyl groups. The bimodality was then attributed to two different types of initiating groups, one from trifluoroacetate (co-ligand of **C1**, that undergoes hydrolysis during workup) and the other from dihydroxyl groups (1,2-diols).[13] The characterisation data for ^{V}PC are also consistent with the hydrolysis of the trifluoroacetate end group. It is proposed that the trifluoroacetates are susceptible to hydrolysis during work-up, particularly as the ester is activated by the electron-withdrawing substituents.[13] A related observation regarding the ease of hydrolysis of trifluoroacetate end-groups was also noted by Darensbourg and co-workers, whereby salen-chromium(trifluoroacetates) catalysed ROCOP of CO_2 and CHO also resulted in the production of di-hydroxyl end-capped polycarbonates with a bimodal molar mass distribution.[16] The trifluoroacetate end-group was identified prior to hydrolysis using anhydrous electrospray mass spectrometry.[16]

The important outcome of the formation of dihydroxyl end-capped polymers is that they can act as precursors in the production of polymers with higher molar mass. It has previously been demonstrated that such polyols are viable initiators for lactide ring-opening polymerisations (ROP), upon addition of a second ROP catalyst, to produce ABA type triblock copoly(ester-*b*-carbonate-*b*-esters).[15]

3.2.2 Syntheses of Block Copolymers PLA-^{V}PC-PLA

The synthesis of PLA-^{V}PC-PLA was then attempted using ^{V}PC macro-initiator. Before preparing any triblocks, it was important to prepare ^{V}PC with monomodal molar mass distribution so as to avoid issues of initiation efficiency and dispersity differentiation in the PLA-^{V}PC-PLA. Previously, Darensbourg and co-workers reported a route to produce polypropylene carbonate (PPC) with a monomodal molar mass distribution by adding 5-20 equivalents (vs. catalyst) of alcohol (as chain transfer agent (CTA)) to the polymerisation.[16] By analogy, the addition of excess CTA would be expected to give ^{V}PC with monomodal molar mass distribution.

The polymerisations were tested with the addition of 5 or 10 equiv. of cyclohexene-diol (CHD) and resulted in polymers maintaining high carbonate linkage contents (> 99%) and a negligible amount of cyclic carbonate (< 1%). Importantly, the addition of 10 equiv. of CHD produced ^{V}PC with monomodal molar mass distributions, as qualified by SEC.

Table 3.1 Polymerisation data obtained from ROCOP of v-CHO and CO_2 with or without the use of CHD as CTA.[a]

Entry	**C1**/diol/v-CHO (equiv.)	% carbonate[b]	% cyclic carbonate[b]	M_n(kgmol^{-1}) (Đ)[c]
1	1/0/1000	> 99	< 1	6.7 (1.18)
2	1/5/1000	> 99	< 1	7.5 (1.21)
3	1/10/1000	> 99	< 1	5.7 (1.17)

[a] Ring-opening copolymerisations were carried out at 80 °C, under 1 bar of CO_2. [b] Determined by comparing the integrals of resonances at 4.75-4.90 ppm (^{V}PC), at 4.00 ppm (cyclic carbonate by-product) and at 3.45 ppm (ether linkages).[c] Determined by SEC, in THF using monodispersed polystyrene standards.

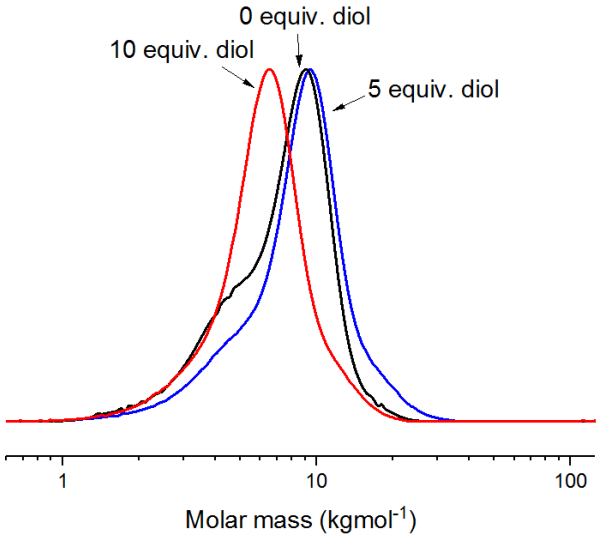


Figure 3.2 Overlaid SEC traces of ^{V}PC produced in the presence of diols (Table 3.1 Entries 1-3).

The isolated polymer (5.7 kgmol^{-1}, Đ = 1.17) was analysed using MALDI-ToF-MS, and two series of chains were observed (Figure 3.3). One corresponded to ^{V}PC chains initiated from a cyclohexane diol moiety, while the other corresponded to chains initiated from v-CHD, *i.e.* the series differed only in the telechelic initiating group. In both cases, ^{V}PC was dihydroxyl-end capped, and thus, it was subsequently used as a macroinitiator for triblock copolymerisation with *rac*-LA using an organocatalyst, 1,5,7,-triazabicyclo[4.4.0]dec-5-ene (TBD), which have been widely used in the ROP of cyclic esters. [17-21]

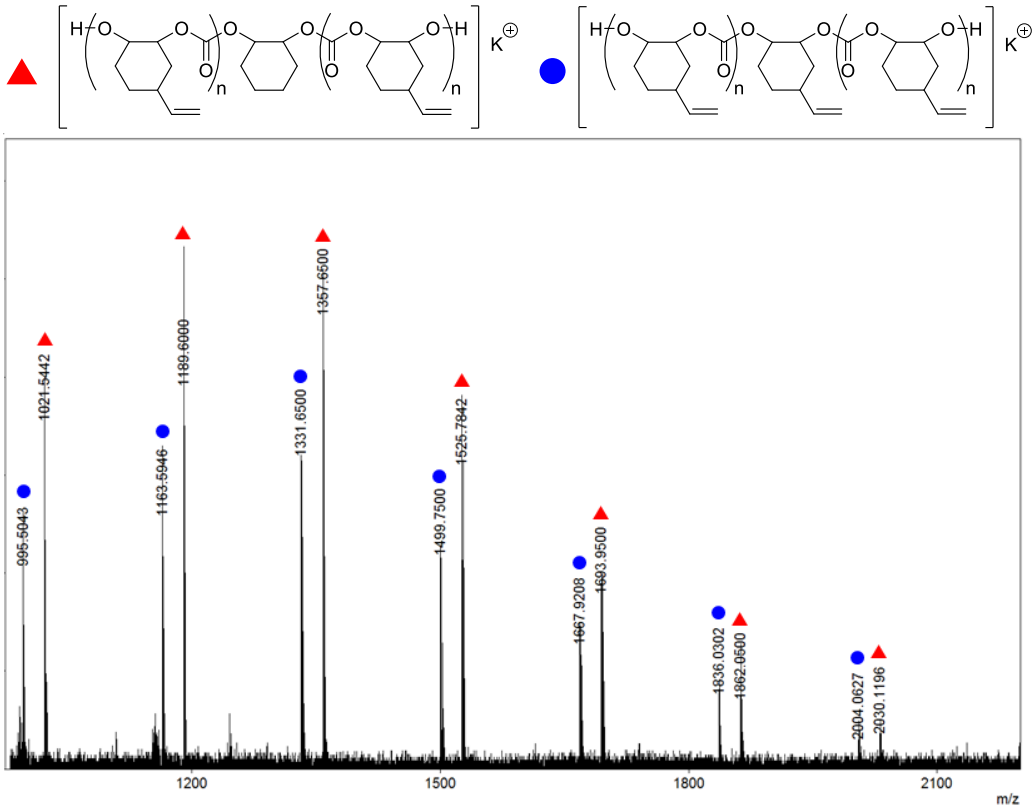


Figure 3.3 MALDI-ToF spectrum of ^{V}PC synthesised with CHD as CTA (5.7 kgmol^{-1}, Đ = 1.17). The major series (red triangles) is assigned to chains initiated by CHD, which are calculated according to: $[(C_9H_{12}O_3)_nC_6H_{12}O_2]K^+$. The minor series (blue circles) consists of α, ω-hydroxyl end-groups, which are calculated according to: $[HO(C_9H_{12}O_3)_nC_8H_{14}O_2]K^+$.

A series of different ABA triblocks was prepared, with controllable compositions and over a range of molar masses from 12.2 to 51.8 kgmol^{-1}, all showing low/moderate dispersities (Đ ≤ 1.30). Figure 3.4 illustrates data demonstrating that all the ROP reactions are well controlled and proceed with a linear increase in molar mass vs. [*rac*-LA]/[^{V}PC]. A reasonable agreement between theoretical and experimental molar masses was observed, as expected for a living polymerisation.

Table 3.2 Polymerisation data for triblock PLA-^{V}PC-PLA[a]

Polymer	$\overline{DP}$	Molar ratio of carbonate: ester linkages[d]	$M_{n,calc}$[e] (kgmol^{-1})	M_n[f] (kgmol^{-1})	Đ[f]
^{V}PC	34[b]	1:0	5.8	5.1	1.17
P1	43[c]	1:2	12.0	12.2	1.24
P2	93[c]	1:3	19.2	16.8	1.30
P3	192[c]	1:9	33.6	30.2	1.29
P4	291[c]	1:10	47.8	44.4	1.30
P5	390[c]	1:20	62.4	51.8	1.28

[a] Reaction conditions: ^{V}PC/TBD = 1/2, $[LA]_0$ = 0.25 M in THF, 25 °C. [b] Calculated on the basis of the ^{1}H NMR integrals of ^{V}PC main chain and end group methine signals (peaks 'c', 'd' and 'e' in Figure 3.5). [c] Calculated on the basis of the ^{1}H NMR integrals of PLA main chain and end group methine signals (peaks 'g' and 'f' in Figure 3.5). [d] Determined by ^{1}H NMR spectroscopy by comparison of the normalised integrals for the ^{V}PC alkene signals at 5.76 ppm and the PLA methine signals at 5.17 ppm. [e] Calculated M_n value obtained from the relation $M_{n,calc}$(^{V}PC) + [LA conversion × M_w(LA)].
[f] Determined using SEC in THF, using monodispersed polystyrene as standard.

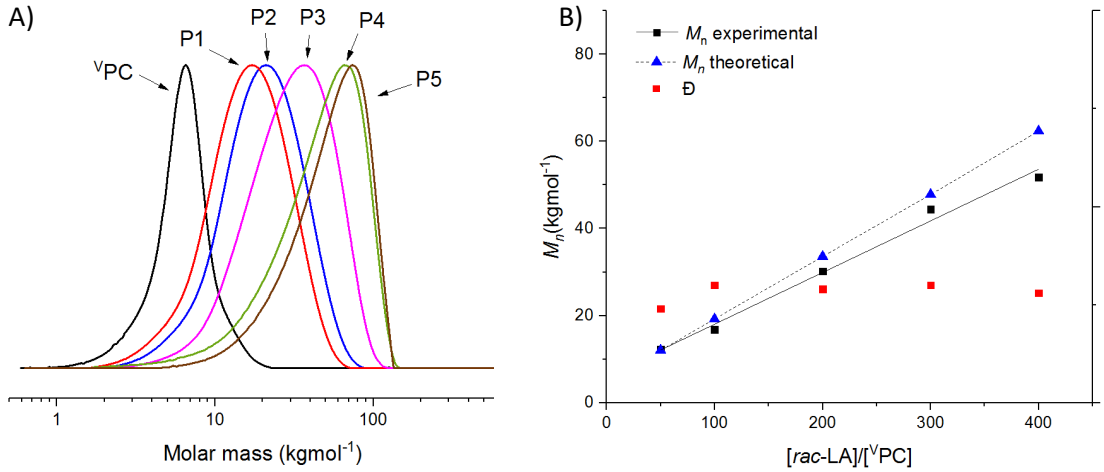


Figure 3.4 A) Overlaid SEC traces of PLA-^{V}PC-PLA formed in Table 3.2. B) Plot of molar masses and dispersities vs. [LA]/[^{V}PC].

The ^{1}H NMR spectrum of the block polymer showed characteristic peaks at 5.15 and 4.89-4.77 ppm, attributed to the main chain methine protons of PLA and ^{V}PC, respectively. The resonances assigned to the ^{V}PC end groups (peaks 'd' and 'e', Figure 3.5) were not observed in the block polymer. A new signal appeared at 4.39

ppm, attributed to the methine proton of the PLA end group. The ^{1}H-^{1}H COSY spectrum showed its correlating ^{1}H resonance at 1.50 ppm, corresponding to the methyl end group signals. The signals of carbonate and ester junction units could not be fully assigned, due to overlap with the alkene group signals. The relative ratio of carbonate: ester linkages in the copolymers was obtained by comparing the integrals for the main chain ester *vs.* carbonate resonances in the ^{1}H NMR spectra (*i.e.* peaks c *vs.* g, Figure 3.5). Thus, the ratio is controlled over the range 1:2 to 1:20, with good agreement between the experimental results and those expected on the basis of polymerisation conversions. The ratios did not change after purification of the copolymers by repetitive precipitation in hexane, which is another strong indicator of block polymer formation. The molar masses all showed clear increases from the polycarbonate macro-initiator to the triblocks, consistent with successful block formation (Figure 3.4).

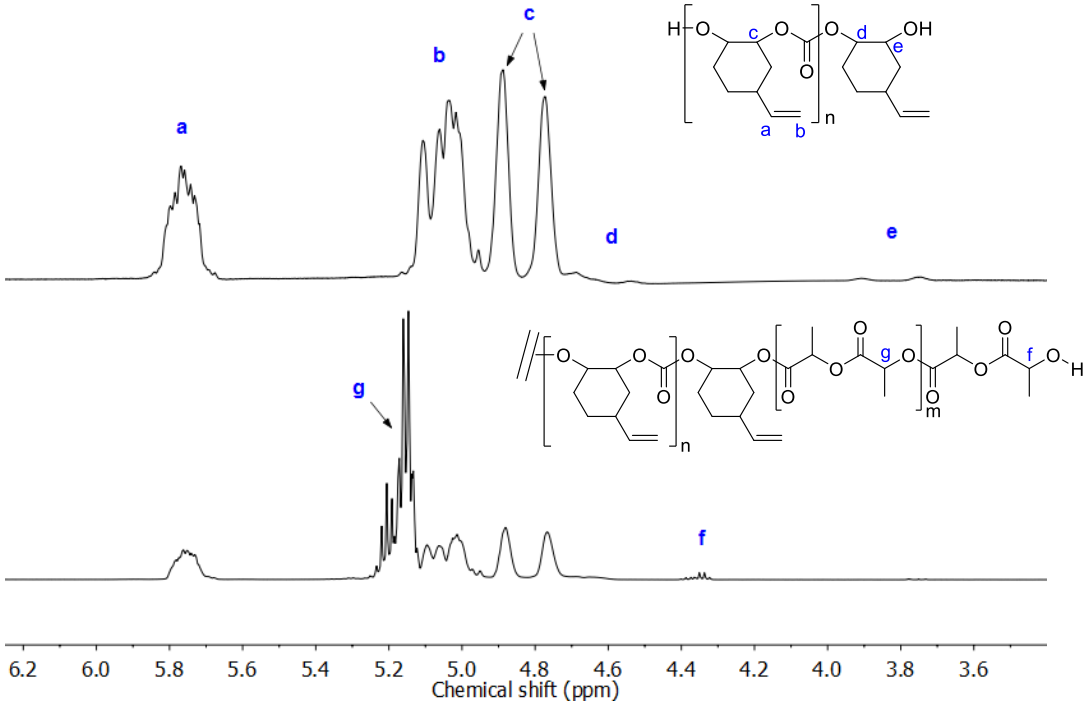


Figure 3.5 ^{1}H NMR spectrum of ^{V}PC showing ^{V}PC end group (peaks 'd' and 'e') and main chain (peak 'c') methine protons, and PLA-^{V}PC-PLA showing PLA main chain (peak 'g') and end group (peak 'f') methine protons (400.0 MHz, $CDCl_3$, 25 ºC).

The $^{13}C\{^{1}H\}$ NMR spectrum of the block copolymer shows two main signals in the carbonyl region. The peak at 153.3 ppm was assigned to the carbonyl signals of ^{V}PC, and those centred at 169.1 ppm were from PLA. Transesterification between the ^{V}PC and PLA blocks would result in the formation of new peaks, typically showing resonances at intermediate chemical shifts between those of the homopolymers. No such signals were observed, suggesting that no significant transesterification was occurring. Multiple peaks observed for the PLA and ^{V}PC blocks are presumably due to a range of different regio- and stereo-structures (*i.e.* PLA and ^{V}PC are atactic).

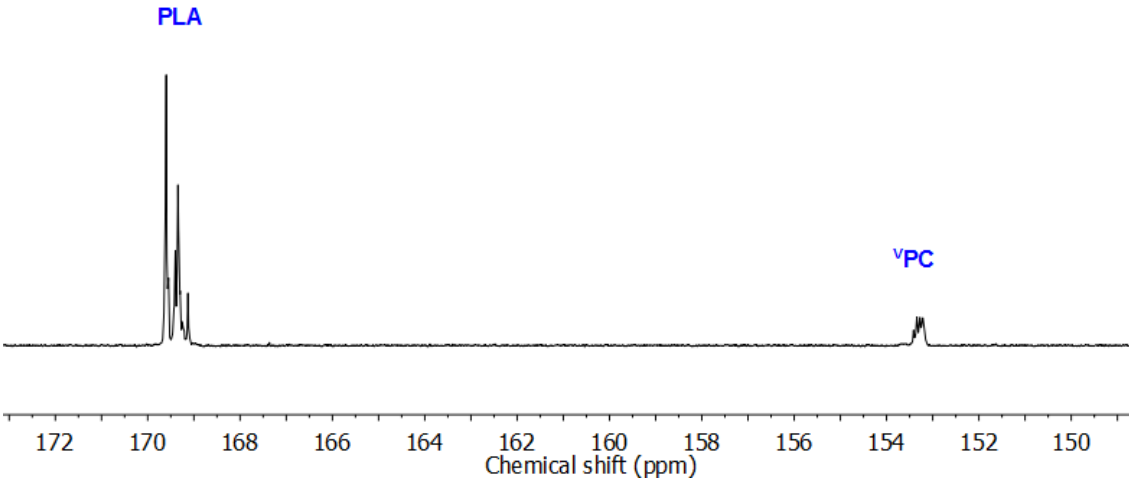


Figure 3.6 $^{13}C\{^{1}H\}$ NMR spectrum showing the carbonyl region of PLA-^{V}PC-PLA (51.8 kgmol^{-1}, Đ = 1.28, $CDCl_3$, 100.7 MHz, 25 ºC).

^{1}H DOSY NMR spectroscopy can be used to distinguish the formation of a block copolymer vs. the formation of homopolymers. A block copolymer should result in a single diffusion coefficient for the signals of both ^{V}PC and PLA. Indeed, the ^{1}H DOSY NMR spectrum shows exactly this effect with signals for PLA and ^{V}PC blocks diffusing at the same rate; these data suggest the successful formation of a block copolymer. In the control experiment, using pure ^{V}PC and PLA of near equivalent molar mass, showed that the ^{1}H NMR signals of different polymers exhibit different diffusion coefficients.

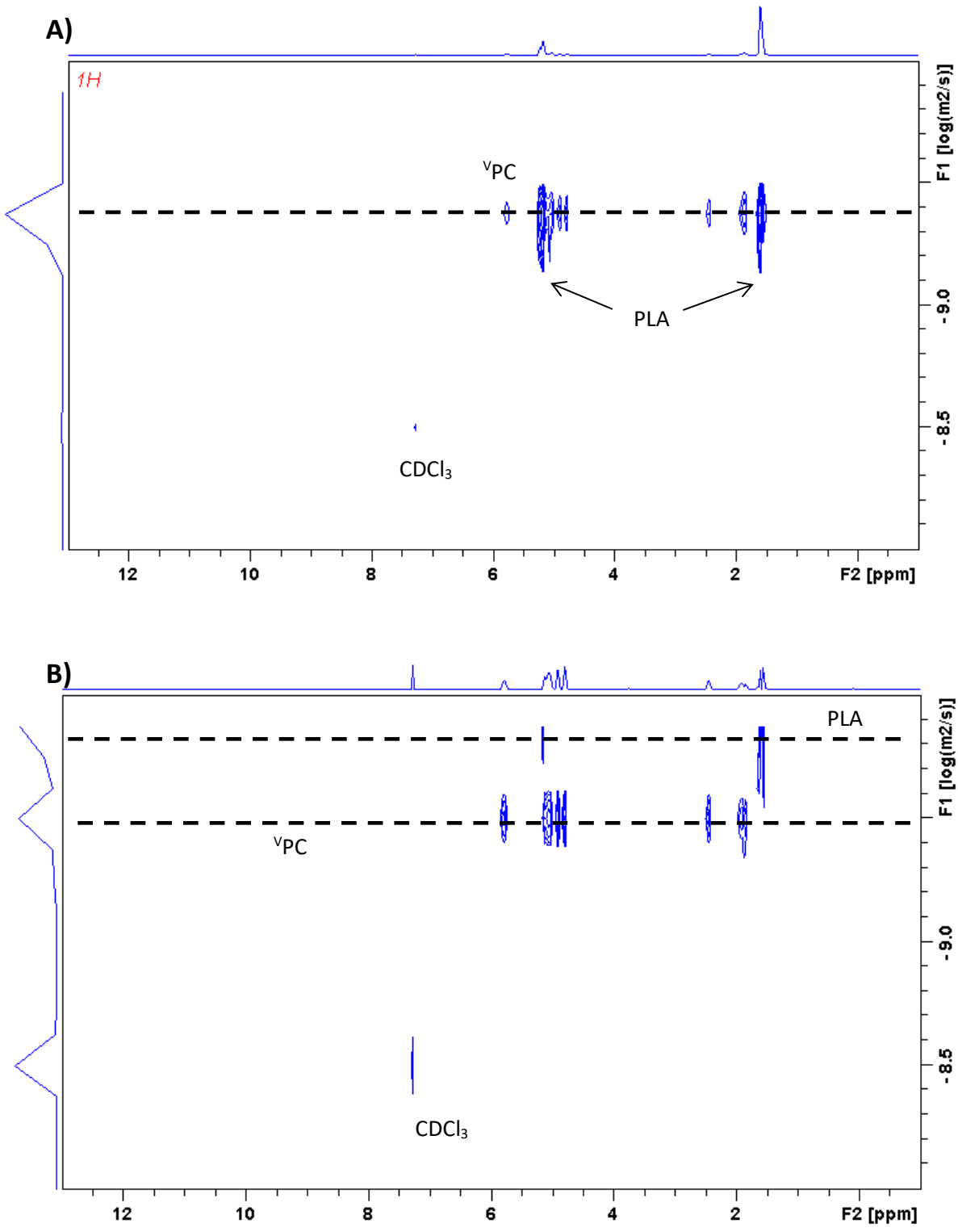


Figure 3.7 ^{1}H DOSY NMR spectra of A) PLA-^{V}PC-PLA (51.8 kgmol^{-1}, Đ = 1.28) and B) a mixture of ^{V}PC and PLA (control).

To further characterise the putative block copolymer, ^{31}P NMR spectroscopy can be used to carry out end group analysis (See Chapter 2). The $^{31}P\{^{1}H\}$ spectrum shows a single resonance at 147.2 ppm, which was assigned to the end group of PLA-^{V}PC-PLA. In comparison, ^{V}PC showed signals at 146.8-146.6 ppm, and PLA showed signals at 147.2 ppm. The result suggests that all the ^{V}PC secondary hydroxyl groups are consumed, and only the PLA hydroxyl groups are detected. These findings reinforce the successful formation of a triblock copolymer, without significant/detectable contamination by diblock copolymers (PLA-^{V}PC) or homopolymers.

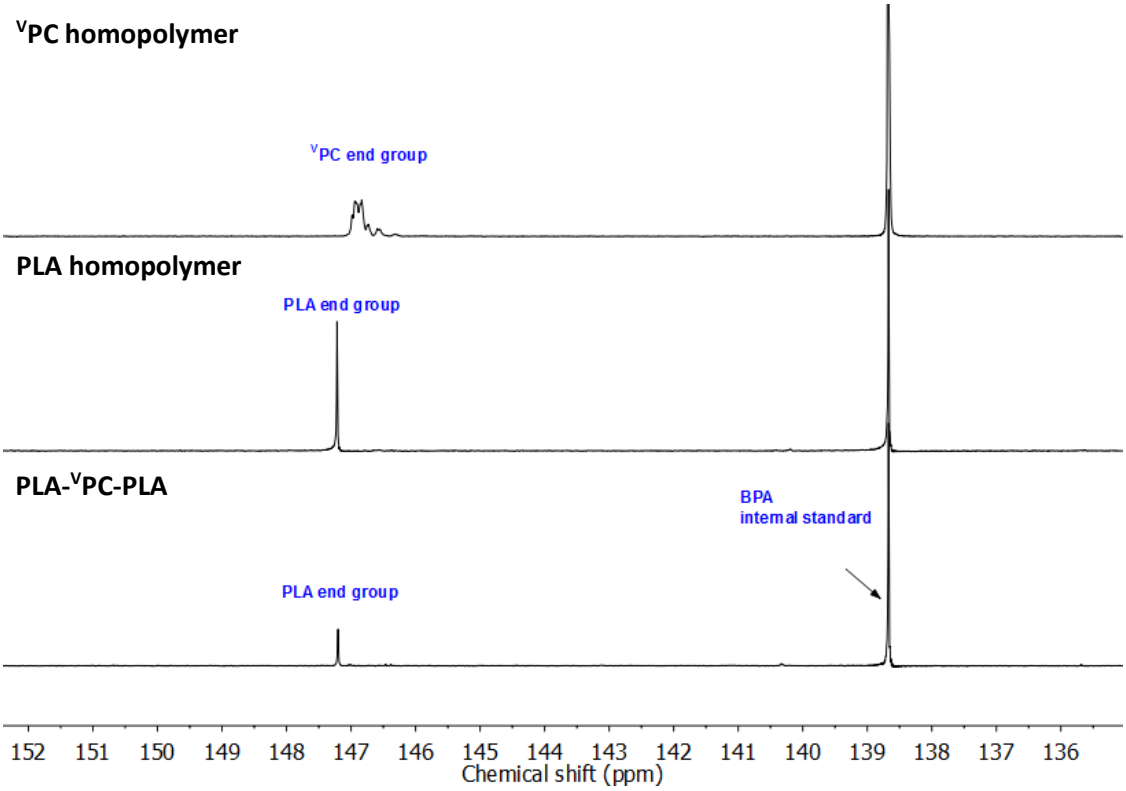
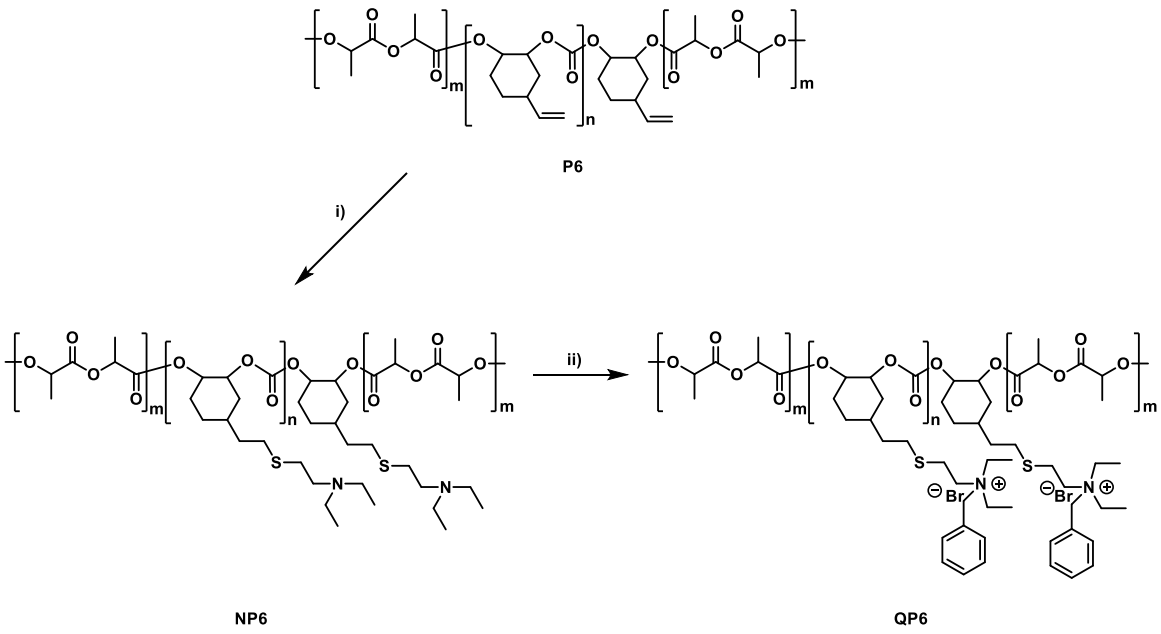


Figure 3.8 Selected region of $^{31}P\{^{1}H\}$ NMR spectra of the product of the reactions between the polymer end groups and 2-chloro-4,4,5,5-tetramethyl dioxaphospholane. ^{V}PC and PLA hydroxyl end groups can be observed at 146.8-146.6 ppm and 147.2 ppm respectively. Bisphenol A (BPA) was used as an internal standard (162.1 MHz, $CDCl_3$, 25 ºC).

3.2.3 Post-polymerisation Modifications

The vinyl group on the central block of PLA-^{V}PC-PLA can easily be transformed into a variety of functional groups.[22] Here, the transformations were used to install functional groups useful for exhibiting antibacterial activity. In particular, the addition of tertiary amine groups, installed *via* the thiol-ene reaction, and their subsequent quaternisation are investigated.



Scheme 3.3 Schematic illustration of the route to NP6 and QP6. Reactions conditions: i) [C=C]/[DMPA]/[thiol] = 1/0.4/2, $[P6]_0$ = 1 M in THF, 25 °C, UV irradiation (365 nm, 10W), 1 h, $NaHCO_3$. iv) [Amine]/[BnBr] = 1/0.2-3, $[NP6]_0$ = 0.1 M DCM, 48 h.

A triblock polymer P6, with M_n = 22.7 kgmol^{-1} (Đ = 1.23), was synthesised using the method described in Section 3.2.2. The polymer was targeted so that the wt% of ^{V}PC was kept at 25 wt% (as determined from ^{1}H NMR spectroscopy) to ensure the material was insoluble in water. The lack of water solubility is essential for antibacterial polymer coating applications since the material must not delaminate or dissolve in water. To add the amine groups to the polymer, the thiol-ene reaction was

applied using a photoinitiator (2,2-dimethoxy-2-phenylacetophenone, DMPA), with four molar equivalents of 2-(diethylamino)ethanethiol hydrochloride. A slight excess of thiol was employed to limit any chain-chain coupling side reactions and to ensure complete functionalisation.[23] The reaction mixture was irradiated with UV light (365 nm, 10W) for an hour and a complete conversion of the vinyl groups was achieved, as determined by ^{1}H NMR spectroscopy. Comparison of the ^{1}H NMR spectra before and after functionalisation indicated the complete disappearance of the vinyl group resonances (5.76 and 5.01-5.09 ppm). The successful incorporation of the thiol was confirmed by the appearances of new resonances at 2.55 ppm, due to the methylene groups adjacent to the S atom and the amine ethyl signals (peaks 'E' and 'F' in Figure 3.9). The ^{1}H NMR spectrum of the product also showed diagnostic amine alkyl group signals at 1.01 ppm (peak 'G' in Figure 3.9). Furthermore, the PLA block signals remained unchanged, suggesting that there was no detectable degradation of the copolymer backbone.

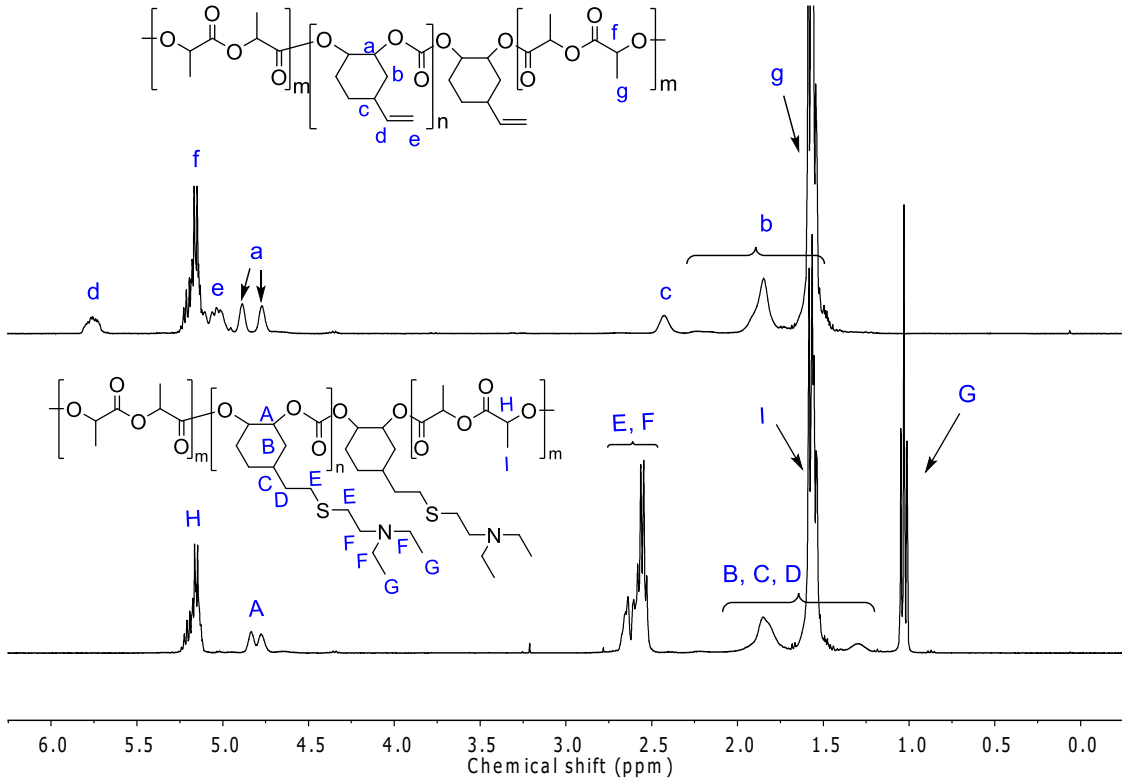


Figure 3.9 Stacked ^{1}H NMR spectra of P6 and NP6 (400.0 MHz, $CDCl_3$, 25 ºC).

Due to its composition, NP6 was soluble in THF and chloroform but insoluble in water. The polymer was also analysed by SEC, in THF, and showed a monomodal molar mass distribution with narrow dispersity (M_n = 36.0 kgmol^{-1}, Đ = 1.25). There was no significant 'tailing' in the higher molar mass region, confirming that interchain cross-linking was suppressed. The slight increase in molar mass after functionalisation is attributed to the addition of the thiol side chains, resulting in a change in hydrodynamic radius and hence retention time (Figure 3.10).

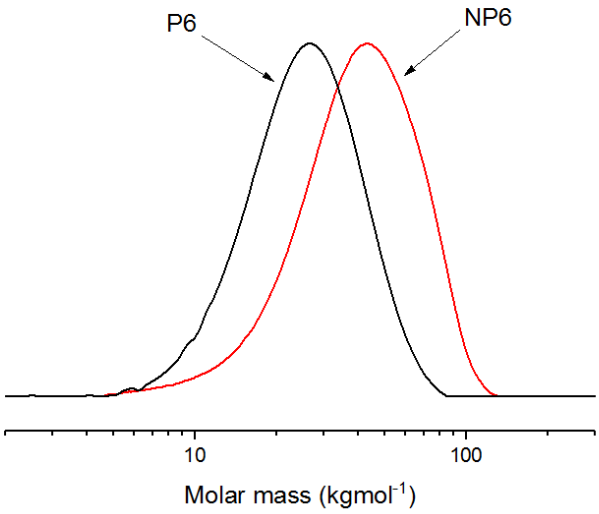


Figure 3.10 Overlaid SEC traces of P6 and NP6.

The antibacterial ammonium moieties were then introduced to NP6 by alkylation reactions using excess benzyl bromide (*vs.* $\overline{DP}$ of ^{V}PC, see Chapter 7 for more details). The use of excess benzyl bromide was necessary to ensure complete quaternisation along the polymer backbone. The final polymer was purified by repeated precipitations into diethyl ether. After quaternisation, the ^{1}H NMR spectrum shows a new peak at 7.52 ppm (peak 'i' in Figure 3.11) and a shift in the methyl group signal to 1.41 ppm (peak 'g' in Figure 3.11). Thus, quantitative quaternisation is suggested, at least within the detection limit of NMR. The quaternised polymer (QP6) showed significantly different solubility from NP6: it is soluble in polar solvents, such as methanol or DMSO. The solubility change was rather unexpected as the proportion of the hydrophobic PLA was still high (~ 75%). SEC analyses in DMF, THF and chloroform were attempted, but results were inconclusive, possibly due to interactions between the quaternary ammonium groups and the column.

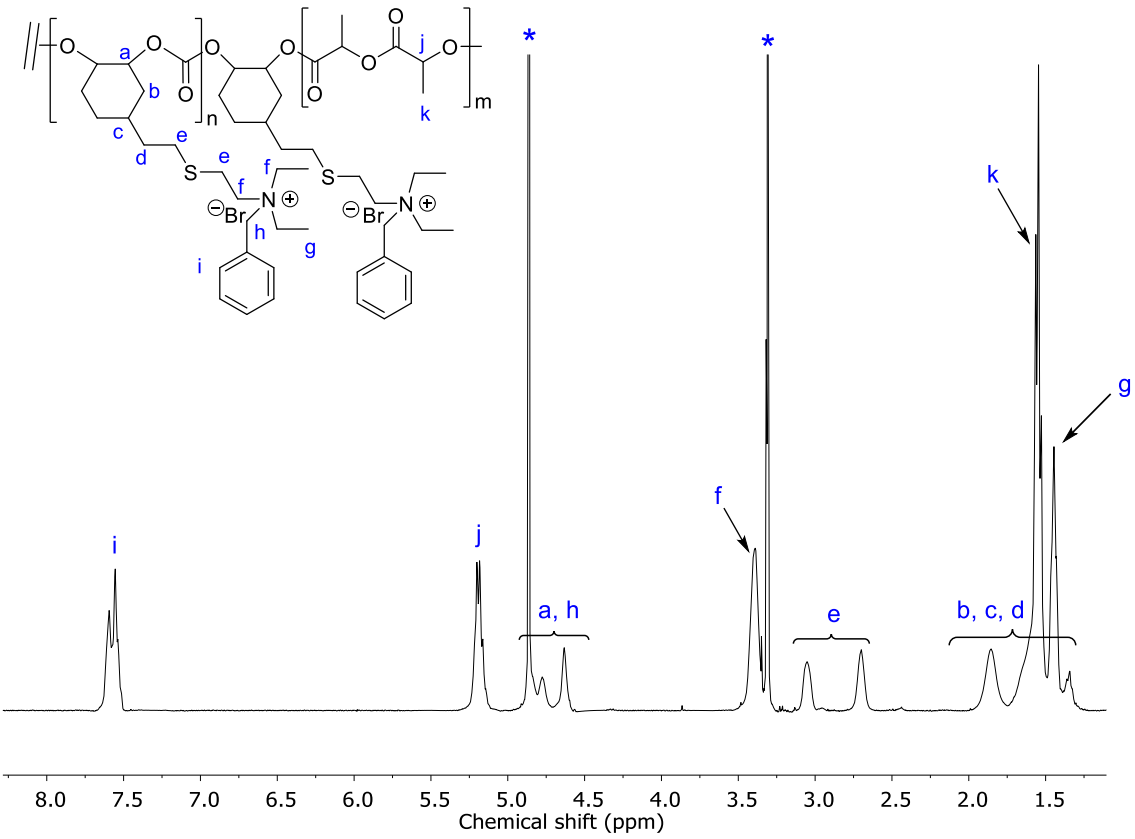


Figure 3.11 ^{1}H NMR spectrum of QP6 (400.0 MHz, CD_3OD, 25 ºC). The asterisk denotes the residual protio-solvent residues.

3.2.4 Assessment of antibacterial activities

The antibacterial activity was investigated using the 'shake-flask' method.[24, 25] Glass slides were cut into uniform pieces, with a surface area of 1 cm^2, and polymer films were drop cast using 200 µL of polymer solutions (5-25 $mg \cdot mL^{-1}$ QP6 in methanol). It is assumed that the bacteria suspension is incubated with 1 mg of QP6 when a 5 $mg \cdot mL^{-1}$ QP6 solution is used to make a film. The polymer films were incubated in direct contact with 2 mL of the target bacterial suspension. After 24 h of incubation, the suspension was serially diluted, and the colony forming units (CFU) were counted. The antibacterial activity is calculated relative to the initial bacteria concentration (~10^5 $CFU \cdot mL^{-1}$).

Since Gram-negative bacteria generally have a more complex cell wall structures than Gram-positive bacteria (the former features a double membrane compared to a single membrane for the latter), they are generally more difficult to kill.[6, 26] In this work, the polymer antibacterial activity was tested against *Escherichia coli (E. coli)* ATCC 25922 as a representative Gram-negative species. Each test result is the average of 9 replicates, after 24 h of exposure. A series were tested, including the control material (P6) and samples of QP6 prepared using different concentrations (Figure 3.12). As expected, the control material did not show any antibacterial activity. The quaternised polymer QP6 resulted in a reduction in $CFU \cdot mL^{-1}$ from 6×10^5 to less than 200, which corresponds to a killing efficiency of at least 99.9% ($P < 0.01$). The most pronounced activity was achieved using the sample prepared with 5 $mg \cdot mL^{-1}$ QP6, which reduced the bacterial numbers to below the detection limit (< 5 $CFU \cdot mL^{-1}$). It was also apparent that the antibacterial activity decreased as the concentration of QP6 polymer increased, possibly due to the differences in surface charge.

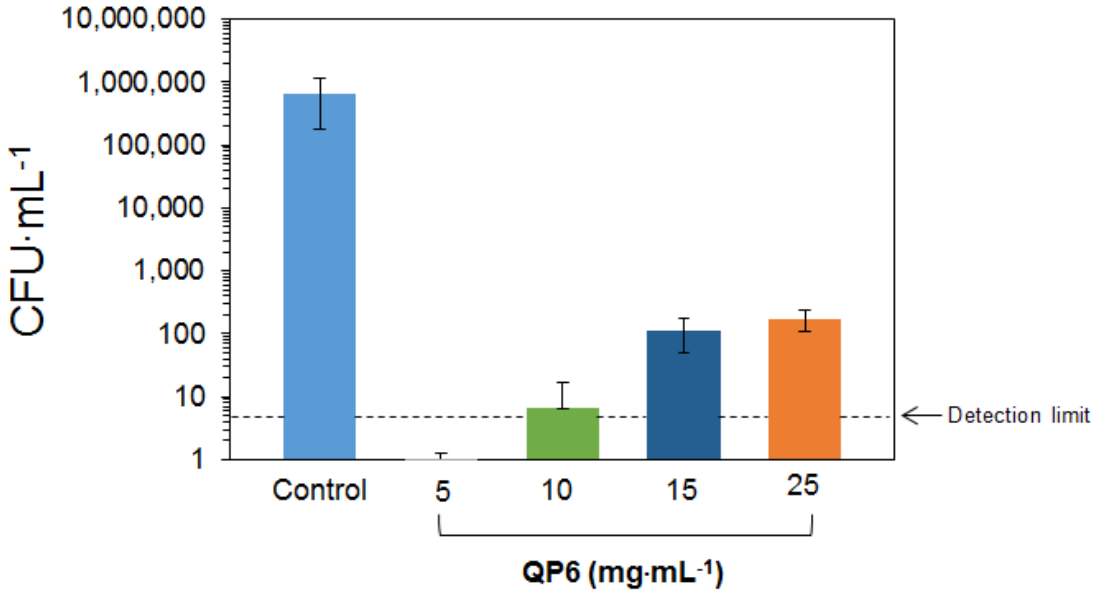


Figure 3.12 Number of *E. coli* ATCC 25922 (colony forming units·mL^{-1}, CFU·mL^{-1}) after exposure to P6 (control) and QP6 prepared using different concentrations for 24 h, at 20 °C. (Initial bacterial counts: ~ 6 × 10^{5} CFU·mL^{-1}, incubated at 37 °C for 18 h). Data correspond to 9 replicates.

To investigate the potential influence of the surface charge on the antibacterial activity, the zeta-potential (ζ-potential) of the polymer films, as a function of pH, was measured. The pH value at which the zeta potential is 0 mV, known as the isoelectric point (IEP), is used as an indicator for the chemistry of the surface.[27]

The uncharged polymer P6 displayed the characteristic behaviour of a weakly acidic surface and showed an isoelectric point (IEP) at pH 4.5. Although P6 did not contain any obvious acidic surface groups, it is possible that the surface charge arises from an enhanced autolysis of water at hydrophobic surfaces, with preferential adsorption of the hydroxide ion.[28] Since most micro-organisms operate under conditions of slightly acidic pH (*i.e.* pH > 4) and the IEP of Gram-negative bacteria is in the range of pH 2-4,[29] P6 is unlikely to undergo any strong electrostatic interaction with the bacterial membrane, and consequently does not show antibacterial activity. However, all the

QP6 polymer films exhibited positive zeta-potential over the whole pH range examined, attributed to the presence of the quaternary ammonium groups. As the antibacterial activities were measured at a pH of 7.4, the zeta-potential values in the pH region of 6-8 were particularly relevant. It was observed that the polymer film with 1 mg QP6 (prepared using 5 mg·mL^{-1} QP6) showed the highest zeta-potential. Moreover, the zeta-potential decreased with increasing masses of QP6, correlating with the trend of decreasing antibacterial activity. It is proposed that QP6 may aggregate at the higher concentrations used for solvent casting and thus fewer quaternary ammonium groups are surface exposed. Another explanation can be that QP6 self-assembles in methanol and the morphology of the self-assembly changes when increasing polymer concentrations.

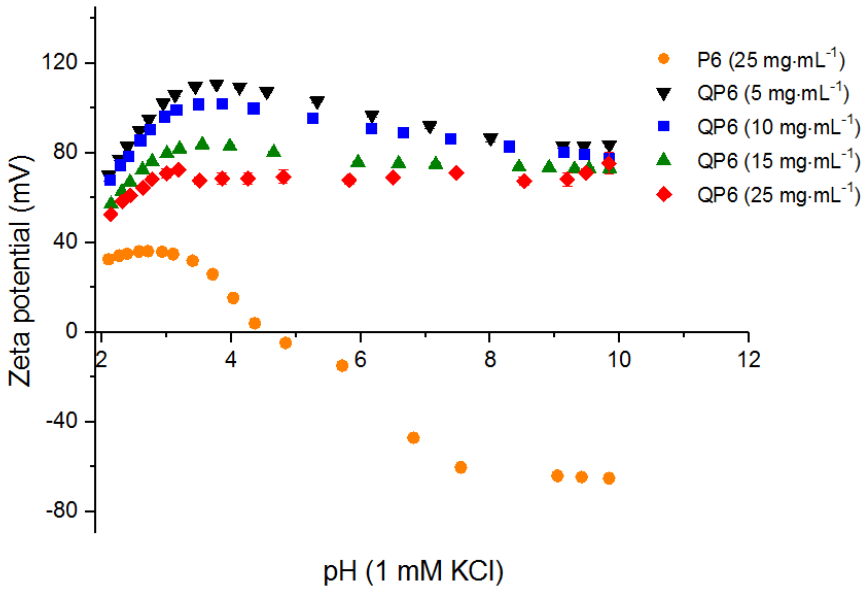


Figure 3.13 Zeta potential (ζ-potential) of P6 and QP6 prepared using different concentrations as a function of pH.

To understand the effect of quaternisation on antibacterial activities, quaternised polymers QP6 with different degrees of quaternisation were synthesised. The degree of quaternisation was varied by reacting the polymer with different amounts of benzyl bromide (from 0.2 to 3 equiv. *vs.* $\overline{DP}$ of ^{V}PC). The extent of quaternisation was determined using ^{1}H NMR spectroscopy by comparing the integrals of the newly introduced ammonium aromatic protons at 7.36-7.54 ppm (peak 'c' in Figure 3.14) with the methine protons on the PLA block at 5.17 ppm (peak 'b' in Figure 3.14). This is not a direct comparison because the ^{V}PC backbone methine protons (peak 'a', Figure 3.14) overlap with the ammonium methylene protons (Peak 'd', Figure 3.14). Nevertheless, the PLA signals remain unchanged throughout the quaternisation and could then be selected as an internal standard. For example, as shown in Figure 3.14, the ratio of PLA methine protons to carbonate main chain units is 1:0.44 in NP6. In $QP_{0.25}$, the ratio of ammonium aromatic protons to the PLA methine protons is 0.27:1. Then the degree of quaternisation is 0.27/5/0.44/2 = 0.25.

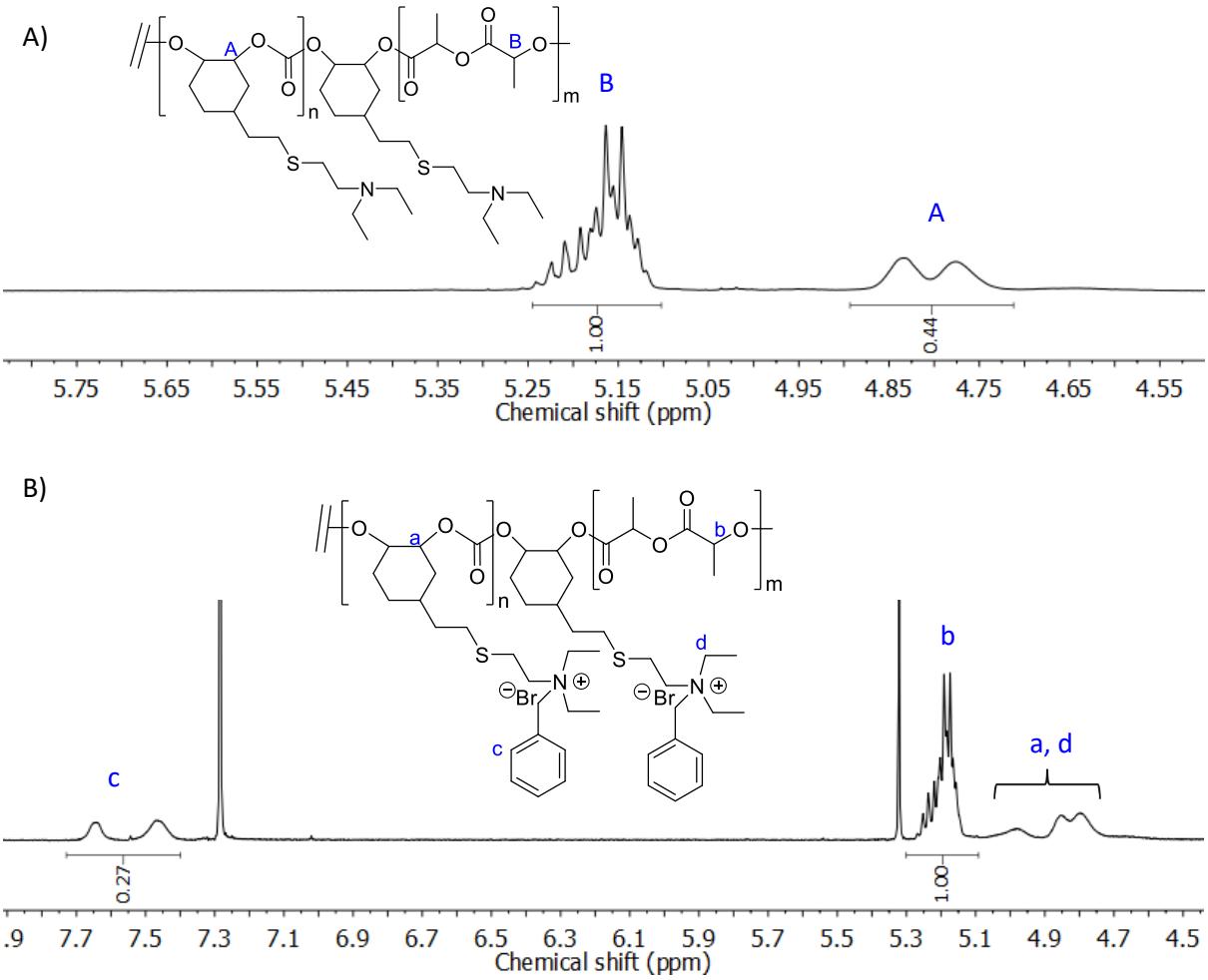


Figure 3.14 A) Enlarged ^{1}H NMR spectrum of NP6, showing the ratio of methine signals of PLA block to the NP6 backbone (400.0 MHz, $CDCl_3$, 25 ºC). B) Enlarged ^{1}H NMR spectrum of $Q_{0.25}$P6, showing the ratio of the methine signals of PLA block to ammonium aromatic signals (400.0 MHz, $CDCl_3$, 25 ºC).

Table 3.3 Data for polymers with different degrees of quaternisation[a]

Polymer	Molar ratio of [Amine]/[BnBr]	Degree of quaternisation[b] (%)
$Q_{1.00}$P6	1:3	100
$Q_{0.78}$P6	1:0.8	78 ± 4
$Q_{0.59}$P6	1:0.6	59 ± 3
$Q_{0.40}$P6	1:0.4	40 ± 2
$Q_{0.25}$P6	1:0.2	25 ± 1

[a] Reaction conditions: $[NP6]_0$ = 0.1 M in DCM, 25 °C, 48 h. [b] Determined by ^{1}H NMR spectroscopy by comparison of the normalised integrals for the ammonium aromatic signals at 7.36-7.54 ppm, the PLA methine signals at 5.17 ppm and the NP6 backbone methane signals at 4.70-4.86 ppm.

As the film prepared from a 5 mg·mL^{-1} QP6 solution showed the highest surface zeta-potential (see above), the same mass concentration was used to test the other polymers with different degrees of quaternisation. All the films were again tested against *E. coli* ATCC 25922. After exposure to the materials for 24 h, a significant reduction in the numbers of viable bacteria was apparent, where CFU·mL^{-1} decreased from 1×10^5 to around 100 (Figure 3.15). Notably, although the fully quaternised polymer displayed the highest antibacterial activity, polymers containing a relatively low percentage of quaternisation (25%) still exhibited significant activity (99.9% reduction in bacterial numbers). However, there was no significant increase in antibacterial activity when the degree of quaternisation changed from 25% to 80%. To investigate this phenomenon, the surface zeta-potential of the films was tested, and the results are shown in Figure 3.15. As expected, the zeta-potential increased with increasing degrees of quaternisation. $Q_{1.00}$P6 showed much higher surface zeta-potential than the other four samples, which is consistent with it also showing the highest antibacterial activity. For the other four QP6 polymers, the increase in zeta-potential was not particularly significant over the pH range relevant for the tests (pH = 7.4) and had a correspondingly little effect on the antibacterial activity observed. In summary, even a low degree of quaternisation results in antibacterial activity for the poly(ester-*b*-carbonate-*b*-ester) films.

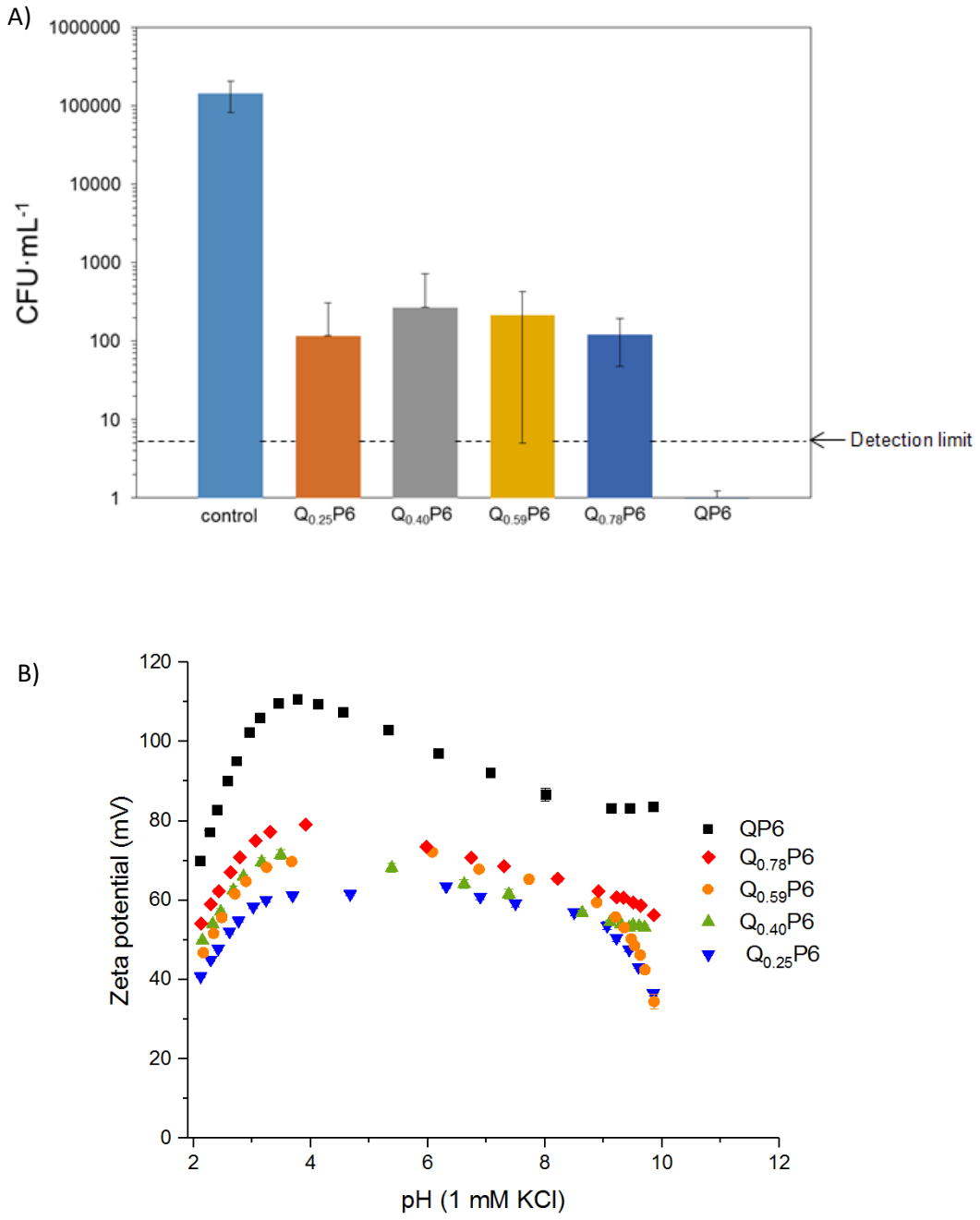


Figure 3.15 A) Antibacterial activities of P6 (control, 5 mg·mL^{-1}) and QP6 samples (5 mg·mL^{-1}) with different degrees of quaternisation against *E. coli*. In all tests, the temperature was maintained at 20 °C in an incubator. (Initial bacterial counts: ~ 1 × 10^5 CFU·mL^{-1}, incubated at 37 °C for 18 h). Data correspond to 9 replicates. B) Zeta potential as a function of pH of QP6 with different degrees of quaternisation.

The reliability of the "shake-flask" method was further tested by examining the polymer surfaces after incubation with bacteria suspension for a pre-determined period. This test was to ensure that there were no bacteria attached to films after 24 h, which might affect the counting. Crystal violet solution was used to stain bacteria for better visualisation by an optical microscope with any violet colour indicating the presence of bacteria on the surface. As shown in Figure 3.16, bacterial attachment was observed within 1 h of incubation, but it was no longer observed after 24 h. The data may be rationalised by an initial interaction between the positively charged QP6 surfaces and slightly negatively charged *E. coli* membrane (ranging from -4.9 to -33.9 mV[30]). During incubation, *E. coli* are attracted to the surface and are killed, after which they apparently detach from the surface (Figure 3.17). For all QP6 samples, there were no remaining bacteria attached to the surface after 24 h incubation, giving confidence in the previous results based on counting from the suspension.

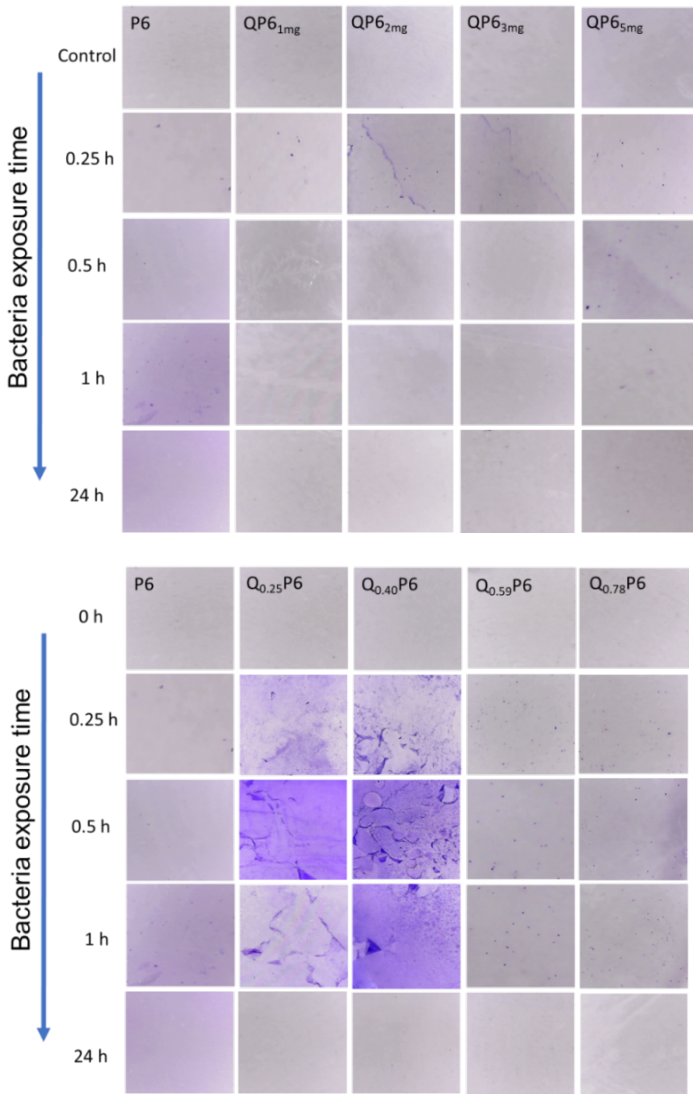


Figure 3.16 Photographs showing bacterial attachment and detachment process, on positively charged surfaces: P6(control), $QP6_{1mg}$, $QP6_{2mg}$, $QP6_{3mg}$, $QP6_{5mg}$, $Q_{0.25}P6$, $Q_{0.40}P6$, $Q_{0.59}P6$ and $Q_{0.78}P6$. Violet colour indicates stained *E. coli* bacteria. 0 h was used as a control as there were no bacteria on the surfaces. Data provided by Gi-byoung Hwang (Department of Chemistry, UCL, UK).

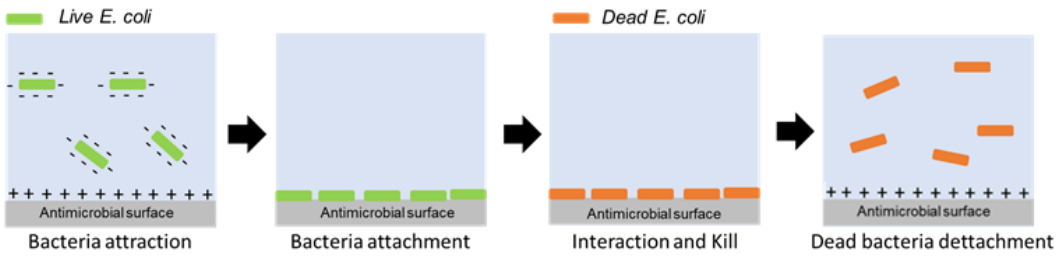


Figure 3.17 Illustration of the attachment and detachment process.

3.2.5 Discussion

Hedrick and Yang have pioneered the development of cationic antibacterial polycarbonates.[1-3] In their reports, the cationic polycarbonates are prepared by ROP of functional cyclic carbonates and subsequent post-polymerisation modification. For example, the ROP of N-substituted cyclic carbonates and subsequent quaternisation with an alkyl halide yields antibacterial polycarbonate.[2]. Alternatively, the ROP of cyclic carbonates featuring alkyl halide side chains was followed by reaction with amines to produce similar products.[1, 3] In their work, the polycarbonates are amphiphilic and self-assemble into either micellar nanoparticles or form hydrogels.[1-3] The hydrogel was tested as an antibacterial material by deposition as 5 × 5 mm^2 surface and tested using the 'shake-flask' method. The materials show 99.9% killing efficiency on *Staphylococcus aureus* (ATCC 29737, Gram-positive), *E. coli* (ATCC 25922, Gram-negative) and *Pseudomonas aeruginosa* (ATCC 9027, Gram-negative) bacteria, and they are also fungicidal against *Candida albicans* (ATCC 10231).[33]A different method, minimal inhibitory concentration determination (MIC), was employed for measuring the antibacterial activity of the polymer nanoparticles. In MIC, the bacteria were incubated in the presence of different concentrations of the polymer self-assemblies, and live bacteria counting was performed on the medium after incubation. As QP6 precipitates out from the incubation medium, its antibacterial activity cannot be directly compared to Hedrick's polycarbonate nanoparticles.

In the field of CO_2-derived polycarbonates, there are a few other examples of antibacterial polymers.[4] Greiner and co-workers reported the first antibacterial poly(limonene carbonate) (PLimC). After 23% amine incorporation into PLimC,

using the thiol-ene reaction, around 87% quaternisation (determined by ^{1}H NMR spectroscopy) was achieved to give a water-insoluble material. Polymer films, each with a mass of 40 mg, were tested against *E.coli* (DSM no. 1077, K12 strain 343/113, DSMZ) using the same "shake-flask" method and showed a killing efficiency of 99.3%.[4] In comparison, QP6 shows greater antibacterial activity, since only 1 mg of $Q_{0.25}$P6 (prepared using 5 mg·mL^{-1} QP6) shows a killing efficiency of 99.9% against the same bacteria.

3.3 Summary and Conclusion

3.3.1 Summary

In conclusion, the di-zinc trifluoroacetate catalyst **C1** showed good activity and very high selectivity for carbonate linkage formation in the copolymerisation of v-CHO and CO_2. It also selectively produced dihydroxyl-capped polycarbonates, which were subsequently used to prepare triblock poly(ester-*b*-carbonate-*b*-ester)s (PLA-^{V}PC-PLA), with good control over molar mass.

PLA-^{V}PC-PLA was modified using the thiol-ene reaction to afford amine side chain substituents with high degrees of functionalisation. The polymer was quaternised and applied as an antibacterial coating by casting films on glass. Films with varying degree of quaternisation were prepared by controlling the reaction conditions, and the influence of the degree of quaternisation on the antibacterial activities was investigated. In comparison with the neutral control polymer, the cationic poly(ester-*b*-carbonate-*b*-ester) exhibited high antibacterial activities against a strain of Gram-negative *E. coli*. A significant reduction in *E.coli* colony forming units was seen even using low polymer mass (1 mg) and at low degrees of quaternisation (25%). The results suggest that the cationic poly(ester-*b*-carbonate-*b*-ester) are promising

antibacterial coating materials that could be applied in various contexts, for example in the fabrication of antibacterial water filters or surfaces. They could also be useful to confer antibacterial properties to PLA, for example in food packaging or coatings on hospital windows/screens.

3.3.2 Outlook

As all the antibacterial tests were only carried out on Gram-negative bacteria, *E. coli*, the efficacy of the polymers against Gram-positive pathogens and fungi is unknown and should also be evaluated and compared with literature reports. The effect of the hydrophilic/hydrophobic ratio of the polymer and the chain length should also be investigated.

This chapter focussed exclusively on functionalising PLA-^{V}PC-PLA to obtain antibacterial activities. In future, other poly(ester-*b*-carbonate-*b*-ester)s should be explored so as to compare and better understand factors enabling antibacterial efficacy. A range of alternating polycarbonate blocks are proposed, including poly(cyclohexadiene carbonate) (^{C}PC), poly(vinyl propylene carbonate) (PVIC) and poly(limonene carbonate) (PLimC). These polycarbonates are suggested because syntheses have literature precedent and they feature alkene groups enabling ammonium side chain addition.[4, 31, 32]

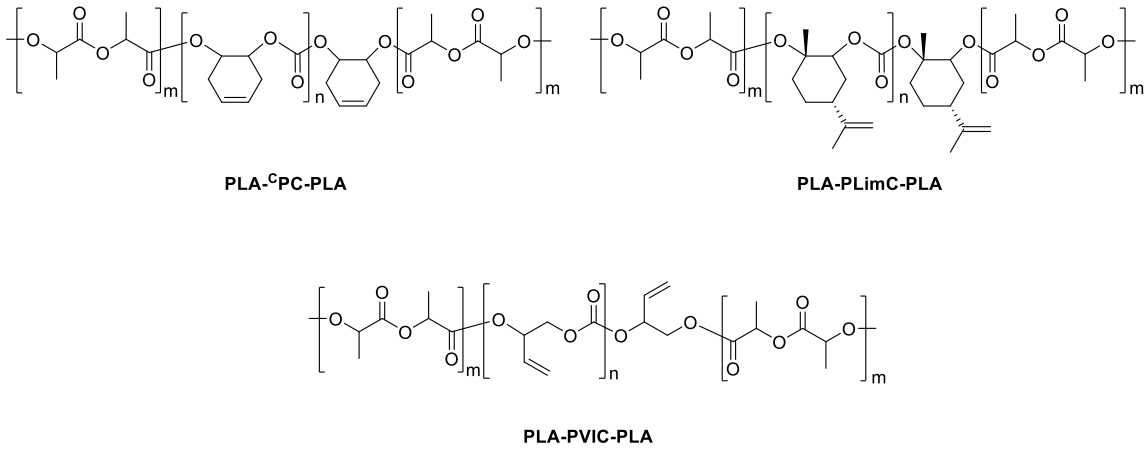


Figure 3.18 Potential polymer precursors for making antibacterial poly(ester-*b*-carbonate-*b*-ester)s.

Work also remains to be done on the characterisation of the antibacterial poly(ester-*b*-carbonate-*b*-ester)s. For example, studies of rheology and processing are important to understand the influence of the substituents on factors such as viscosity, melt flow index, so as to recommend polymer processing methods, *e.g.* extrusion, hot-pressing and solvent casting. It will also be of interest to see whether the addition of elastomeric (after functionalisation) polycarbonate blocks results in any toughening on PLA block. Toughening is typically characterised by a tensile stress-strain measurement and if observed is valuable for load-bearing applications, such as screws and plates for fracture fixation.[33]

3.4 References

1. V. W. L. Ng, J. P. K. Tan, J. Leong, Z. X. Voo, J. L. Hedrick and Y. Y. Yang, *Macromolecules*, 2014, **47**, 1285-1291.
2. A. Pascual, J. P. K. Tan, A. Yuen, J. M. W. Chan, D. J. Coady, D. Mecerreyes, J. L. Hedrick, Y. Y. Yang and H. Sardon, *Biomacromolecules*, 2015, **16**, 1169-1178.
3. F. Nederberg, Y. Zhang, J. P. K. Tan, K. Xu, H. Wang, C. Yang, S. Gao, X. D. Guo, K. Fukushima, L. Li, J. L. Hedrick and Y.-Y. Yang, *Nat. Chem.*, 2011, **3**, 409-414.

4. O. Hauenstein, S. Agarwal and A. Greiner, *Nat. Commun.*, 2016, **7**, 11862.
5. F. Siedenbiedel and J. C. Tiller, *Polymers*, 2012, **4**, 46.
6. Y. Qiao, C. Yang, D. J. Coady, Z. Y. Ong, J. L. Hedrick and Y.-Y. Yang, *Biomaterials*, 2012, **33**, 1146-1153.
7. A. Wendy, A. Allan and T. Brian, *Polym. Int.*, 1998, **47**, 89-144.
8. F.-T. Tsai, Y. Wang and D. J. Darensbourg, *J. Am. Chem. Soc.*, 2016, **138**, 4626-4633.
9. M. R. Kember and C. K. Williams, *J. Am. Chem. Soc.*, 2012, **134**, 15676-15679.
10. G.-P. Wu, D. J. Darensbourg and X.-B. Lu, *J. Am. Chem. Soc.*, 2012, **134**, 17739-17745.
11. A. J. McBain, R. G. Ledder, L. E. Moore, C. E. Catrenich and P. Gilbert, *Appl. Environ. Microbiol.*, 2004, **70**, 3449-3456.
12. M. He and C. C. Chu, *J. Appl. Polym. Sci.*, 2013, **130**, 3736-3745.
13. N. Yi, J. Unruangsri, J. Shaw and C. K. Williams, *Faraday Discuss.*, 2015, **183**, 67-82.
14. S. Paul, C. Romain, J. Shaw and C. K. Williams, *Macromolecules*, 2015, **48**, 6047-6056.
15. M. R. Kember, J. Copley, A. Buchard and C. K. Williams, *Polym. Chem.*, 2012, **3**, 1196-1201.
16. D. J. Darensbourg and G.-P. Wu, *Angew. Chem., Int. Ed.*, 2013, **52**, 10602-10606.
17. B. G. G. Lohmeijer, R. C. Pratt, F. Leibfarth, J. W. Logan, D. A. Long, A. P. Dove, F. Nederberg, J. Choi, C. Wade, R. M. Waymouth and J. L. Hedrick, *Macromolecules*, 2006, **39**, 8574-8583.
18. L. Mespouille, O. Coulembier, M. Kawalec, A. P. Dove and P. Dubois, *Prog. Polym. Sci.*, 2014, **39**, 1144-1164.
19. P. Olsén, K. Odelius, H. Keul and A.-C. Albertsson, *Macromolecules*, 2015, **48**, 1703-1710.
20. R. C. Pratt, B. G. G. Lohmeijer, D. A. Long, R. M. Waymouth and J. L. Hedrick, *J. Am. Chem. Soc.*, 2006, **128**, 4556-4557.
21. H. Misaka, R. Kakuchi, C. Zhang, R. Sakai, T. Satoh and T. Kakuchi, *Macromolecules*, 2009, **42**, 5091-5096.

22. J.-F. Zhang, W.-M. Ren, X.-K. Sun, Y. Meng, B.-Y. Du and X.-H. Zhang, *Macromolecules*, 2011, **44**, 9882-9886.
23. Y. H. Lim, G. S. Heo, S. Cho and K. L. Wooley, *ACS. Macro. Lett.*, 2013, **2**, 785–789.
24. R. J. B. Pinto, P. A. A. P. Marques, C. P. Neto, T. Trindade, S. Daina and P. Sadocco, *Acta Biomater.*, 2009, **5**, 2279-2289.
25. D. Ochs, *Plastics Additives Handbook*, 2000, 647-680.
26. M. E. Falagas and I. A. Bliziotis, *Int. J. Antimicrob. Agents*, 2007, **29**, 630-636.
27. R. Zimmermann, S. Dukhin and C. Werner, *J. Phys. Chem. B*, 2001, **105**, 8544-8549.
28. J. K. Beattie, *Lab Chip*, 2006, **6**, 1409-1411.
29. V. P. Harden and J. O. Harris, *J. Bacteriol.*, 1953, **65**, 198-202.
30. J. Li and L. A. McLandsborough, *Int. J. Food Microbiol.*, 1999, **53**, 185-193.
31. D. J. Darensbourg and F.-T. Tsai, *Macromolecules*, 2014, **47**, 3806-3813.
32. M. Winkler, C. Romain, M. A. R. Meier and C. K. Williams, *Green Chem.*, 2015, **17**, 300-306.
33. K. S. Anderson, K. M. Schreck and M. A. Hillmyer, *Polym. Rev.*, 2008, **48**, 85-108.

Chapter 4

Poly(phosphoester-carbonate) as Potential Platform Materials That Are Capable of Full Degradation

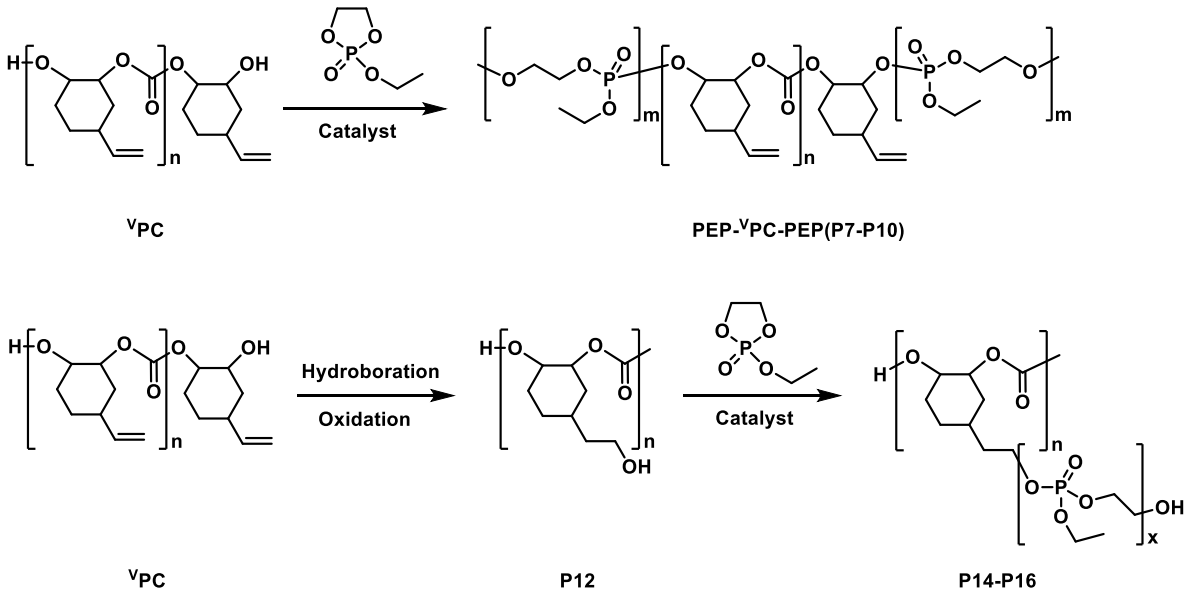
4.1 Background and Aims

Amphiphilic polymers refer to polymers that contain both a hydrophobic and a hydrophilic unit.[1] The incompatibility between the units induces microphase separation and finally results in the self-assembly in selected solvents.[2-6] Amphiphilic polymers are widely applied in the biomedical field as drug carriers and gene vectors.[7] Degradable polymeric carriers are particularly advantageous because they can be broken down into small molecules which can be excreted or absorbed by the human body.[8, 9]

This Chapter targets the synthesis of amphiphilic poly(phosphoester-*b*-carbonate-*b*-phosphoester) polymers for the preparation of self-assembled nanostructures for drug delivery, where the polyphosphoester block is hydrophilic and the polycarbonate is hydrophobic. The use of polyphosphoester (PPE) is particularly interesting because PPEs have hydrophilicity that can be easily tuned and they are known to undergo enzymatic degradation by alkaline phosphatases or phosphodiesters.[10-14] In addition, copolymers of PPE and PLA have been formulated into microspheres for several preclinical and clinical studies, primarily for sustained local delivery of paclitaxel.[15] However, the studies into poly(phosphoester-*b*-carbonate-*b*-phosphoester) polymers are still at an early stage.[16-18] Polycarbonates can undergo hydrolytic degradation *via* alkaline hydrolysis, and they do not generate acidic by-products during degradation.[8, 19, 20] More importantly, polycarbonates degrade primarily *via* surface erosion mechanisms, where the rate of degradation at the surface of the material exceeds that of the bulk.[21, 22] The ability to undergo surface erosion may be desirable for drug delivery if drug release occurs at a predictable rate.[21, 22]

The synthesis of the target materials is proposed by ROP of hydrophilic cyclic phospholane monomers using telechelic polycarbonate macro-initiator, which can be prepared using ROCOP of v-CHO and CO_2. By varying the compositions, various new amphiphilic block polymers and their self-assemblies will be investigated. Vesicle formation is targeted as these structures are capable of delivering hydrophilic drugs.[23]

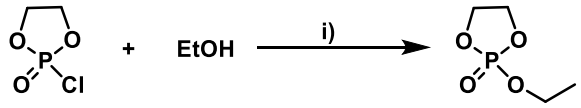
Currently, the post-polymerisation modification of alkene-containing polycarbonates relies significantly on thiol-ene reactions.[24-27] There are still many opportunities for the development of alternative and complimentary post-polymerisation reactions. This Chapter also focuses on the development of hydroboration-oxidation reactions on the polymers to improve hydrophilicity and enhance cell adhesion. As compared to installing hydroxyl groups by the thiol-ene reactions, hydroboration-oxidation delivers the hydroxyls closer to the polymer backbone, which may limit changes to T_g values and associated processing temperatures. The syntheses of graft polymers from these hydroxyl groups will also be explored as the incorporation of side chains can increase the M_n and add low T_g portions to improve further the processability (as low M_n polycarbonate is very brittle).[24]



Scheme 4.1 Structures of polymers targeted in this Chapter.

4.2 Results and Discussions

4.2.1 Synthesis of cyclic phospholane monomer



Scheme 4.2 Synthetic route of ethyl ethylene phosphate: i) triethylamine, THF, -20 °C, 18 h (Yield: 48% after distillation twice).

Prior to any polymer synthesis, the preparation of monomers was undertaken. The cyclic phospholane monomer ethyl ethylene phosphate (EP) was synthesised, in one step, from commercially available 2-chloro-2-oxo-1,3,2-dioxaphospholane by condensation with ethanol, according to a previously reported procedure (Scheme 4.2).[28] Its ^{1}H NMR spectrum shows three resonances at 1.37, 4.20 and 4.40 ppm, assigned to the various methylene and methyl protons (Figure 4.1). The ^{31}P NMR spectrum exhibits a single resonance at 17.5 ppm (Figure 4.1).

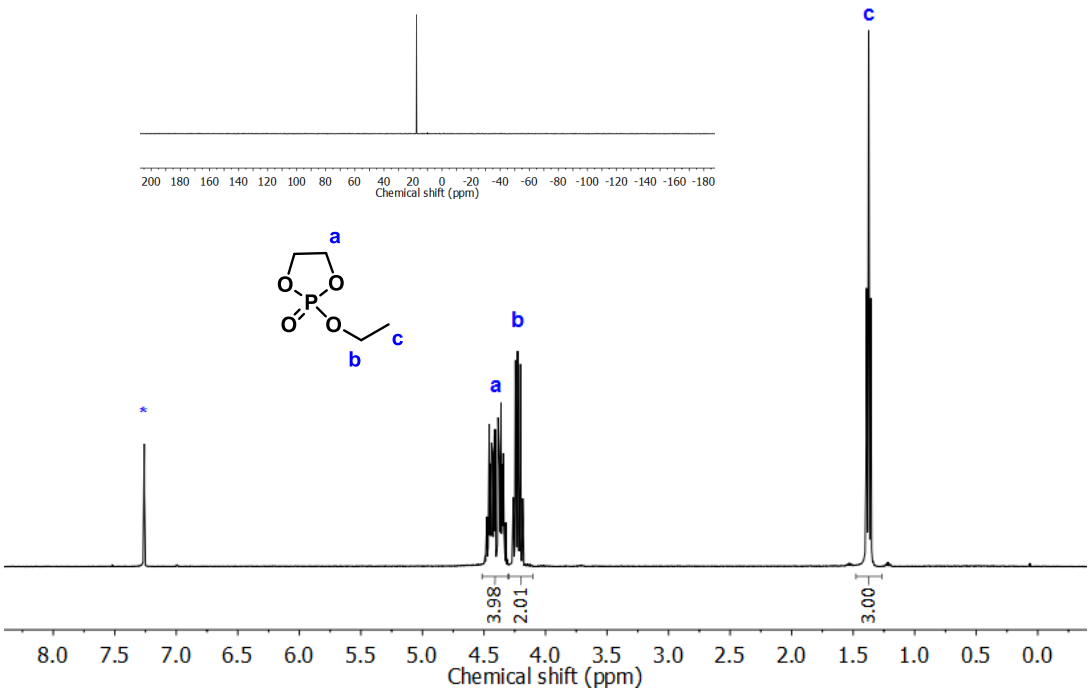
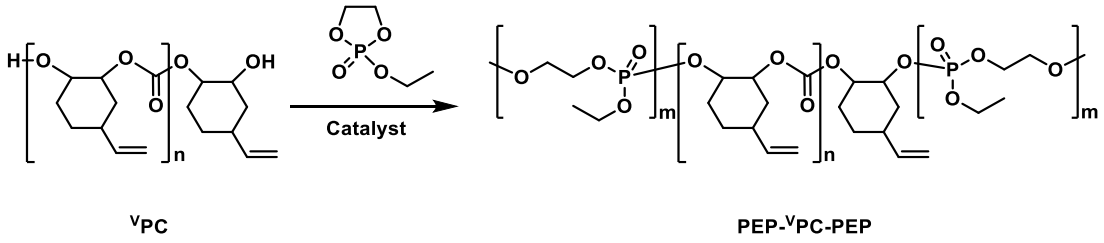


Figure 4.1 ^{1}H NMR and ^{31}P{^{1}H} NMR spectra of EP (^{1}H: 400.0 MHz, $CDCl_3$, 25 ºC; ^{31}P: 162.1 MHz, $CDCl_3$, 25 ºC), in line with the previous report.[28] The asterisk denotes the protio-solvent

4.2.2 Syntheses of block poly(phosphoester-*b*-carbonate-*b*-phosphoester)s with different block ratios

The block poly(phosphoester-carbonate) was synthesised *via* a combination of ring-opening polymerisation (ROP) and ring-opening copolymerisation (ROCOP). The *α,ω*-dihydroxyl end-capped ^{V}PC macroinitiator, $^{V}PC_{38}$, was prepared by the ROCOP of v-CHO and CO_2, as described in Chapter 3. The block poly(phosphoester-*b*-carbonate-*b*-phosphoester)s, PEP-^{V}PC-PEP, were synthesised through the ROP of EP monomer, using $Sn(Oct)_2$ as the catalyst and ^{V}PC as the initiator (Scheme 4.3). All the polymerisations were stopped when the conversions reached approximately 70%

because it was reported previously that transesterification reactions became dominant at higher conversions.[13]



Scheme 4.3 Synthetic route of PEP-^{V}PC-PEP using ^{V}PC as the macroinitiator. Reaction conditions: $[^{V}PC]_0/[Sn(Oct)_2]_0/[EP]_0$ = 1/2/15-100, DCM, 25 °C.

After polymerisation, the polymers PEP-^{V}PC-PEP were purified by precipitation in cold diethyl ether and analysed by NMR spectroscopy. The ^{31}P NMR spectrum of a representative copolymer is shown in Figure 4.2. An apparent shift in the ^{31}P NMR spectrum resonances to about -1.32 ppm was observed, indicating complete ring-opening of the monomer. The signal at -0.28 ppm is assigned to the end group of the polymer chain (Figure 4.2).

The ^{1}H NMR spectrum shows characteristic peaks at 4.25 and 4.89-4.77 ppm, attributed to the PEP main chain methylene protons and ^{V}PC main chain methine protons (peaks 'a' and 'h', Figure 4.3). A new peak at 3.78 ppm is assigned to the PEP end groups, (peak 'h'' in Figure 4.3). By comparing the end group region of the block copolymers (Figure 4.4) with that of PEP and ^{V}PC homopolymers, it can be seen that all the hydroxyl end groups in ^{V}PC homopolymers are consumed in the formation of the triblock copolymer.

DOSY and ^{31}P NMR end group analyses were also attempted to confirm the block structure. However, the tests were not successful, likely due to aggregation of polymer in solution (*i.e.* $CDCl_3$ and DMSO-d_6).

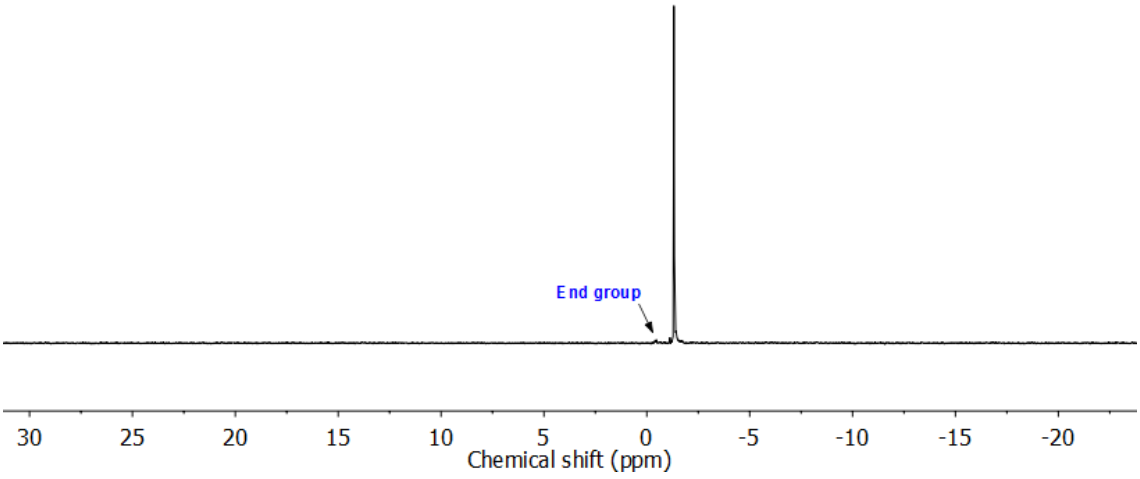


Figure 4.2 $^{31}P\{^{1}H\}$ NMR spectrum of PEP-^{V}PC-PEP (162.1 MHz, $CDCl_3$, 25 ºC).

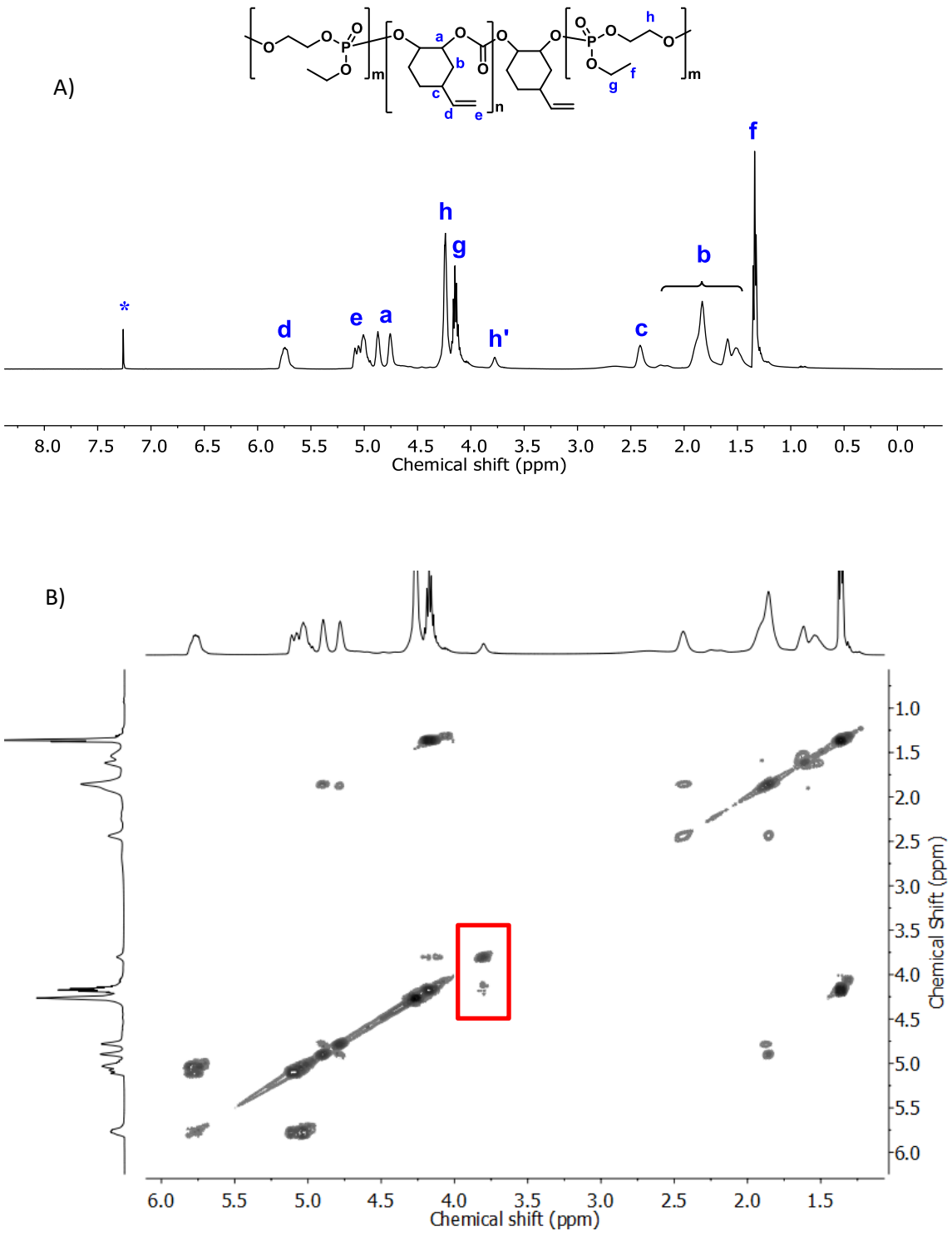


Figure 4.3 A) ^{1}H NMR spectrum of PEP-^{V}PC-PEP and B) ^{1}H-^{1}H COSY NMR spectrum of PEP-^{V}PC-PEP ($CDCl_3$, 400.0 MHz, 25 ºC). The signal at 3.78 ppm was assigned to the –OH end group of PEP block.

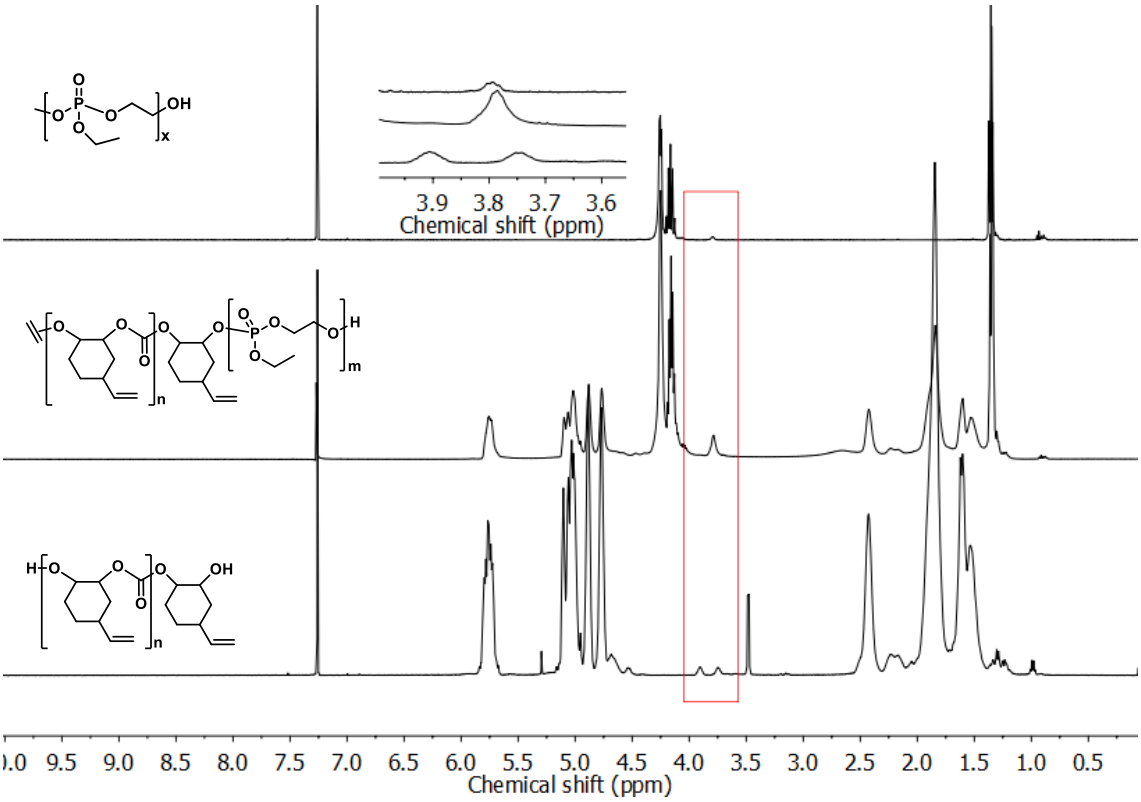


Figure 4.4 Stacked ^{1}H NMR spectra of PEP (Top), PEP-^{V}PC-PEP (Middle) and ^{V}PC (Bottom) ($CDCl_3$, 400 MHz, 25 ºC). The end group region is enlarged.

The $\overline{DP}$ values were obtained by comparing the integrals for the PEP end groups versus main chain methylene resonances in the ^{1}H NMR spectra (*i.e.* peaks h' and h + g in Figure 4.3 A). It was found that the calculated molar masses were in good agreement with either the theoretical molar masses or the values determined by SEC, indicating good polymerisation control (Table 4.1). Due to the high aqueous solubility of the polyphosphoester block, the resulting triblock copolymers showed self-assembly behaviour in water. As the ratio of hydrophobic/hydrophilic blocks would be expected to make a difference in the morphology of polymeric self-assemblies, PEP-^{V}PC-PEP triblock copolymers with different block ratios were prepared.[29]

Table 4.1 Syntheses of the PEP-^{V}PC-PEP with different compositions.

Entry	Polymer	wt% of ^{V}PC	$M_{n,theo}$ (kg/mol)[c]	$M_{n,NMR}$ (kg/mol)[d]	$M_{n,SEC}$ (kg/mol)[e]	$Đ^{e}$
1	$^{V}PC_{38}$[a]	100	n/a	6.2	6.4[f]	1.14[f]
2	PEP_{37}-$^{V}PC_{38}$-PEP_{37} (**P7**) [b]	36	16.2	17.2	14.6	1.28
3	PEP_{19}-$^{V}PC_{38}$-PEP_{19} (**P8**) [b]	52	12.1	11.9	11.9	1.44
4	PEP_{9}-$^{V}PC_{38}$-PEP_{9} (**P9**)[b]	71	9.1	8.7	8.8	1.43
5	PEP_{6}-$^{V}PC_{38}$-PEP_{6} (**P10**)[b]	77	8.0	8.0	7.9	1.15

[a]Polymerisation condition: Polymersiations were run in neat v-CHO with a loading of catalyst/CTA/v-CHO=1/10/1000 at 80 ºC for 20 h (See Chapter 7 for more details) [b]Polymerisation condition: [^{V}PC]/[Sn(Oct)$_2$]/[EP] = 1/2/15-100, [EP]$_0$ = DCM, at 25 ºC for 1-5 h. [c] Theoretical molar mass of Entries 2-5 was determined by ([EP] × conversion ×$M_{[EP]}$) + $M^{NMR}{}_{[^{V}PC]}$. [d]Calculated on the basis of the ^{1}H NMR integrals, the methine end group was used as internal reference for Entry 1, while ^{V}PC-OH was used as internal reference for Entries 2-5 (Comparing the integrals of peak d and peak h + g in Figure 4.3 A.[e]Determined using Size exclusion chromatography in DMF, using monodispersed polystyrene as standard. [f]Determined using Size exclusion chromatography in THF, using monodispersed polystyrene as standard.

Due to the aggregation of the triblock copolymers in THF, the SEC analysis was performed using DMF. Characterisation of ^{V}PC by SEC using DMF was not achieved because of its insolubility. Although the molar masses of the triblock cannot be compared with that of the macroinitiator, all the triblock copolymers display monomodal molar mass distributions (Figure 4.5). Additionally, there was no observable precipitation in the polymer solution in DMF, suggesting no significant contamination of ^{V}PC homopolymer.

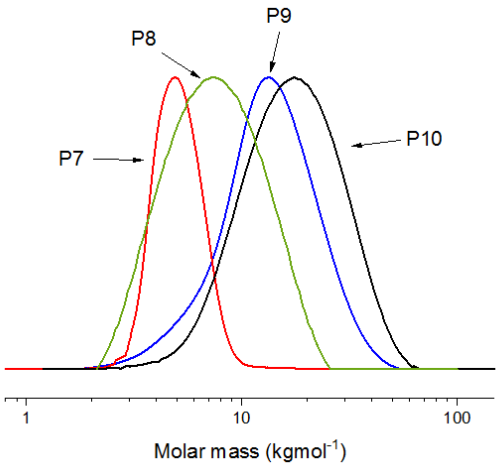


Figure 4.5 Overlaid SEC traces of **P7-P10** (Table 4.1 Entries 2-5).

There are many factors that control the morphology of the self-assembled nanostructures, such as the hydrophilic/hydrophobic ratio, polymer concentration, salt concentration, pH, temperature and the nature of the solvent.[29] Among these factors, the volume ratio of the hydrophilic to hydrophobic block is considered to be particularly important, and empirically values greater than 1:1 usually afford micelles, while values smaller than 1:2 favour the formation of vesicles.[29] Thus, a range of poly(phosphoester-*b*-carbonate-*b*-phosphoester) block polymers, with different hydrophilic/hydrophobic ratios, should allow access to different morphologies. The weight contents of the hydrophobic block (^{V}PC) in the triblock copolymers were 36, 52, 71 and 77 wt%, respectively (Table 4.1, entries 2-5). In control experiments, ^{V}PC and PEP were also tested for their ability to self-assemble, but, ^{V}PC precipitated immediately upon contact with water and PEP was completely soluble at 25 ºC.

4.2.3 Self-assembly of the amphiphilic block poly(phosphoester-*b*-carbonate-*b*-phosphoester)

The self-assembled structures were prepared *via* the 'solvent switch' method, which is commonly used in the field.[30] In this approach, PEP-^{V}PC-PEP copolymers were firstly dissolved in DMF (0.5-10 mg·mL^{-1}), followed by the dropwise addition of excess DI water at 25 ºC. DI water is used as an anti-solvent and it reduces the block polymer solubility and thus induces self-assembly. The excess DMF was removed by dialysis, prior to any measurements. Dynamic light scattering (DLS) was used to characterise the self-assemblies and to establish the formation of structures with low polydispersities (PDI).

Table 4.2 DLS analysis of the self-assembled nanostructures of PEP-^{V}PC-PEP, prepared in Table 4.1 (size distribution by intensity).[a]

Entry	Polymer	D_h (nm)[b]	PDI[b]	Proposed morphology
1	**P7**	22 ± 1	0.38 ± 0.02	micelles
2	**P8**	24 ± 2	0.17 ± 0.01	micelles
3	**P9**	305 ± 6	0.31 ± 0.03	vesicles
4	**P10**	252 ± 2	0.05 ± 0.02	vesicles

[a] All self-assembled nanostructures were prepared using the 'solvent-switch' method (see Chapter 7 for details). [b] Determined using DLS.

DLS results show monomodal size distributions of particles in all four samples. The hydrodynamic diameters of **P7** and **P8** were 22 ± 1 nm (PDI: 0.38 ± 0.02) and 24 ± 2 nm (PDI: 0.17 ± 0.01), indicating the formation of micelle structures. For **P9** and **P10**, the hydrodynamic diameters were 305 ± 6 nm (PDI: 0.31 ± 0.03) and 252 ± 2 nm (PDI: 0.05 ± 0.02), suggesting the formation of vesicle structures. The reliability of the DLS results was verified by both the raw correlation data and the cumulant fit curves (Figure 4.6). Very low cumulant fit errors (< 0.005) and flat baselines were observed in the raw correlation data, indicating that the results are reliable. The morphologies of the resulting nanostructures were further confirmed by transmission electron microscopy (TEM).

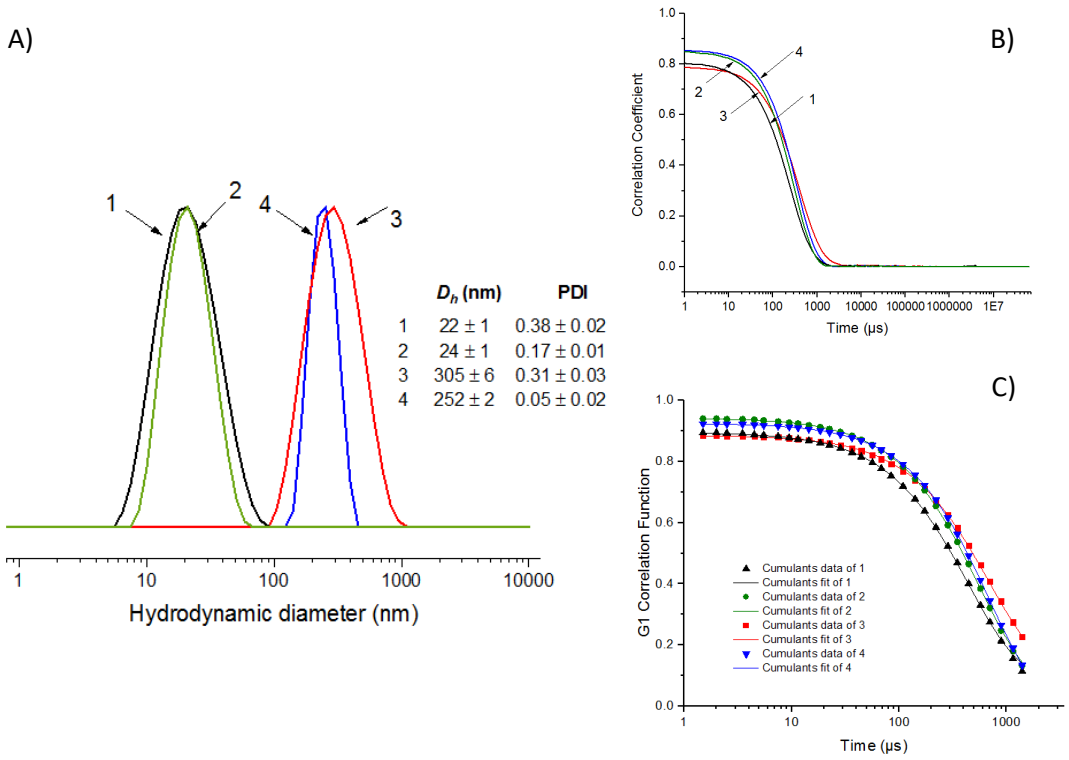


Figure 4.6 A) Hydrodynamic diameter (D_h) and polydispersity index (PDI) (size distribution by intensity), B) Cumulant fit and C) Correlation functions of DLS studies of the self-assembled nanostructures (1-4 correspond to entries 1-4 in Table 4.2, respectively).

4.2.4 TEM characterisation

TEM was used to examine the material's morphology (Table 4.2). All TEM samples were stained with uranium acetate to increase the contrast (see more details in Chapter 7). The characterisation was conducted by Dr Edward R. White and Dr Mahmoud Ardakani at Imperial College London. As illustrated in Figure 4.7, and in line with the DLS results, PEP-^{V}PC-PEP with lower hydrophobic weight content (52 wt%, **P8**) formed spherical micelles (Figure 4.7 A and B). PEP-^{V}PC-PEP with higher hydrophobic weight content (77 wt%, **P10**) formed much larger hollow aggregates with clearly definable bilayer structure, indicating vesicle formation (Figure 4.7 C and D). The membrane thickness of the vesicles was found to be 25 ± 8 nm. The average diameters of the vesicles, as established by TEM, were slightly lower than those

determined in solution using DLS measurements. This was consistent with the previous literature studying polymeric vesicles *via* TEM in the dried state.[31, 32] The TEM images, together with the DLS results, demonstrate the influence of varying the hydrophobic/hydrophilic block ratio in tuning the morphology of self-assembled nanostructures. The concept is already well-known for other amphiphilic copolymers[29] but has yet to be demonstrated for this particular type of polymer.

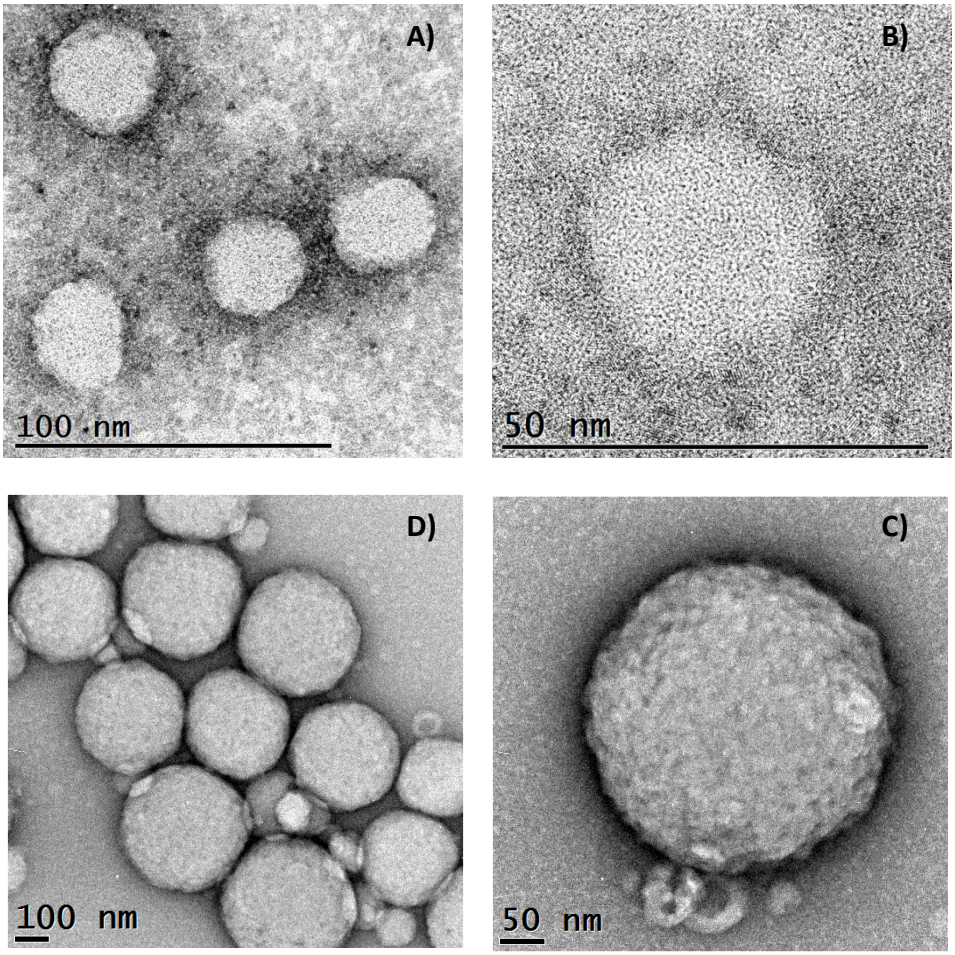


Figure 4.7 TEM images of representative self-assembled nanostructures from PEP-^{V}PC-PEP: A) & B) micelles formed from **P8** and C) & D) vesicles formed from **P10**.

4.2.5 Model Drug Release Experiments

After confirming the vesicle formation, it was of interest to study their potential in drug delivery. First, a zeta potential measurement was performed to evaluate their stability. As a rough approximation, colloidal systems having zeta potentials ranging from ± 40 to ± 60 mV are considered as showing 'good stability'.[33] In this case, the rather high zeta potential (-47.8 ± 0.7 mV, $|\zeta| > 40$mV) indicates good colloidal stability, relevant to any future use in medicine. The drug loading efficiency was evaluated using Rhodamine B (RhB); RhB is a hydrophilic fluorescent dye, which is a commonly used model drug.[34, 35] A hydrophilic model drug was selected because hydrophilic drugs are often subject to low intracellular absorption due to their poor permeability through the cell membrane, which consists of a lipid bilayer.[36, 37] Rapid clearance is another drawback of delivery of the hydrophilic drug. By encapsulating the hydrophilic drug in a polymeric drug delivery vehicle, its release can be sustained, and repetitive injections can be avoided.[36, 37]

Prior to any drug delivery experiments, a fluorescence calibration was conducted using known concentrations of RhB in PBS buffer (the PO_4^{3-} concentration of the PBS buffer = 10 mM; and the pH value = 7.4). The vesicles' drug loading efficiency (DLE) was determined by DLE (%) = $\frac{M_e}{M_f} x\ 100\%$, where M_e represents the weight of drug encapsulated in vesicles and M_f represents the weight of drug used in total (See Chapter 2 and Chapter 7).

The DLE was found to be 32%, which is moderate compared to previous reports (20-35%).[38-41] The *in vitro* release behaviour of RhB-loaded **P10** vesicles was monitored in 10.0 mM PBS buffer, at 37 °C and pH 7.4 either with or without the presence of enzymes. The drug release experiment is based on a 'dialysis bag' method, where the

separation of encapsulated RhB and released RhB is achieved by the use of a dialysis membrane.[42] In order to verify the reliability of the result, a control experiment was conducted, where a free RhB solution of the same concentration as the encapsulated RhB solution was put into another dialysis bag, and its release was monitored. As shown in Figure 4.8, the release of encapsulated RhB was much slower than that of the free RhB control although the initial 'burst' release behaviours were similar. After *ca.* 16 h, the RhB in the control experiment was almost completely released. However, at the same time, only 60 ± 2% RhB was released from the vesicles, indicating the controlled release of RhB.

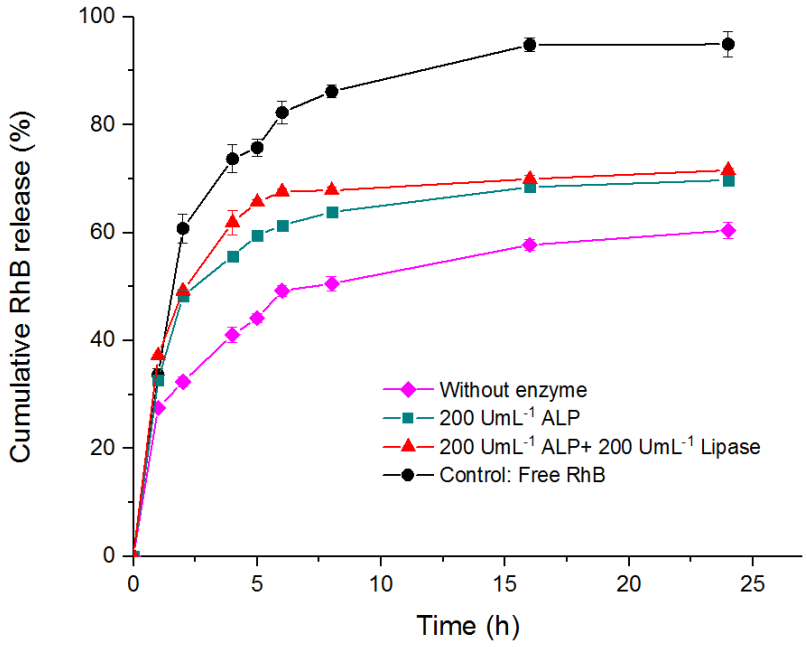


Figure 4.8 Cumulative release profiles of RhB-loaded **P10** at 37 ºC in PBS buffer (10.0 mM, pH 7.4).

Previous reports demonstrated that alkaline phosphatase (ALP) and *Rhizopus arrhizus* lipase can be applied to the degradation of polyphosphoesters and polycarbonates, respectively.[43-45] Therefore, ALP and *Rhizopus arrhizus* lipase were used to study the effect of enzymes on the cumulative release from the vesicles. When the vesicles were

incubated with ALP (200 UmL^{-1}), a faster release was observed compared to the one without any enzyme present. This faster release is possibly due to the disruption of the hollow sphere structure, resulting from some degradation of the polyphosphoester block. Furthermore, culturing the vesicles in PBS medium with both ALP and *Rhizopus arrhizus* lipase led to a slight further increment in the release. It is possible that ALP degrades the PEP corona enabling the degradation of the ^{V}PC membrane by the lipase, resulting in enhanced RhB release. Nonetheless, only approximately 12% increase in the cumulative release over 24 h was observed with both enzymes compared to that without enzymes, suggesting incomplete vesicles disruption. Nevertheless, the addition of enzymes caused an initial 'burst' release similar to that seen with the control.

4.2.6 *In vitro* Degradation Study of PEP-^{V}PC-PEP

4.2.6.1 Enzymatic Degradation of PEP-^{V}PC-PEP under Physiological Conditions

To further investigate the enzymatic degradation, **P10** vesicles were incubated in the culture medium (10.0 mM PBS, 37 ºC, pH 7.4) in the presence of enzymes, and the size of self-assembly was monitored using DLS. A control experiment (*i.e.* without enzymes) was conducted to test particle stability.

Culturing the vesicles for 24 h with lipase did not significantly change the diameter, as shown in Figure 4.9B. This is presumably because the PEP corona protects the ^{V}PC membrane from the lipase. In the presence of ALP, a change in size from monomodal narrow distributions to bi-/multi-modal distributions was observed, suggesting the disassociation and/or aggregation of the nanoparticles. However, the average diameter of the vesicles was not dramatically affected, after 24 h of incubation with either ALP alone or ALP and lipase. The colloidal structures of most vesicles appear to be

maintained; this may be attributed to either low activity of ALP, under physiological conditions, or to the rigidity of the hydrophobic ^{V}PC membrane. These findings are in agreement with the cumulative release data shown previously, where the cumulative release is accelerated with enzymes, but a complete release of RhB was not achieved.

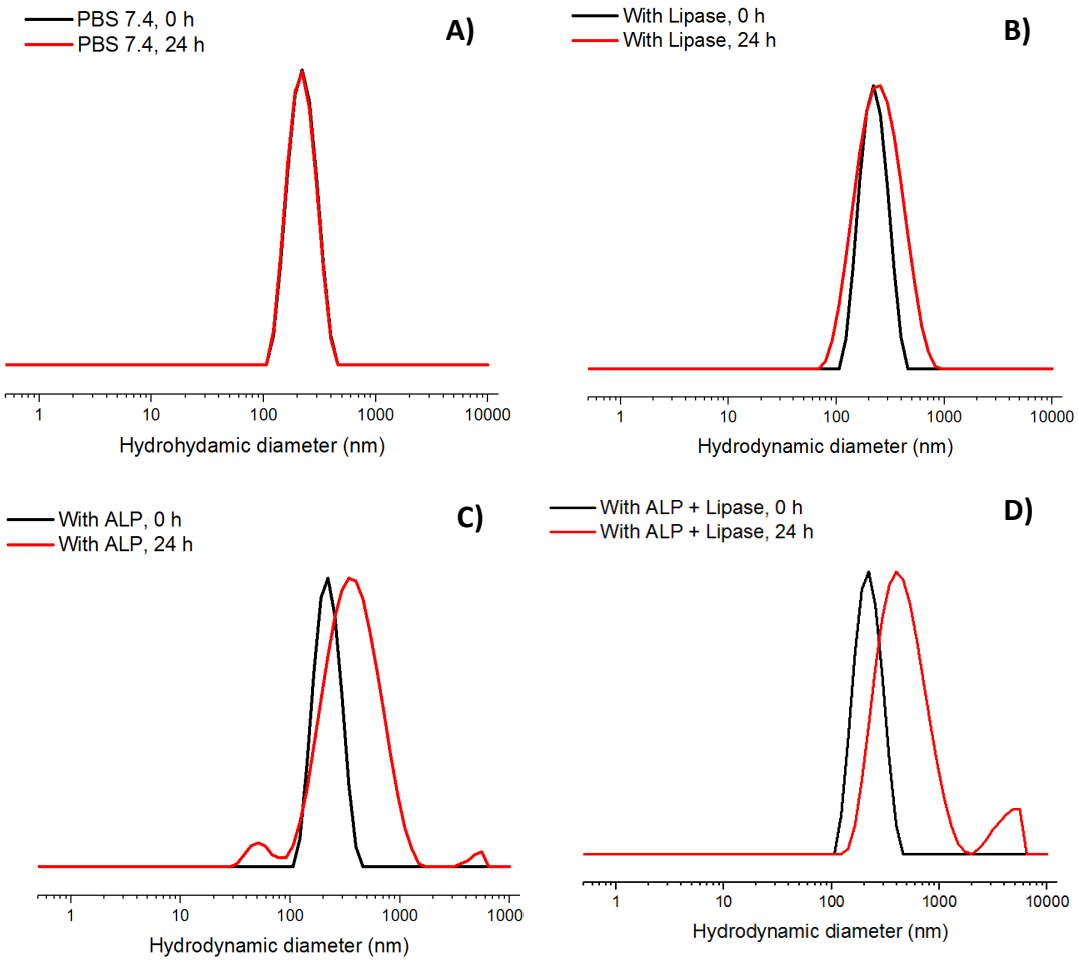


Figure 4.9 Hydrodynamic diameter variation of PEP-^{V}PC-PEP in PBS buffer with or without enzymes during the experimental period: A) PBS buffer (10.0 mM, 37 ºC, pH 7.4), B) 200 UmL^{-1} *Rhizopus arrhizus* lipase, C) 200 UmL^{-1} ALP, and D) 200 UmL^{-1} *Rhizopus arrhizus* lipase and 200 UmL^{-1} ALP (size distribution by intensity).

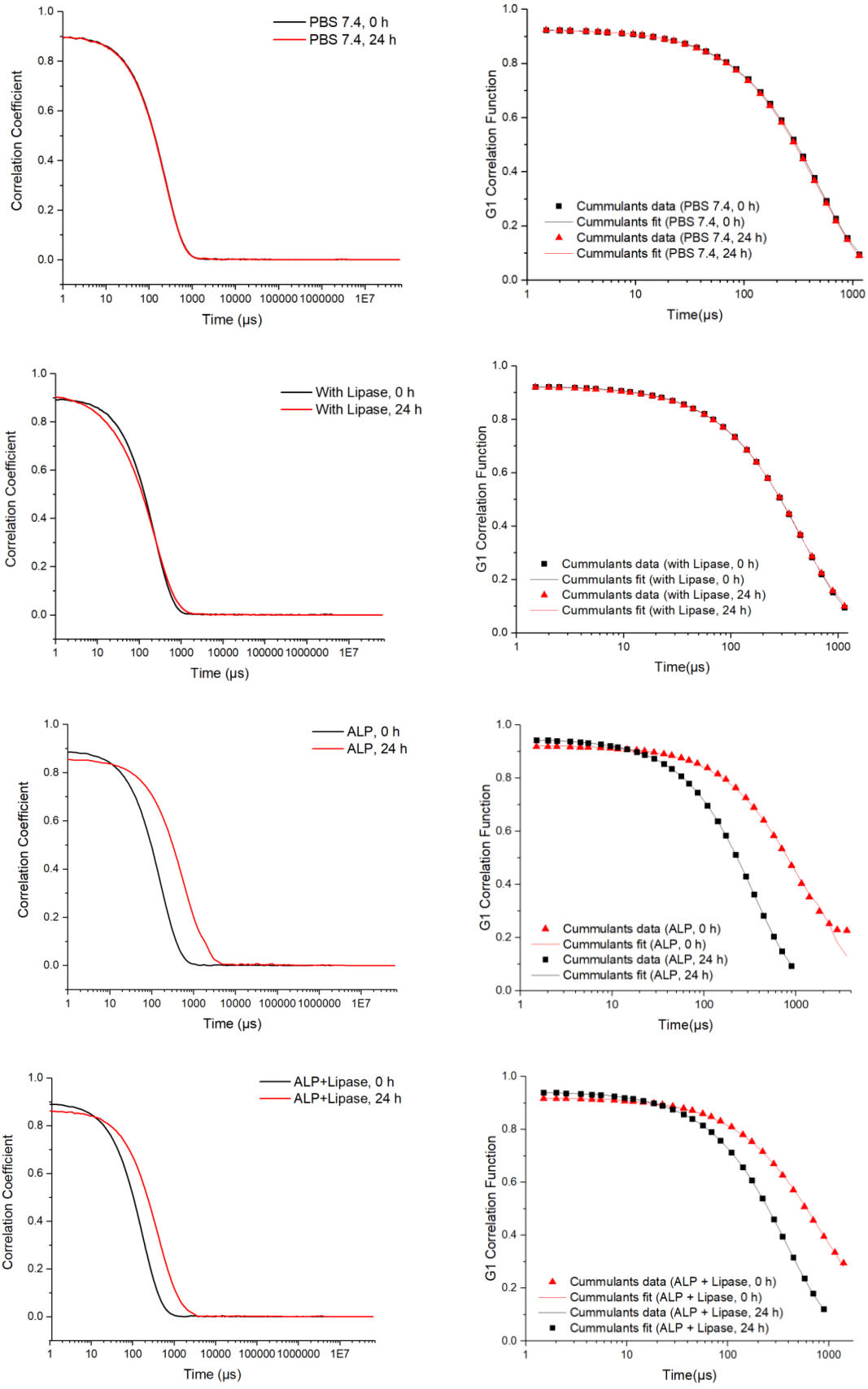


Figure 4.10 Cumulant fit and correlation functions of DLS studies in **Figure 4.9**.

4.2.6.2 Hydrolytic Degradation of PEP-^{V}PC-PEP

It was previously reported that although ALP is stable at physiological conditions, its optimum pH is pH 8-10 with the highest activity being observed at 9.8. [46-48] In addition to enzymatic degradation, phosphoester linkages can also be cleaved by spontaneous hydrolysis (at either acidic or basic pH).[46-48] Therefore, the vesicle stabilities over a range of pH values were assessed by DLS, prior to further enzyme degradation tests.

The hydrolytic degradation experiments were carried out at neutral (pH 7.4), acidic (pH 5.0), and basic pH values (pH 8.8 and 10.0) at 37 °C for 24 h. Experiments at pH 5.0 and 10.0 resulted in significant vesicle instability after 24 h (Figure 4.11A and D), as judged by the change in hydrodynamic diameter and broader PDI. According to a previous report, the phosphoester side chains tend to hydrolyse faster under acidic conditions, whereas under basic conditions main chain phosphoester scission is favoured.[46] It is hypothesised that the hydrolysis of either the PEP backbone or the ethoxy side chains causes destabilisation of the vesicles, resulting in a decrease in hydrodynamic diameter. At neutral (pH 7.4) or slightly basic pH (pH 8.8) values, good stability of vesicles was maintained after 24 h (Figure 4.11 B and C).

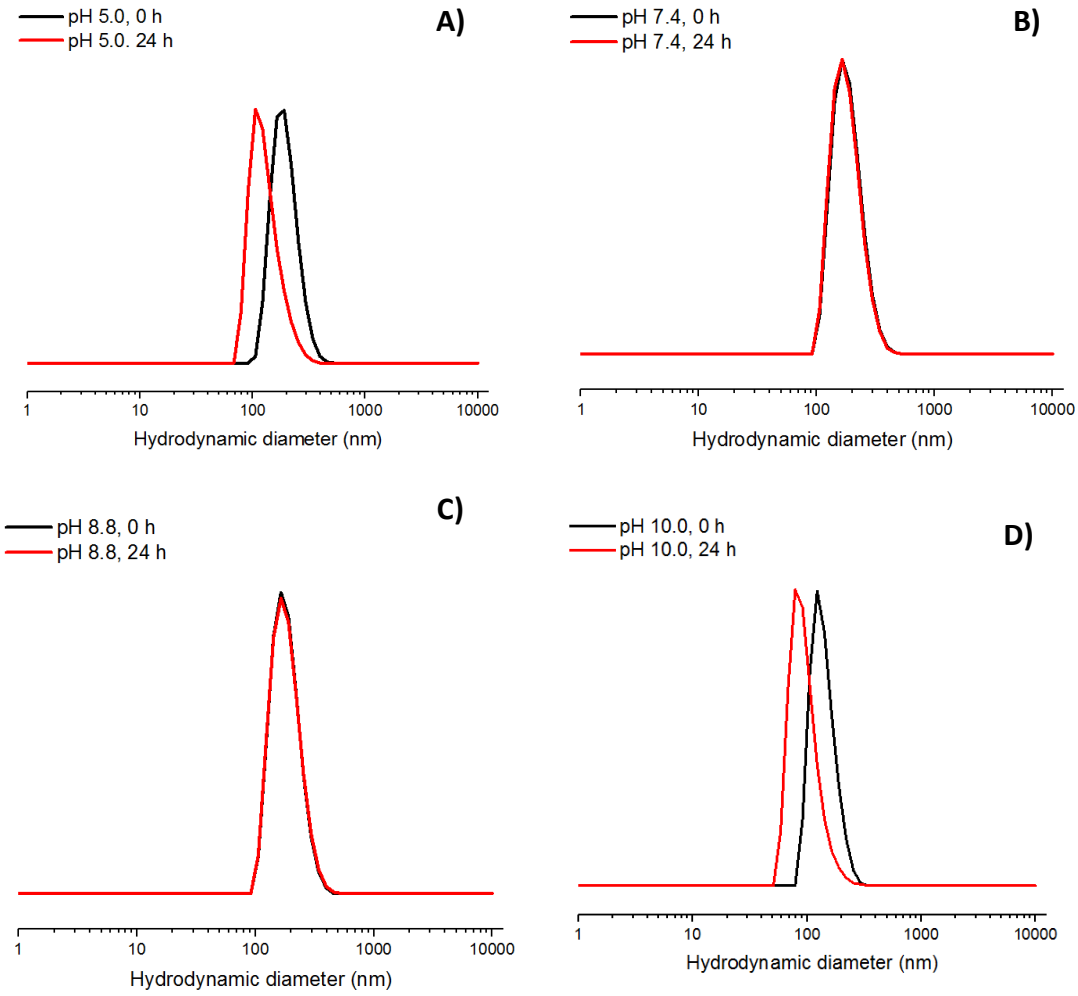


Figure 4.11 Hydrodynamic diameter variation of PEP-^{V}PC-PEP at various pH conditions (size distribution by number).

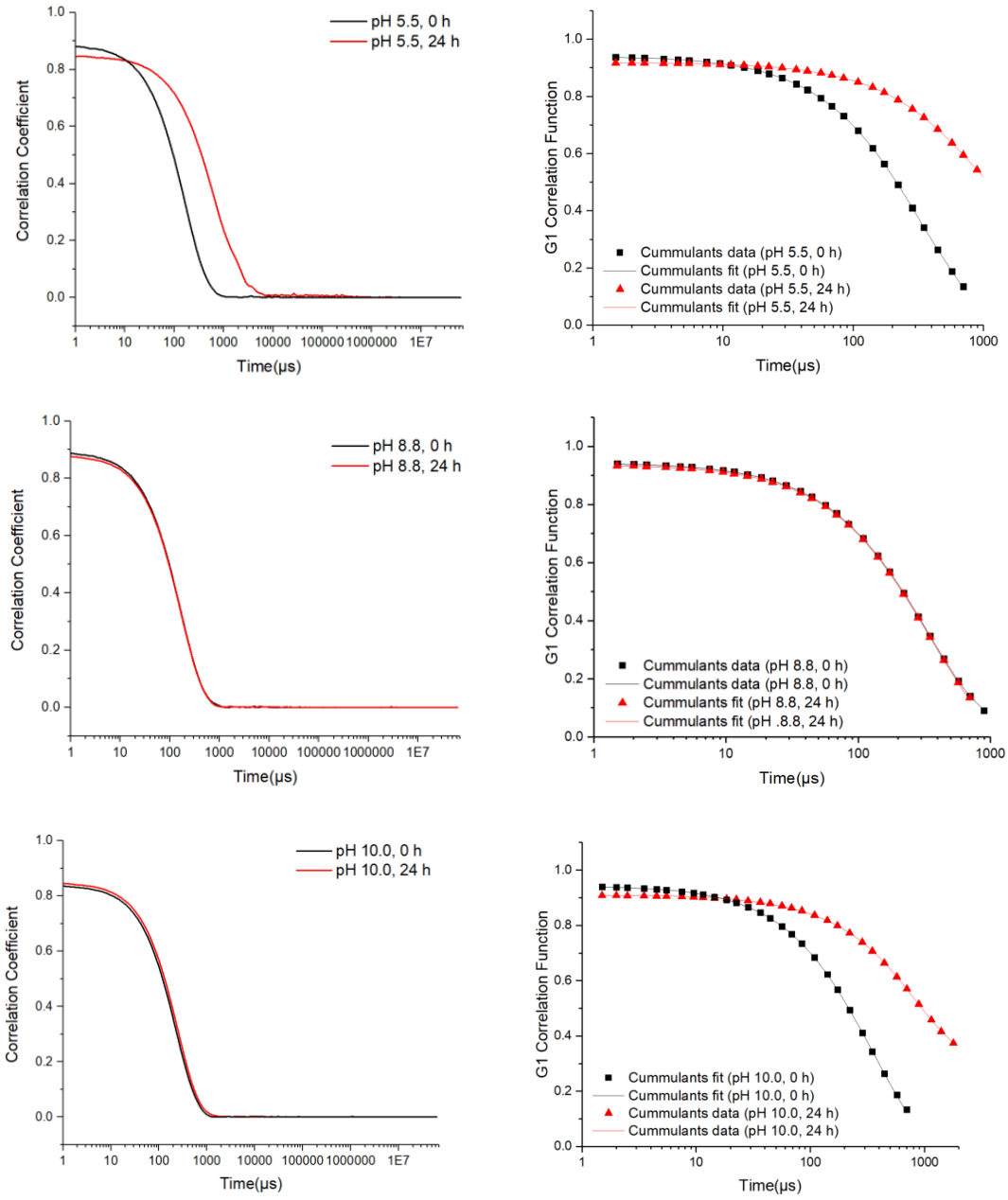


Figure 4.12 Cumulant fit and correlation functions of DLS studies in **Figure 4.11**.

4.2.6.3 Enzymatic Degradation of PEP-^{V}PC-PEP under Basic Conditions

As the size of vesicles, in pH 8.8 aqueous solutions at 37 °C, remained consistent over 24 h, this pH was used for the subsequent enzyme degradation study. The experiments were conducted by adding different amounts of ALP to the PEP-^{V}PC-PEP vesicle solutions, which were placed in a shaker at a rate of 600 rpm, at 37 °C, for 24 h. Since the mean count rate (displayed in kcps-kilo counts per second) given by DLS is proportional to both the size and the number of self-assemblies, as long as the attenuator is fixed,[49-51] the biodegradation process can be inferred using DLS. As shown in Figure 4.13, the degradation at pH 8.8 was much faster than under physiological conditions and was dependant on the concentration of ALP, *i.e.* a shift to smaller sizes and an increase in polydispersity were observed with increasing ALP concentrations. Accordingly, the count rates decreased with more ALP present. By comparison, the count rate of the control remained constant over 24 h. When the vesicle solution was incubated with 200 UmL^{-1} ALP for 24 h, the count rate decreased from around 470 ± 7 kcps to 25 ± 3 kcps. The solution turned turbid and visible precipitation was observed, suggesting that the degradation of PEP by ALP resulted in the release and precipitation of copolymer fragment.

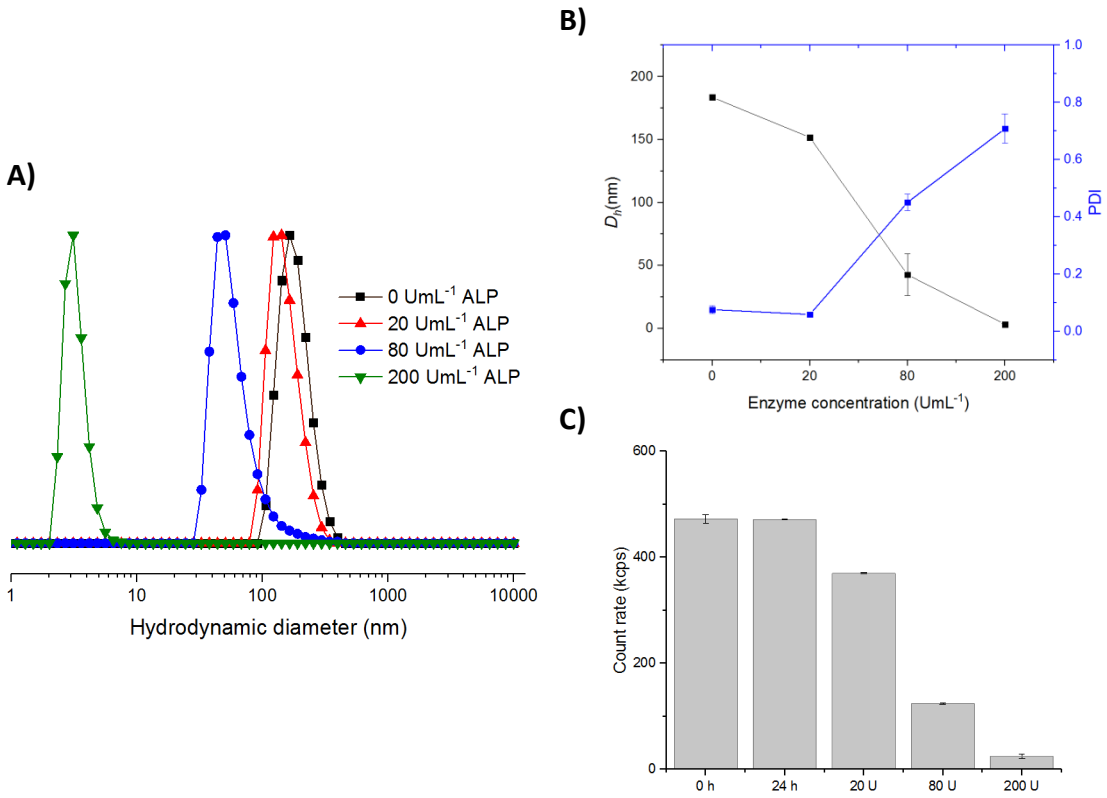


Figure 4.13 ALP catalysed biodegradation of PEP-^{V}PC-PEP with different enzyme concentrations at pH 8.8 and 37 °C, monitored by DLS. A) & B) Hydrodynamic diameter variation (size distribution by number) and C) Mean count rate variation of the polymer vesicle solutions after 24 h incubation.

To investigate further the rate of the enzyme-mediated biodegradation, the vesicles were incubated with 200 UmL^{-1}ALP at pH 8.8, and 37 ºC and the biodegradation process was monitored using DLS. As shown in Figure 4.14, the diameter continuously decreased from 200 nm to around 5 nm within 1 h and remained constant with extended culture time, which strongly indicates the disruption of the ordered structure (vesicle morphology). Mean count rate studies further confirm the vesicle degradation, where the count rate decreased from 453 ± 7 to 27 ± 10 kcps within 1 h.

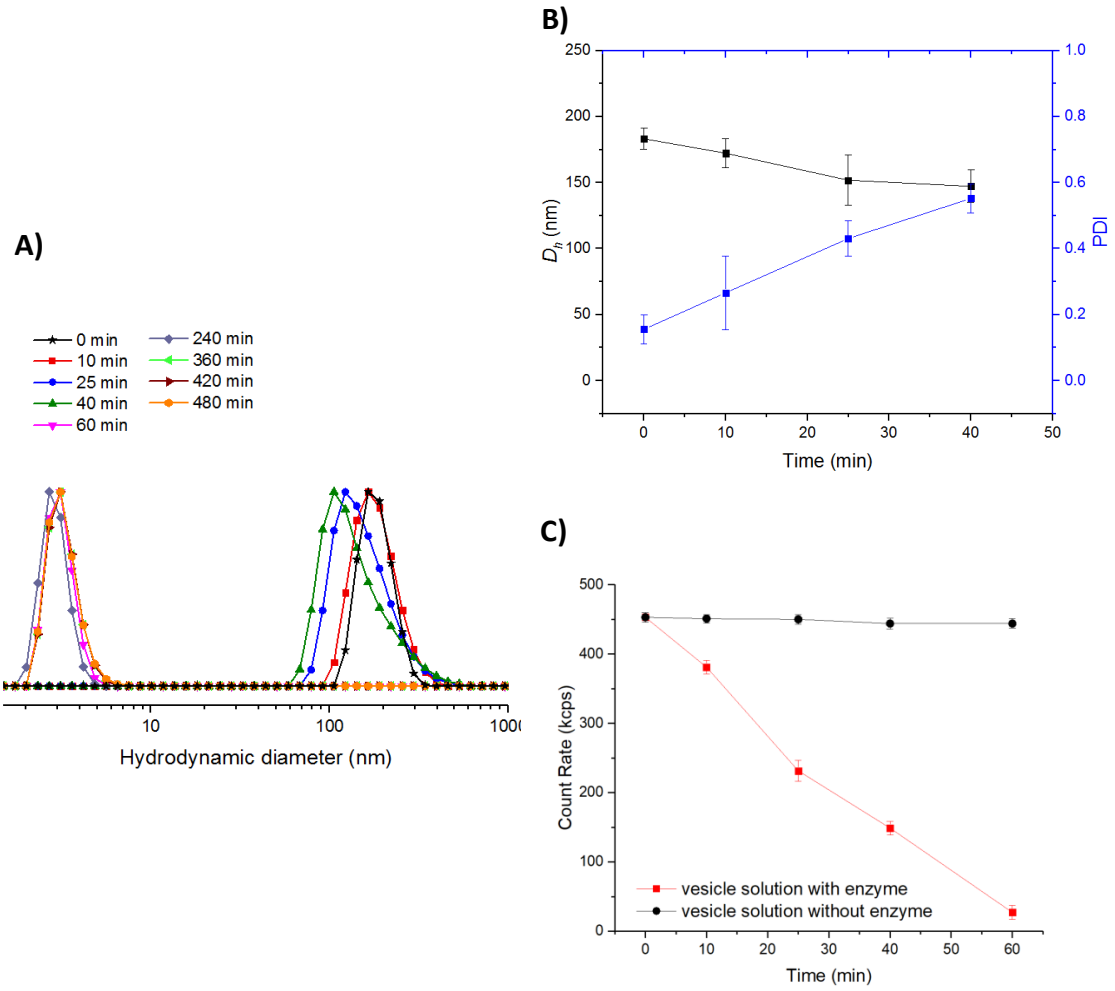


Figure 4.14 A) & B) Hydrodynamic diameter variation of **P10** vesicle solutions with 200 UmL^{-1} ALP at pH 8.8 and 37 °C, as monitored by DLS (size distribution by number) and C) Mean count rate variation of **P10** vesicle solutions.

The change in molar mass during enzyme degradation was also monitored by SEC (Figure 4.15 A). After 1.0 h, the M_n of PEP-^{V}PC-PEP decreased from 7.9 to 6.8 $kgmol^{-1}$, with an increase in dispersity from 1.20 to 1.44. Upon degradation, a shoulder peak appeared in the low molar mass region. Such a bimodal molar mass distribution is consistent with the formation of copolymer fragment due to cleavage of the phosphoester bond by ALP. After 2 h, visible precipitation was observed, and no polymer signal was detectable by SEC (in DMF); the precipitate is likely ^{V}PC which has a very low solubility in DMF.

The insoluble degradation product was dissolved in THF and analysed using SEC (in THF) after further incubating the polymer vesicle solution with ALP until ^{31}P NMR spectroscopy confirmed the complete disappearance of all ^{31}P signals. It was observed that the SEC trace of the degradation product matched with that of the ^{V}PC macroinitiator used to generate the triblock. It seems that under these conditions, there was no significant degradation of the polycarbonate block.

After lyophilisation, the precipitated degradation products were analysed by ^{1}H NMR spectroscopy, and the data was compared with the spectrum of PEP-^{V}PC-PEP (Figure 4.16). The ^{1}H NMR spectra show that signals assigned to protons of the PEP block almost disappear, while signals assigned to protons of ^{V}PC remain present.

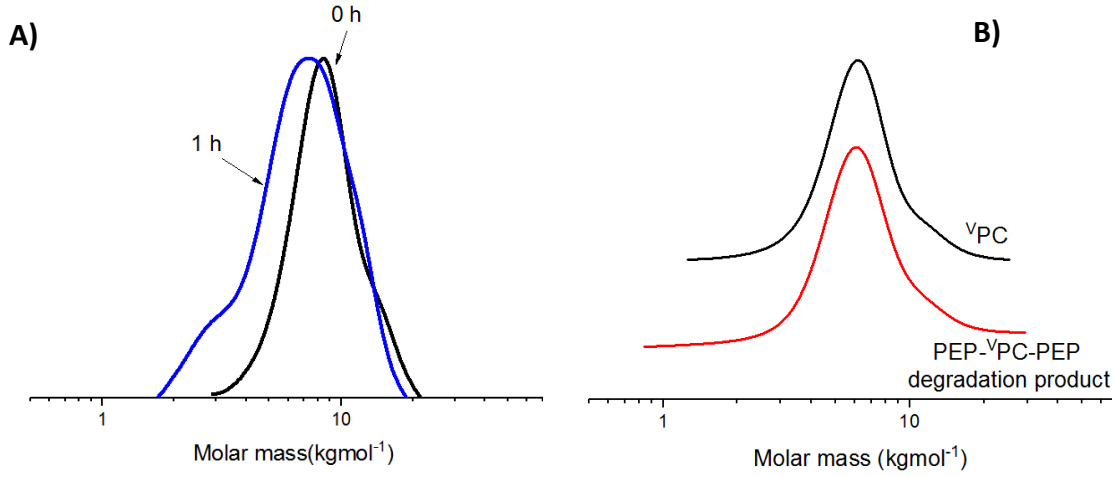


Figure 4.15 SEC traces of the biodegradation products after treating with 200 UmL^{-1} ALP at pH 8.8 and 37 ºC. A) Overlaid SEC traces before and after treating with ALP for 1 h, obtained from SEC in DMF using monodispersed polystyrene as standard and B) Stacked SEC traces of ^{V}PC and the degradation products of PEP-^{V}PC-PEP, obtained from SEC in THF using monodispersed polystyrene as standard.

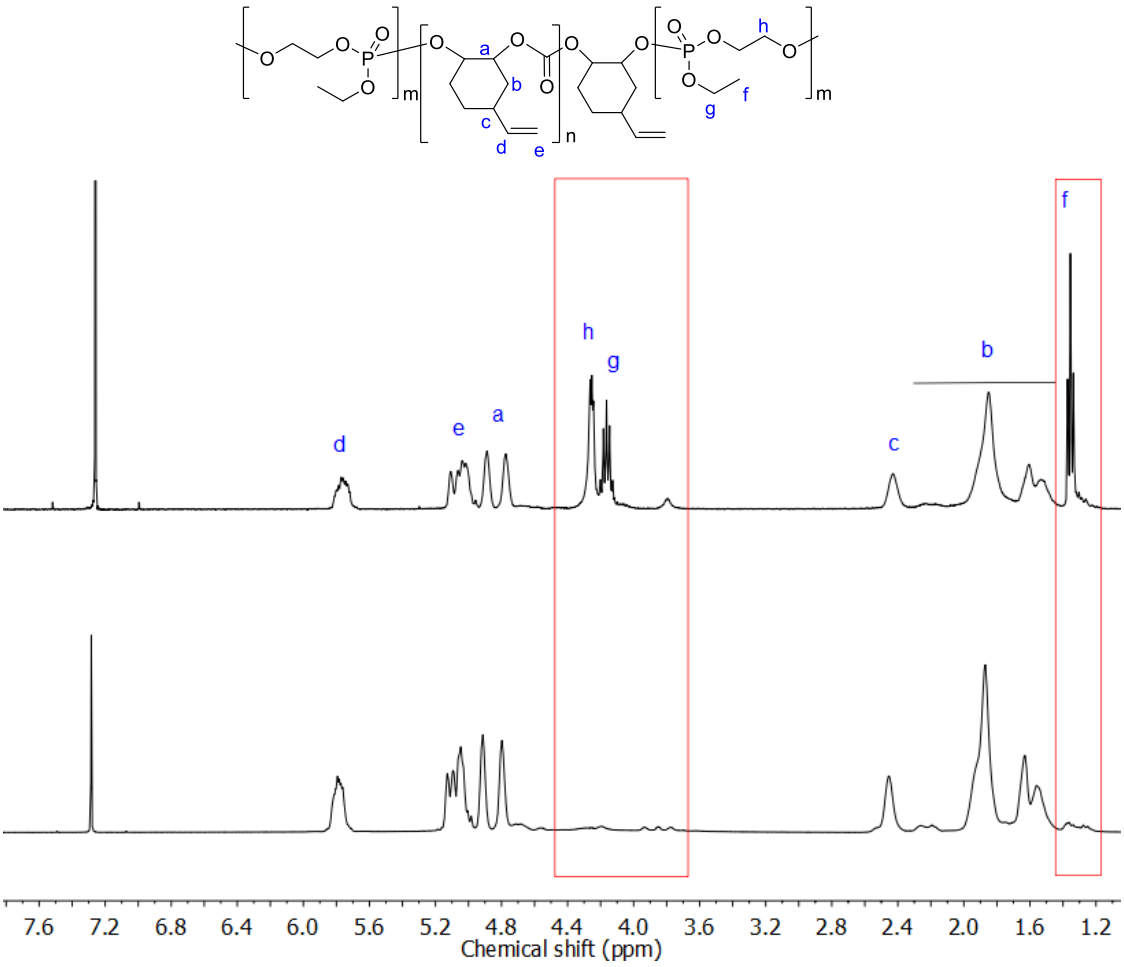


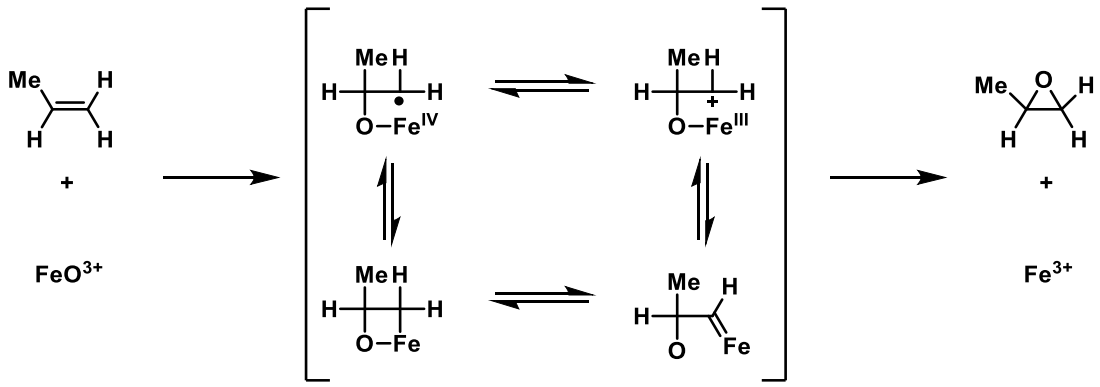
Figure 4.16 Stacked ^{1}H NMR spectra of PEP-^{V}PC-PEP before (Top) and after enzyme degradation (Bottom) for 24 h ($CDCl_3$, 400 MHz, 25 ºC).

4.2.6.4 Cytotoxicity Tests

The cytotoxicity of both the polymers and their degradations products are important considerations in evaluating any applications in medicine. The phosphoester PEP releases ethylene glycol upon degradation, and this product was found to be non-toxic at concentrations as high as 10 mg·mL^{-1}.[52] Wooley and co-workers identified all the degradation products of PEP-based polyphosphoester micelles to be phosphoric acids and ethylene glycol, which both showed negligible cytotoxicity and low immunotoxicity.[53]

In this work the other biodegradation product is ^{V}PC. To investigate its biocompatibility and those of its corresponding degradation products, cytotoxicity tests were conducted using the Alamar Blue test and a Live/Dead viability assay. These experiments were conducted by Mr Chunching Li (working with Prof. Molly M. Stevens at Imperial College London). ^{V}PC is hydrophobic, so the tests were performed using a polymer extract medium. An organo-tin stabilised polyvinyl chloride (PVC) and low-density polyethylene (PE) were used as the positive and the negative controls, respectively. MC3T3-E1 cells were selected as the model cell line because they exhibit typical behaviours of proliferation and differentiation of immature cells and they have been widely used in the testing of new drug carriers and in bone tissue engineering.[54, 55]

The cell viability after 72 h incubation with ^{V}PC (200 mg·mL^{-1}) remained > 85% (normalised to the untreated cells) suggesting very low cytotoxicity to MC3T3-E1 cells (Figure 4.17). The cytotoxicity of its degradation products was determined by first achieving complete hydrolytic degradation by reaction of ^{V}PC with 1 N NaOH solution, at 80 ºC for 48 h. The neutralised degradation solution was then subjected to serial dilution and added to the cell culture medium, using methods described previously.[56] The cytotoxicity of the degradation products was dose-dependent, with significant toxicity observed at high concentrations (> 1000 μg·mL^{-1}, Figure 4.18). The toxicity likely results from an increased intracellular concentration of alkene groups; generally alkenes are expected to be oxidised by cytochrome P450 (CYP) monooxygenase into epoxides, which are generally very reactive.[57] It may be that any oxygenated products bind readily to proteins or nucleic acids, leading to hepatotoxicity.[58]



Scheme 4.4 Oxidation of Propylene by P450.[59]

Although the alkene groups certainly cause cytotoxic effects, post-polymerisation modifications can be used to transform them into groups with higher biocompatibility.

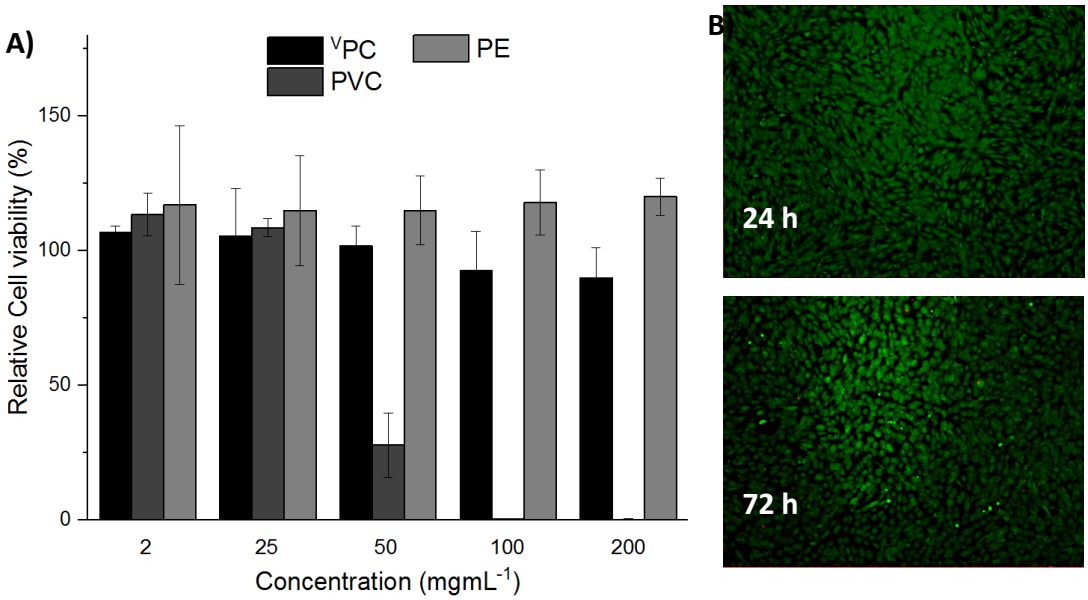


Figure 4.17 A) Viability of MC3T3-E1 cells (%) treated with ^{V}PC extract medium and controls (PVC and PE) after 72 h incubation, determined by Alamar Blue test and B) Cell viability of ^{V}PC (200 mg·mL^{-1}) using a Live/Dead staining method after 24 and 72 h incubation with MC3T3-E1 cells. Data correspond to experiment run at least in triplicate.

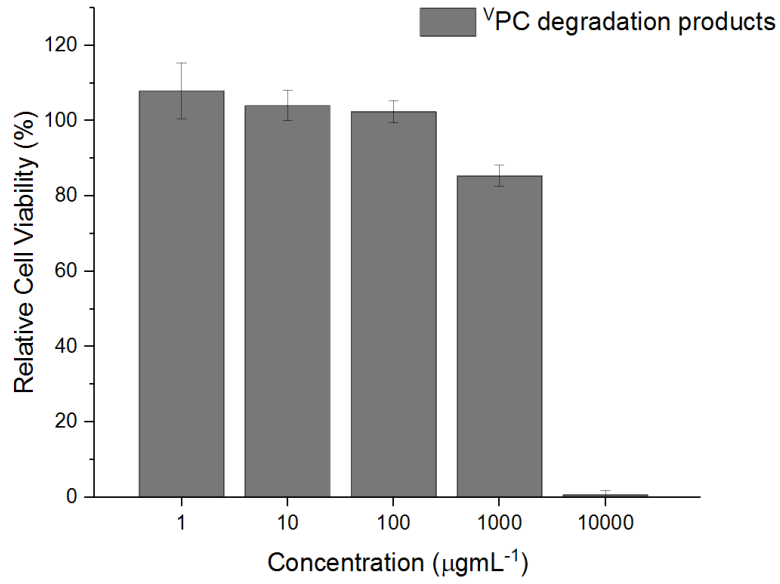


Figure 4.18 Viability of MC3T3-E1 cells (%) treated with ^{V}PC degradation products after 72 h. Data correspond to experiment run at least in triplicate.

4.2.7 Hydroboration-oxidation

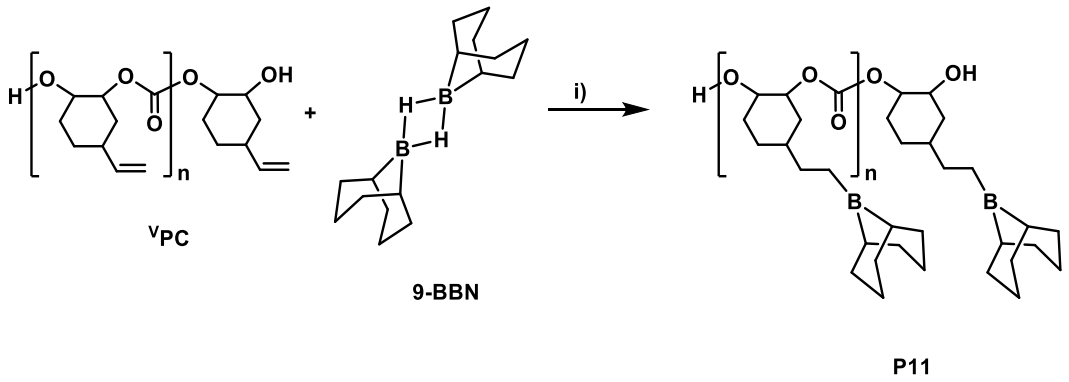
Although hydroboration is routinely used in organic chemistry to functionalise alkenes through subsequent oxidation or coupling reactions, its use in polymer chemistry remains more limited.[60-62] It has been used with various unsaturated hydrocarbon polymers; there is only one example of its use with an oxygenated polymer.[62] In this particular case, the pendant alkene groups on poly(β-hydroxyalknaote) (PHA) were transformed using hydroboration, which significantly increased the glass transition temperature (T_g) values from -54 ºC to -4 ºC.[62] No further reactions on the boronate functional polymer were conducted.

Hydroboration involves the addition of a B-H moiety from an organoborane reagent to an olefin, resulting in the formation of a new C-B bond.[63] Commercially available organoborane reagents include BH_3 adduct reagents, such as BH_3•THF or BH_3•SMe_2, monosubstituted boranes such as [(1R,2S,3R,5R)-2,6,6-trimethylbicyclo[3.1.1]hept-3-yl]borane ($IpcBH_2$) and disubstituted boranes such as 9-borabicyclo(3.3.1)nonane (9-BBN) or disiamylborane (Sia_2BH).

Preliminary investigations into hydroboration of the unsaturated polycarbonate applied the volatile borane adduct, BH_3•THF, was employed. Adding excess BH_3•THF into a THF solution of ^{V}PC, under an inert atmosphere, resulted in rapid formation of a gel. The product was almost totally insoluble in both common polar and apolar organic solvents. It is worth mentioning that the solid product isolated after drying could not reform the original gel-like material (*e.g.* by addition of excess THF). The product appears likely to be a highly cross-linked polycarbonate since BH_3•THF can perform both inter- and intra-molecular hydroboration reactions. To overcome

this, 9-BBN was applied since it is also known for selective hydroboration, based on its steric hindrance.[64]

4.2.7.1 Hydroboration of ^{V}PC using 9-BBN



^{V}PC 9-BBN P11

Scheme 4.5 Reaction between ^{V}PC and 9-BBN. i) THF, 25 °C, 1.5 h.

The hydroboration reaction between ^{V}PC and a slight excess of 9-BBN (1.2 equiv.) was performed under an inert atmosphere, in THF, at 25 °C. After 1.5 h, all the volatiles were removed *in vacuo,* and the polymer residue was washed with hexane to remove the unreacted 9-BBN. The product (**P11**) was isolated in high yield (> 80%) (Scheme 4.5). It was both air and moisture sensitive which prevented characterisation using SEC or DSC, but NMR studies showed complete functionalisation of ^{V}PC. Two signals at 5.04-5.11 and 5.77 ppm, corresponding to the vinyl protons in ^{V}PC, are completely absent in the spectrum of **P11**. New resonances, corresponding to 9-BBN protons, are observed at 1.19, 1.67 and 1.83 ppm (peaks 'a', 'd' and 'e', respectively, in Figure 4.19), which illustrates the successful incorporation of 9-BBN to the ^{V}PC.

The $^{13}C\{^{1}H\}$ NMR spectrum shows characteristic resonances at 153.5, 73.6, 33.3, 31.3 and 22.4 ppm (peaks 'K', 'J', 'H', 'F' and 'A', respectively, in Figure 4.19), which are assigned to the polymer carbonyl group and the backbone carbon atoms, C_β, C_γ, and C_α of 9-BBN, respectively. **P11** also gives rise to a broad resonance at +89 ppm in the ^{11}B NMR spectrum (Figure 4.20).

The NMR spectra confirm that the hydroboration only occurs at the alkene functional groups and is tolerant to the carbonate linkages. Although the hydroboration of carbonyl compounds is known, it generally requires metal catalysts to occur at an appreciable rate.[6-8] Furthermore, in the polymers, the electron-deficient carbonyl groups would be expected to react more slowly with B-H groups. This is in line with the ^{11}B NMR spectrum which does not show any resonances at 50-60 ppm, *i.e.* the typical region for RO-$\underline{B}_{9\text{-BBN}}$ signals (R is alkyl) (Figure 4.20).

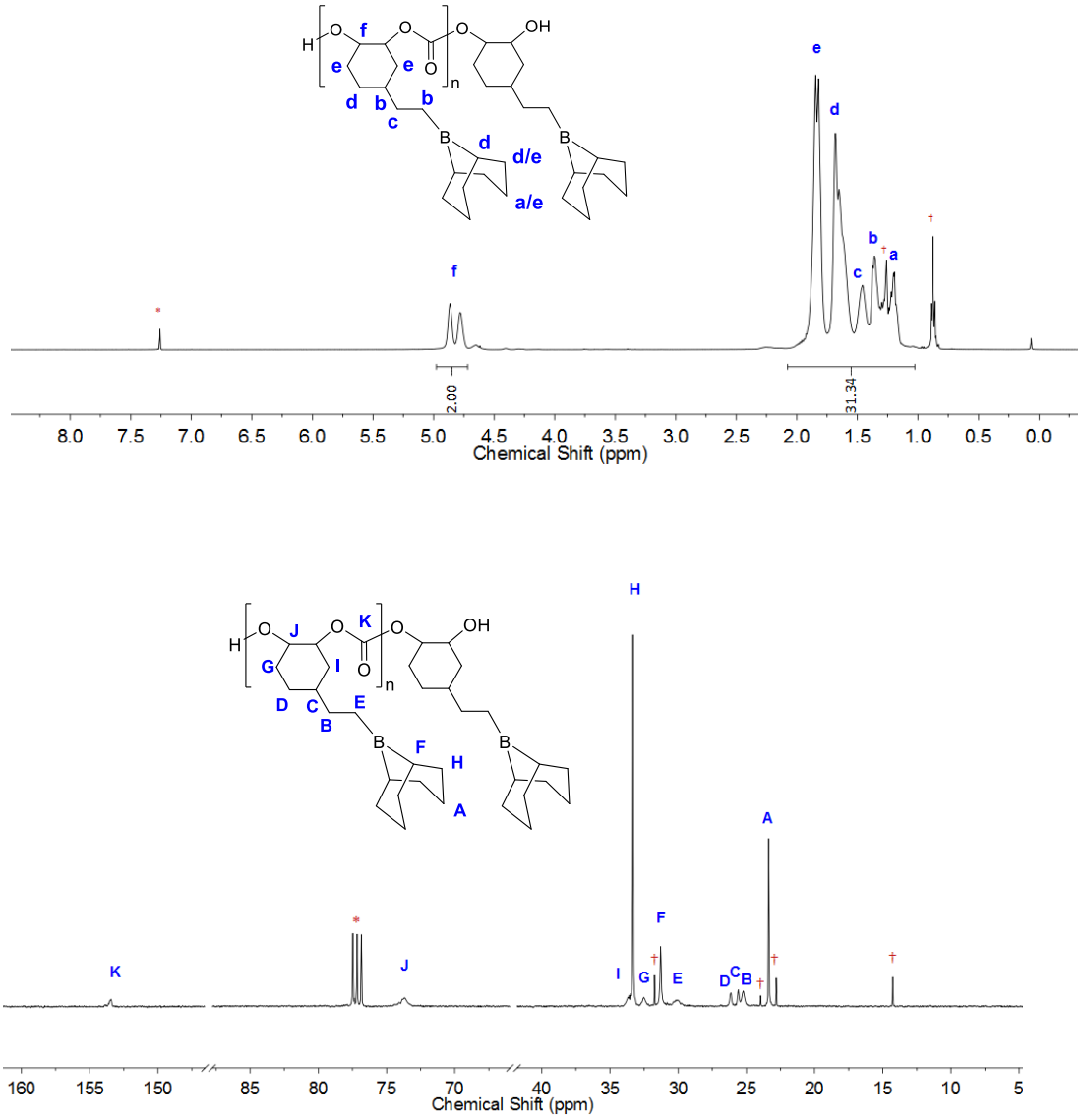


Figure 4.19 ^{1}H NMR spectrum and ^{13}C{^{1}H} NMR spectrum of **P11** (9-BBN functionalised ^{V}PC, ^{1}H NMR: $CDCl_3$, 400 MHz, 25 ºC, ^{13}C{^{1}H} NMR: $CDCl_3$, 100.7 MHz, 25 ºC). Asterisks and daggers denote residue protio-solvent and residue hexane, respectively.

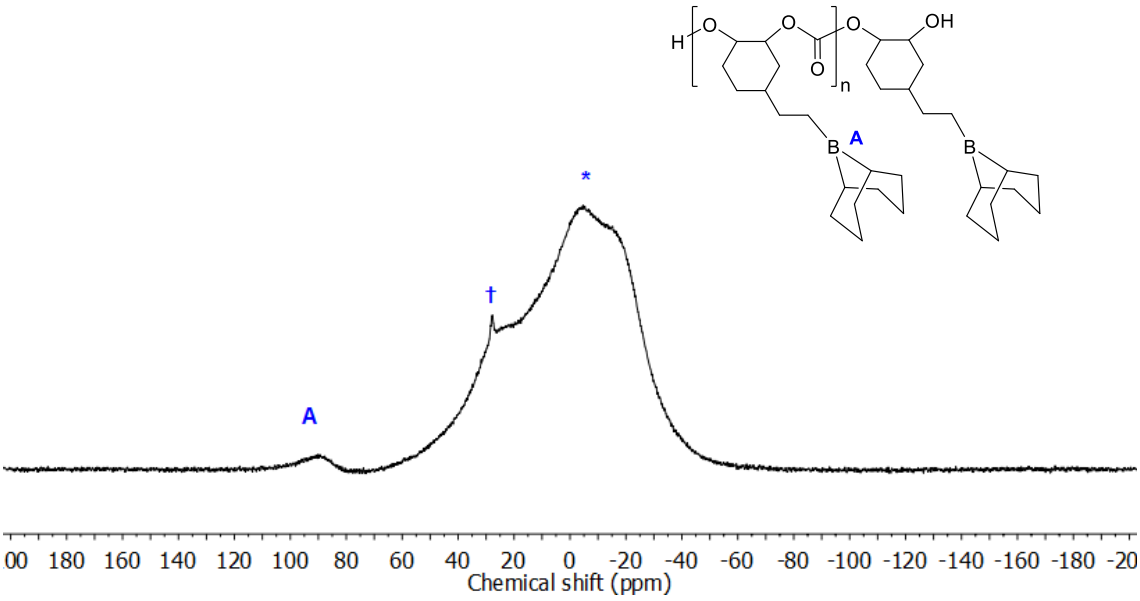


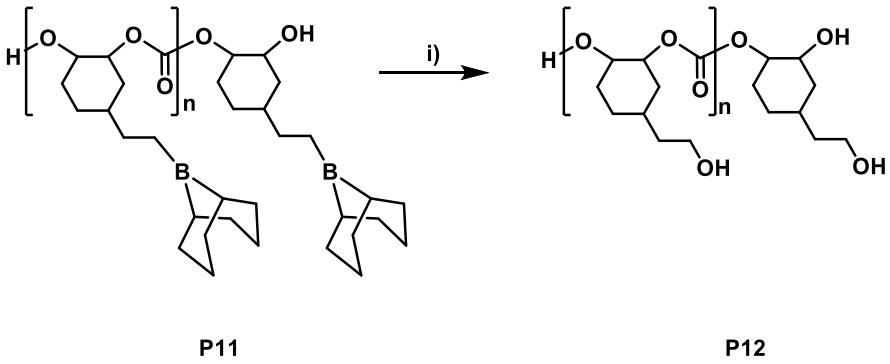
Figure 4.20 ^{11}B NMR spectrum of the product obtained from the reaction between ^{V}PC and 9-BBN (160.0 MHz, $CDCl_3$, 25 ºC). An asterisk and a dagger denote glass and residue 9-BBN, respectively

*4.2.7.2 Oxidation of **P11***

The oxidation of **P11** is targeted to add hydroxyl groups to the polymer backbone. Such oxidation reactions are usually accomplished using H_2O_2 as the oxidising agent, with a high concentration NaOH solution. However, the polycarbonate is expected to degrade under such conditions, so alternative reactions are required. Pelter *et al.*[65] and Keller *et al.*[66] have shown *m*-chloroperbenzoic acid (mCPBA) may be used as an alternative oxidant. For example, successful hydroboration-oxidation of (but-3'-enyl)-2,5-di(4'-butyloxybenzoyloxy)benzoate was achieved using 9-BBN and a large excess mCPBA ([mCPBA]/[9-BBN] = 5.2/1), importantly the ester groups remained unreacted.[66]

Thus, **P11** was reacted with a slight excess of mCPBA, in THF under an inert atmosphere, for 1.5 h. The reaction was quenched by addition of a methanol/water

mixture (10:1 v/v), and the polymer was purified by precipitation in water. The purified polymer **P12** was isolated in around 80% yield.



P11 **P12**

Scheme 4.6 Oxidation of polymer **P11.** i) 3.4 equiv of mCPBA, THF, 25 °C, 2 h.

The solubility of **P11** changed after oxidation: it was no longer soluble in chloroform and only sparingly soluble in THF. Its solubility was enhanced in polar solvents, including methanol and DMF, however, it was not soluble in water. To access its hydrophilicity, static water contact angle measurements were carried out on a film. Polymer films were prepared by solvent casting (30 $mg \cdot mL^{-1}$ in methanol, 100 μL) onto glass slides, which were then dried *in vacuo* at 25 °C for 48 h. ^{V}PC could not be coated onto glass using this method, and so it was solvent cast from a chloroform solution (500 $mg \cdot mL^{-1}$) to afford a polymer film. An uncoated glass slide was tested as a control. The ^{V}PC film showed a static water contact angle of 87 ± 2° and the glass slide was 84 ± 1°. The water contact angle of the film of **P12** was 51 ± 2°. The value decreased by nearly 36°, due to the increased hydrophilicity of **P12** after hydroboration-oxidation.

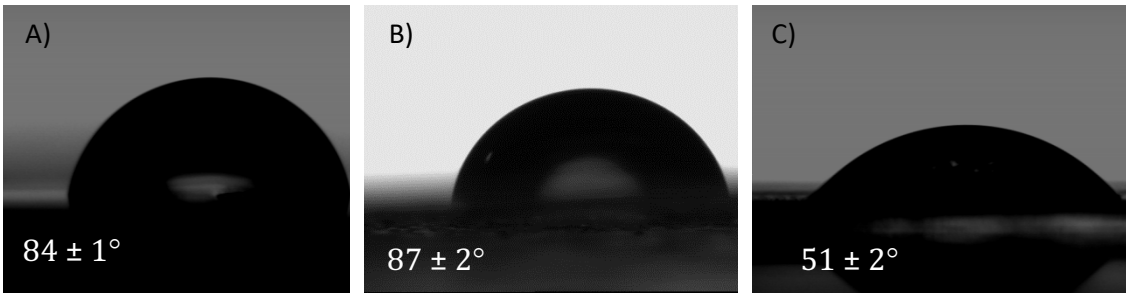


Figure 4.21 Photographs of water droplets on different surfaces: A) uncoated glass, B) ^{V}PC and C) **P12**.

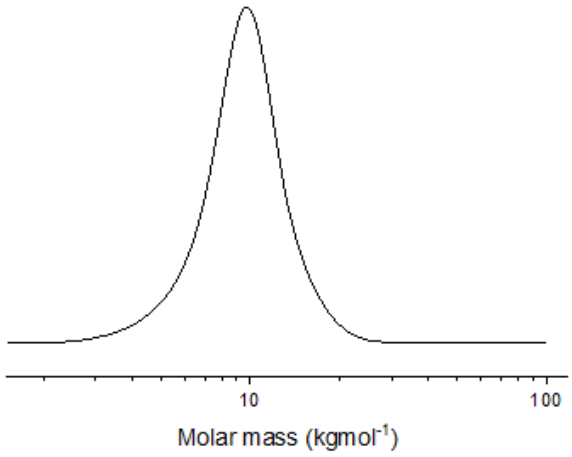


Figure 4.22 SEC trace of **P12**.

Characterisation of **P12** by SEC is complicated by its insolubility in THF, so it was analysed in DMF. Although the molar mass cannot be directly compared with ^{V}PC, a monomodal molar mass distribution and M_n of 8.8 kgmol^{-1} (Đ = 1.12) indicate that the polycarbonate was not significantly degraded.

Polymer **P12** was also fully characterised using ^{1}H, COSY, ^{13}C{^{1}H}, ^{11}B and ^{1}H-^{13}C{^{1}H} two-dimensional NMR studies. Its ^{1}H NMR spectrum shows a key triplet resonance at 3.58 ppm, assigned to the methylene protons next to the hydroxyl groups (peak 'e' in Figure 4.23). The signal at 4.77 ppm (peak 'f' in Figure 4.23) is assigned to the polycarbonate backbone protons, and the integrals are the same as for ^{V}PC. This

also suggests that no significant polymer degradation occurred during oxidation. Furthermore, no resonances assigned to 9-BBN are observed in the ^{1}H NMR spectrum. The ^{11}B NMR spectrum also shows no signals, implying the complete conversion of the boron intermediate to an alcohol functionalized polymer **P12**.

The ^{13}C{^{1}H} NMR spectrum of **P12** shows all the expected resonances which are correlated to the ^{1}H NMR spectrum. The key signals of the carbon bonded to the hydroxyl group and the polycarbonate backbone carbon atoms were observed at 60.6 and 75.4 ppm, respectively.

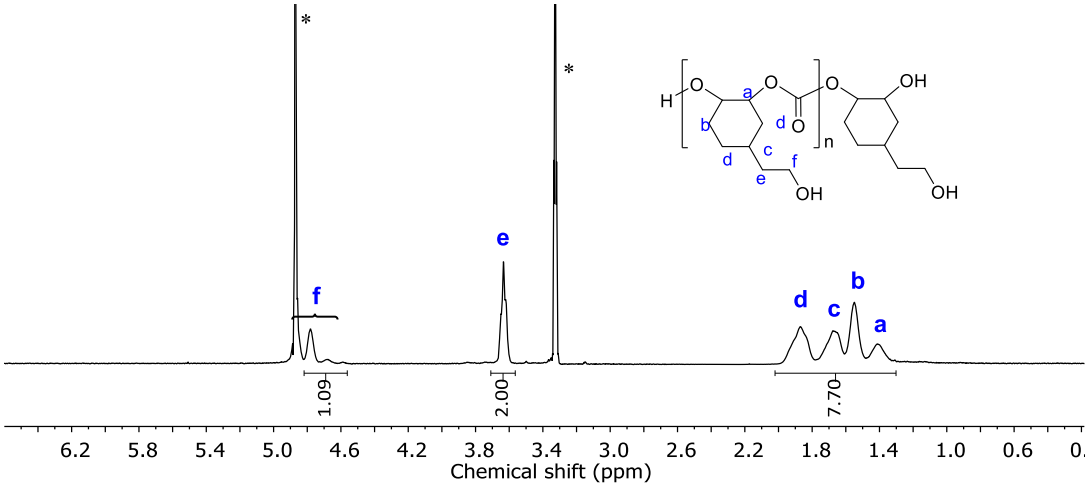
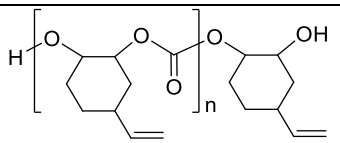
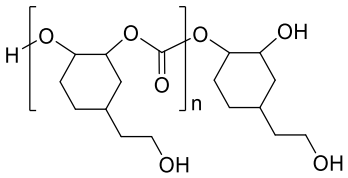
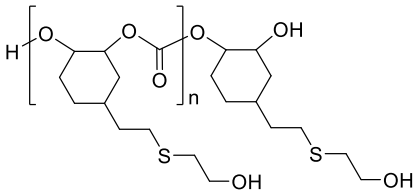


Figure 4.23 ^{1}H NMR spectrum of polymer **P12** (methanol-d_4, 400 MHz, 25 ºC). Asterisks denote residue protio-solvent.

Table 4.3 Thermal properties of polymer ^{V}**PC**, **P12** and **P13**.

Material		M_n (kgmol^{-1})	Đ	T_g[a] (°C)
	^{V}**PC**	5.7[a]	1.17[a]	101
	**P12**	8.8[b]	1.12[b]	88
	**P13**	6.6[a]	1.12[a]	57

[a] Acquired from the second heating cycles in DSC thermograms [b] Determined using SEC in THF, using monodispersed polystyrene as standards. [c] Determined using SEC in DMF, using monodispersed polystyrene as standards.

Thermal analysis of polymer **P12** was carried out using DSC (second heating cycle) and showed a glass transition temperature (T_g) at 88 °C (Figure 4.24). The T_g was compared to analogous polymers with similar M_n, *i.e.* ^{V}PC and derivative **P13** (Table 4.4). It was observed that the T_g values of **P12** (88 °C) and **P13** (57 °C) are lower than that of the parent ^{V}PC (101 °C). This is presumably due to the reduced packing efficiency of the branched polymers since the T_g values depend on chain flexibility. This trend in T_g values is in line with similar observations using poly(cyclohexadiene carbonate) (^{C}PC), poly(2-vinyloxirane carbonate) (PVIC) and their hydroxyl and carboxylic acid functionalised derivatives.[67]

The characterisations by NMR spectroscopy, SEC, water contact angle measurements and DSC all suggest complete post-polymerisation functionalisation of ^{V}PC, without any significant polymer degradation. It is worth noting that the two-step hydroboration-oxidation was carried out to identify the products formed at each step.

However, the hydroboration-oxidation reaction can also be performed in a one-pot manner, without isolating the hydroborated polymer product, which is more applicable to bulk functionalisation studies.

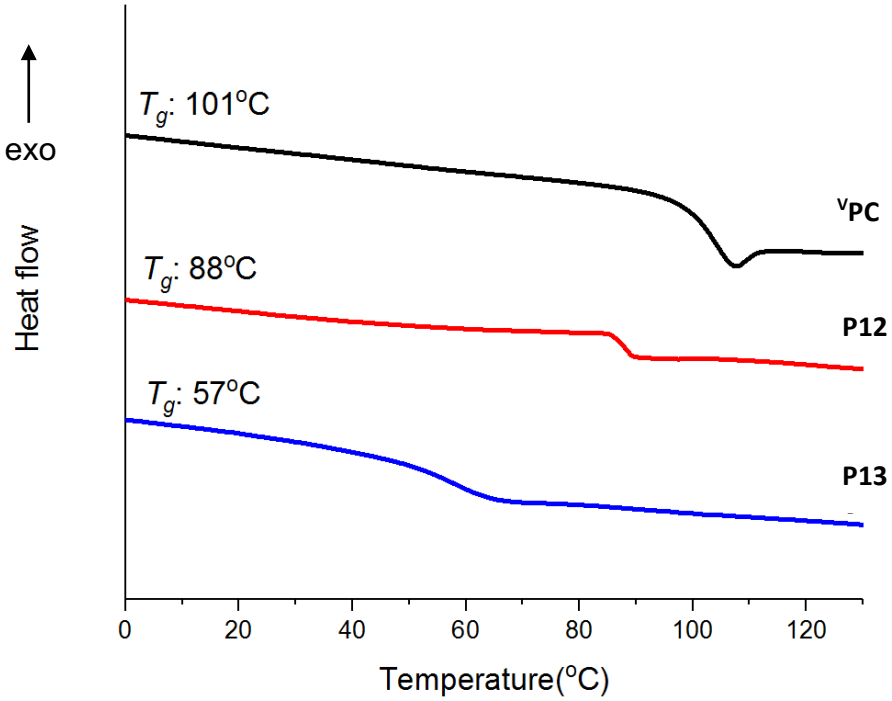


Figure 4.24 Overlaid DSC traces of ^{V}PC (Top), **P12** (Middle) and **P13** (Bottom).

*4.2.7.3 Cytotoxicity test and cell attachment test using **P12***

Cytotoxicity tests were then carried out to establish the change in biocompatibility after hydroboration-oxidation (using MC3T3-E1 cells). At a concentration of 200 mg·mL^{-1}, **P12** exhibited high biocompatibility, compared to the negative control PE. The degradation products also showed no significant toxicity at concentrations as high as 5000 μg·mL^{-1}. These results indicate an important improvement over ^{V}PC degradation products, which showed toxicity at a concentration of 1000 μg·mL^{-1}.

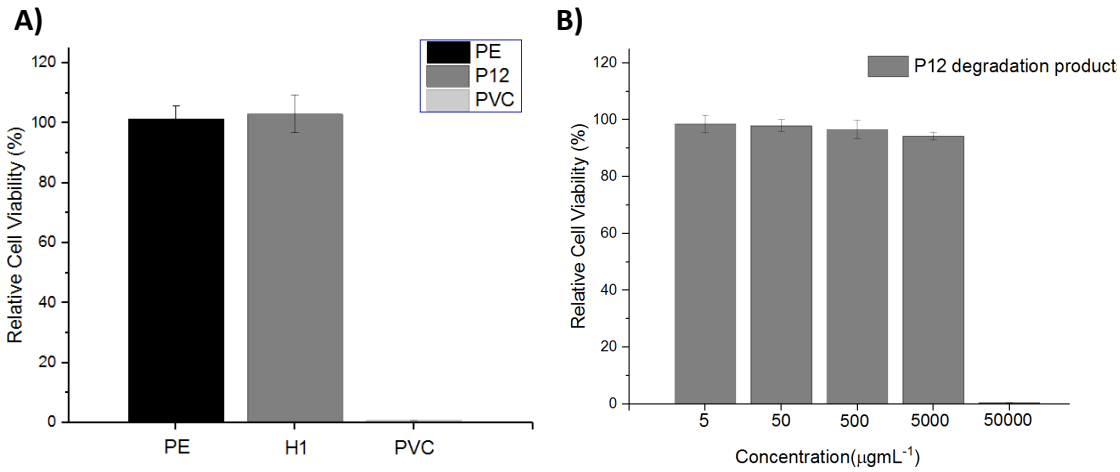


Figure 4.25 A) The viability of MC3T3-E1 cells (%) treated with **P12** extract medium and controls (PVC and PE) after 72 h incubation, determined by Alamar Blue test and B) Viability of MC3T3-E1 cells (%) treated with **P12** degradation products and controls after 72 h incubation, determined by Alamar Blue test. Data correspond to experiment run at least in triplicate.

The cellular response of MC3T3-E1 osteoblasts to **P12** was also investigated. In particularly, cell adhesion and spreading experiments were conducted for up to 24 h in serum-containing media. Prior to any tests, freshly prepared **P12** coatings were sterilised by exposure (60 s) to UV light (254 nm central wavelength and 2.5 $mW \cdot cm^{-2}$ power density). The cells were then seeded on the **P12** coatings in a cell plate (without any protein pre-treatment). The coatings were incubated overnight to ensure sufficient time for attachment and spreading. After 24 h incubation, they were analysed using confocal microscopy: a large number of spread cells were observed. In the control experiments, negligible cell attachment was observed because cells were rounded on the surface and as such were easily removed (*e.g.* during washings).

The *in vitro* cell data indicated that **P12** presented relatively low cytotoxicity and good cell adhesion, suggesting an improvement in biocompatibility using hydroboration-oxidation.

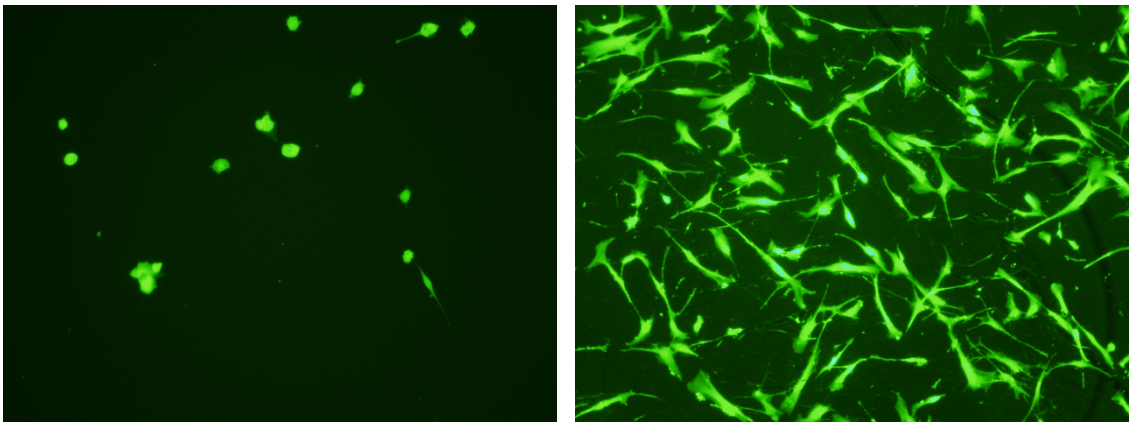


Figure 4.26 Confocal microscopy images of MC3T3-E1 cells on A) ^{V}**PC** and B) **P12** polymer coatings.

4.2.8 Syntheses of brush poly(carbonate-*g*-phosphoester)

The polymer side chain hydroxyl groups can also be used to initiate other polymerisations and form 'brush' polymers. Brush polymers are a special class of graft polymers with side chains densely linked to a polymer backbone that present a 'stretched' chain conformation. Brush polymers have attracted attention due to the relative ease in changing the chemical composition or graft density to tune physical/chemical properties, and future applications in medicines and photonics are suggested.[68-72] So far, most brush polymers are composed of non-degradable backbones and/or side chains, which limits their actual use in medical applications.[71-74] To meet medical requirements, both side chain and backbone should be degradable and biocompatible. Previous reports demonstrated successful syntheses of fully degradable graft polymer poly(carbonate-*g*-ester)s, using CO_2-derived polycarbonates as backbone material. The hydroxyl-functionalised polycarbonate macroinitiators were obtained by functionalising the alkenes *via* thiol-ene reaction.[68, 75] The hydroboration-oxidation method may be a superior means to introduce hydroxyl groups and enable the synthesis of graft polymers because the hydroxyl groups can be introduced closer to the polymer backbone, without any incorporation of sulfur atoms.

P12 was tested as the backbone and the hydroxyl side chains were used to initiate PEP polymerisation. **P12** is insoluble in DCM, so DMF was selected as the reaction solvent. To ensure EP ROP is initiated in DMF, a test reaction was performed using [EP]/[OH] ratio of 50, with $Sn(Oct)_2$ as the catalyst (CHD as the initiator), at 25 ºC. After 20 h, around 75% conversion to polymer was achieved (TOF = 2 h^{-1}).

Based on this result, a series of brush copolymers were prepared using **P12** as the macroinitiator. Polymerisations were stopped at around 50% EP conversion to avoid any significant transesterification reactions. The chemical structure, composition and molar mass of the final polymers were characterised using ^{1}H NMR spectroscopy and SEC. The ^{1}H NMR spectrum of the final polymer shows characteristic peaks at 4.25 ppm and 1.36 ppm, due to the PEP methylene and methyl protons (peaks 'G', 'H' and 'I', Figure 4.27). The PEP end group signals were observed at 3.78 ppm (peak 'J', Figure 4.27). By comparing the integrals of the end group signals versus the side chain methyl protons at 1.36 ppm, the $\overline{DP}$ of PEP was estimated to be 2, 3 and 5 for the brush copolymers, respectively (Table 4.4).

Table 4.4 Graft copolymerisation of EP onto **P12** backbone.

Entry	Polymer	$\overline{DP}^c$	$M_{n,theo}$ (kgmol^{-1})^d	$M_{n,SEC}$ (kgmol^{-1})^e	$Đ^e$	$T_{g,DSC}$ (^oC)^f
1	P12[a]	0	7.5	7.1[e]	1.12[e]	88
2	P14[b]	2	16.6	14.9	1.09	-2
3	P15[b]	3	23.6	16.7	1.23	-14
4	P16[b]	5	37.3	23.3	1.37	-22

[a] Obtained from hydroboration-oxidation of ^{V}PC. See Chapter 7 for details [b] Polymerisation condition: $[EP]_0/[P12]_0$ = 20/1, 1 wt% of $Sn(Oct)_2$, DMF, at 25 °C for 24 - 72 h. [c] $\overline{DP}$ was determined using ^{1}H NMR spectroscopy by the relative integrals of PEP end groups and main chain signals, at 4.25 and 3.78 ppm, respectively. [d] Theoretical molar mass of Entry 1 was determined on the basis of ($M^{NMR}_{[^VPC]}$ + $M_{[hydroxyl\ group]}$ × no. of vinyl groups), while the theoretical molar mass of Entry 2-4 was determined on the basis of ([EP] × conversion × $M_{[EP]}$)+$M^{NMR}_{[H1]}$ [e]Determined using SEC in DMF, using monodispersed polystyrene as standard. [f]Determined using DSC

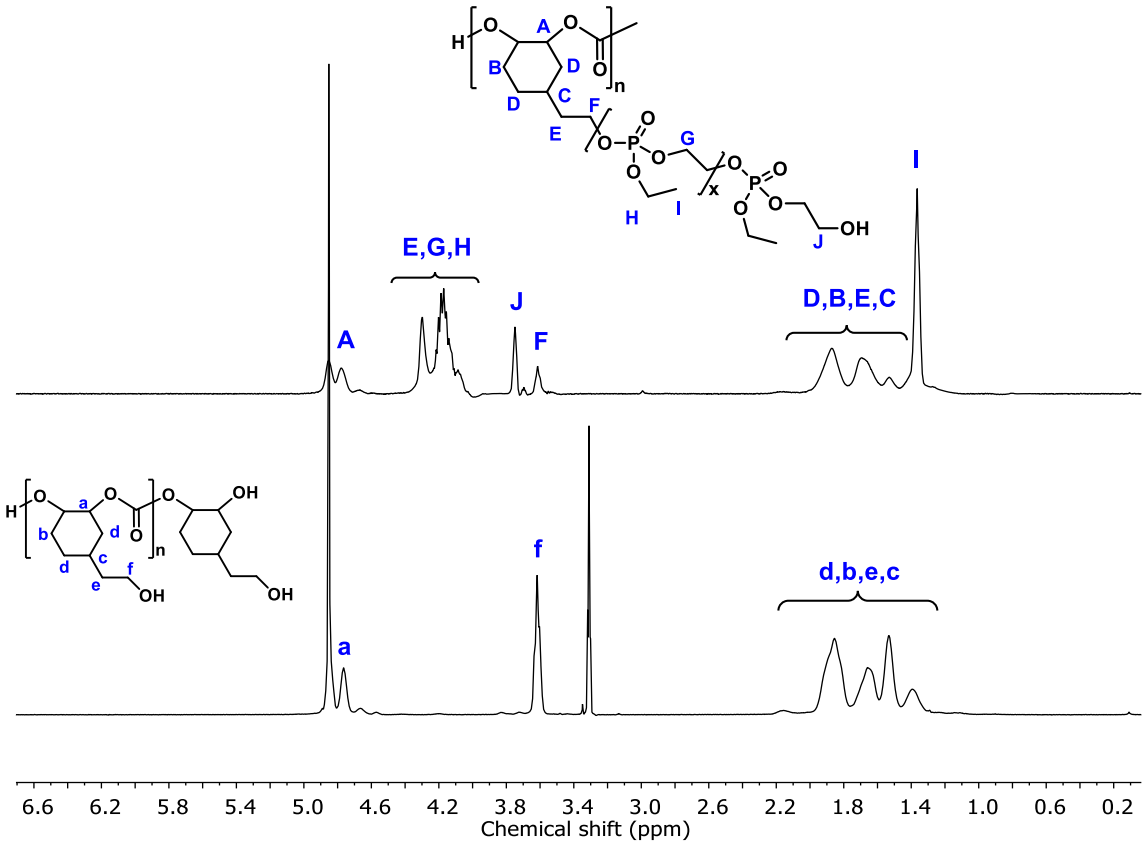


Figure 4.27 Stacked ^{1}H NMR spectra of **P12** and poly(carbonate-*g*-phosphoester) (methanol-d_4, 400 MHz, 25 ºC).

As seen in Figure 4.28, SEC curves of all the brush polymers are monomodal with narrow polydispersities (< 1.40). A shift to higher molar masses was observed with a higher degree of polymerisation, suggesting some control over side chain $\overline{DP}$. The difference between $M_{n,GPC}$ and $M_{n,theo}$ is attributed to the difference in hydrodynamic radii between graft polymer and linear chains; such differences are commonly observed for brush polymers.[68, 76]

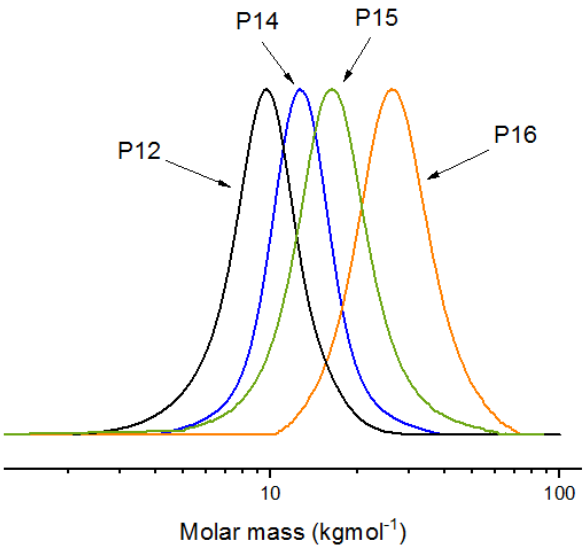


Figure 4.28 Overlaid SEC curves of **P12**, **P14**, **P15** and **P16**. DMF was used as a solvent and monodispersed polystyrene as a standard.

The thermal behaviour of the brush polymers was also investigated using DSC (Figure 4.29). The glass transition temperatures of **P12** and PEP are 88 and -50 °C respectively. A single T_g was observed for all brush polymers, and with increasing phosphoester segments in the side chains, the T_g decreases. The T_g values of the polymers vary from 88 °C to -22 °C after grafting short PEP chains, offering the potential to prepare materials that change from plastics to elastomers.

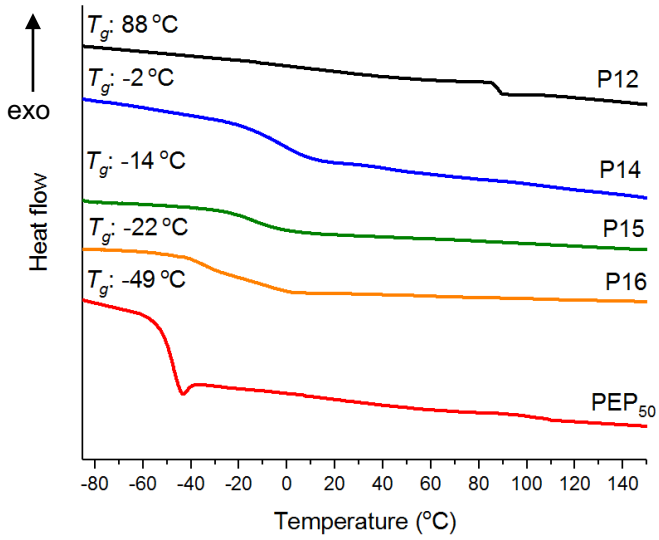


Figure 4.29 DSC curves of **P12**, **P14**, **P15**, **P16** and PEP_{50}.

4.3 Conclusions

4.3.1 Summary

The ring-opening polymerisation of ethyl ethylene phosphate using telechelic polycarbonate macro-initiators yielded amphiphilic ABA-type block copolymers. The relative hydrophilic/hydrophobic ratios were controlled and the polymeric materials afforded different self-assembly morphologies, including micelles and vesicles, as characterised by DLS and TEM imaging. Both the loading and release characteristics using Rhodamine B demonstrate the potential for the materials to be applied in controlled drug release applications in the future. In this study, the self-assembled structures were rapidly disrupted in the presence of alkaline phosphatase, under slightly basic conditions (pH = 8.8), as monitored by DLS and SEC. After degradation, the remaining product was ^{V}PC. Although ^{V}PC itself demonstrates no apparent cytotoxicity against MC3T3-E1 cell line, its degradation products are toxic at a concentration higher than 1000 $\mu g \cdot mL^{-1}$.

Hydroboration-oxidation has been demonstrated as a viable method to functionalise ^{V}PC with hydroxyl groups, and the product showed monomodal molar mass distributions with low dispersity. The incorporation of hydroxyl groups improved the hydrophilicity, cell compatibility and cell attachment of the polymers, as assessed by water contact angle measurements and cell studies. The hydroxyl groups were also used to initiate ROP of EP to prepare poly(carbonate-*g*-phosphoester) brush polymers with tunable thermal properties. It should be noted that this is the first work discussing the cell attachment of polycarbonates from CO_2/epoxide ROCOP and the cell viability of their degradation products.

4.3.2 Outlook

In future, toxicity assay should be carried out to establish how the nanostructures (*e.g.* micelles, vesicles and their degradation products) impact cell behaviour using both cancer cells (*e.g.* cervical carcinoma cell line) and healthy cells (*e.g.* human dermal fibroblasts). So far, only the delivery of RhB has been investigated, the delivery of hydrophobic drugs (e.g. paclitaxel and Levonorgestrel) is certainly worth investigation in future. The delivery of proteins are also of interest since many are very difficult to administer due to rapid degradation and poor cell membrane permeation.[77, 78]

It may also be possible to transform the alkene groups into stimuli-responsive groups (*e.g.* by pH, thermal or sugar-triggers, Figure 4.28). Such a material might function with the polyphosphoester block showing enzymatic degradation and the polycarbonate block being triggered to assemble/disassemble.

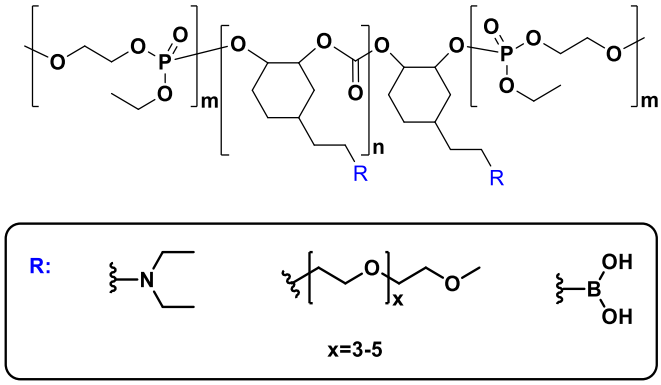


Figure 4.30 Potential dual-responsive polymers.

4.4 References

1. X.-B. Xiong, Z. Binkhathlan, O. Molavi and A. Lavasanifar, *Acta Biomater.*, 2012, **8**, 2017-2033.
2. J. Li, M. Huo, J. Wang, J. Zhou, J. M. Mohammad, Y. Zhang, Q. Zhu, A. Y. Waddad and Q. Zhang, *Biomaterials*, 2012, **33**, 2310-2320.
3. K. Cai, X. He, Z. Song, Q. Yin, Y. Zhang, F. M. Uckun, C. Jiang and J. Cheng, *J. Am. Chem. Soc.*, 2015, **137**, 3458-3461.
4. H. Wei, L. R. Volpatti, D. L. Sellers, D. O. Maris, I. W. Andrews, A. S. Hemphill, L. W. Chan, D. S. H. Chu, P. J. Horner and S. H. Pun, *Angew. Chem., Int. Ed.*, 2013, **52**, 5377-5381.
5. J. M. Priegue, D. N. Crisan, J. Martínez-Costas, J. R. Granja, F. Fernandez-Trillo and J. Montenegro, *Angew. Chem., Int. Ed.*, 2016, **55**, 7492-7495.
6. S.-J. Gwak, C. Macks, D. U. Jeong, M. Kindy, M. Lynn, K. Webb and J. S. Lee, *Biomaterials*, 2017, **121**, 155-166.
7. F. Zhang, S. Zhang, S. F. Pollack, R. Li, A. M. Gonzalez, J. Fan, J. Zou, S. E. Leininger, A. Pavía-Sanders, R. Johnson, L. D. Nelson, J. E. Raymond, M. Elsabahy, D. M. P. Hughes, M. W. Lenox, T. P. Gustafson and K. L. Wooley, *J. Am. Chem. Soc.*, 2015, **137**, 2056-2066.
8. B. D. Ulery, L. S. Nair and C. T. Laurencin, *J. Polym. Sci., Part B: Polym. Phys.*, 2011, **49**, 832-864.
9. K. Kataoka, A. Harada and Y. Nagasaki, *Adv. Drug Delivery Rev.*, 2001, **47**, 113-131.
10. T. Steinbach and F. R. Wurm, *Angew. Chem., Int. Ed.*, 2015, **54**, 6098-6108.

11. K. Knop, R. Hoogenboom, D. Fischer and U. S. Schubert, *Angew. Chem., Int. Ed.*, 2010, **49**, 6288-6308.
12. T. Wolf, T. Steinbach and F. R. Wurm, *Macromolecules*, 2015, **48**, 3853-3863.
13. T. Steinbach, S. Ritz and F. R. Wurm, *ACS Macro Lett.*, 2014, **3**, 244-248.
14. H. Wang, L. Su, R. Li, S. Zhang, J. Fan, F. Zhang, T. P. Nguyen and K. L. Wooley, *ACS Macro Lett.*, 2017, **6**, 219-223.
15. Y. C. Wang, Y. Y. Yuan, J. Z. Du, X. Z. Yang and J. Wang, *Macromol. Biosci.*, 2009, **9**, 1154-1164.
16. X.-Z. Yang, Y.-C. Wang, L.-Y. Tang, H. Xia and J. Wang, *J. Polym. Sci. Part A: Polym. Chem.*, 2008, **46**, 6425-6434.
17. Y.-C. Wang, Y. Li, X.-Z. Yang, Y.-Y. Yuan, L.-F. Yan and J. Wang, *Macromolecules*, 2009, **42**, 3026-3032.
18. G.-P. Wu and D. J. Darensbourg, *Macromolecules*, 2016, **49**, 807-814.
19. J. Xu, E. Feng and J. Song, *J. Appl. Polym. Sci.*, 2014, **131**, 39822.
20. K. Fukushima, *Biomater. Sci.*, 2016, **4**, 9-24.
21. T. Artham and M. Doble, *Macromol. Biosci.*, 2008, **8**, 14-24.
22. Z. Zhang, R. Kuijer, S. K. Bulstra, D. W. Grijpma and J. Feijen, *Biomaterials*, 2006, **27**, 1741-1748.
23. J. D. Robertson, G. Yealland, M. Avila-Olias, L. Chierico, O. Bandmann, S. A. Renshaw and G. Battaglia, *ACS Nano*, 2014, **8**, 4650-4661.
24. M. Scharfenberg, J. Hilf and H. Frey, *Adv. Funct. Mater.*, 1704302.
25. R. J. Williams, I. A. Barker, R. K. O'Reilly and A. P. Dove, *ACS Macro Lett.*, 2012, **1**, 1285-1290.
26. D. M. Stevens, A. Rahalkar, B. Spears, K. Gilmore, E. Douglas, M. Muthukumar and E. Harth, *Polym. Chem.*, 2015, **6**, 1096-1102.
27. S. Tempelaar, L. Mespouille, P. Dubois and A. P. Dove, *Macromolecules*, 2011, **44**, 2084-2091.
28. C.-S. Xiao, Y.-C. Wang, J.-Z. Du, X.-S. Chen and J. Wang, *Macromolecules*, 2006, **39**, 6825-6831.
29. J. Du and R. K. O' Reilly, *Soft Matter*, 2009, **5**, 3544-3561.
30. L. Zhang and A. Eisenberg, *J. Am. Chem. Soc.*, 1996, **118**, 3168-3181.
31. A. O. Moughton and R. K. O' Reilly, *Chem. Commun.*, 2010, **46**, 1091-1093.
32. C. Fernyhough, A. J. Ryan and G. Battaglia, *Soft Matter*, 2009, **5**, 1674-1682.

33. R. W. O' Brien, B. R. Midmore, A. Lamb and R. J. Hunter, *Faraday Discuss. Chem. Soc.*, 1990, **90**, 301-312.
34. J. Du and S. P. Armes, *J. Am. Chem. Soc.*, 2005, **127**, 12800-12801.
35. B. S. Tucker and B. S. Sumerlin, *Polym. Chem.*, 2014, **5**, 1566-1572.
36. W. Huang, C. Shi, Y. Shao, K. S. Lam and J. Luo, *Chem. Commun.*, 2013, **49**, 6674-6676.
37. J. Fang, H. Nakamura and H. Maeda, *Adv. Drug Delivery Rev.*, 2011, **63**, 136-151.
38. A. Kowalczuk, R. Trzcinska, B. Trzebicka, A. H. E. Müller, A. Dworak and C. B. Tsvetanov, *Prog. Polym. Sci.*, 2014, **39**, 43-86.
39. S. Louguet, B. Rousseau, R. Epherre, N. Guidolin, G. Goglio, S. Mornet, E. Duguet, S. Lecommandoux and C. Schatz, *Polym. Chem.*, 2012, **3**, 1408-1417.
40. M.-H. Xiong, Y. Bao, X.-Z. Yang, Y.-C. Wang, B. Sun and J. Wang, *J. Am. Chem. Soc.*, 2012, **134**, 4355-4362.
41. Y. Zhang, H. F. Chan and K. W. Leong, *Adv. Drug Delivery Rev.*, 2013, **65**, 104-120.
42. P. Calvo, J. L. Vila-Jato and M. J. Alonso, *J. Pharm. Sci.*, 1996, **85**, 530-536.
43. Z. Zhao, J. Wang, H.-Q. Mao and K. W. Leong, *Adv. Drug Delivery Rev.*, 2003, **55**, 483-499.
44. C. Wachiralarpphaithoon, Y. Iwasaki and K. Akiyoshi, *Biomaterials*, 2007, **28**, 984-993.
45. T. Suyama and Y. Tokiwa, *Enzyme Microb. Technol.*, 1997, **20**, 122-126.
46. J. Baran and S. Penczek, *Macromolecules*, 1995, **28**, 5167-5176.
47. Y.-C. Wang, L.-Y. Tang, Y. Li and J. Wang, *Biomacromolecules*, 2009, **10**, 66-73.
48. Y. Iwasaki, C. Nakagawa, M. Ohtomi, K. Ishihara and K. Akiyoshi, *Biomacromolecules*, 2004, **5**, 1110-1115.
49. Q. Liu, J. Chen and J. Du, *Biomacromolecules*, 2014, **15**, 3072-3082.
50. W. Agut, A. Brulet, D. Taton and S. Lecommandoux, *Langmuir*, 2007, **23**, 11526-11533.
51. C. Jumeaux, R. Chapman, R. Chandrawati and M. M. Stevens, *Polym. Chem.*, 2015, **6**, 4116-4122.
52. J. Liu, W. Huang, Y. Pang, X. Zhu, Y. Zhou and D. Yan, *Biomacromolecules*, 2010, **11**, 1564-1570.

53. Y. H. Lim, G. S. Heo, Y. H. Rezenom, S. Pollack, J. E. Raymond, M. Elsabahy and K. L. Wooley, *Macromolecules*, 2014, **47**, 4634-4644.
54. Q. Gan, D. Dai, Y. Yuan, J. Qian, S. Sha, J. Shi and C. Liu, *Biomed. Microdevices*, 2012, **14**, 259-270.
55. D. C. Genetos, D. J. Geist, D. Liu, H. J. Donahue and R. L. Duncan, *J. Bone Miner. Res.*, 2005, **20**, 41-49.
56. M. D. Timmer, H. Shin, R. A. Horch, C. G. Ambrose and A. G. Mikos, *Biomacromolecules*, 2003, **4**, 1026-1033.
57. F. P. Guengerich, *Chem. Res. Toxicol.*, 2001, **14**, 611-650.
58. E. L. Loechler, M. M. Teeter and M. D. Whitlow, *J. Biomol. Struct. Dyn.*, 1988, **5**, 1237-1257.
59. J. T. Groves, G. E. Avaria-Neisser, K. M. Fish, M. Imachi and R. L. Kuczkowski, *J. Am. Chem. Soc.*, 1986, **108**, 3837-3838.
60. T. C. Chung, M. Raate, E. Berluche and D. N. Schulz, *Macromolecules*, 1988, **21**, 1903-1907.
61. F. Moingeon, J. Roeser, P. Masson, F. Arnaud and S. Mery, *Chem. Commun.*, 2008, 1341-1343.
62. C. Guillaume, N. Ajellal, J.-F. Carpentier and S. M. Guillaume, *J. Polym. Sci., Part A: Polym. Chem.*, 2011, **49**, 907-917.
63. C. Sandford and V. K. Aggarwal, *Chem. Commun.*, 2017, **53**, 5481-5494.
64. H. C. Brown, E. F. Knights and C. G. Scouten, *J. Am. Chem. Soc.*, 1974, **96**, 7765-7770.
65. A. Pelter, L. Hughes and J. M. Rao, *J. Chem. Soc., Perkin Trans. 1*, 1982, 719-722.
66. P. Keller, D. L. Thomsen and M. H. Li, *Macromolecules*, 2002, **35**, 581-584.
67. D. J. Darensbourg and F.-T. Tsai, *Macromolecules*, 2014, **47**, 3806-3813.
68. J.-F. Zhang, W.-M. Ren, X.-K. Sun, Y. Meng, B.-Y. Du and X.-H. Zhang, *Macromolecules*, 2011, **44**, 9882-9886.
69. X. Jiang, M. C. Lok and W. E. Hennink, *Bioconjugate Chem.*, 2007, **18**, 2077-2084.
70. R. Djalali, S.-Y. Li and M. Schmidt, *Macromolecules*, 2002, **35**, 4282-4288.
71. H.-i. Lee, J. Pietrasik, S. S. Sheiko and K. Matyjaszewski, *Prog. Polym. Sci.*, 2010, **35**, 24-44.

72. S. S. Sheiko, B. S. Sumerlin and K. Matyjaszewski, *Prog. Polym. Sci.*, 2008, **33**, 759-785.
73. H.-i. Lee, W. Jakubowski, K. Matyjaszewski, S. Yu and S. S. Sheiko, *Macromolecules*, 2006, **39**, 4983-4989.
74. K. L. Beers, S. G. Gaynor, K. Matyjaszewski, S. S. Sheiko and M. Möller, *Macromolecules*, 1998, **31**, 9413-9415.
75. J. Geschwind, F. Wurm and H. Frey, *Macromol. Chem. Phys.*, 2013, **214**, 892-901.
76. D. Han, X. Tong and Y. Zhao, *Macromolecules*, 2011, **44**, 5531-5536.
77. T. Smart, H. Lomas, M. Massignani, M. V. Flores-Merino, L. R. Perez and G. Battaglia, *Nano Today*, 2008, **3**, 38-46.
78. T. Rezai, J. E. Bock, M. V. Zhou, C. Kalyanaraman, R. S. Lokey and M. P. Jacobson, *J. Am. Chem. Soc.*, 2006, **128**, 14073-14080.

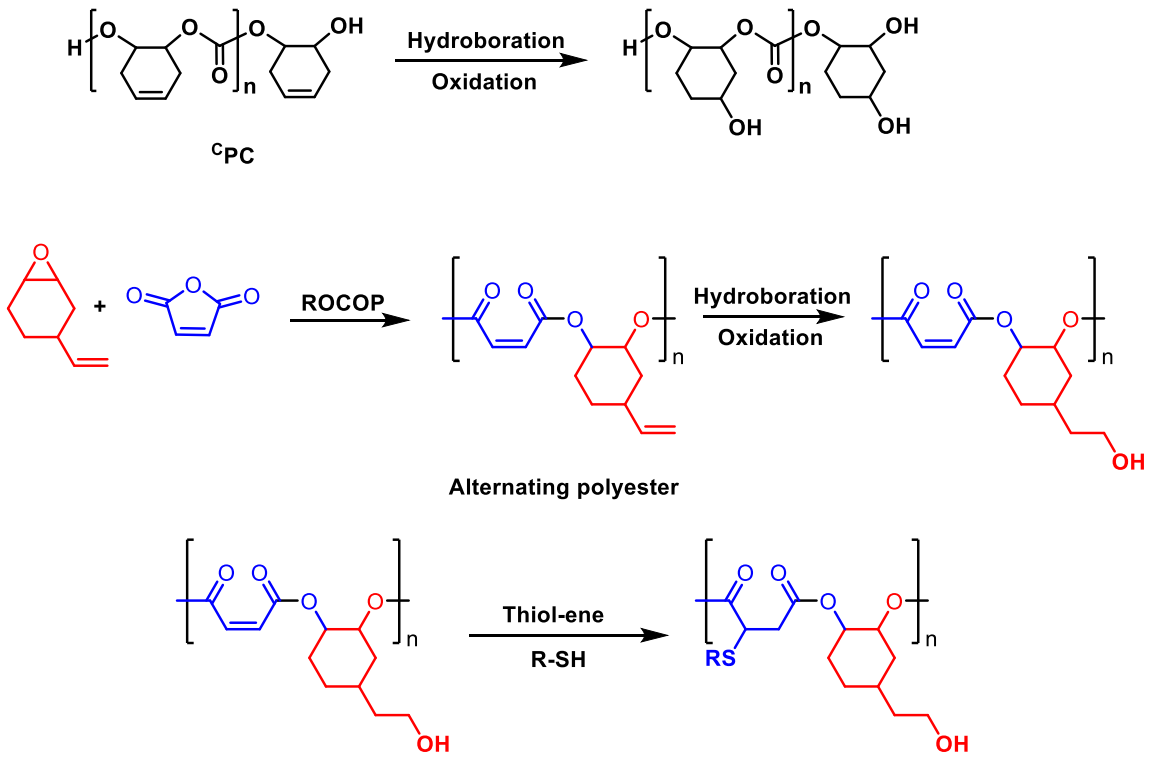
Chapter 5

Selective Post-polymerisation Modifications in Functionalising Unsaturated Polycarbonates and Polyesters

5.1 Background and Aims

There is an increasing interest in functionalised polymers, both to modify physical and chemical properties and to conjugate biomolecules.[1, 2] In the previous chapter, hydroboration-oxidation was used to functionalise the pendant alkene groups of ^{V}PC into hydroxyl groups. The incorporation of hydroxyl groups improved its hydrophilicity and allowed better cell adhesion. Currently, a major challenge is to develop orthogonal functionalisation reactions to introduce multiple groups onto a single polymer backbone and to control their positions precisely.[3, 4] This chapter will investigate methods to pattern polymers by specifically using hydroboration-oxidation and thiol-ene reactions. The strategy relies on the difference in reactivities of different types of alkene. In this context, a terminal alkene is defined as an alkene group with substituents on only one carbon, and an internal alkene features substituents at both carbons. It is worth noting selective patterning cannot easily be achieved using only thiol-ene reactions, due to its extremely rapid and complex kinetics (*i.e.* the rate-limiting step differs for different alkenes and thiols).[5]

Here, hydroboration-oxidation reactions will be investigated using ^{C}PC, internal alkene-containing polycarbonate, to compare the reactivity with previously examined ^{V}PC (terminal alkene-containing polycarbonate). Next, polymers containing two different alkene functionalities will be synthesised. The selective reaction of the terminal alkene groups to form hydroxyl groups will be investigated together with the sequential thiol-ene reactions on the internal alkene to incorporate a second substituent, *e.g.* alkyl, amine, carboxyl and methoxy-oligo(ethylene glycol). The material properties before and after functionalisation will be compared so as to understand the potential of this patterning method.

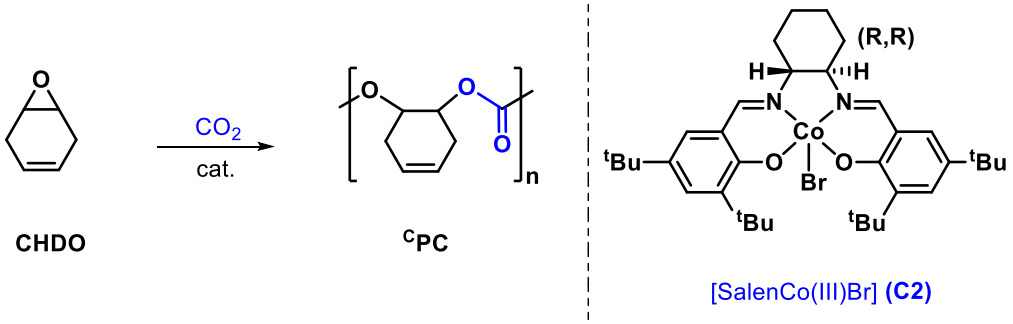


Scheme 5.1 Structures of polymers targeted in this work.

5.2 Results and Discussion

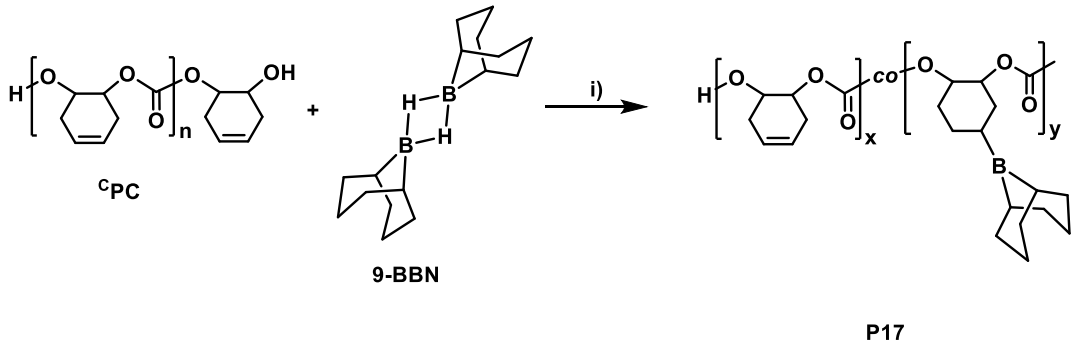
5.2.1 Hydroboration-oxidation of poly(cyclohexadiene oxide) (^{C}PC)

Poly(cyclohexadiene oxide) (^{C}PC) was first synthesised *via* cyclohexadiene oxide (CHDO)/CO_2 ROCOP using **C2** as the catalyst, bis(triphenylphosphine)iminium bromide (PPNBr) as the co-catalyst, and n-propanol as the chain-transfer agent (CTA), according to a previous report.[6] The polymerisation was performed at 20 bar CO_2 pressure and 30 °C. By varying the monomer loadings, the ^{C}PC showed M_n values from 2.0 to 6.2 kgmol^{-1}, with narrow dispersities (≤ 1.2).



Scheme 5.2 ROCOP of CHDO and CO_2 using **C2**. **C2** was applied in combination with a co-catalyst (PPNBr).

The previously successful hydroboration-oxidation methodology used with ^{V}PC was applied to ^{C}PC (M_n = 2.1 kgmol^{-1}, Đ = 1.13) (Scheme 5.2). However, these conditions were totally unsuccessful even with prolonged reaction times. The hydroboration of ^{C}PC required higher reaction temperatures (70 °C) and a reaction time of 5 h. The crude product was purified by washing with hexane and was dried *in vacuo*.



Scheme 5.3 Hydroboration of ^{C}PC with 9-BBN. i) THF, 70 °C, 5 h.

The hydroborated polymer **P17** was characterised using ^{1}H, ^{13}C{^{1}H}, ^{11}B and ^{1}H-^{13}C{^{1}H} two-dimensional NMR spectroscopy. The ^{1}H and ^{13}C NMR spectra show broad resonances which hamper complete assignment. Nevertheless, high conversion (> 70%) of alkene groups from ^{C}PC to **P17** was indicated by a change in intensity of the resonance at 5.57 ppm (peak 'a', Figure 5.1) corresponding to the alkene protons. The backbone polymer resonance at 4.96 ppm for ^{C}PC (peak 'b', Figure 5.1) shifted to 4.70 ppm for **P17** (peak 'b'', Figure 5.1). For **P17**, the broad resonances at 1.0–2.5 ppm were assigned to 9-BBN protons. A broad resonance at +89 ppm was observed in the ^{11}B NMR spectrum, which was assigned to the coordinated 9-BBN boron atom (Figure 5.2). SEC analysis was not carried out due to the air sensitivity of **P17**.

The reaction did not proceed to reach full conversion even when raising the temperature to 80 °C. Other attempts to achieve higher conversion of the alkene groups by use of chlorinated solvent or longer reaction times were also unsuccessful. It is possible that the sterically hindered 9-BBN substituent prevents or slows substitution of some adjacent monomers. The use of a less sterically hindered borane may overcome this problem, but will also likely lead to chain cross-linking side reactions.

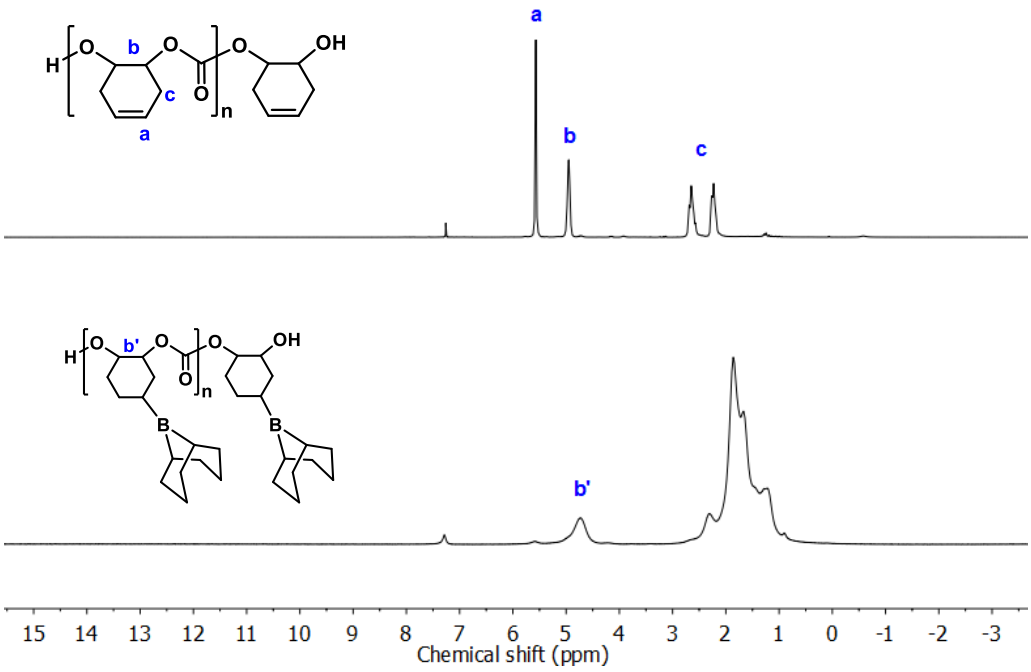


Figure 5.1 Stacked ^{1}H NMR spectra of ^{C}PC (Top) and the corresponding hydroborated product **P17** (Bottom) ($CDCl_3$, 400.0 MHz, 25 ºC).

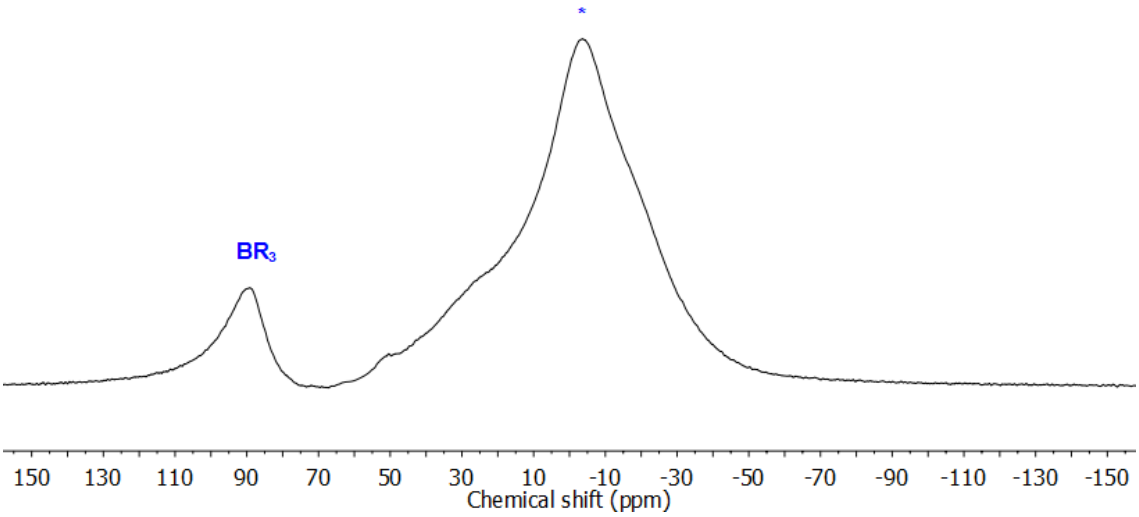
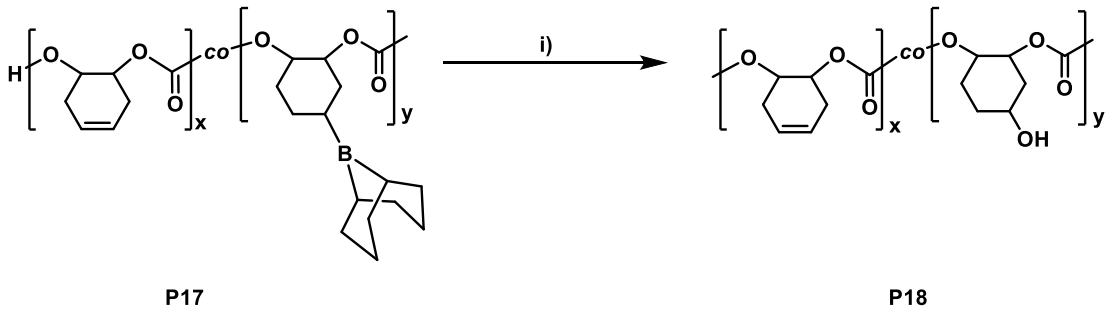


Figure 5.2 ^{11}B NMR spectrum of the product obtained from the reaction between ^{C}PC and 9-BBN after reacting at 80 °C for 24 h (160.0 MHz, $CDCl_3$, 25 ºC). An asterisk denotes glass.



Scheme 5.4 Oxidation of polymer **P17.** i) 3.4 equiv. of mCPBA, THF, 25 °C, 2 h

The same oxidation conditions (mCPBA, 2 h at 25 °C) used to prepare hydroxylated ^{V}PC were adopted in the oxidation of **P17** (Scheme 5.4). The crude polymer was isolated in a yield of around 75%. The hydroxyl functionalised polymer **P18** was primarily characterised by ^{1}H, ^{13}C{^{1}H}, COSY and ^{1}H-^{13}C{^{1}H} NMR spectroscopy. In the ^{1}H NMR spectrum, the alkene resonances at 5.58 ppm (peak 'c', Figure 5.3) were still present, indicating the incomplete conversion to hydroxyl groups. Some successful oxidation was confirmed by the signals at 3.59 ppm (peak 'i', Figure 5.3), which was due to methine protons adjacent to the hydroxyl. This resonance also coupled with the adjacent methylene protons (peaks 'h' and 'g', Figure 5.3). The signals at 4.57-4.86 ppm were assigned to functionalised polymer backbone protons (peaks 'd' and 'e', Figure 5.3). However, these peaks overlapped with the signals of the unfunctionalised backbone (peak 'a', Figure 5.3). The degree of functionalisation was calculated to be 75% by comparing the integrals of backbone protons (H_a + H_d + H_e) and H_c.

SEC analysis of polymer **P18** shows a single peak at M_n of 3.1 kDa (Đ = 1.13), suggesting that the polymer backbone remains unreacted during the hydroboration-oxidation. The polymer is amorphous, and thermal analysis shows only one T_g at 102 °C, which is 10 °C lower than that of ^{C}PC (Figure 5.4).

The static water contact angle measurements were conducted on both ^{C}PC and **P18**. ^{C}PC has a water contact angle of 85 ± 1°, whereas **P18** has a water contact angle of 65 ± 1°. The decrease in water contact angle suggests the increase in hydrophilicity even after partial functionalisation.

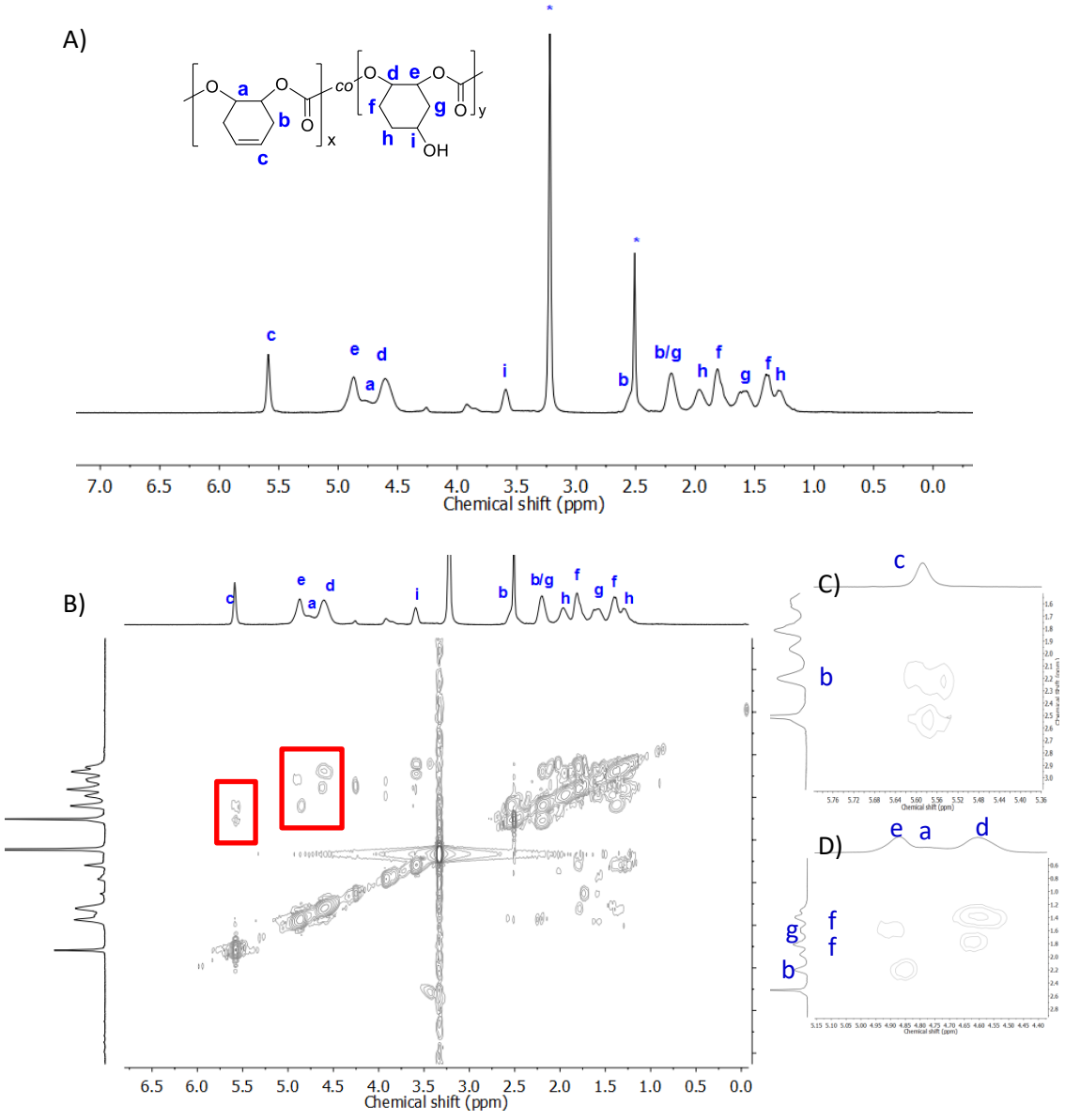


Figure 5.3 A) ^{1}H NMR spectrum of polymer **P18** (DMSO-d_6, 400.0 MHz, 25 ºC). B) A) ^{1}H-^{1}H COSY NMR spectrum of polymer **P18** (DMSO-d_6, 400.0 MHz, 25 ºC). C) An enlarged ^{1}H-^{1}H COSY NMR spectrum corresponding to the selected area in B). The signals at (5.58, 2.21) and (5.58, 2.54) ppm are assigned to the coupling between H_c and H_b on the ^{C}PC moiety. D) An enlarged ^{1}H-^{1}H COSY NMR spectrum

corresponding to the selected area in B). The signals at (4.90, 1.63), (4.62, 1.38) and (4.62, 1.77) ppm are assigned to the coupling between H_e and H_g and the coupling between on the H_d and H_f on the hydroxyl-functionalised ^{C}PC moiety. The signal at (4.85, 2.21) ppm is assigned to the coupling between H_a and H_b.

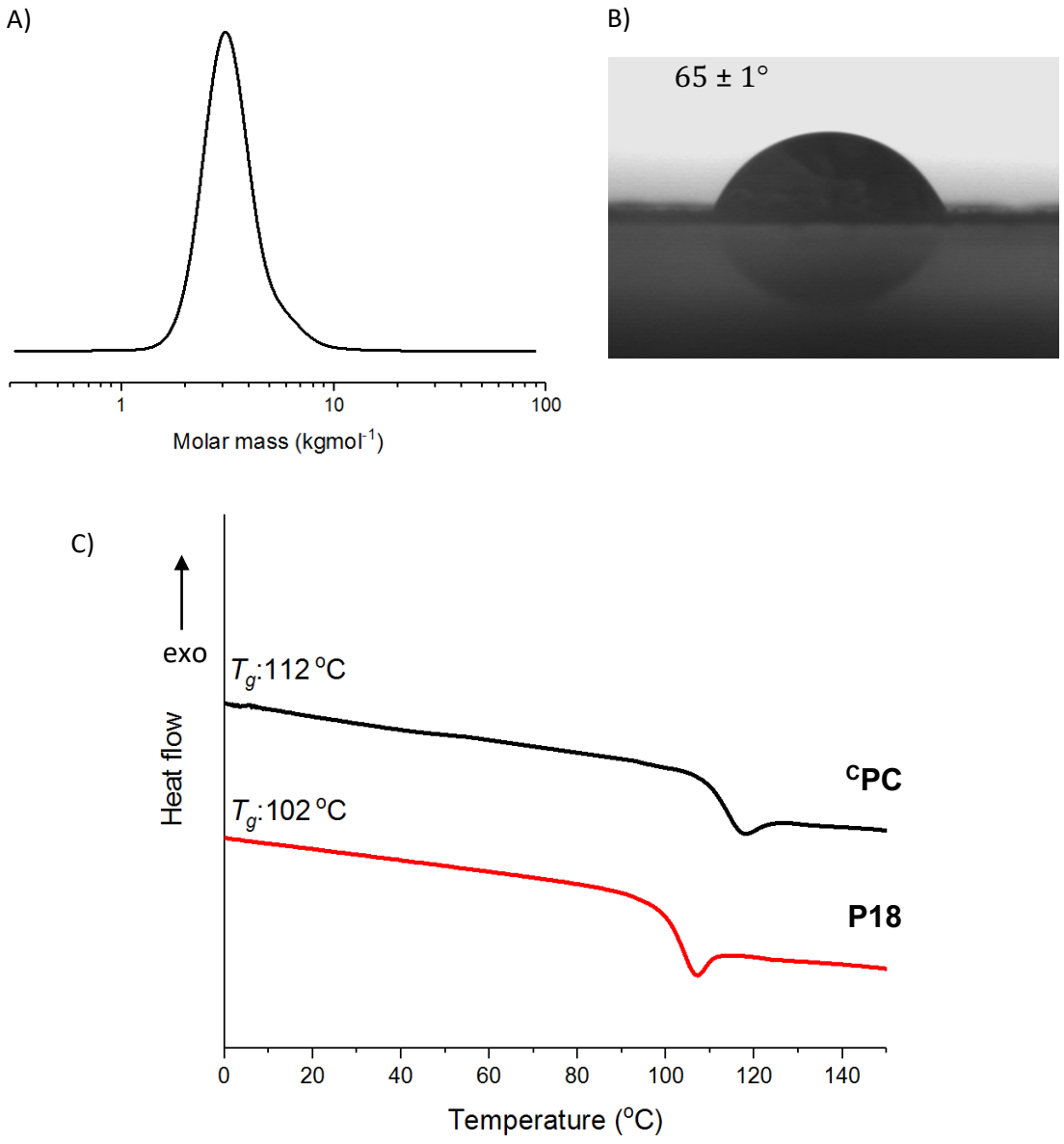


Figure 5.4 A) SEC trace of polymer **P18**, B) Photographs of water droplets on **P18** and C) Overlaid DSC traces of ^{C}PC and **P18**.

5.2.2 Selective post-polymerisation modification on a mixture of ^{V}PC and ^{C}PC

The different reactivity between polymers featuring internal and terminal alkenes opens up the possibility of using hydroboration-oxidation to selectively functionalise polymers containing both types of alkenes. This concept was explored first using mixtures of two polymers.

An initial NMR scale reaction between ^{V}PC, ^{C}PC and 9-BBN, at a ratio of 1: 1: 2.2, was carried out. The reaction was monitored at regular time intervals, and the conversion of the different alkene functionalised polymers was calculated by relative integration of the alkene signals at 5.77 ppm (^{V}PC) and 5.57 ppm (^{C}PC) (Figure 5.5). The NMR scale experiment revealed that hydroboration occurred faster with ^{V}PC and reached completion within 2 h at 25 °C. No further reaction was observed, and ^{C}PC remained unreacted in the presence of excess 9-BBN over 16 h at 25 °C (spectrum D, Figure 5.5). The NMR scale experiment is consistent with the observations made during independent hydroboration reactions of ^{V}PC and ^{C}PC. Clearly, the reactivity of ^{V}PC is greater than ^{C}PC. The higher reactivity with terminal alkene groups is in line with an investigation carried out by Brown *et al.*[7] In their report, the relative rates of hydroboration using 9-BBN showed that 1-hexene was 1000 times more reactive than cyclohexene, suggesting that the nature of alkene groups affects the reactivity significantly.[7]

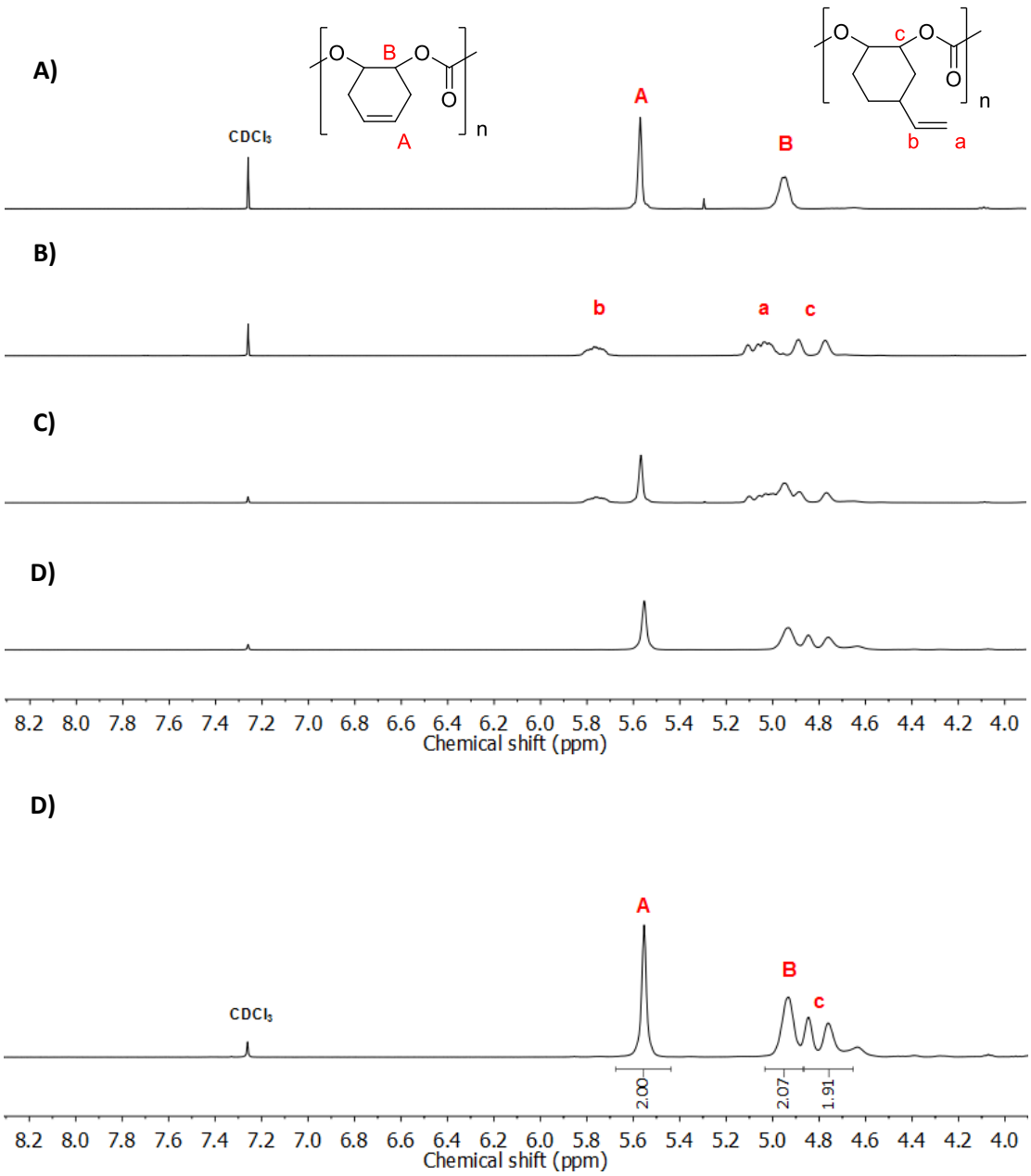


Figure 5.5 Stacked ^{1}H NMR spectra of ^{V}PC, ^{C}PC and their reaction mixture at different reaction temperatures and times (400.0MHz, $CDCl_3$, 25 °C): A) Purified ^{C}PC, B) Purified ^{V}PC, C) Mixture of ^{C}PC and ^{V}PC, D) Mixture of ^{C}PC and ^{V}PC, 2.2 equiv. 9-BBN, $CDCl_3$, 25 °C,16 h.

To quantify the particular relative rates here, the mixture of ^{V}PC, ^{C}PC and 9-BBN, at a ratio of 1/1/2.2, was monitored using ^{1}H NMR spectroscopy, in the presence of an internal standard (mesitylene). Figure 5.6 shows the stacked ^{1}H NMR spectra, and Figure 5.7 shows the conversion of alkenes (^{V}PC vs. ^{C}PC) versus time. It can be seen that the hydroboration of the terminal alkene group on ^{V}PC (peak 'b' in Figure 5.6)

occurred immediately and reached around 80% conversion within *ca.* 60 mins. During this time, the internal alkene group on ^{C}PC (peak 'A' in Figure 5.6) remained unreacted, as confirmed using the internal standard (mesitylene, peak 'd' in Figure 5.6). The conversion of the terminal alkene group on ^{V}PC increases linearly with reaction time. The linear conversion versus time relationship indicates that the reaction is zero order in alkene and the pseudo-first order rate constant is 5.62 ± 0.06 × 10^{-5} s^{-1}. This zero-order dependence also correlates with Brown's finding, in which hydroboration reactions with reactive alkenes exhibit overall first-order dependence, *i.e.* the reactions are first-order in 9-BBN dimer and zero order in alkene.[7]

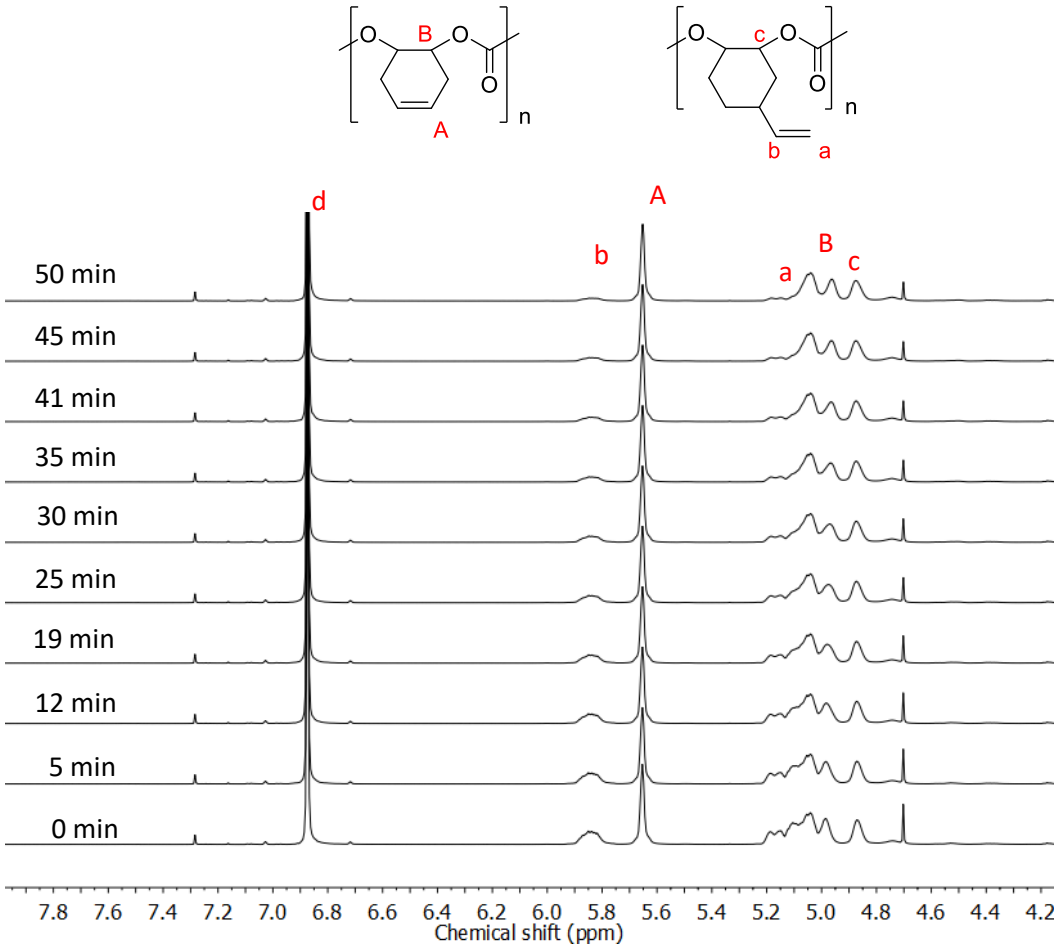


Figure 5.6 ^{1}H NMR spectra of reactions between a mixture of ^{V}PC and ^{C}PC and 9-BBN.

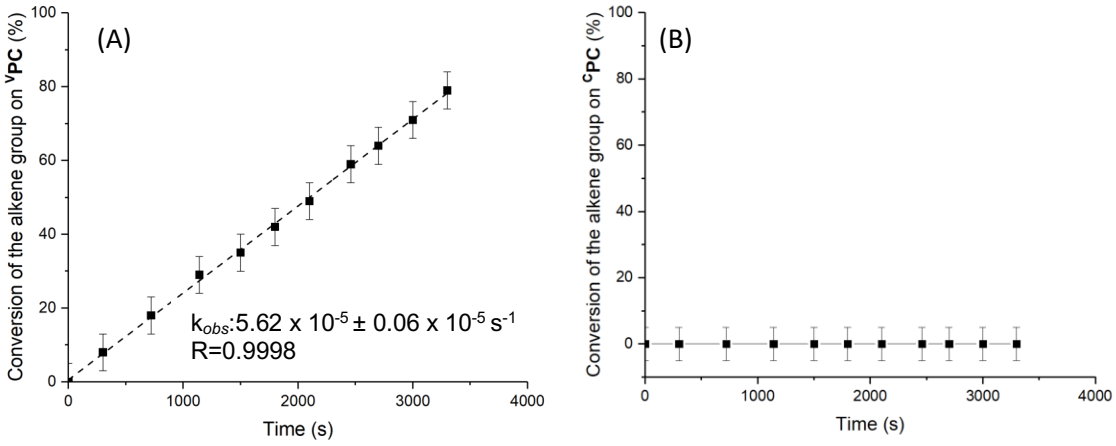
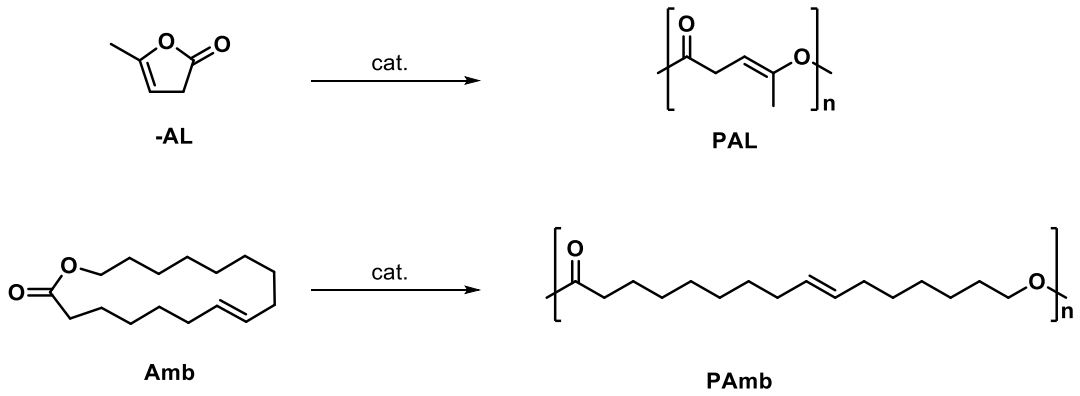


Figure 5.7 Conversion of the alkene groups ((A): ^{V}PC and (B): ^{C}PC) versus reaction time. Conversion determined by comparing the integrals of H_b and H_A with internal standards.

In conclusion, hydroboration using 9-BBN provides a successful means to functionalise unsaturated polycarbonates selectively, with terminal alkenes showing a much higher reactivity.

5.2.3 Syntheses of unsaturated polyesters

So far, only mixtures of two differently unsaturated polycarbonates have been investigated. To broaden the scope and utility, various unsaturated monomers were targeted, including commercially available alkene-functionalised α-angelica lactone (AL) and ambrettolide (Amb). It was envisaged that the homopolyesters produced from these lactones could be used as macroinitiators for block copolymers featuring terminal and internal alkenes in the same polymer chain.



Scheme 5.5 Ring-opening polymerisation (ROP) of α-angelica lactone (AL) and ambrettolide (Amb).

α-Angelica lactone (AL), a five-membered unsaturated lactone, is bio-derived from levulinic acid.[8] Triazabicyclodecene (TBD), 1,8-diazabicycloundec-7-ene (DBU) and $Sn(Oct)_2$ were investigated as catalysts for its polymerisation of AL, but all reactions resulted in low conversions and the formation of oligomers. The ROP reactions did not proceed to any significant $\overline{DP}$ even over prolonged reaction times (2-4 days). The difficulty presumably arises due to AL having low ring strain, which limits the equilibrium and disfavours high molar mass polymer formation.[8]

Ambrettolide (Amb) is also naturally occurring and is found in the Ambrette seeds, which is widely used in the fragrance industry.[9] The ROP of Amb to form polyambrettolide (PAmb) was investigated, using TBD or $Sn(Oct)_2$ as catalysts, with CHD as the co-initiator. The results of polymerisation are shown in Table 5.1.

Table 5.1 Polymerisation data for ROP of Amb

Entry	Cat.	Initiator[b]	Time (h)	Conv. (%)	M_n[b] (kgmol^{-1})	Đ[b]
1	$Sn(Oct)_2$	CHD	55	~30	11.5	2.00
2	TBD	CHD	55	full	59.5	2.10
3	TBD	CHD	24	~90	43.0	1.96

[a] Reaction conditions: equivalence ratio of [cat.]/[Amb]=1/300, neat Amb, 120 °C. [b] Determined using Size exclusion chromatography in THF, using monodispersed polystyrene as standard.

All ROP reactions were conducted at 120 °C for 55 h, and the polymerisations were quenched by exposing the mixture to air or benzoic acid. When using the TBD catalyst, near complete conversion of Amb to PAmb was achieved. Under the same conditions, only 30% conversion was achieved using $Sn(Oct)_2$. SEC analyses showed that the dispersities were all very broad (~ 2.00), suggesting significant transesterification side reactions. The broad dispersity is likely caused by the low ring-strain, which resulted in similar rates of polymerisation and transesterification.[10, 11]

The difference in the ROP of these two lactones can be explained by the varied thermodynamic driving force for the polymerisation. For small ring-sizes (< 7 membered ring), the driving force is the relief of enthalpic ring strain from the lactone.[12] However, for lactones that possess larger rings (> 10 membered ring), changes in enthalpy upon ring-opening are minimal, and ROP becomes entropy-driven through an increase of conformational freedom.[13, 14] This entropy-driven process has been previously studied for ω-pentadecalactone (PDL) (C_{15}), which is the most widely explored macrolactone (ΔH°_p = 3 kJ·mol^{-1} and ΔS°_p = 23 J·mol^{-1}·K^{-1} ([PDL]eq = 0.016 M at 100 °C).[13]

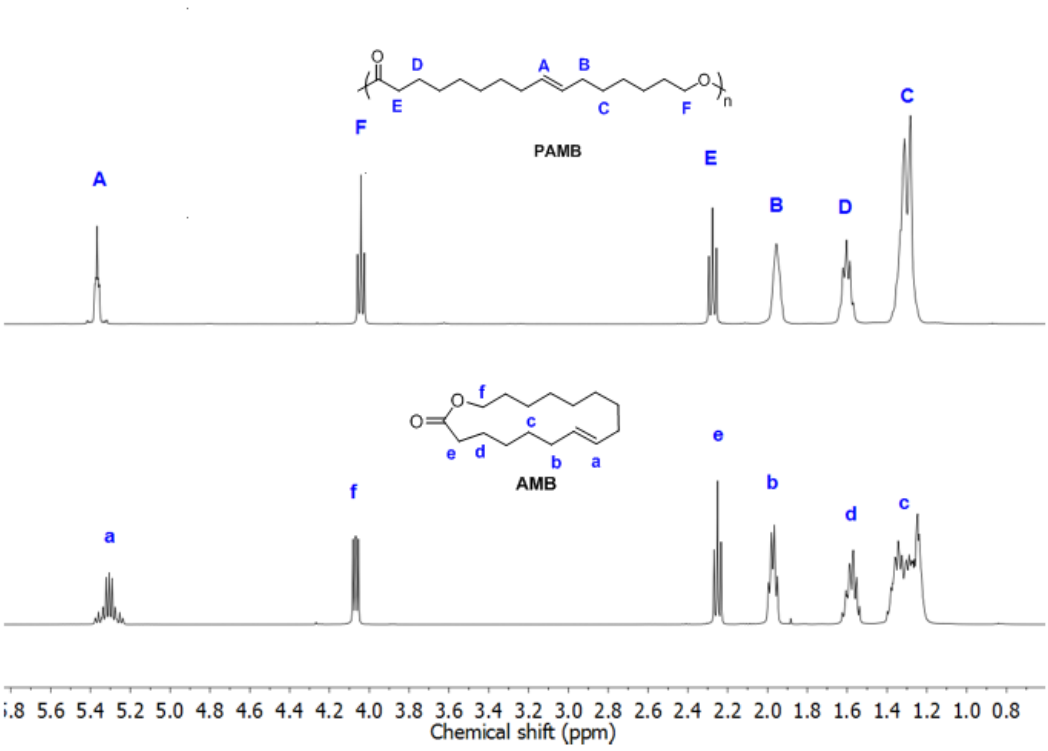


Figure 5.8 Stacked ^{1}H NMR spectra of PAmb (Top) and Amb (Bottom) ($CDCl_3$, 400.0 MHz, 25 °C).

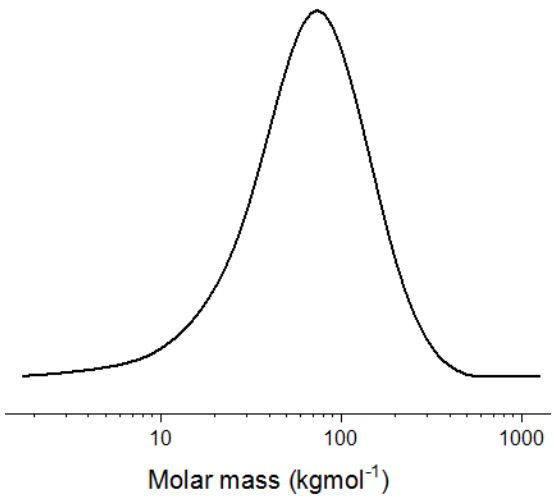
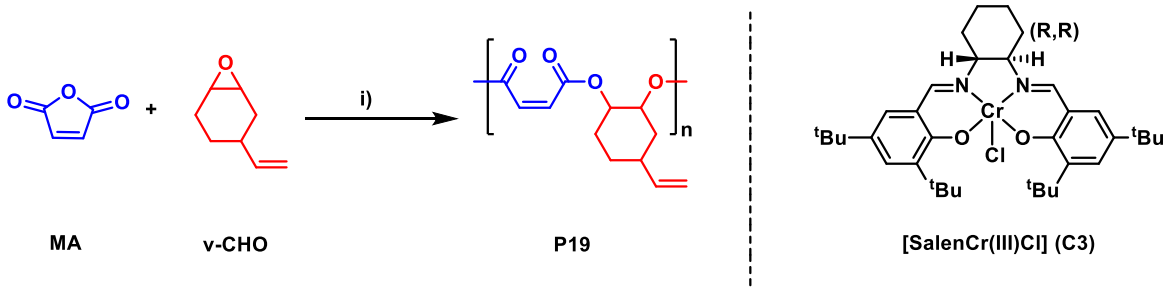


Figure 5.9 SEC trace of PAmb (Table 5.1, Entry 3).

5.2.4 The syntheses of unsaturated alternating polyesters

Block copolymers from unsaturated polycarbonates and polyesters were not accessible using AL or Amb ROP, due to either high thermodynamic stability (AL) or broad dispersity values (Amb). Next, unsaturated alternating polyesters were targeted, using ROCOP of unsaturated anhydrides and epoxides to install different alkene groups into the same polymer backbone.



Scheme 5.6 ROCOP of MA and v-CHO, and the structure of catalyst investigated for the ROCOP. i) [**C3**]/[PPNCl]/[CHD]/[MA]/[v-CHO] = 1/1/10/100/100-130, [v-CHO] = 1 M in toluene, 60-80 °C, 6 h.

The ROCOP of maleic anhydride (MA) and v-CHO to produce poly(vinyl-cyclohexene maleate) (^{V,M}PE, **P19**) was targeted, using Cr(III) salen catalyst and a co-catalyst bis(triphenylphosphine)iminium chloride (PPNCl). The reaction did not result in any polymer formation without the co-catalyst after 6 h but when 1 equiv. PPNCl was used (as co-catalyst), the reactions in toluene, either at 60 or 80 °C, resulted in near quantitative conversion to polyester (based on anhydride). The use of PPNCl results in chloride group initiation, which causes bimodal distributions.[15, 16] Therefore, excess diol (10 equiv. vs. catalyst) was added to suppress the chloride initiation process and to achieve monomodal molar mass distributions.

Table 5.2 Polymerisation data for ROCOP of MA and v-CHO.[a]

Entry	[SalenCr(III)Cl]/PPNCl/ CHD/MA/v-CHO	Temp (℃)	Conv.[b] (%)	M_n[c] (kgmol^{-1})	Đ[c]
1	1/0/10/100/100	80	0	N/A	N/A
2	1/1/10/100/100	80	86	2.2	1.13
3	1/1/10/100/100	60	100	2.0	1.25
4	1/1/10/100/130	60	100(MA), 78 (v-CHO)	2.4	1.13

[a] Polymerisation conditions: [v-CHO] = 1 M in toluene, 6 h. [b] Determined from the normalised relative integrals in the ^{1}H NMR spectrum. [c] Determined using SEC in THF, using monodispersed polystyrene as standard.

The MALDI spectrum shows peaks separated by 222 m/z, which corresponds to the [MA-*alt*-vCHO] repeating unit, in line with a formation of highly alternating polyester chains, end-capped by α,ω-dihydroxyl groups (Figure 5.10).

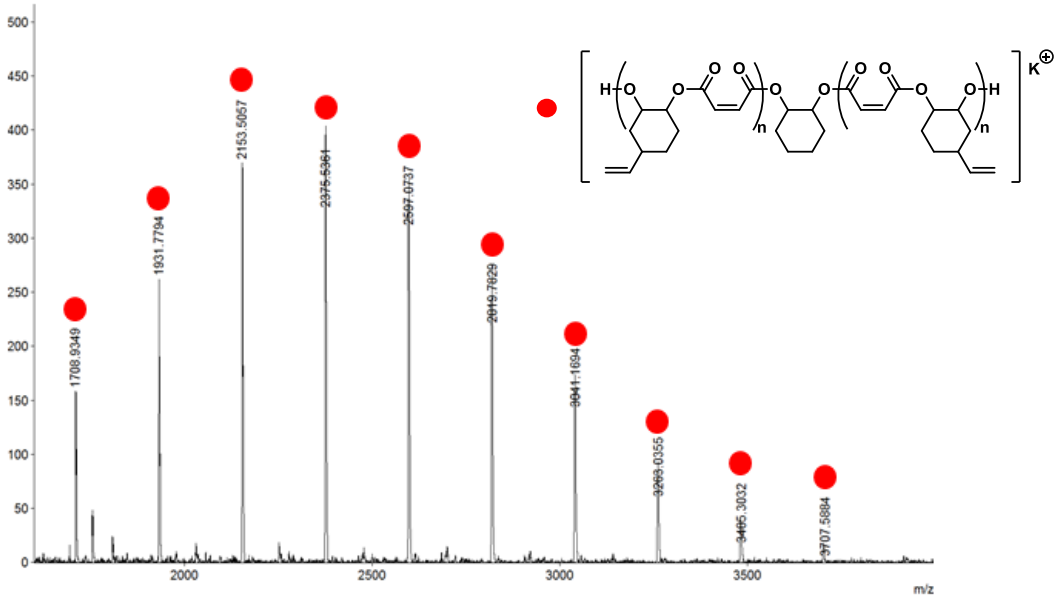


Figure 5.10 MALDI-ToF spectrum of **P19** synthesised with CHD as the CTA (Table 2, Entry 4). The polyester series show m/z = [116.16(cyclohexanediol) + (222.24 × n) (MA-*alt*-v-CHO) + 39.1 (K^+)].

The hydroxyl end-capped polyester was also analysed by ^{1}H NMR spectroscopy, which showed no ether linkage formation (Figure 5.11). Peaks at 6.24 and 5.78 ppm, corresponding to signals 'F' and 'D' in the ^{1}H NMR spectrum (Figure 5.11), were assigned to the internal and terminal alkene groups, respectively. Moreover, the ^{13}C NMR spectrum shows two characteristic maleate resonances at 130.0 and 160.5 ppm (Peaks 'F' and 'G' in Figure 5.12), corresponding to the alkene and carbonyl carbon centres, respectively. Multiple signals, assigned to the end groups, were observed at 2.8-4.5 ppm, due to regioirregularities in the polymer chain. For this polymer, head-to-tail (HT), tail-to-tail (TT) and head-to-head (HH) sequences were all formed, although HT sequences are expected to be favoured due to reduced steric hindrance.

The molar mass could not be determined by NMR methods due to the complex chain end signals. Nevertheless, the resultant polymer displayed a monomodal molar mass distribution with M_n of 2.0 kgmol^{-1} (Đ = 1.25), as determined by SEC. The molar mass is in close agreement with the theoretical values (2.2 kgmol^{-1}), calculated based on the use of 10 equiv. of CTA.

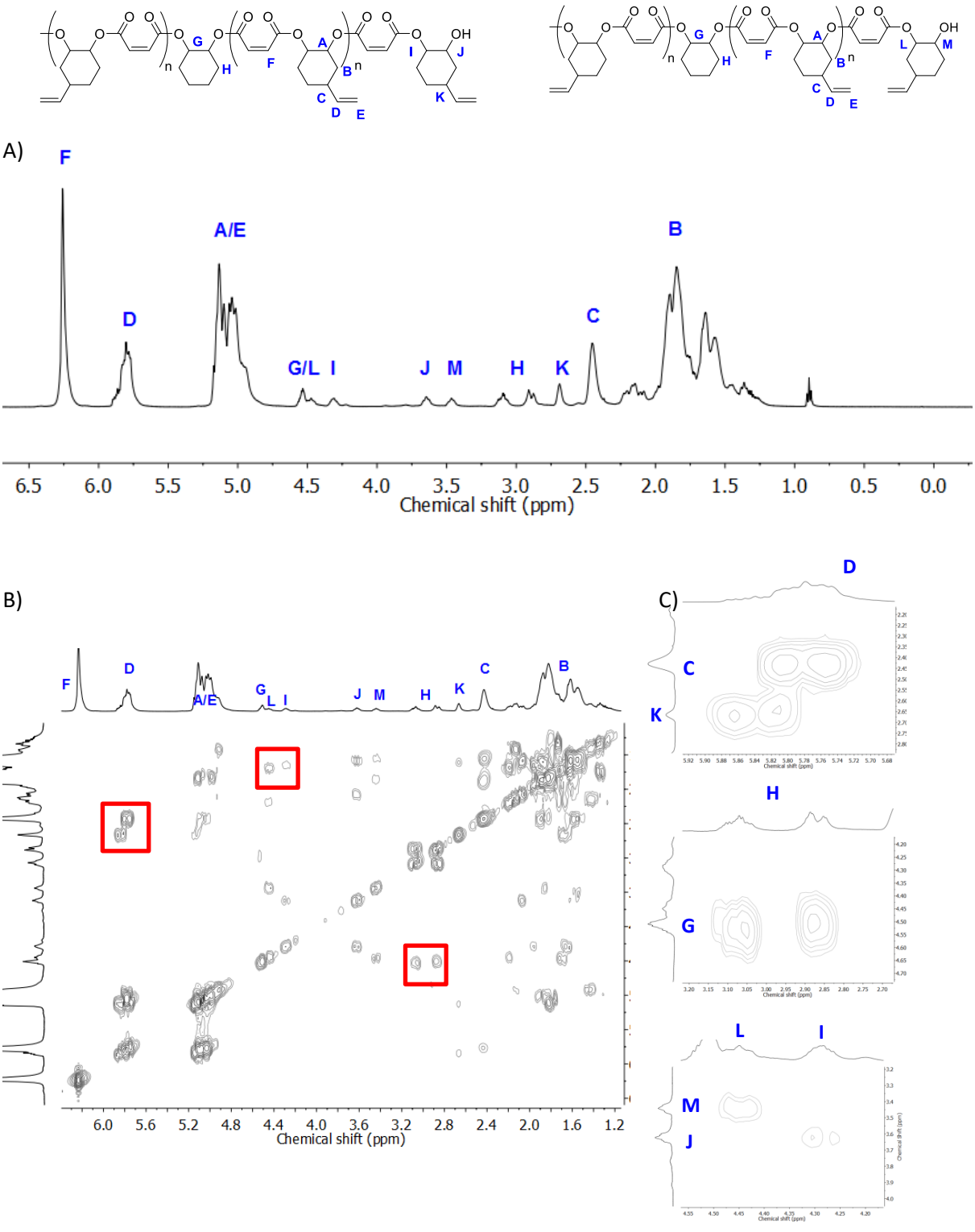


Figure 5.11 A) ^{1}H NMR spectrum of **P19** ($CDCl_3$, 500.0 MHz, 25 °C). B) ^{1}H-^{1}H COSY NMR spectrum of **P19** ($CDCl_3$, 500.0 MHz, 25 °C). C) Enlarged ^{1}H-^{1}H COSY NMR spectra corresponding to the selected area in B). The signals at (5.86, 2.67) and (5.81, 2.43) are assigned to the correlation between vinyl groups and the adjacent methine protons on the end group and backbone respectively. The signals at (3.06,

4.50) and (2.88, 4.50) are assigned to the correlation between the methylene protons H_G and H_H on the 'cyclohexylene junction' group. The signals at (4.43, 3.47) and (4.30, 3.62) are assigned to the correlation between backbone methylene protons.

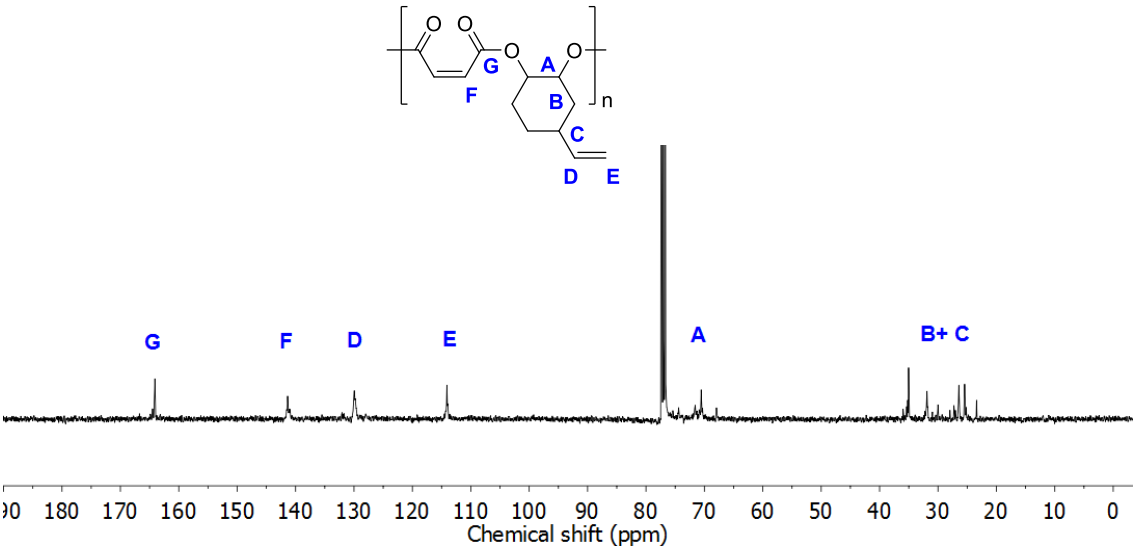


Figure 5.12 ^{13}C NMR spectrum of **P19** (400.0 MHz, $CDCl_3$, 25 °C).

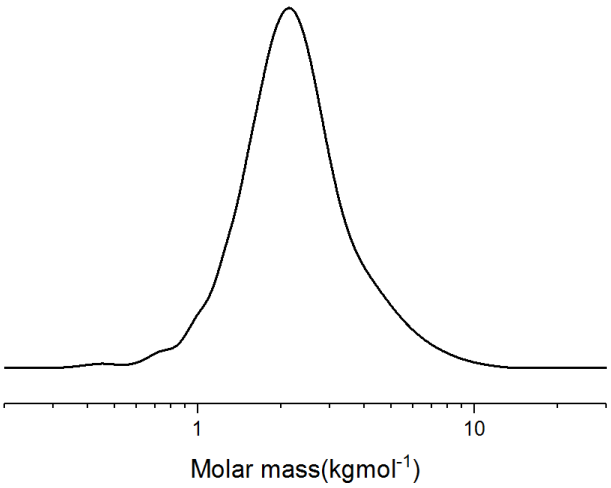


Figure 5.13 SEC trace of **P19** (Table 5.2, Entry 3).

5.2.5 Selective hydroboration of ^{V,M}PE (P19)

The new polyester, **P19**, features both internal and terminal alkene moieties and so allows investigation of selective post-polymerisation reactions to sequentially functionalise each alkene. To test the concept, an NMR hydroboration reaction between **P19** and slightly excess of 9-BBN ([alkene]/[9-BBN] = 1/1.5) was monitored using ^{1}H NMR spectroscopy. The stacked ^{1}H NMR spectra of the reaction mixture are shown in Figure 5.14.

Hydroboration of the terminal alkene group (peak 'B' in Figure 5.14) went to completion within 40 min, but there was no consumption of the internal alkene over this time (peak 'A' in Figure 5.14). Also, the hydroboration showed a first-order dependence on alkene concentration, after an initiation period of about 5 min. This was different from the hydroboration with alkene groups on ^{V}PC, which showed a zero-order dependence. Brown *et al.,* showed that there are two steps in the hydroboration using 9-BBN, the first is the dissociation of the 9-BBN dimer, and the second step is the reaction of the 9-BBN with the alkene. For more reactive alkenes, the rate-determining step (RDS) is the dissociation of the 9-BBN dimer, resulting in a zero-order dependence in alkene concentration. For less reactive alkenes, the RDS is the reaction between the alkene and the borane, resulting in a first-order dependence in alkene concentration.[7] Based on the change in reaction order, the alkene groups in **P19** are less reactive than those in ^{V}PC. This reactivity difference may arise from differences in hydrodynamic radii and conformation of ^{V}PC and **P19** in solution (*i.e.* THF).

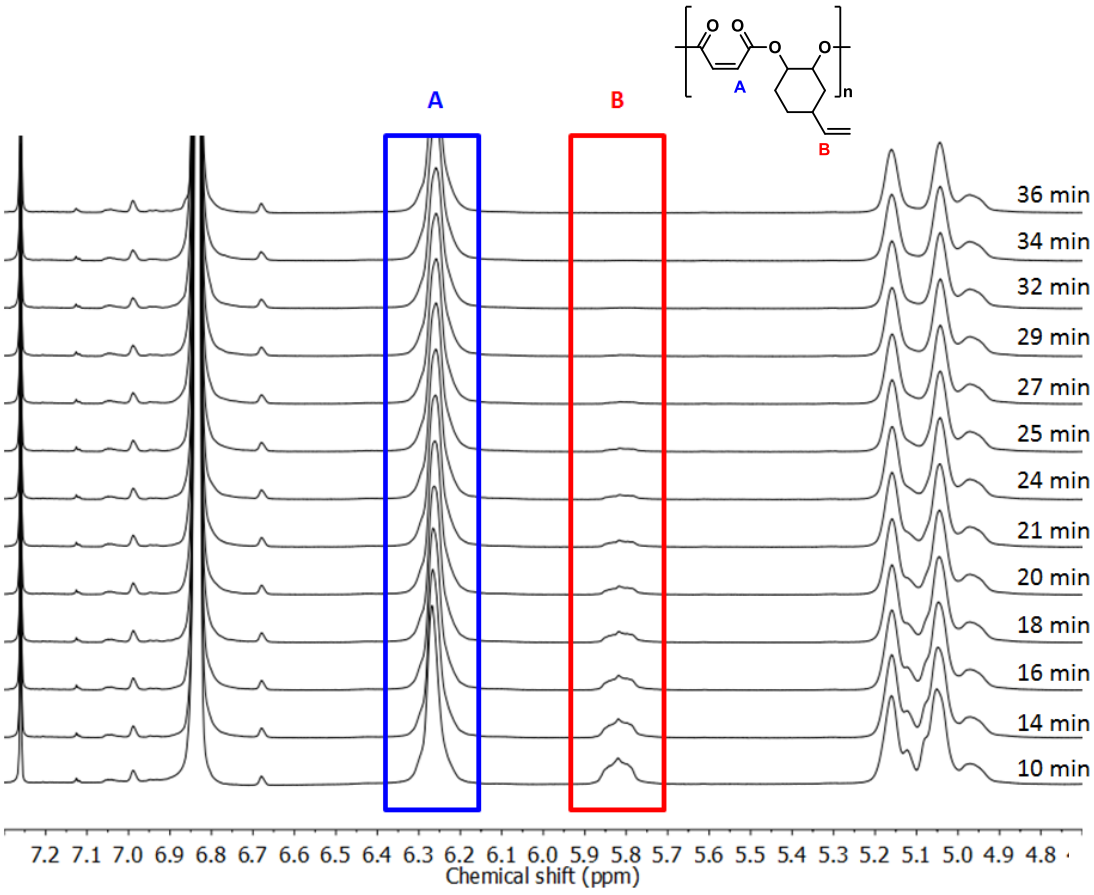


Figure 5.14 Changes in the ^{1}H NMR resonance of the alkene groups during the reaction of **P19** with 9-BBN ($CDCl_3$, with mesitylene as an internal standard).

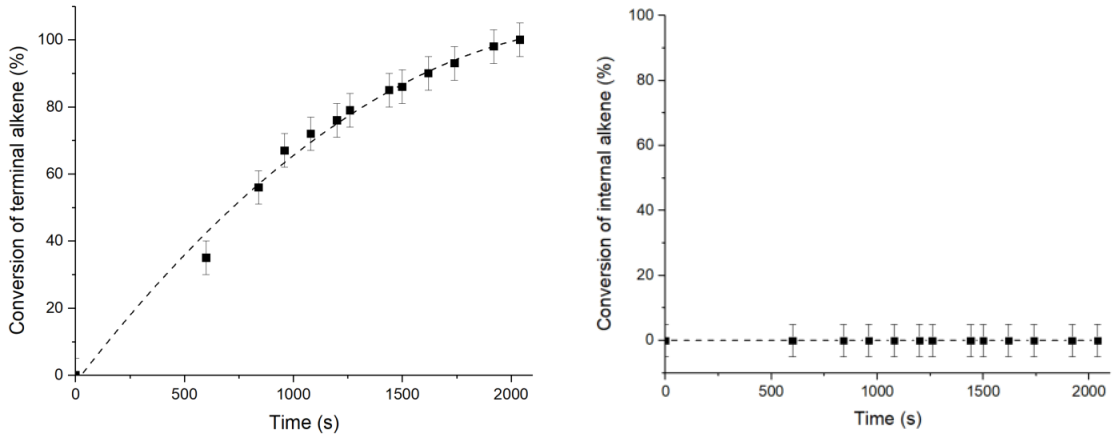


Figure 5.15 Percentage conversions of the alkene groups (terminal and internal) versus reaction time. Conversion determined by comparing the integrals of H_A and H_B with internal standards.

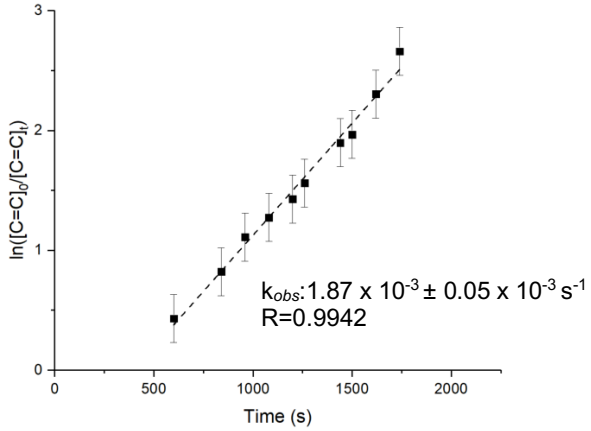
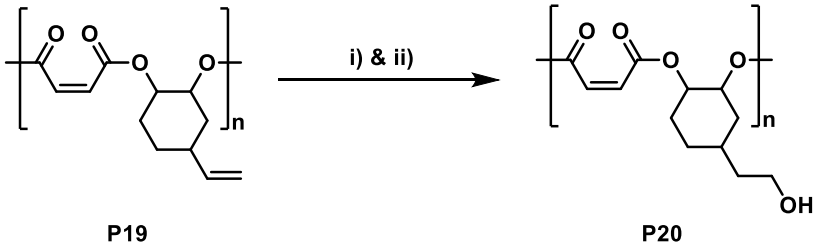


Figure 5.16 Plot of $\ln([C=C]_0/[C=C]_t)$ vs time of terminal alkene groups.

The NMR investigation confirmed that hydroboration occurs selectively at the terminal alkene group and any internal alkenes remain unreacted. Therefore, further post-polymerisation modification can be performed on the internal alkene groups.



Scheme 5.7 Hydroboration-oxidation of **P19**. i)1.5 equiv. 9-BBN, THF, 25 °C, 1 h. ii) 3.4 equiv. mCPBA, THF, 25 °C, 2 h.

The hydroboration-oxidation of ^{V,M}PE was conducted using the same method as described previously and afforded the hydroxyl functionalised polyester **P20**. The reaction proceeded selectively at the terminal alkene groups, without altering the polyester backbone or the molar mass. The ^{1}H NMR spectrum of **P20** confirms the disappearance of the terminal alkene signals at 5.04-5.11 and 5.77 ppm. Also, new signals evolved at 4.36 and 3.42 ppm (peaks 'G' and 'E' in Figure 5.17), which were assigned to the hydroxyl group and its neighbouring methylene protons, respectively. The signal at 6.48 ppm (peak 'F' in Figure 5.17) was assigned to the maleate internal

alkene protons, while the one at 4.87 ppm was contributed by the cyclohexyl backbone protons (peak 'A' in Figure 5.17). These two signals remain unchanged after the hydroboration-oxidation reaction, suggesting that the polyester backbone stays intact, which was further verified by SEC characterisation in DMF (Figure 5.18).

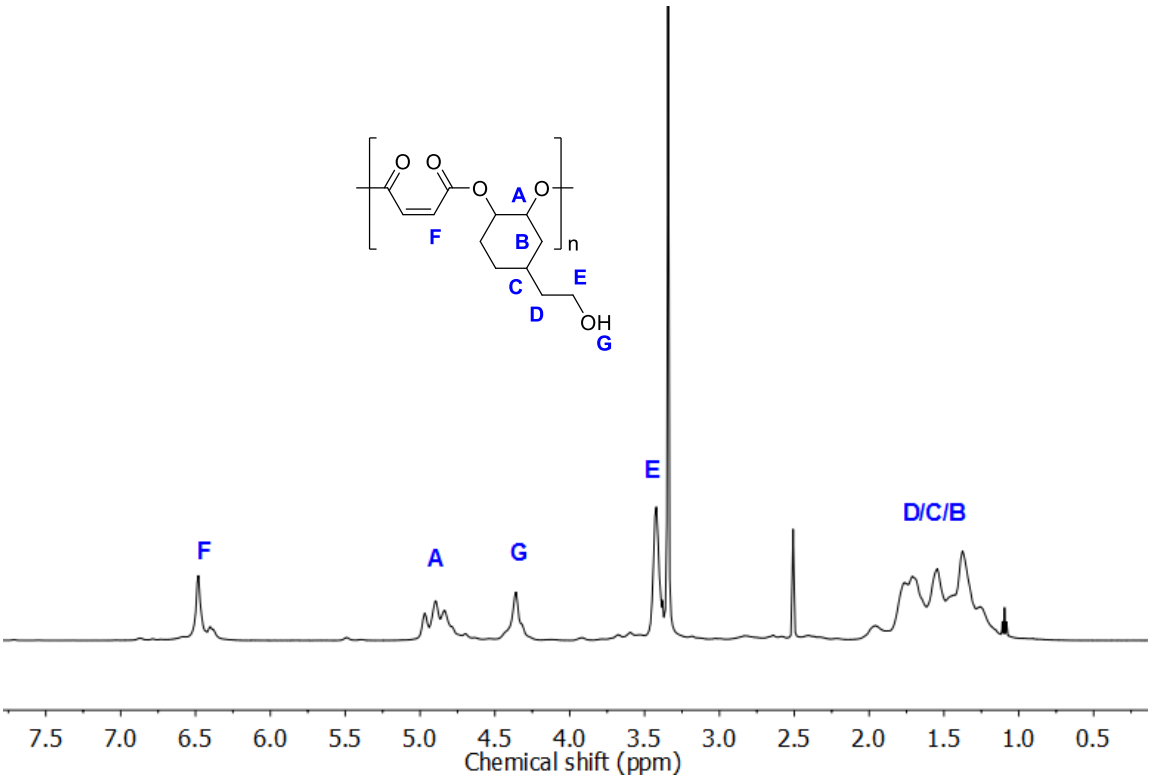


Figure 5.17 ^{1}H NMR spectrum of **P20** (DMSO-d_6, 400.0 MHz, 25 °C).

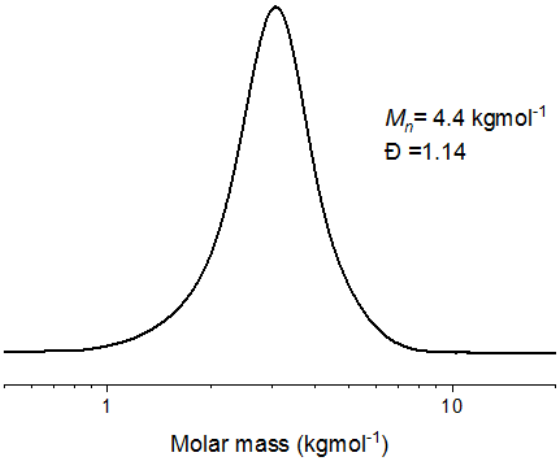
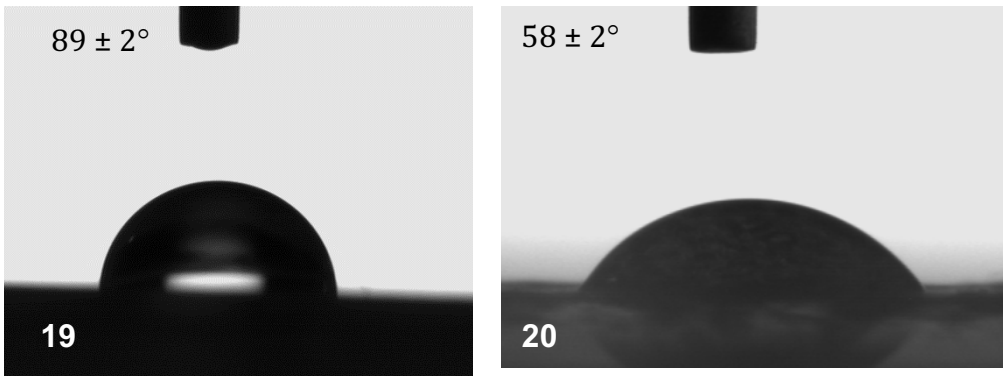


Figure 5.18 SEC trace of **P20**.

Introducing a hydroxyl group into each repeat unit of **P19** significantly changes the polymer solubility. The obtained polyester **P20** no longer dissolves in THF. Thus DMF SEC was used instead to assess its molar mass and dispersity. A monomodal peak was observed, with M_n of 4.4 kgmol^{-1} (Đ = 1.19). Its glass transition temperature (T_g) value of was 98 °C, as assessed using differential scanning calorimetry (DSC), which is higher than **P19**. This increase may arise from inter-/intra chain hydrogen bonding between hydroxyl (H-bond donor) and ester groups (H-bond acceptor). Moreover, equivalent hydrogen bonding induced T_g increments were observed for other polymers with hydroxyl substituents.[17, 18] The water contact angle of **P20** was 58°, which is lower than that of **P19**, suggesting an increase in hydrophilicity.

Overall, the characterisation data suggest hydroboration-oxidation is successful in enabling the selective functionalisation of the terminal alkene groups while leaving the internal alkene groups unreacted.

A)



B)

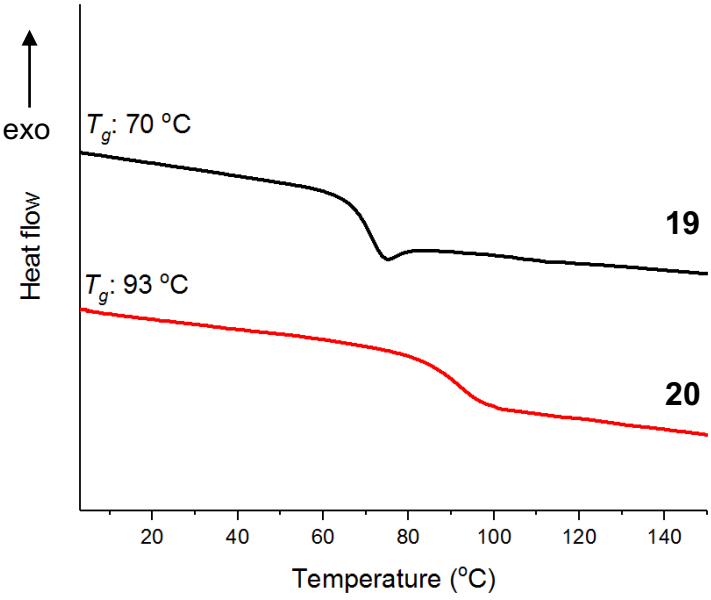
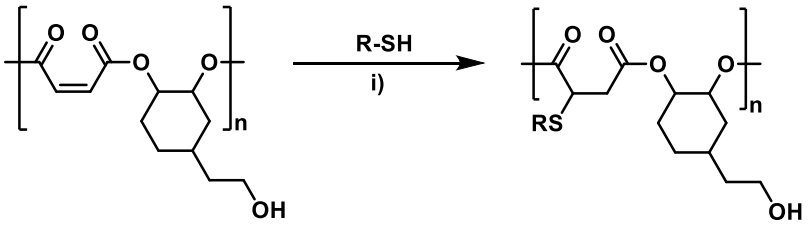


Figure 5.19 A) Photographs of water droplets on **P19** and **P20**. B) Overlaid DSC traces of **P19** and **P20**.

5.2.6 Thiol-ene reaction with P20



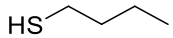
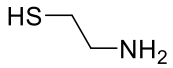
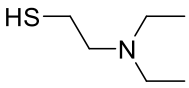
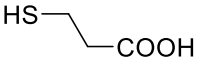
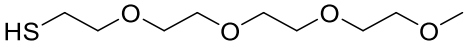
P20 P21-25

Scheme 5.8 Thiol-ene reaction between **P20** and various thiols. Reaction conditions: i) [C=C]/[DMPA]/thiol=1/0.4/4, DMSO, irradiated under UV (365 nm, 10 W) for 1h.

An orthogonal reaction platform from a single backbone is advantageous to control the functional group positions precisely.[3, 4] Here, the common precursor was **P20** and subsequently a series of radical-mediated thiol-ene reactions were used to functionalise the remaining internal alkene groups.

In the reactions, **P20** was reacted with various thiols (4 equiv. per alkene group), *via* UV-induced thiol-ene reactions, using DMPA as the UV initiator (see Chapter 7). The polymers were characterised using ^{1}H NMR spectroscopy, DSC and static water contact angle measurements (Table 5.3).

Table 5.3 Functionalisation of **P20** *via* photo-induced radical thiol-ene reactions.[a]

Polymer	Thiol	T_g[b] (°C)	Water contact angle[c] (º)	M_n(Đ)[d] (kgmol^{-1})
21		69	53 ± 1	5.0 (1.14)
22		78	38 ± 1	5.7(1.86)
23		86	31 ± 2	10.0 (1.96)
24		8	29 ± 1	3.5 (1.34)
25		-8	46 ± 1	6.0 (1.19)

[a] Reaction conditions: [alkene]/[DMPA]/thiol=1/0.4/4, [alkene]$_0$=0.25 M in DMSO, irradiated under UV(365 nm, 10W) at 25°C for 1h. [b]Acquired from the second heating cycles in DSC [c] Measured using a Drop Shape Analysis System and the values were averaged based on the values on three different areas on the polymer surface. [d] Determined *via* SEC in DMF, calibrated using monodispersed polystyrene as standard.

In all cases, ^{1}H NMR spectroscopy revealed complete disappearance of the signal at 6.48 ppm, assigned to the maleate alkene protons, indicating the complete consumption of internal alkene groups. However, the NMR signals were very broad at ambient temperature, possibly due to inter-/intra-molecular hydrogen bonding. **P21** was characterised using ^{1}H VT-NMR spectroscopy, specifically at elevated temperature (80 ºC), to suppress the H-bonding effect. New signals were observed in the high-temperature NMR spectrum (peaks 'F'' and 'I'' in Figure 5.20) due to the methine and methylene hydrogens next to the thioether group, indicating a successful thiol-ene reaction. The ^{13}C NMR spectrum also confirms the consumption of the internal alkene group and the appearance of new peaks at 42 ppm, due to the carbon centre adjacent to the thioether group (Figure 5.21).

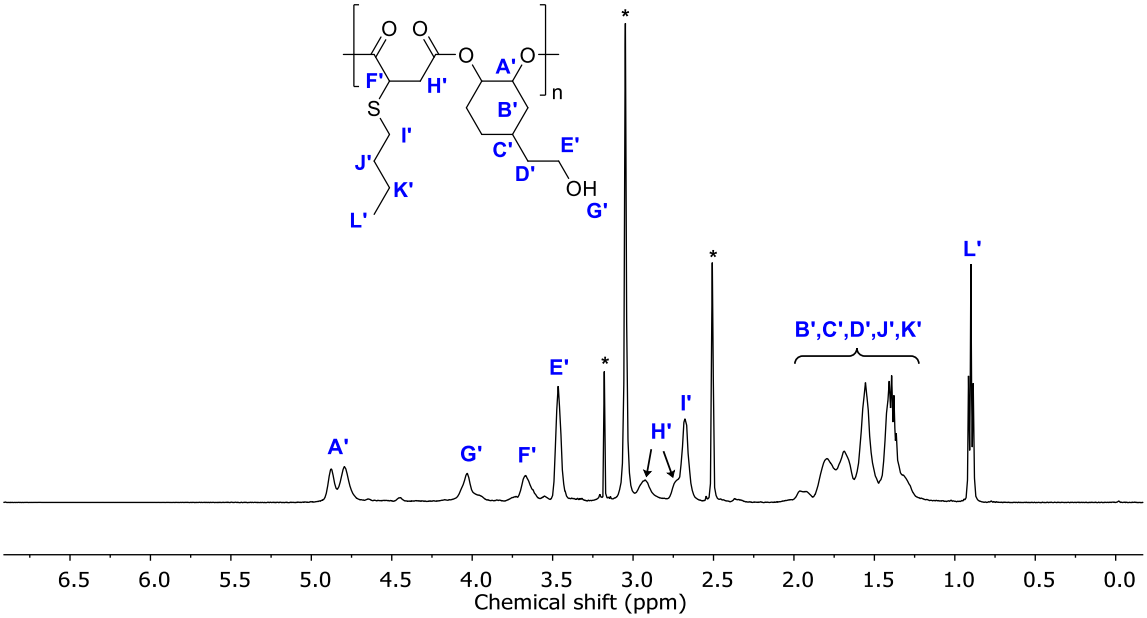


Figure 5.20 ^{1}H NMR spectrum of **P21** (DMSO-d_6, 500.0 MHz, 80 ºC).

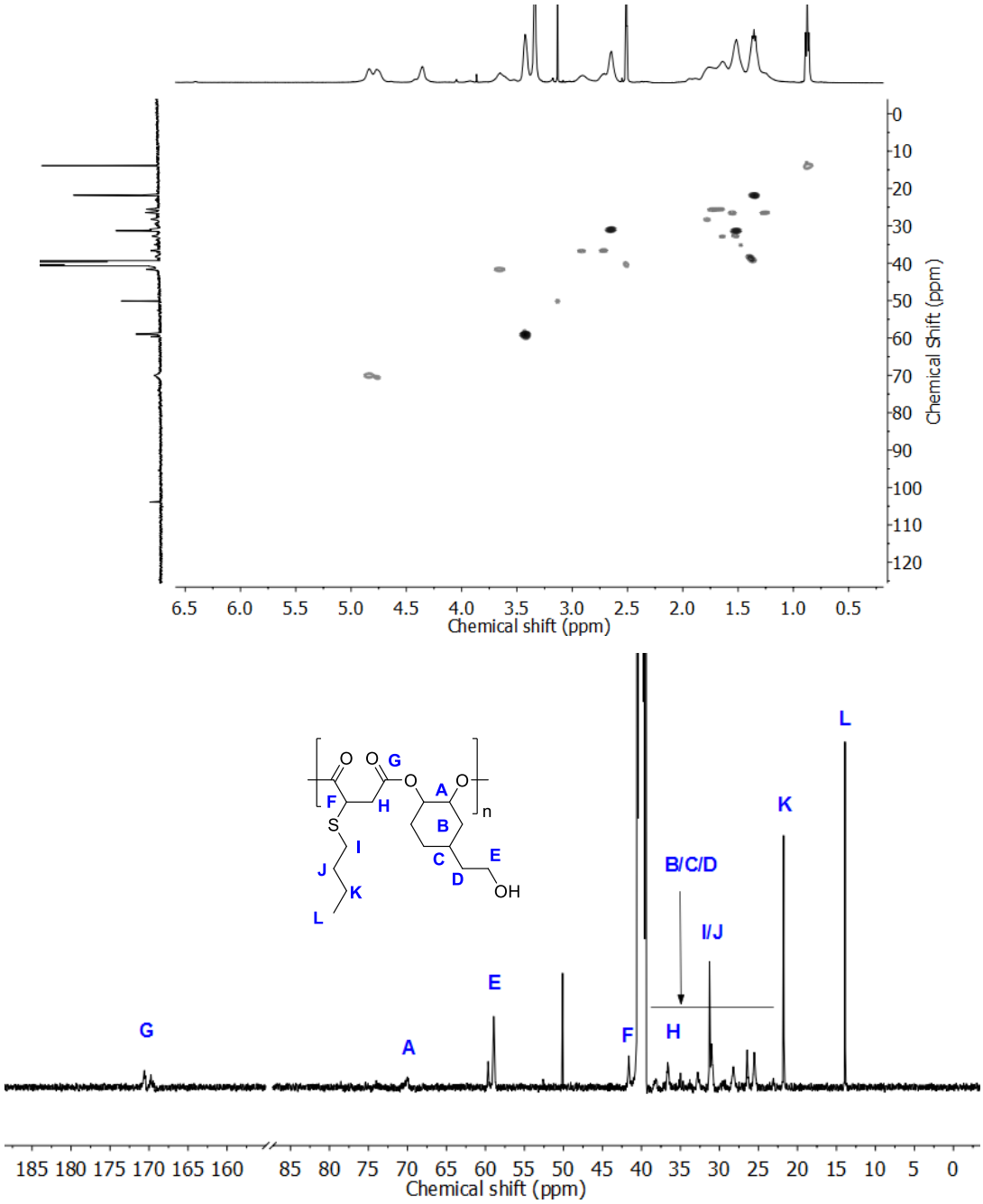


Figure 5.21 Top: ^{1}H-^{13}C HSQC NMR spectrum of **P21**. Bottom: ^{13}C NMR spectrum of **P21** (DMSO-d_6, 500.0 MHz, 40 ºC).

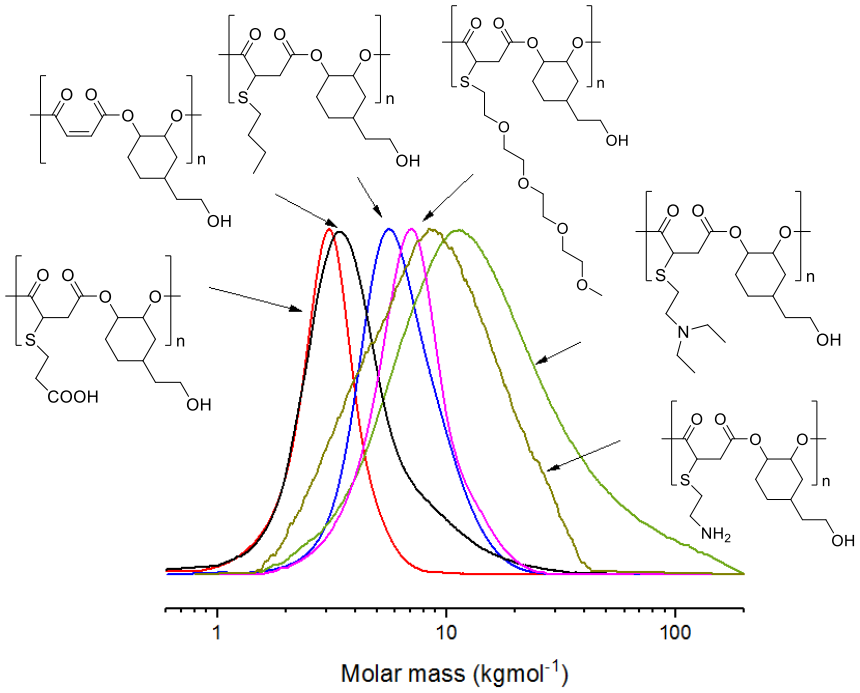


Figure 5.22 Stacked SEC traces of polymers **20-25**.

The thiol-ene reactions between **P20** and 1-butanethiol/tetraethylene glycol monoethyl ether thiol afforded polymers **P21** and **P25**, respectively, with increased molar mass and narrow dispersities (Table 5.3 and Figure 5.22). For other three polymers, the molar masses were a little more unexpected. This could possibly be attributed to both inter-/intra- polymer interactions and interactions between the SEC column and polymer functional groups (amine or carboxylic groups) in each repeat unit. Such column-polymer interactions have also been observed by other researchers working with amine/acid functionalised polymers.[19-21]

The T_g values of the modified polymers were also investigated by DSC. The polymers (**P21**-**P25**) display T_g values lower than their precursor P**20** (93 °C), presumably due to the introduction of flexible thioether chains in each repeat unit.[22] For polymers **P22** and **P23**, the T_g values are relatively higher, possibly due to the inter-chain interactions between the amine and carbonate groups. The steric hindrance of the side

groups attached to **P23** is proposed to reduce flexibility and increase T_g (compared to **P22**).

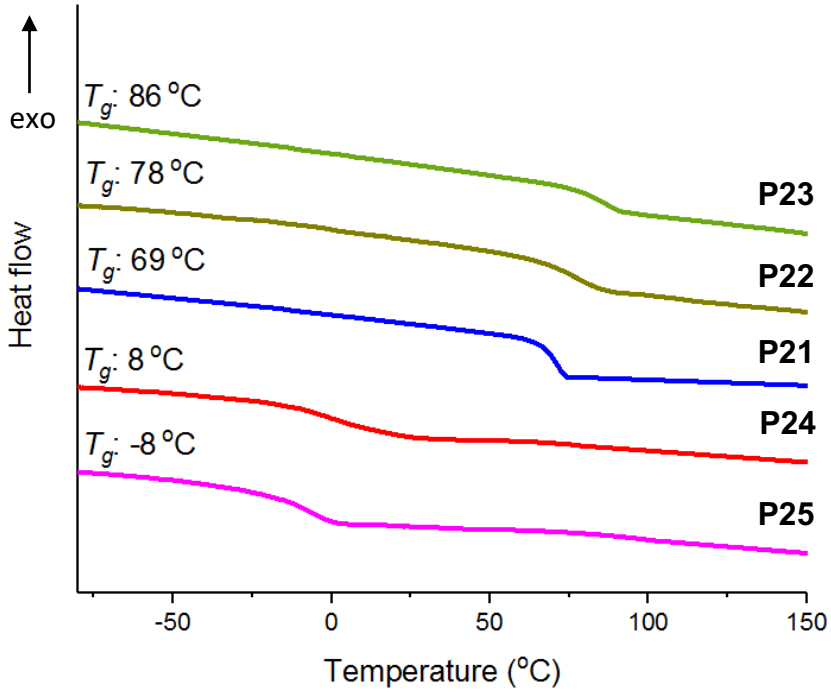


Figure 5.23 Overlaid DSC traces of polymers **P21-25**.

One curious finding is that polymer **P21** forms self-assembled nanostructures in water. According to dynamic light scattering (DLS) data (Figure 5.24), the hydrodynamic diameter of **P21** was determined to be 136 ± 1 nm (PDI: 0.12 ± 0.01). Very low cumulant fit errors (< 0.005) and the flat baseline in the raw correlation data verified the reliability of these DLS results (Figure 5.24). Meanwhile, the zeta potential was also determined to evaluate the stability of the nanostructures. The absolute value of the zeta potential (|ζ|) suggests the extent of the electrostatic repulsion between neighbouring colloidal nanoparticles.[23, 24] Therefore, a higher absolute value indicates higher colloidal stability, suggesting higher electrostatic repulsion, which thus prevents aggregation.[24] Usually, colloidal systems having zeta potentials from ± 40 to

± 60 mV are considered to have 'good stability'.[24] In this case, the rather high zeta potential (-67.5 ± 0.4 mV, $|\zeta| > 65$ mV) reveals high colloidal stability.

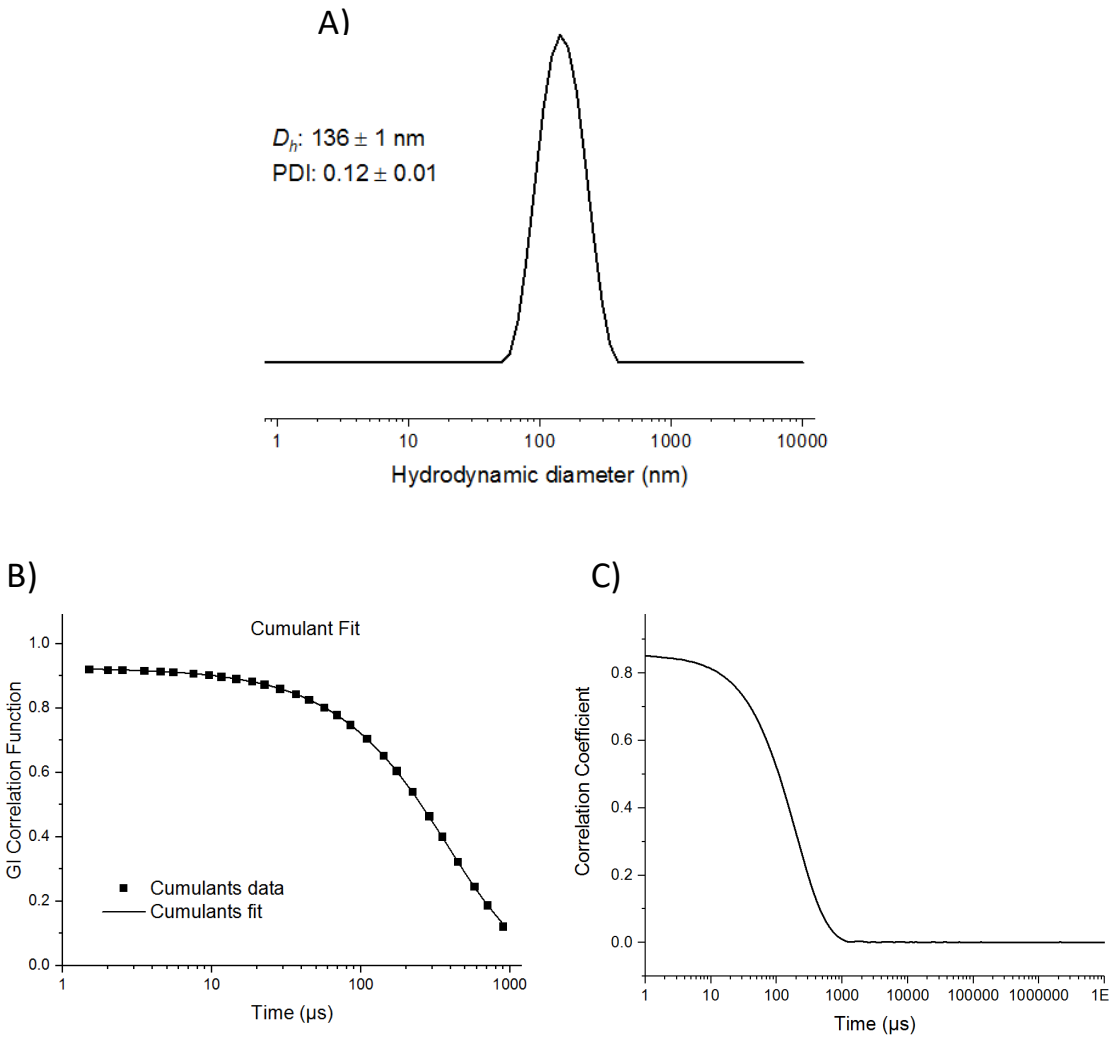


Figure 5.24 DLS data collected from an aqueous solution of **P21** (10 mg·mL^{-1}, size distribution by intensity). A) Hydrodynamic diameter (D_h) and polydispersity index (PDI) of the self-assemblies. B) Cumulant fit and C) Correlation functions of DLS study

The nanostructures were analysed using TEM, which revealed a micelle-like morphology (Figure 5.25). The size of these micelles (*ca.* 25 ± 5 nm) were considerably smaller than indicated from the DLS results (~ 136 nm). In contrast to self-assembled nanostructures formed by amphiphilic block copolymers, there is

usually a less clear boundary between hydrophilic and hydrophobic regions of self-assembled nanostructures formed by amphiphilic homopolymers.[37] It could be that some of the polar hydroxyl groups in **P21** are trapped together with water inside the micelle core during the self-assembly process, leading to a significant expansion in micelle radius, which has previously been observed using other amphiphilic homopolymers.[25, 26] The difference in sizes between TEM and DLS, may result from the dehydration of such nanostructures during TEM sample preparation. Indeed, related effects were also observed in the previous report using poly(2-hydroxy-3-phenoxypropyl acrylate).[25]

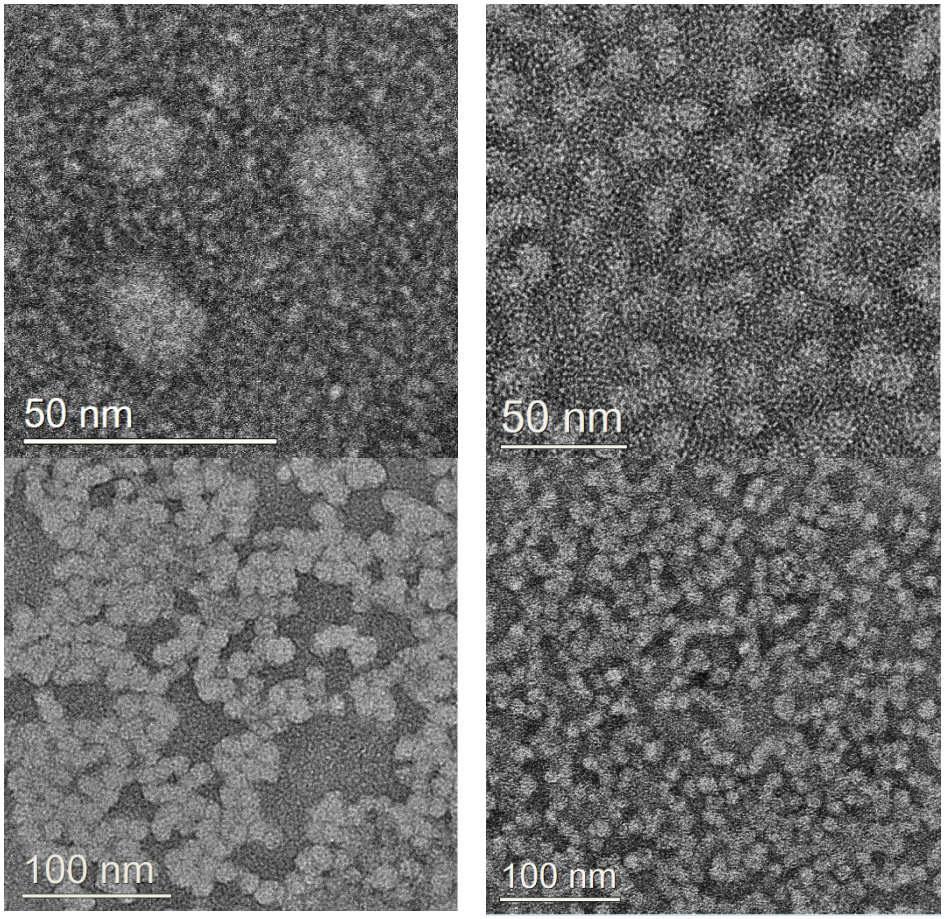


Figure 5.25 TEM image of the micelles formed from polymer **P21** in aqueous solution (10 mg·mL^{-1}).

This unusual self-assembly behaviour was only observed using **P21**. It may be that **P21** has an optimised volume ratio of hydrophilic/hydrophobic components resulting in the self-assembly. Other polymer chain lengths and hydrophobic/hydrophilic ratios required to investigate further.

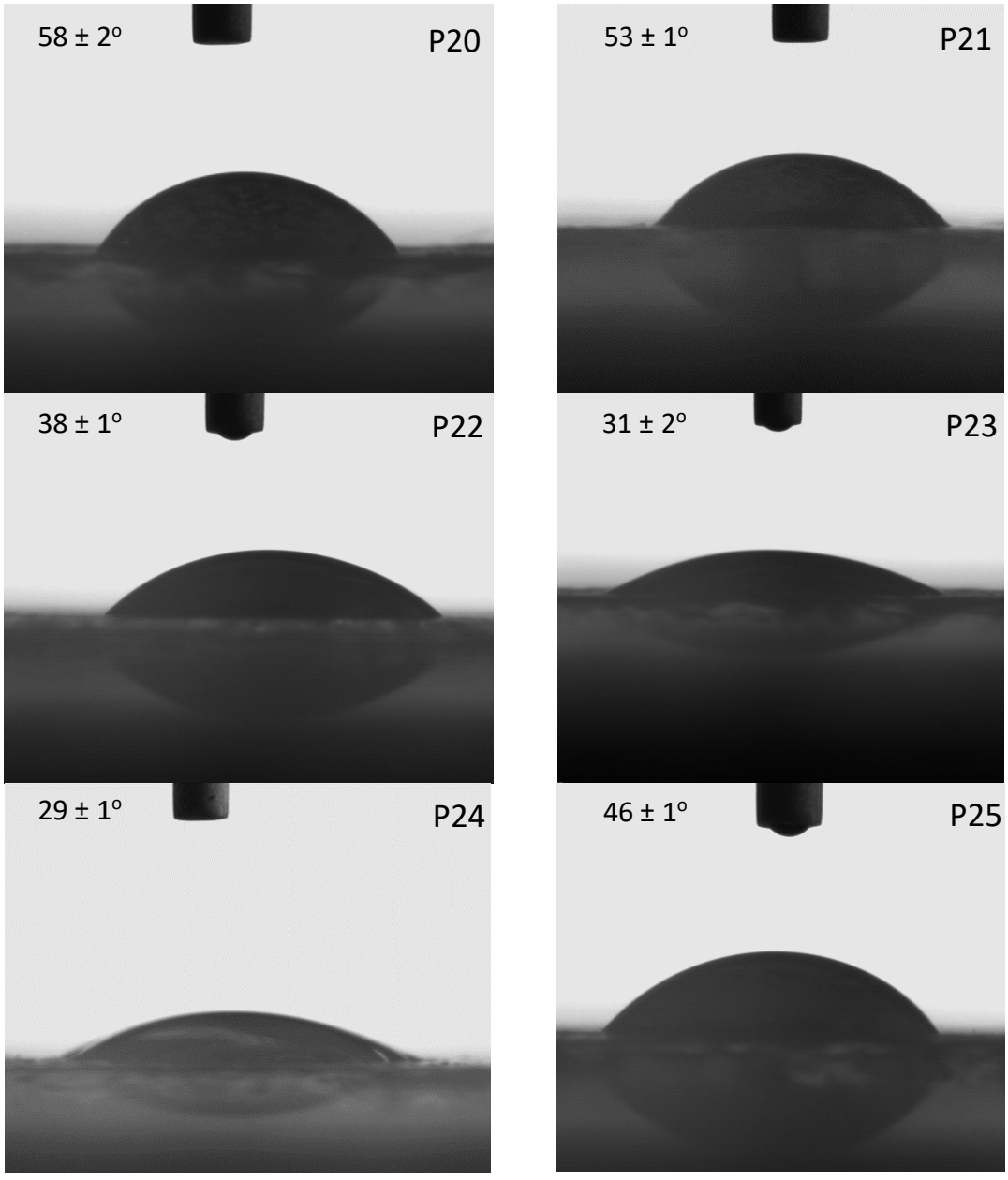


Figure 5.26 Photographs of water droplets on polymers (**P20**-**P25**) coated glass surfaces.

The hydrophilicity was further assessed using water contact angle measurements. The water contact angles of polymers **P22**-**P25** were lower than **P21**, suggesting they have higher hydrophilicity. This, in turn, supports the hypothesis that the failure of **P22**-**P25** to form nanostructures may be due to high hydrophilicity.

5.3 Summary and Outlook

5.3.1 Summary

In summary, a new approach to prepare a series of dual-functionalised polyesters, using selective reactions with internal and terminal alkenes, is reported. Firstly, a hydroboration-oxidation reaction allowed selective transformation of all the terminal alkenes (v-CHO unit), leaving the internal alkenes (maleate unit) unreacted. Secondly, the internal alkenes were transformed to thioether, methoxy-oligo(ethylene glycol), acid and amine functionalities. This selective approach readily affords orthogonally functionalised polyesters with a near perfect AB alternating sequence. The resulting polymers are all amorphous and show tuneable thermal properties, with T_g values ranging from -8 ºC to 86 ºC.

5.3.2 Outlook

In this Chapter, the possibility to introduce two different substituents to a single polymer backbone has been demonstrated. A future target will be to demonstrate similar patterning using other alternating polymers so as to understand its generality and scope. Some potential polymer structures for further investigation are shown in Figure 5.27; they all possess both terminal and internal alkene groups. Although the synthesis of polymer **3** has been achieved by epoxide/anhydride ROCOP, using (BDI)ZnOAc catalysts (BDI = β-diiminate),[27] the other polymers are not yet reported.

It is proposed that they may be synthesised using related conditions used to prepare ^{V,M}PE.

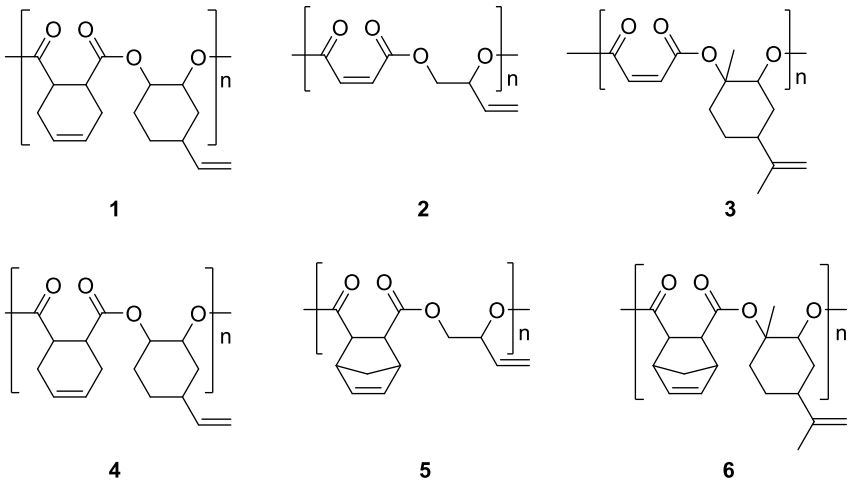
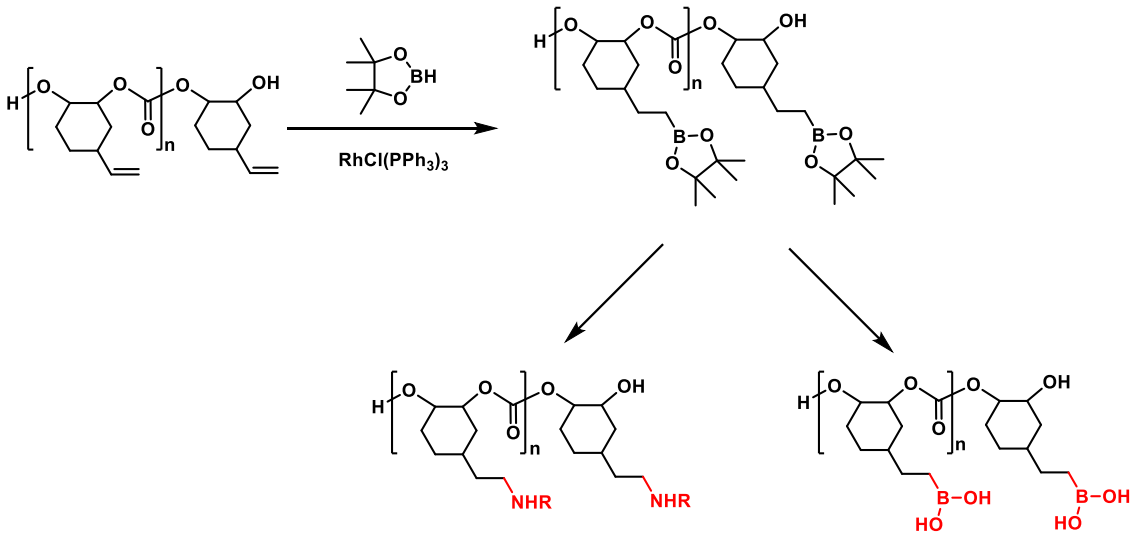


Figure 5.27 Potential alternating polyesters for achieving selective post-polymerisation modification.

More importantly, the scope of the reactions should be expanded to include other functional groups and to introduce favourable biomedical properties (Scheme 5.9). For example, boronic ester-functionalized polymers, synthesised by hydroboration using pinacolborane with Wilkinson's catalyst, could be used as the platform for other transformations.[28] Amine substituents could be obtained by amination of the boronic esters, whereas hydrolysis should lead to the boronic acids.[29] In terms of applications, amines could be used to conjugate proteins or peptides.[30] Boronic acids could be used to coordinate monosaccharides and, thus, self-assembled structures of boronic acid-containing polymers may dissociate in response to changes in sugar concentration, which could be relevant to treatment of diabetes and related applications.[31]



Scheme 5.9 Proposed synthetic route for obtaining amine and boronic acid-containing polymers.

5.4 References

1. W. Chin, C. Yang, V. W. L. Ng, Y. Huang, J. Cheng, Y. W. Tong, D. J. Coady, W. Fan, J. L. Hedrick and Y. Y. Yang, *Macromolecules*, 2013, **46**, 8797-8807.
2. Y.-M. Li, T. Jiang, Y. Lv, Y. Wu, F. He and R.-X. Zhuo, *Colloids Surf., B*, 2015, **132**, 54-61.
3. R. Kakuchi and P. Theato, *Polym. Chem.*, 2014, **5**, 2320-2325.
4. M. Malkoch, R. J. Thibault, E. Drockenmuller, M. Messerschmidt, B. Voit, T. P. Russell and C. J. Hawker, *J. Am. Chem. Soc.*, 2005, **127**, 14942-14949.
5. B. H. Northrop and R. N. Coffey, *J. Am. Chem. Soc.*, 2012, **134**, 13804-13817.
6. M. Winkler, C. Romain, M. A. R. Meier and C. K. Williams, *Green Chem.*, 2015, **17**, 300-306.
7. H. C. Brown, K. K. Wang and C. G. Scouten, *Proc. Natl. Acad. Sci. U. S. A.*, 1980, **77**, 698-702.
8. T. Chen, Z. Qin, Y. Qi, T. Deng, X. Ge, J. Wang and X. Hou, *Polym. Chem.*, 2011, **2**, 1190-1194.
9. V. Sanz and E. Seoane, *J. Chem. Soc., Perkin Trans. 1*, 1982, 1837-1839.
10. M. P. F. Pepels, M. Bouyahyi, A. Heise and R. Duchateau, *Macromolecules*, 2013, **46**, 4324-4334.

11. M. P. F. Pepels, P. Souljé, R. Peters and R. Duchateau, *Macromolecules*, 2014, **47**, 5542-5550.
12. M. A. Hillmyer and W. B. Tolman, *Acc. Chem. Res.*, 2014, **47**, 2390-2396.
13. D. K. Schneiderman and M. A. Hillmyer, *Macromolecules*, 2016, **49**, 2419-2428.
14. S. Strandman, J. E. Gautrot and X. X. Zhu, *Polym. Chem.*, 2011, **2**, 791-799.
15. E. Hosseini Nejad, C. G. W. van Melis, T. J. Vermeer, C. E. Koning and R. Duchateau, *Macromolecules*, 2012, **45**, 1770-1776.
16. K. Nakano, M. Nakamura and K. Nozaki, *Macromolecules*, 2009, **42**, 6972-6980.
17. C. Schubert, C. Osterwinter, C. Tonhauser, M. Schömer, D. Wilms, H. Frey and C. Friedrich, *Macromolecules*, 2016, **49**, 8722-8737.
18. M. Scharfenberg, S. Hofmann, J. Preis, J. Hilf and H. Frey, *Macromolecules*, 2017, **50**, 6088-6097.
19. M. Miyamoto, K. Naka, M. Tokumizu and T. Saegusa, *Macromolecules*, 1989, **22**, 1604-1607.
20. C. S. Patrickios, W. R. Hertler, N. L. Abbott and T. A. Hatton, *Macromolecules*, 1994, **27**, 930-937.
21. Y. Miyaki, M. Iwata, Y. Fujita, H. Tanisugi, Y. Isono and T. Fujimoto, *Macromolecules*, 1984, **17**, 1907-1912.
22. D. J. Darensbourg and F.-T. Tsai, *Macromolecules*, 2014, **47**, 3806-3813.
23. J. Z. Du and S. P. Armes, *Langmuir*, 2009, **25**, 9564-9570.
24. R. W. O' Brien, B. R. Midmore, A. Lamb and R. J. Hunter, *Faraday Discuss. Chem. Soc.*, 1990, **90**, 301-312.
25. Y. Zhu, L. Liu and J. Du, *Macromolecules*, 2013, **46**, 194-203.
26. J. Zhang, K. Liu, K. Mullen and M. Yin, *Chem. Commun.*, 2015, **51**, 11541-11555.
27. R. C. Jeske, A. M. DiCiccio and G. W. Coates, *J. Am. Chem. Soc.*, 2007, **129**, 11330-11331.
28. C. Guillaume, N. Ajellal, J.-F. Carpentier and S. M. Guillaume, *J. Polym. Sci., Part A: Polym. Chem.*, 2011, **49**, 907-917.
29. C. Sandford and V. K. Aggarwal, *Chem. Commun.*, 2017, **53**, 5481-5494.
30. N. Murthy, J. Campbell, N. Fausto, A. S. Hoffman and P. S. Stayton, *Bioconjugate Chem.*, 2003, **14**, 412-419.

31. G. F. Whyte, R. Vilar and R. Woscholski, *J. Chem. Bio.*, 2013, **6**, 161-174.

Chapter 6

Conclusions and Outlook

6.1 Conclusions

The interest in epoxide and CO_2/anhydride copolymerisation in the last decade has led to a myriad of alternating polycarbonate/polyesters. Nevertheless, the majority of current research remains at the polymer synthesis stage and the potential to use these products remains unexplored. This thesis outlined initial attempts to investigate alternating polyesters/polycarbonates for biomedical applications, including antibacterial materials and self-assembly for drug-delivery. To target these uses, modifications to the polymers' physical/chemical properties were accomplished through either post-polymerisation modification or copolymerisation reactions. It is worth noting that prior to this thesis, there has been almost no investigation for related applications. Furthermore, a novel selective and orthogonal functionalisation strategy has been developed to enable sequential patterning of a perfectly alternating polyester backbone.

6.2 Outlook

6.2.1 Antibacterial poly(ester-*b*-carbonate-*b*-ester) polymers

Cationic block polymers synthesised in this thesis showed good antibacterial activities. In future, the optimisation of the antibacterial efficacy should be investigated by changing the polycarbonate block, with the most promising candidate, in terms of both thermal/mechanical and antibacterial properties, being considered for large-scale synthesis trials. A possible option to improve the synthesis would be to apply 'switch' catalysis using mixtures of epoxide/CO_2 and lactide to prepare the polymer in a 'one-pot' process. Such a procedure has been recently described to prepare related block copolymers, using a single catalyst that switches between both

ROCOP and ROP cycles in a one-pot reaction.[1-3] The 'switch' strategy could reduce costs associated with scale-up as there is no need to isolate and purify intermediary products.

In future, the antibacterial block polymers could be used for various applications, including antibacterial packaging (*e.g.* for food and even sensitive medicines) and wound healing materials. For packaging uses, it is important to study gas barrier properties, as absorption of ambient vapour or liquid can increase plasticisation, resulting in a decrease in mechanical properties.[4, 5] Barrier properties usually begin with understanding rates of water vapour and oxygen transmission.[6] For wound healing applications it may be preferable to replace PLA with PLGA since the latter material is more rapidly degradable and is amorphous (whereas PLA is usually semi-crystalline).[7] Importantly, a hemolytic assay should be conducted to test for toxicity (*e.g.* using human dermal fibroblast). Cell proliferation and morphology tests are also recommended to ensure the polymer can support healthy cell growth. If these results are promising, wound healing measurements could be performed using animal models. If any cytotoxicity effects are observed, the bromide counter-anion could be substituted, since prior studies showed a change in anion altered selectivity for pathogenic microbes and mammalian cells.[8, 9] The anions shown in Figure 6.1 are proposed because they have a track record in selective antimicrobials and the use of such anions on these block polymers would certainly be worth exploring.[8, 9]

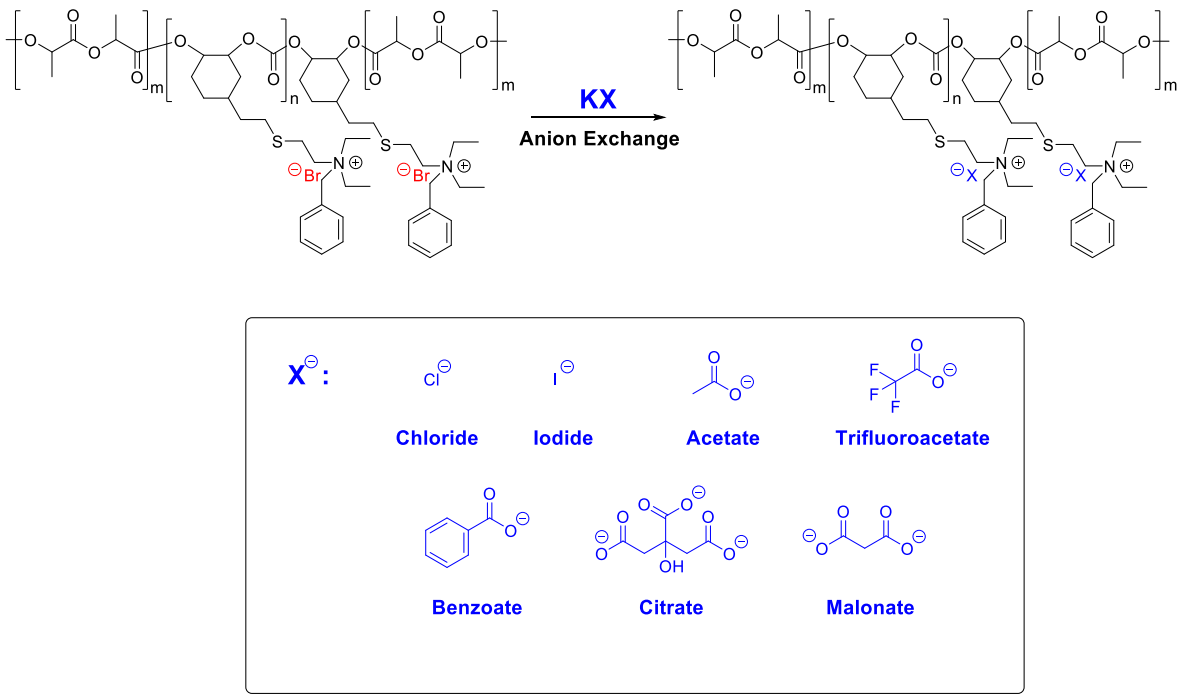


Figure 6.1 Schematic representation of the anion exchange reaction and anions to be explored in future studies.

6.2.2 Poly(phosphoester-carbonate)s

In Chapter 4, the syntheses of block and graft polymers were described. Preliminary *in vitro* studies on enzymatic degradation of the poly(phosphoester-*b*-carbonate-*b*-phosphoester), using alkaline phosphatase, showed promise. Nevertheless, it is of interest to study the enzyme degradation of polyphosphoester *in vivo* as *in vitro* studies usually employ a large excess of a specific enzyme, in a buffered solution, to accelerate the process.[10, 11] As such, the *in vitro* study does not take into account factors such as the oxygen concentrations, the number of metal ions or the inflammation response. Therefore, it is important to understand how the enzyme behaves *in vivo* because the complexity of the human body may change degradation behaviour.

A further application using the vesicles would be to encapsulate sensitive hydrophilic therapeutics (*e.g.* siRNA) since the polycarbonate membrane may protect them from nuclease action.[12, 13] Currently, However, the delivery of such hydrophilic therapeutics still represents a challenge because of their low membrane permeability.[13] One strategy would be to incorporate active transporters, such as transmembrane proteins Aquaporins, target a specific water-channel. This might be possible by adding Aquaporins during self-assembly formation.[14, 15] Vesicle permeability can then be investigated using a stopped-flow method, where the vesicles are mixed with osmotic solutions of NaCl and any shrinkage is monitored by dynamic light scattering methods; these data can be used to calculate permeability.[16]

There are many challenges remaining in the field of polymeric drug delivery. Firstly, there are significant drawbacks associated with the widely employed 'dialysis bag' method to determine the drug loading efficiency and drug release profile. In this method, the diffusion of drugs from the polymer is followed by diffusion across the dialysis membrane and, thus, does not reflect any real rate of drug release relevant to the body. Therefore, assessment of the reliability of the obtained data against release *in vivo* would be very useful. A few alternative approaches to measure controlled release have been developed with the majority targeted towards electroactive elements.[17-19] For example, differential pulse polarography was used to assess continuous drug release from Piroxicam, Chloramphenicol, and Diazepam.[17, 18] However, the sensors appear to be specific to a particular drug. The development of relevant mathematical models to predict drug release behaviours is also important to further develop this work.

The preparation of polyphosphoesters is currently only in academic laboratories. The energy-intensive and multi-step monomer synthesis is likely to limit large-scale production.[3] Thus, investigations into alternative processes to the polymers are essential. A preparation method based on polymerising phosphate salts, analogously to that used for DNA synthesis may be the ultimate goal.[20]

6.2.2 Hydroboration-oxidation and selective post-polymerisation modifications

Chapter 5 demonstrated the synthesis of alternating polyesters with two different alkene groups and the sequential patterning of these polymers using hydroboration-oxidation and thiol-ene reactions. The incorporation of hydroxyl groups improved the materials' hydrophilicity and cell adhesion. It is also possible that the biodegradation may be enhanced, as the presence of these hydroxyl groups is expected to enhance water uptake and provide binding sites for serine hydrolases.[21, 22]

The alternating sequence may be relevant in targeting and permeating cell membranes. In such applications, the terminal alkene groups could be functionalised with hydroxyl groups as the hydroxyl groups to facilitate cell adhesion. The introduction of an adjacent guanidinium group is also of interest since guanidinium-rich polymers have been shown to be cell-penetrating.[23-25] Such target polymers could be prepared through thiol-ene reactions with internal alkene groups and a guanidium-functional thiol. To enhance such cell targeting/penetrating behaviour, self-assembled nanostructures may be required, especially for the delivery of macromolecular therapeutics such as antibodies, recombinant proteins and nucleic acids.[26] It is proposed that exposed hydroxyl groups may induce self-assembly through hydrogen-bonding interactions.[27] In addition, block copolymers encompassing hydrophobic blocks may be synthesised to drive self-assembly *via* hydrophilic/hydrophobic

interactions. The block copolymers could be synthesised through a two-stage epoxide/anhydride ROCOP using either the macro-initiator or sequential monomer addition approach. In addition to the commonly employed thiol-ene post functionalisation, literature precedents suggest that norbornene moieties can be further reacted by efficient inverse-electron-demand Diels-Alder reactions.[28, 29] Thus, a triple orthogonal functionalisation strategy may be realised when combined with the hydroboration-oxidation and thiol-ene reactions (Figure 6.2).

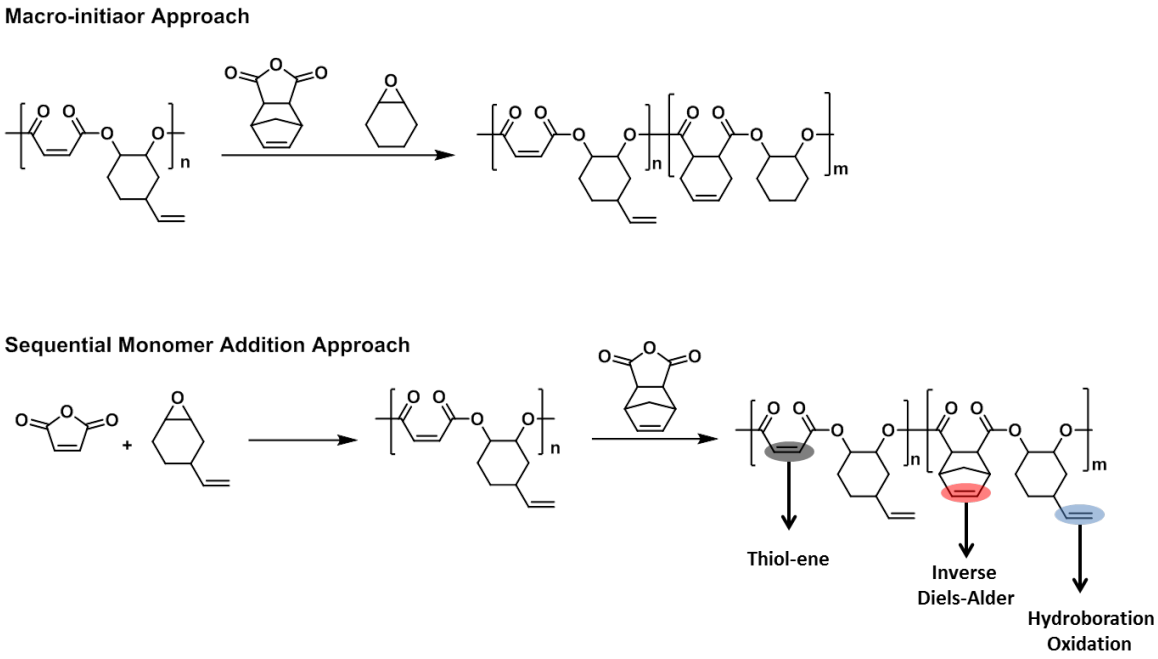


Figure 6.2 Synthetic strategies to make alternating block polyesters for further functionalisation.

6.3 References

1. C. Romain and C. K. Williams, *Angew. Chem., Int. Ed.*, 2014, **53**, 1607-1610.
2. Y. Zhu, C. Romain and C. K. Williams, *J. Am. Chem. Soc.*, 2015, **137**, 12179-12182.
3. T. Stößer, T. T. D. Chen, Y. Zhu and C. K. Williams, *Philos. Trans. R. Soc., A*, 2018, **376**.
4. M. Saša, G. Kata, I. Marica, H. Sandra and C. Nada, *J. Appl. Polym. Sci.*, 2006, **99**, 1590-1599.
5. T. V. Duncan, *J. Colloid Interface Sci.*, 2011, **363**, 1-24.
6. C. Silvestre, D. Duraccio and S. Cimmino, *Prog. Polym. Sci.*, 2011, **36**, 1766-1782.
7. R. A. Jain, *Biomaterials*, 2000, **21**, 2475-2490.
8. S. Dutta, A. Shome, T. Kar and P. K. Das, *Langmuir*, 2011, **27**, 5000-5008.
9. I. Mehmet, T. J. P. K., O. R. J., S. S. Ana, M. David, Y. Y. Yan, H. J. L. and S. Haritz, *Macromol. Biosci.*, 2016, **16**, 1360-1367.
10. Y.-C. Wang, L.-Y. Tang, T.-M. Sun, C.-H. Li, M.-H. Xiong and J. Wang, *Biomacromolecules*, 2008, **9**, 388-395.
11. M. H. Xiong, Y. J. Li, Y. Bao, X. Z. Yang, B. Hu and J. Wang, *Adv. Mater.*, 2012, **24**, 6175-6180.
12. G. Jens, A. Dietmar, W. Linge, B. Giuseppe and V. Brigitte, *Angew. Chem., Int. Ed.*, 2012, **51**, 4448-4451.
13. E. Wagner, *Acc. Chem. Res.*, 2012, **45**, 1005-1013.
14. R. P. Brinkhuis, F. P. J. T. Rutjes and J. C. M. van Hest, *Polym. Chem.*, 2011, **2**, 1449-1462.
15. R. Kasper, B. Patric, L. Karolina, O. Ozana, B. Nico and M. Wolfgang, *Adv. Funct. Mater.*, 2011, **21**, 1241-1259.
16. M. Kumar, M. Grzelakowski, J. Zilles, M. Clark and W. Meier, *Proc. Natl. Acad. Sci. U. S. A.*, 2007, **104**, 20719-20724.
17. K. M. Rosenblatt, D. Douroumis and H. Bunjes, *J. Pharm. Sci.*, 2007, **96**, 1564-1575.
18. N. Charalampopoulos, K. Avgoustakis and C. G. Kontoyannis, *Anal. Chim. Acta*, 2003, **491**, 57-62.

19. J. P. K. Tan, C. H. Goh and K. C. Tam, *Eur. J. Pharm. Sci.*, 2007, **32**, 340-348.
20. S. Tobias and W. F. R., *Angew. Chem., Int. Ed.*, 2015, **54**, 6098-6108.
21. J. Z. Long and B. F. Cravatt, *Chem. Rev.*, 2011, **111**, 6022-6063.
22. M. Tang, M. Purcell, J. A. M. Steele, K.-Y. Lee, S. McCullen, K. M. Shakesheff, A. Bismarck, M. M. Stevens, S. M. Howdle and C. K. Williams, *Macromolecules*, 2013, **46**, 8136-8143.
23. C. J. McKinlay, R. M. Waymouth and P. A. Wender, *J. Am. Chem. Soc.*, 2016, **138**, 3510-3517.
24. P. A. Wender, D. J. Mitchell, K. Pattabiraman, E. T. Pelkey, L. Steinman and J. B. Rothbard, *Proc. Natl. Acad. Sci. U. S. A.*, 2000, **97**, 13003-13008.
25. J. B. Rothbard, T. C. Jessop, R. S. Lewis, B. A. Murray and P. A. Wender, *J. Am. Chem. Soc.*, 2004, **126**, 9506-9507.
26. M. W. Tibbitt, C. B. Rodell, J. A. Burdick and K. S. Anseth, *Proc. Natl. Acad. Sci. U. S. A.*, 2015, **112**, 14444-14451.
27. Y. Zhu, L. Liu and J. Du, *Macromolecules*, 2013, **46**, 194-203.
28. R. Baumgartner, Z. Song, Y. Zhang and J. Cheng, *Polym. Chem.*, 2015, **6**, 3586-3590.
29. R. J. Williams, I. A. Barker, R. K. O'Reilly and A. P. Dove, *ACS Macro Lett.*, 2012, **1**, 1285-1290.

Chapter 7

Experimental Section

7.1 General Procedures

7.1.1 Materials

All solvents and reagents were obtained from commercial sources (Sigma-Aldrich, VWR International, Alfa Aesar and Fisher) and used as received unless otherwise stated. All manipulations were carried out using a standard Schlenk line or dry-box techniques under an inert atmosphere of nitrogen. All glassware was dried at 160 °C for 20 h and cooled under vacuum prior to use. Solvents were dried by passing through a column of appropriate drying agent, degassed and stored under nitrogen atmosphere.

Ligand H_2L, catalyst **C1**, 1,4-cyclohexadiene oxide (CHDO), ethyl ethylene phosphate (EP) were synthesised according to the previously published literature.[1-3] Cyclohexene oxide (CHO) and vinyl-1-cyclohexene-1,2-epoxide (v-CHO) were fractionally distilled over calcium hydride prior to use and stored under an inert atmosphere. v-CHO was stored at - 35 ºC. Trans-1,2-cyclohexene diol (CHD) was recrystallised from ethyl acetate and stored under nitrogen atmosphere. *rac*-Lactide (*rac*-LA) (Purac) was recrystallised from isopropanol once, then from dry toluene twice, sublimated and dried under high vacuum for 72 h prior to use. 1,5,7-Triazabicyclo[4.4.0]dec-5-ene (TBD) was dissolved in THF, dried over 3 Å molecular sieves, filtered and sublimated after removing THF. Bis(triphenylphosphine)iminium chloride (PPNCl) was purified by recrystallisation from diethyl ether and acetonitrile. Maleic anhydride (MA) was recrystallised from benzene, sublimated and stored under nitrogen atmosphere. Methylene diphenyl diisocyanate (MDI) was purified *via* dissolving in hexane and filtering the insoluble impurity, followed by removing all the solvent. Dialysis tubing (14000 Da molar mass cutoff (MWCO)) was obtained from

BioDesign Inc. of New York. High-pressure reactions were carried out in a Parr 5513 25 mL bench reactor using CP grade (99.99%) carbon dioxide (BOC) purified by passing through a VIVI p600-1 CO_2 gas purifying column. High-purity CO_2 for low-pressure reactions was obtained by passing research grade CO_2 (99.99995%) purchased from BOC (Linde Gas) through a high-performance purifier (drierite column).

7.1.2 Measurements

NMR: ^{1}H (400.0 MHz), $^{13}C\{^{1}H\}$ (101.0 MHz), $^{31}P\{^{1}H\}$ (162.1 MHz) and 2D NMR (COSY, HSQC, HMBC) spectra were recorded using a Bruker AV 400 spectrometer at 298 K (unless otherwise stated). NMR spectra were processed and analysed using MestReNova software.

DOSY NMR: DOSY NMR experiments were performed at 298 K on a Bruker 500 AVANCE III HD NMR spectrometer operating at a frequency of 500.13 MHz for proton resonance under TopSpin (version 3.2, Bruker Biospin, Karlsruhe) and equipped with a z-gradient bbfo/5mm tuneable "SmartProbe"^{TM} probe and a GRASP II gradient spectroscopy accessory providing a maximum gradient output of 53.5 G/cm (5.35G/cmA). Diffusion-ordered NMR data was acquired using the Bruker pulse program ledbpgp2s with a spectral width of 5500Hz (centred on 4.5 ppm) and 32768 data points. A relaxation delay of 12 s was employed along with a diffusion time (large delta) of 100 ms and a longitudinal eddy current delay (LED) of 5 ms. Bipolar gradient pulses (little delta/2) of 2.2 ms and homospoil gradient pulses of 0.6 ms were used. The gradient strengths of the two homospoil pulses were -17.13% and -13.17%. 32 experiments were collected with the bipolar gradient strength, initially at 5% (1st experiment), linearly increased to 95% (32nd experiment). All gradient pulses were smooth-square shaped (SMSQ10.100) and after each application a recovery

delay of 200 μs used. The experiment was run with 24 scans per increment, employing one stimulated echo with two spoiling gradients. DOSY plots were generated by using the DOSY processing module of TopSpin. Parameters were optimised empirically to find the best quality of data for presentation purposes.

End group analysis by $^{31}P\{^{1}H\}$ NMR spectroscopy: Literature procedure for hydroxyl end group analysis by $^{31}P\{^{1}H\}$ NMR spectroscopy was followed.[3] A stock solution was prepared by dissolving 400 mg of bisphenol A (BPA) and 5.5 mg of $Cr(acac)_3$ in 10 mL of pyridine. A 400 μL of the polymer solution (30 $mg \cdot mL^{-1}$ in $CDCl_3$) and 40 μL of the stock solution were mixed in a 5 mm NMR tube. After adding 40 μL of 2-chloro-4,4,5,5,-tetramethyl dioxaphospholane to the tube, the reaction mixture was allowed to react for 18 h prior to characterisation.

SEC: The molar mass and dispersities were determined using a Shimadzu LC-20AD, with HPLC grade THF as the eluent at a flow rate of 1.0 $mL \cdot min^{-1}$ at 40 ºC. Two Mixed Bed PSS SDV linear S columns were used in series, and the polymer samples were dissolved in HPLC grade THF and filtered prior to analysis. In some cases, a different Agilent SEC instrument was used to characterise the molecular weights and dispersities of hydrophilic polymers, with PSS GRAM columns in series using DMF (+ 0.075% w/v LiBr) as the eluent at a flow rate of 0.8 $mL \cdot min^{-1}$ at 40 ºC. Retention times were normalised using water as a flow rate marker. In both cases, molar masses were calculated relative to a set of monodisperse polystyrene standards.

MALDI-ToF MS: All MALDI-ToF measurements were performed using Micromass MALDI micro MX spectrometer. Potassium trifluoroacetate (KTFA) was used as the ionising agent. For polycarbonate homopolymers, dithranol was used as the matrix. Trans-2-[3-(4-tert-butylphenyl)-2-methyl-2-propenylidene]malononitrile (DCTB) was

used as the matrix for polyesters. The polymer, the matrix and the ionising agent were dissolved in THF separately at a concentration of 10 $mg \cdot mL^{-1}$ and mixed at a loading of 1: 1: 1. The mixed solution was spotted on a stainless steel MALDI plate repeatedly (3 times) and left to dry for 16 h. All the spectra were recorded using reflectron mode and analysed using mmass software.

***Thermal analyses**:* The thermal properties were measured using DSC3+ (Mettler Toledo, Ltd). A sealed empty crucible was used as a reference, and the DSC was calibrated using indium. About 5 mg of sample was placed in an empty crucible and heated from 25 °C to 150 °C, at a rate of 10 $°C \cdot min^{-1}$, under N_2 flow (80 $mL \cdot min^{-1}$), and were kept at 150 °C for 2 min to erase the thermal history. Subsequently, the samples were cooled to -80 °C, at a rate of 10 $^oC \cdot min^{-1}$, and kept at -80 $°C \cdot min^{-1}$ for a further 2 mins, followed by a heating procedure from -80 °C to 150 °C, at a rate of 10 $°C \cdot min^{-1}$. Each sample was run for three heating-cooling cycles. The glass transition temperatures (T_g) reported are taken from the third cycle. The DSC data collection and analysis were carried out using STARe software (Mettler-Toledo).

***Water contact angle measurements**:* Static water contact angles were measured using a Drop Shape Analysis System (EasyDrop, Krüss, Germany). A 30 µL drop of ultra-pure water (MilliQ water, Millipore, MA, USA) was placed on the polymer film surfaces, and the static water contact angle was measured. The measurements were performed on three different areas of each slide, and the values were averaged.

Antibacterial assay: The bactericidal activity of the samples was tested on *Escherichia coli* (strain ATCC 25922). *E. coli* was stored at 70 ºC in Brain-Heart-Infusion broth (BHI, Oxoid Ltd., Hampshire, England, UK) with 20% (v/v) glycerol, and was propagated on MacConkey agar (Oxoid Ltd., Hampshire,

England, UK). 10 mL of BHI broth was inoculated with one bacteria colony and cultured at 37 ºC with shaking at 200 rpm. After 18 h of incubation, the bacteria were harvested by centrifugation at 5000 rpm for 10 min, washed twice by phosphate buffered saline (PBS), and 10^4-fold diluted in PBS to obtain ~ 10^5 CFU·mL^{-1}. The polymer samples were immersed in 2 mL of this suspension and incubated at 20 ºC with shaking at 100 rpm for 24 h. After the incubation, the bacteria suspension was serially diluted, plated onto MacConkey agar, and incubated at 37 ºC for 24 h to obtain colony counts.

Surface charge measurements: The surface charge, i.e. the ζ-potential, of the coated samples was determined with a SurPASS electrokinetic analyser from Anton Paar (Graz, Austria) from the streaming current between pH 10 and 2 (as controlled by titrating 0.05 mol·L^{-1} KOH and 0.05 mol·L^{-1}HCl). The coated glass substrates were mounted on the sample holder with double-sided adhesive tape. The sample holders were then installed in an adjustable gap cell at a gap width of 100 μm. 1 mM KCl as electrolyte solution was pumped through the cell with the pressure being steadily increased up to 300 mbar. The ζ-potential was determined from the measured streaming current using the Helmholtz-Smoluchowski equation:

$$\frac{\Delta I_{str}}{\Delta P} = \zeta(I_{str}) \frac{\varepsilon_0 \varepsilon_r A_c}{\eta L}$$

[I_{str} is streaming current, P is the applied pressure, ε_0 is vacuum permittivity, ε_r is relative liquid permittivity, η is the electrolyte viscosity, A_c is the cross-section of the streaming channel and L is the length of the streaming channel]

Bacteria attachment assay: The samples were placed in 2 mL of bacterial suspension containing ~ 10^8 CFU·mL^{-1}, and then incubated at 20 ºC with shaking at

100 rpm for 0, 0.25, 0.5, 1, and 24 h. after that, the sample were gently washed by DI water and immersed in 5 mL of 0.1% crystal violet solution for 10 min to stained bacteria attached on the samples. The stained sample was washed by DI water and dried for 24 h. The images of samples were taken by an optical microscope (ModelIMT-2, Olympus Ltd, Tokyo, Japan).

DLS: The DLS measurements were conducted using a Zetasizer Nano series instrument (Malvern Instrument). The scattering angle was set at 173^{o}, and all the aqueous aggregate solutions were put into disposable PMMA cuvettes for analysis. Data processing was carried out using cumulant analysis of the experimental correlation function and analysed *via* the Stokes-Einstein equation.

Zeta potential: The physical stability of the nanostructures is characterised by the zeta potential using a Zetasizer Nano series instrument (Malvern Instruments). Data collection and processing were carried out using Zetasizer software (version 7.11 from Malvern Instruments).

TEM: Amorphous carbon-coated copper TEM grids (Agar Scientific) were plasma glow-discharged for 15 s to generate a hydrophilic surface. Individual samples (2-4 μL) were placed onto the freshly discharged grids for 5 mins, before being blotted with a filter paper to remove excess solutions. Uranium acetate (0.5 wt%) was used to stain the sample by placing onto the sample-loaded grids for 5 mins and then removing the excessive staining solution. The grids were dried in a fume hood overnight prior to characterisation. In Chapter 4, the characterisation of vesicles and micelles formed from poly(phosphoester-*b*-carbonate-*b*-phosphoester) was conducted by Dr Edward R. White (Imperial College London) and Dr Mahmoud Ardakani (Imperial College London) on a JEOL JEM 2100F scanning transmission electron

microscope, equipped with an Oxford X-Max 80 SDD EDX detector, at an operating voltage of 200 kV. In Chapter 5, the characterisation of micelles formed from alternating polyesters was conducted by Miss Tianyi Chen (working with Prof. Peter Nellist at University of Oxford) on a JEOL 3000F scanning transmission electron microscope, equipped with an Oxford X-Max 80 SDD EDX detector.

Fluorescence Spectroscopy: Fluorescence experiments were carried out to evaluate the drug-loading efficiency. Rhodamine-B was used as a model drug and the fluorophore. Experiments were conducted using a Horiba Jobin Yvon FluoroLog-3 equipped with a Hamamatsu R928 PMT detector and a double-grating emission monochromator. The spectra were corrected to take into account the energy profile of the lamp and the detector sensitivity at each wavelength using the manufacturer correction file.

Cytotoxicity/Cell viability Tests: ATCC-MC3T3-E1 preosteoblasts were used for cytotoxicity test according to the ISO-10993-5 procedure. Cells were cultured at 37 °C, 5% CO_2, in Minimum Essential Medium α (α-MEM) supplemented with 10% fetal bovine serum (FBS), 1% non-essential amino acids (NEAA), 1% L-Glutamine and 1% Penicillin-Streptomycin. Cells were placed in 96-well tissue culture plates at 9400 cells/well and incubated for 48 h to form a subconfluent monolayer. Test polymer, a non-toxic high-density PE tubing negative control and organo-tin stabilised PVC positive control were sterilised with 70% ethanol for 30 min, washed three times with sterile PBS, and pre-treated with complete medium composed of α-MEM supplemented with 5% FBS, 1% NEAA, 1% L-Glutamine and 1% Penicillin-Streptomycin for 24 h. Fresh medium was then substituted at 5 $mL \cdot g^{-1}$. Serial dilutions of the extract (1, 10, 25, 50 and 100% of the extract) were performed using the complete medium as diluent. The extract mediums were conditioned for 24 h at

37 °C, 5% CO_2. The subconfluent ATCC-MC3T3-E1 monolayers were then cultured in the conditioned medium, and the cell viability will be assessed on day 0, day 1 and day 3. After the designated incubation time, the metabolic activity of the samples was assessed by alamarBlue^{TM} which was diluted 1:10 in cell medium, incubated for 3 h and analysed at 570 nm and 600 nm on a Perkin Elmer Envision multimode plate reader. Cell viability was demonstrated using the LIVE/DEAD viability assay. At each time point, assayed samples were incubated with LIVE/DEAD solution (2 μM Calcein-AM and 4 μM ethidium homodimer in cell culture media) at 37°C, 5% CO_2 for 30 min. After the incubation, the residual ethidium homodimer and un-reacted Calcein-AM were washed away by warm PBS and added with phenol-red free culture media. Microscopy was carried out using an Olympus BX-51 reflected fluorescence microscope (Olympus UK Ltd., London) within 30 min after staining.

Cell Attachment Tests: ATCC-MC3T3-E1 preosteoblasts were cultured at standard conditions (37 °C, 5% CO_2) in Minimum Essential Medium α (α-MEM) supplemented with 10% fetal bovine serum (FBS), 1% non-essential amino acids (NEAA), 1% L-Glutamine and 1% Penicillin-Streptomycin. Polymers were placed in 24-well non-tissue treated plate, washed with PBS and sterilised under UV light for 3 h. The cell suspension was deposited in an empty well as a control. Cell adhesion was allowed to proceed for 24 h and was visualised by staining with Calcein-AM. The morphology of the attached cells was visualised using a Leica SP5 MP/FLIM inverted confocal microscopy.

7.1.3 Synthesis of C1

Preparation of 4-tert-butyl-2,6-diformylphenol (compound 1, ***Scheme 7.1)***[1]

4-*tert*-Butyl-phenol (10.0 g, 66.6 mmol) and hexamethylenetetramine (14.9 g, 106.6 mmol) were placed in a round bottom flask, and CF_3COOH (52.0 mL, 692.0 mmol) was added slowly to this reaction mixture while stirring. The reaction mixture was left to reflux for 14 h at 125 °C. Then the mixture was refluxed for 4 hours at 150 ºC using a Dean-Stark condenser to remove water (which formed as a side product). 3M HCl was added (100.0 mL) after cooling the reaction mixture to 100 °C. The resulting mixture was refluxed for another 40 min, at 100 °C, and then kept at -20 ºC for 14 h. The precipitate produced was filtered, washed twice with cold MeOH (-78 °C) and dried under vacuum to yield yellow crystals (8.27 g, 60.2%).

^{1}H NMR ($CDCl_3$, 400 MHz) δ / ppm: 11.48 (s, 1H, -O<u>H</u>), 10.24 (s, 2H, -C(O)<u>H</u>), 7.98 (s, 2H, Ar-<u>H</u>), 1.35 (s, 9H,Ar-C-(C<u>H</u>$_3$)$_3$). ^{1}H NMR spectrum is shown in **Figure 7.1**.

Preparation of $[H_4L](ClO_4^-)_2$ (compound 2, ***Scheme 7.1)***[1]

4-tert-Butyl-2,6-diformylphenol (4.0 g, 19.4 mmol), $NaClO_4$ (9.5 g, 77.6 mmol), acetic acid (2.2 mL, 38.8 mmol) and 300 mL of MeOH were placed in a round-bottom flask and heated to 70 °C with stirring. 2,2-dimethyl-1,3-propanediamine (2.3 mL 19.4 mmol) dissolved in MeOH (100.0 mL) was added slowly to the solution when it began to boil. The reaction mixture was then cooled to 25 °C and stirred for 18 h. The volume of the resulting red/orange solution was reduced to ca. 120 mL and left to stand for 16 h to yield a red crystalline precipitate. The red crystalline precipitate was filtered and washed with cold MeOH (-78 °C) to yield red crystals (4.6 g, 64%).

^{1}H NMR (DMSO-d_6, 400 MHz) δ / ppm: 13.61 (br s, 4H, N<u>H</u>/O<u>H</u>), 8.69 (d, 4H, N=C<u>H</u>), 7.66 (s, 4H, Ar-<u>H</u>), 3.88 (s, 8H, C<u>H</u>$_2$), 1.29 (s, 12H, C<u>H</u>$_3$), 1.15 (s, 18H, C<u>H</u>$_3$). ^{1}H NMR spectrum is shown in **Figure 7.2**.

*Preparation of [H_4L] (compound 3, **Scheme 7.1**)*[1]

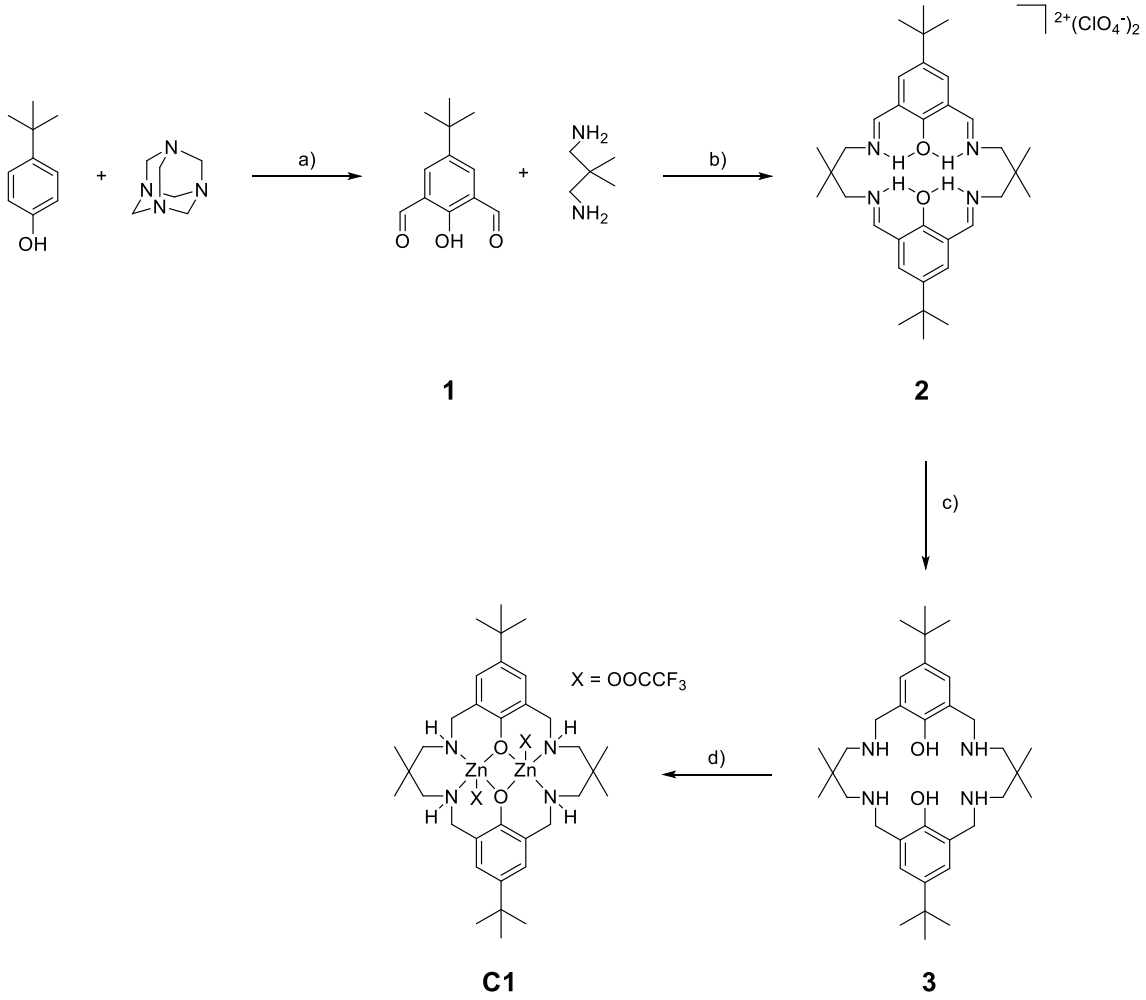
[H_4L](ClO_4^-)$_2$ was suspended in MeOH (300.0 mL), and $NaBH_4$ (4.2 g, 110.0 mmol) was added slowly to this suspension. After adding $NaBH_4$, the red-orange suspension turned to a clear solution and was allowed to stir for 1 h. Distilled water (150.0 mL) was then added to the solution slowly, and the solution became cloudy. Once the white precipitate persistently appeared, the mixture was left to stand for 16 h. The precipitate was filtered, washed with cold water (30.0 mL) and dried under vacuum to yield a white crystal (2.1 g, 89%).

^{1}H NMR ($CDCl_3$, 400 MHz) δ / ppm: 6.93 (s, 4H, Ar-<u>H</u>), 3.73 (s, 8H, C<u>H</u>$_2$), 2.51 (s, 8H, C<u>H</u>$_2$), 1.25 (s, 18H, C<u>H</u>$_3$), 1.01 (s, 12H, C<u>H</u>$_3$). ^{1}H NMR spectrum is shown in **Figure 6.3**.

*Preparation of [$LZn_2(CF_3COO)_2$] (**C1**, **Scheme 7.1**)*[1]

$Zn(CF_3COO)_2.xH_2O$ was dried under a vacuum at 40°C in the presence of P_2O_5 for 48 h. H_2L (2.0 g, 3.6 mmol) was dissolved in methanol (150.0 mL) and $Zn(CF_3COO)_2.xH_2O$ (2.1 g, 7.2 mmol) was added. After stirring the reaction mixture for 18 hours, methanol was removed *in vacuo*. The product was taken up in dichloromethane and filtered. After removing dichloromethane *in vacuo*, a white powder (2.7 g, 82%) was obtained and dried under vacuum at 40 °C, in the presence of P_2O_5 for 72 h.

^{1}H NMR ($CDCl_3$, 400MHz) δ / ppm: Major isomer δ 6.91 (s, 4H, Ar-H), 4.32-4.26 (m, 4H, Ar-CH_2-N), 3.24 (d, J = 12.0 Hz, 4H, Ar-CH_2-N), 2.98 (m, 4H, N-CH_2-C), 2.68 (d, J = 11.5 Hz, 4H, N-CH_2-C), 2.38 (t, J = 12.7 Hz, 4H, NH), 1.24 (s, 18H, Ar-CH_3), 1.18 (s, 6H, N-C-CH_3), 1.03 (s, 6H, N-C-CH_3). ^{19}F NMR (d^4-methanol, 400MHz) δ / ppm: -77.09(s). ^{1}H and ^{19}F NMR spectra are shown in **Figure 7.4** and **Figure 7.5**.



Scheme 7.1 Synthetic route of **C1**. Reaction conditions: a) HMTA, CF_3COOH, 125 °C, 24h; 3M HCl, 100 °C, 40 min. b) $NaClO_4$, AcOH, MeOH, 70 °C, 4 h. c) $NaBH_4$, MeOH, 25 °C, 1h; H_2O, 18 h. d) $Zn(CF_3COO)_2$, MeOH, 25°C, 18 h.

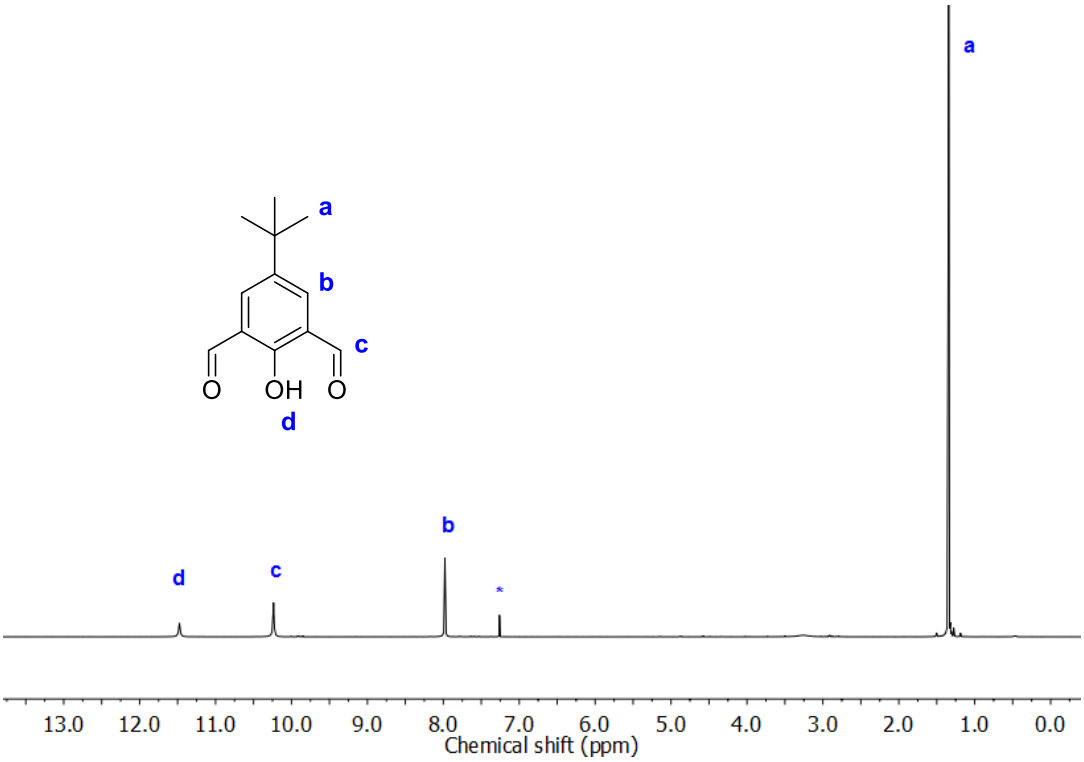


Figure 7.1 ^{1}H NMR spectrum of 4-tert-butyl-2,6-diformylphenol (400.0 MHz, $CDCl_3$). The asterisk denotes the residue protio-solvent.

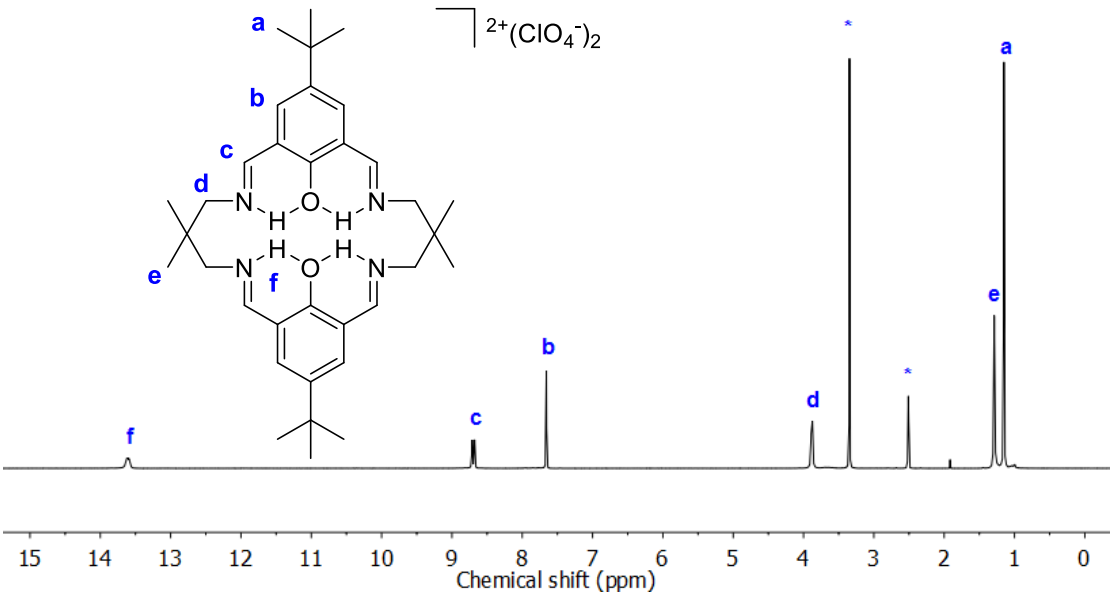


Figure 7.2 ^{1}H NMR spectrum of $[H_4L](ClO_4^-)_2$ (400.0 MHz, DMSO-d_6). The asterisk denotes the residue protio-solvent.

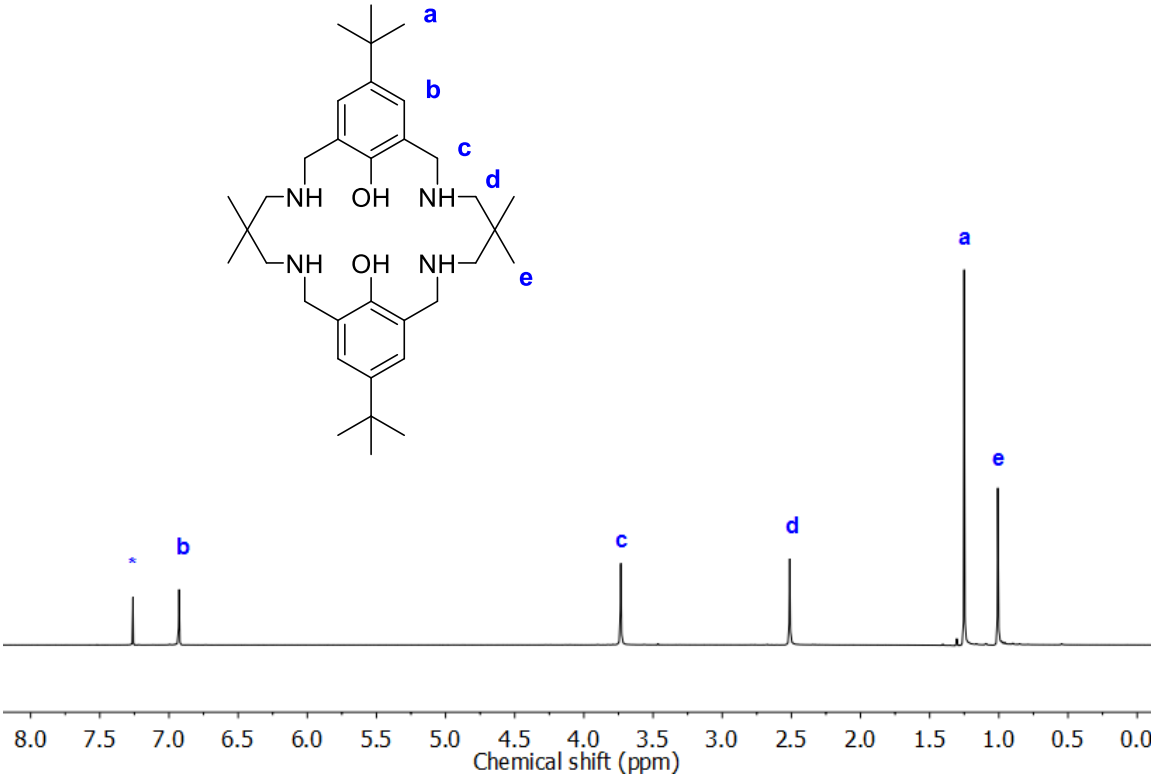


Figure 7.3 ^{1}H NMR spectrum of [H_4L] (400.0 MHz, $CDCl_3$). The asterisk denotes the residue protio-solvent.

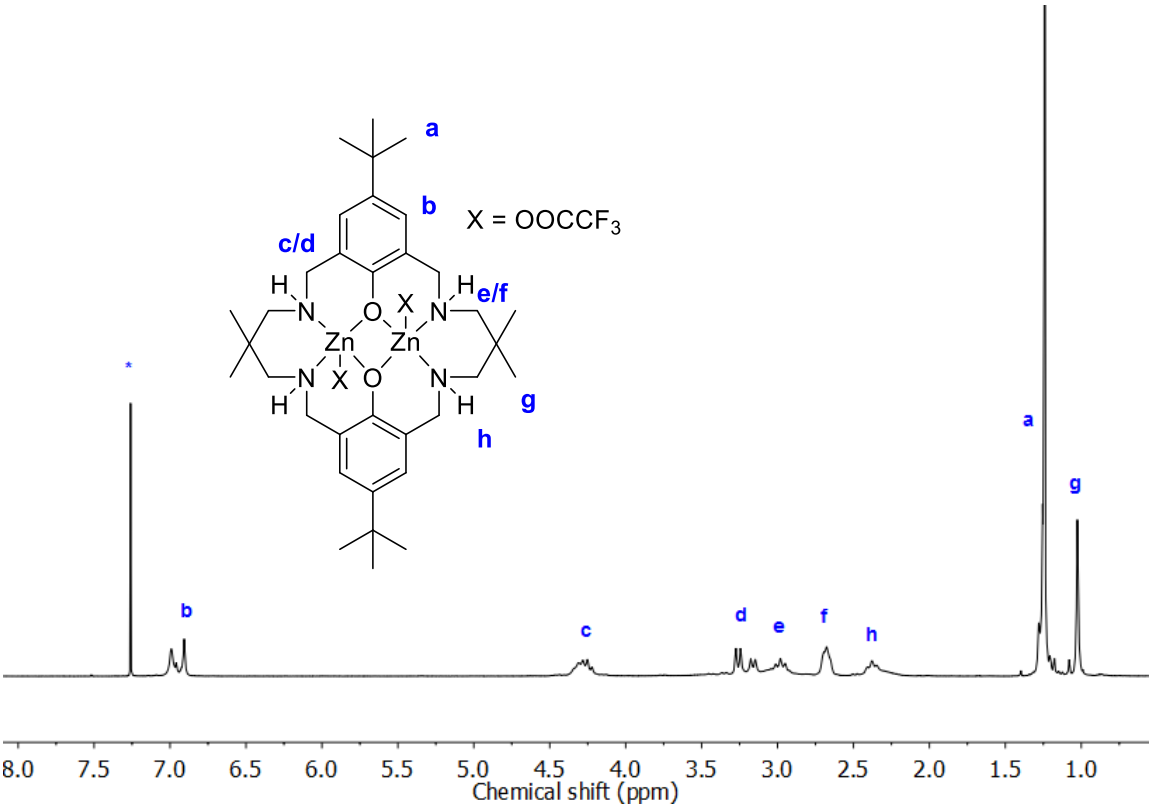


Figure 7.4 ^{1}H spectrum of **C1** (400.0 MHz, $CDCl_3$). The asterisk denotes the residual protio-solvent.

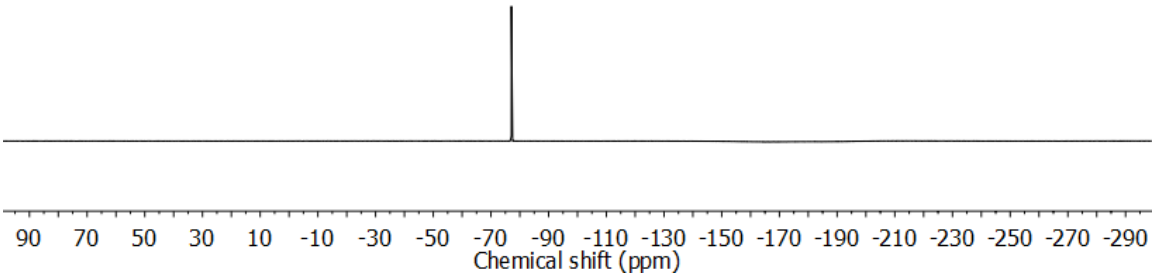
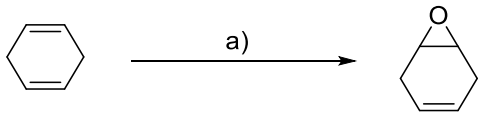


Figure 7.5 $^{19}F\{^{1}H\}$ NMR spectrum of $[LZn_2(O_2CCF_3)_2]$ (**C1**) (376.6 MHz, $CDCl_3$).

7.1.4 Syntheses of monomers/compounds

*Preparation of 1,4-cyclohexadiene oxide (CHDO)(**Scheme 7.2**)*[2]



Scheme 7.2 Synthetic route of 1,4-cyclohexadiene oxide (CHDO). a) mCPBA, DCM, H_2O, $NaHCO_3$, 25 °C, 3h.

To a solution of $NaHCO_3$ (12.1 g, 150.0 mmol) in water (70.0 mL) was added a solution of 4-cyclohexadiene (9.1 mL, 100.0 mmol) in dichloromethane (200.0 mL). m-CPBA (59.3 g, 95.0 mmol) was added in several portions to the pre-cooled mixture in an ice-bath at 0 °C. The reaction mixture was stirred at 0 °C for an hour, then allowed to warm to 25 °C and stirred for further 3 h. After which time, an aqueous solution of $Na_2S_2O_3$ (100.0 mL) was added to the solution mixture and stirred for an hour. The organic layer was separated, and the aqueous layer was extracted with dichloromethane (3 × 50.0 mL). The combined organic layer was washed with a saturated $NaHCO_3$ solution (100.0 mL) following by brine (100.0 mL), and dried over Na_2SO_4. All volatiles were removed, and the crude product was further purified by fractional distillation to give a colourless liquid (6.4 g, 67%).

^{1}H NMR ($CDCl_3$, 400.0 MHz) δ / ppm: 5.43 (s, 2 H, C<u>H</u>=C<u>H</u>), 3.24 (s, 2 H, OC<u>H</u>), 2.56 (d, 2 H, C<u>H</u>$_2$), 2.43 (d, 2 H, C<u>H</u>$_2$).

^{13}C NMR ($CDCl_3$, 100.7 MHz) δ / ppm: 121.6, 51.1, 25.1.^{1}H NMR and ^{13}C NMR spectra are shown in **Figure 7.6** and **Figure 7.7**.

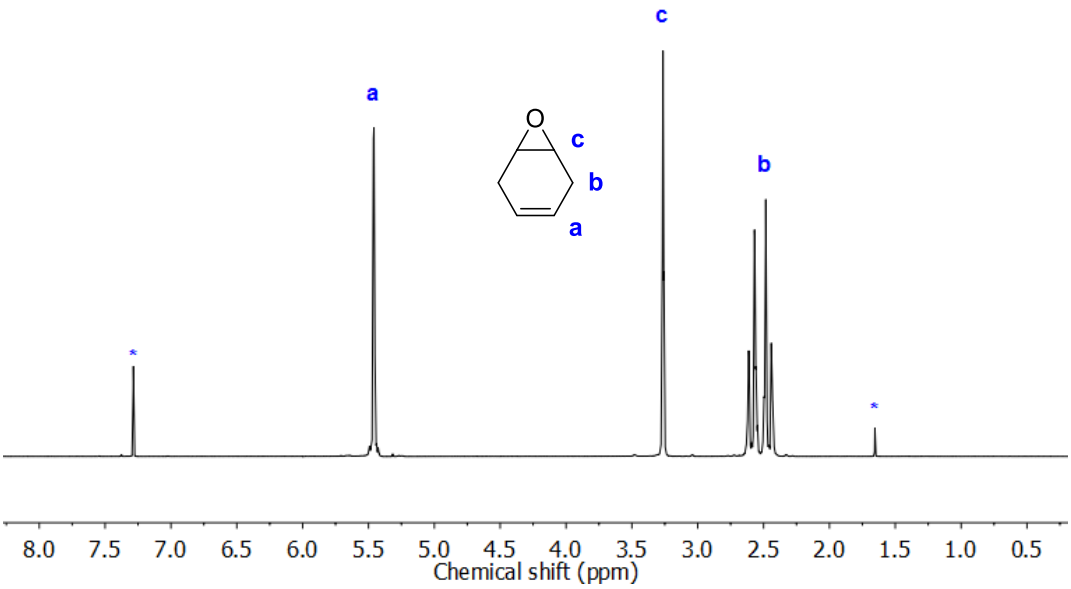


Figure 7.6 ^{1}H NMR spectrum of CHDO (400.0 MHz, $CDCl_3$). The asterisk denotes the residual protio-solvent and residue solvents.

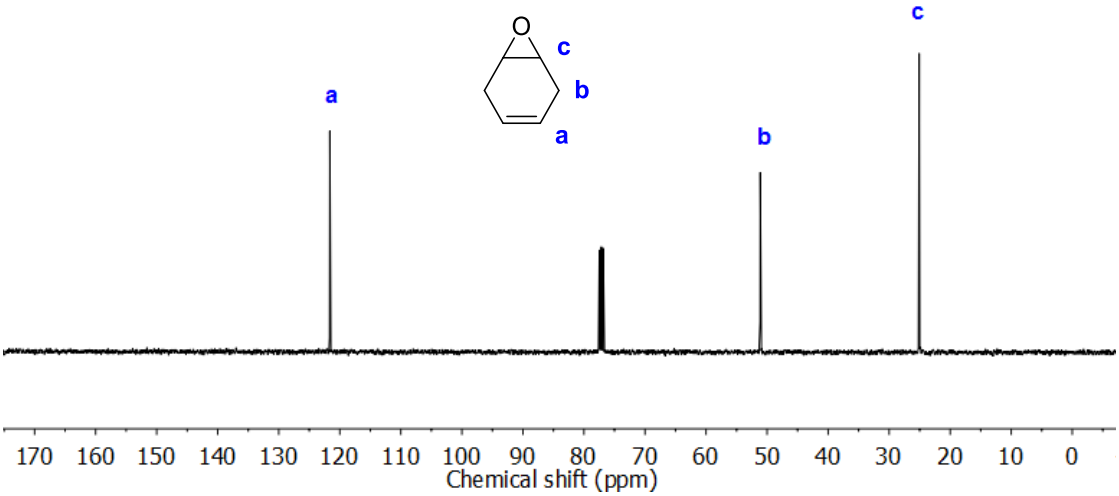


Figure 7.7 $^{13}C\{^{1}H\}$NMR spectrum of CHDO (100.7 MHz, $CDCl_3$).

Preparation of ethyl ethylene phosphate (EP)[3]

Ethanol (10.0 g, 218.0 mmol) and triethylamine (22.0 g, 218.0 mmol) were dissolved in 50 mL of dry THF. After cooling the reaction mixture to -20 °C and stirring for 20 min, 2-chloro-2-oxo-1,3,2-dioxaphospholane (COP, 31.0 g, 218.0 mmol) was added dropwise under nitrogen atmosphere. The reaction was stirred for 18 h, and the precipitate was filtered off. The filtrate was concentrated under reduced pressure and fractionally distilled to give a colourless liquid (16.0 g, 48%).

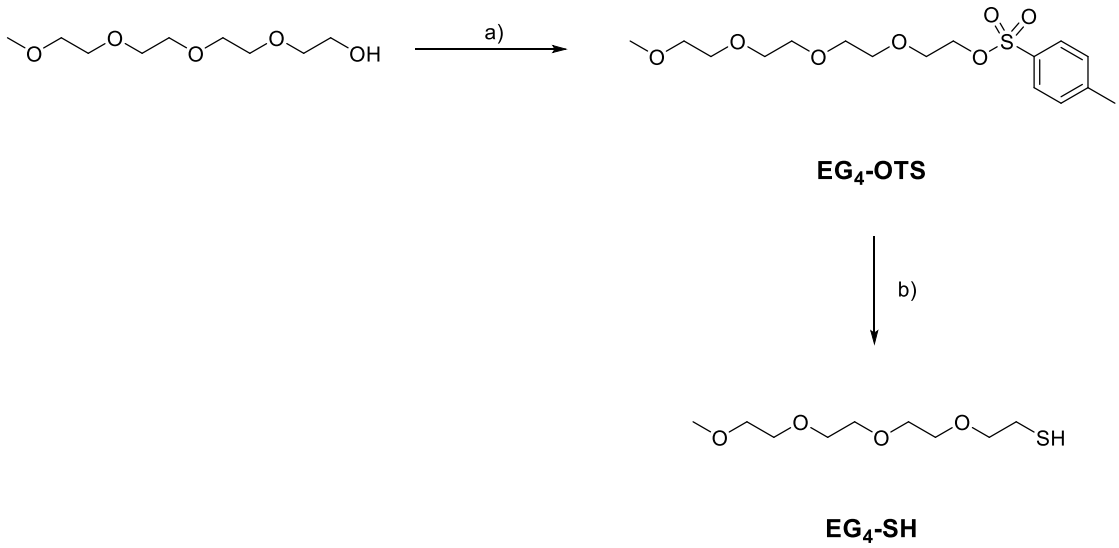
^{1}H NMR ($CDCl_3$, 400.0 MHz) δ / ppm: 4.4 (m, 4H, $OC\underline{H_2}C\underline{H_2}O$), 4.2 (m, 2H, $OC\underline{H_2}CH_3$), 1.37 (t, 3H, $OCH_2C\underline{H_3}$).

$^{31}P\{^{1}H\}$ NMR ($CDCl_3$, 162.1 MHz) δ / ppm: 17.5 (s).

Preparation of tetraethylene glycol monoethylether monotosylate (EG_4-OTs, ***Scheme 7.3****)*[4]

A 250 mL round bottom flask was charged with a solution of tetraethylene glycol monoethyl ester (10.0 g, 48.0 mmol) in THF (20 mL). The solution was cooled to 0 °C in an ice-bath, prior to the addition of an aqueous NaOH (5 M, 27.0 mL, 134.0 mmol). Then a solution of p-toluenesulfonyl chloride (16.5 g, 86.4 mmol) in THF (20.0 mL) was added dropwise to the cold, stirring solution. The reaction was then warmed to RT and stirred for 16 h. Water (50.0 mL) was then added to the reaction, and the solution mixture was extracted with DCM (3 × 50.0 mL). The organic fractions were washed with water (2 × 50.0 mL) following by brine (50.0 mL), then dried over magnesium sulfate. All volatiles were removed under reduced pressure, giving a pure product as colourless oil without any further purification (13.1 g, 75%).

^{1}H NMR ($CDCl_3$, 400 MHz) δ / ppm: 7.79 (d, 2H, ^{3}J = 8.3 Hz, Ar-H), 7.32 (d, 2H, ^{3}J = 8.3 Hz, Ar-H), 4.14 (m, 2H, OCH_2), 3.51-3.69 (m, 14H, OCH_2), 3.35 (s, 3H, OCH_3) and 2.42 (s, 3H, CH_3). ^{1}H NMR spectrum is shown in **Figure 7.8**.



Scheme 7.3 Synthetic route of EG_4-OTs and EG_4-SH. a) mCPBA, DCM, H_2O, $NaHCO_3$, 25 °C, 3h

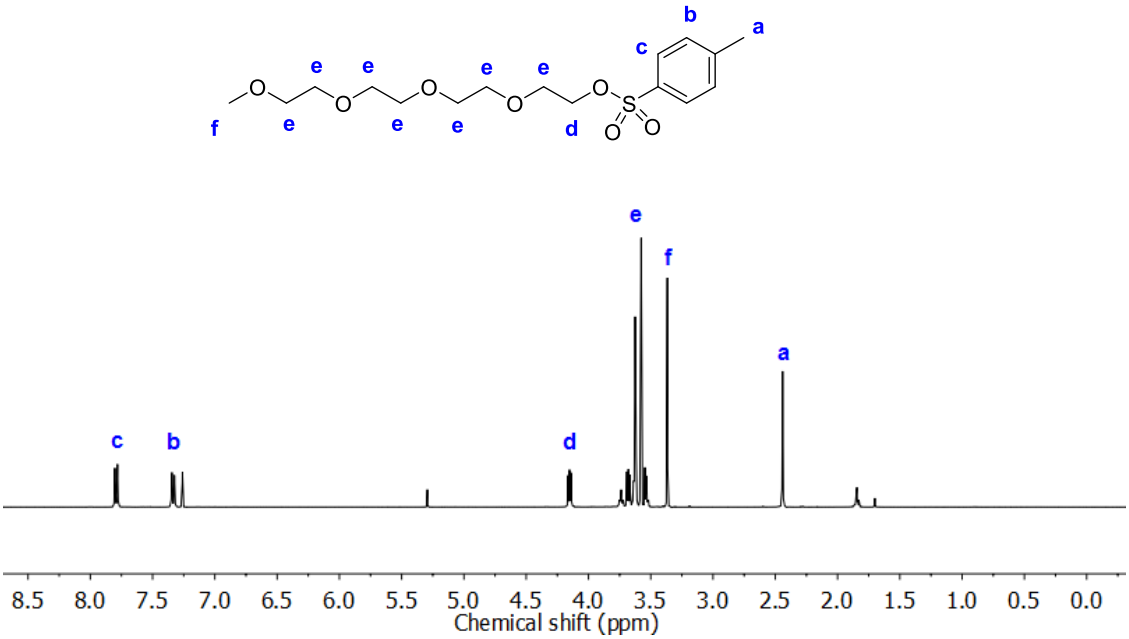


Figure 7.8 ^{1}H NMR spectrum of EG_4-OTs (400.0 MHz, $CDCl_3$).

Preparation of tetraethylene glycol monoethylether thiol (EG_4-SH, ***Scheme 7.3)***[4]

To a 100 mL round bottom flask were added tetraethylene glycol monoethylether monotosylate (11.8 g, 33.9 mmol), thiourea (2.6 g, 33.0 mmol) and absolute ethanol (30.0 mL). The reaction was refluxed under a flow of nitrogen over a period of 7 h. After which time, a solution of NaOH (1.6 g, 40.7 mmol) in distilled H_2O (10.0 mL) was added, and reflux continued for 17 h. The reaction mixture was neutralised with conc. HCl, concentrated to approximately 20 mL and extracted with CH_2Cl_2 (3 × 20.0 mL). The combined organic layer was washed with brine (3 x 20.0 mL) and dried over anhydrous Na_2SO_4. All volatiles were removed *in vacuo*, giving pale yellow oil as a pure product (6.1 g, 81%).

^{1}H NMR ($CDCl_3$, 400 MHz) δ / ppm: 3.51-3.64 (14H, m, OC<u>H</u>$_2$), 3.36 (3H, s, OC<u>H</u>$_3$), 2.66 (2H, q, SC<u>H</u>$_2$), 1.57 (1H, t, S<u>H</u>). ^{1}H NMR spectrum is shown in **Figure 7.9**.

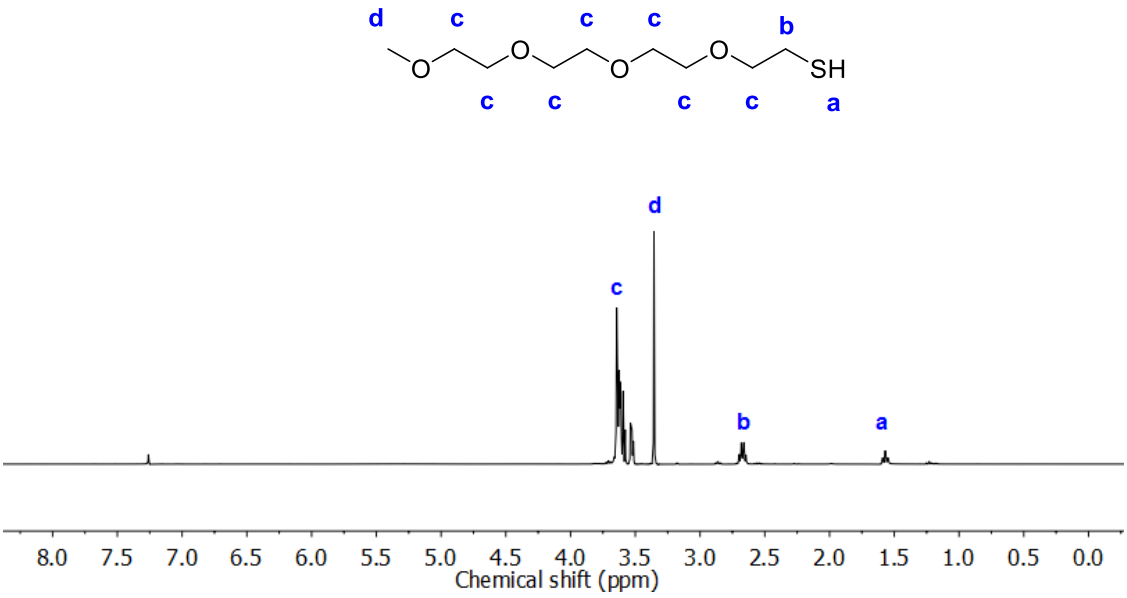
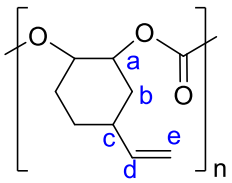


Figure 7.9 ^{1}H NMR spectrum of EG_4-SH (400.0 MHz, $CDCl_3$).

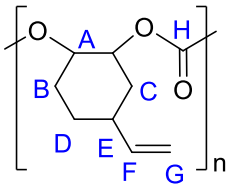
7.2 Copolymerisation of CO2 and epoxides

7.2.1 CO_2/v-CHO copolymerisation at 1 bar of CO_2 (^{V}PC)

v-CHO (2.2 ml, 16.5 mmol) and C1 (15.0 mg, 16.0 μmol) was added to a Schlenk tube, degassed and left for stirring under 1 atm CO_2 at 80 °C for a pre-determined period. The crude reaction mixture was dried *in vacuo* to remove unreacted v-CHO. The polymer was dissolved in dichloromethane, filtered through a silica plug and purified by precipitation from methanol to yield a white solid.



Labelling scheme for ^{1}H NMR assignment



Labelling scheme for ^{13}C{^{1}H} NMR assignment

^{1}H NMR ($CDCl_3$, 400 MHz) δ / ppm: 5.76 (m, 1H, H_d), 5.03 (m, 2H, H_e), 4.89-4.77 (m, 2H, H_a), 2.43 (m, 1H, H_c), 1.90-1.40 (m, 6H, H_b).

^{13}C{^{1}H} NMR ($CDCl_3$, 100.7 MHz) δ / ppm: 153.3 (C_H), 141.7 (C_F), 114.1 (C_G), 73.5 (C_A), 35.0 (C_E), 31.7 (C_B), 26.2 (C_D), 25.5 (C_C). ^{1}H NMR and ^{13}C NMR spectra are shown in **Figure 7.10** and **Figure 7.11**.

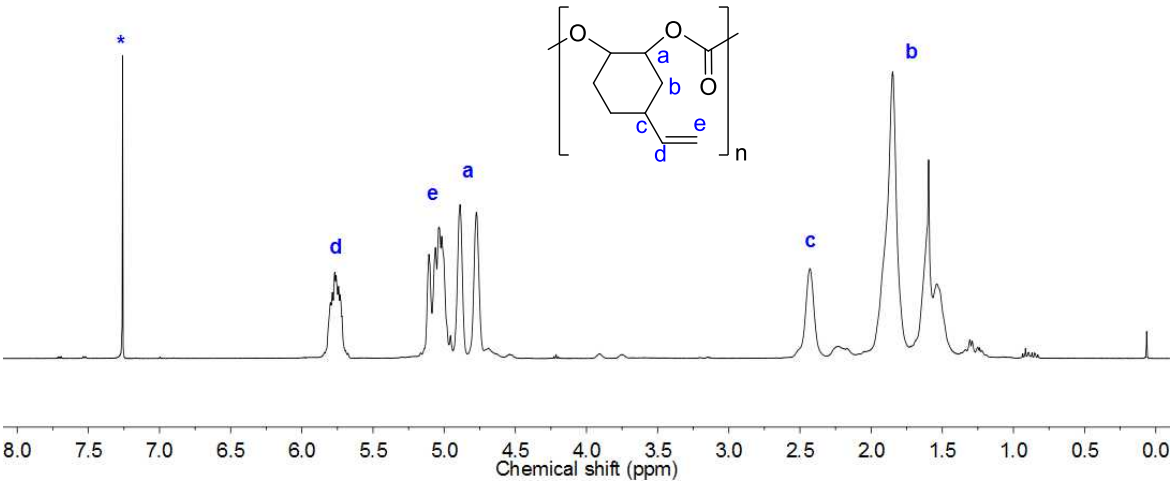


Figure 7.10 ^{1}H NMR spectrum of ^{V}PC (400.0 MHz, $CDCl_3$, 298 K) The asterisk denotes the residual protio-solvent.

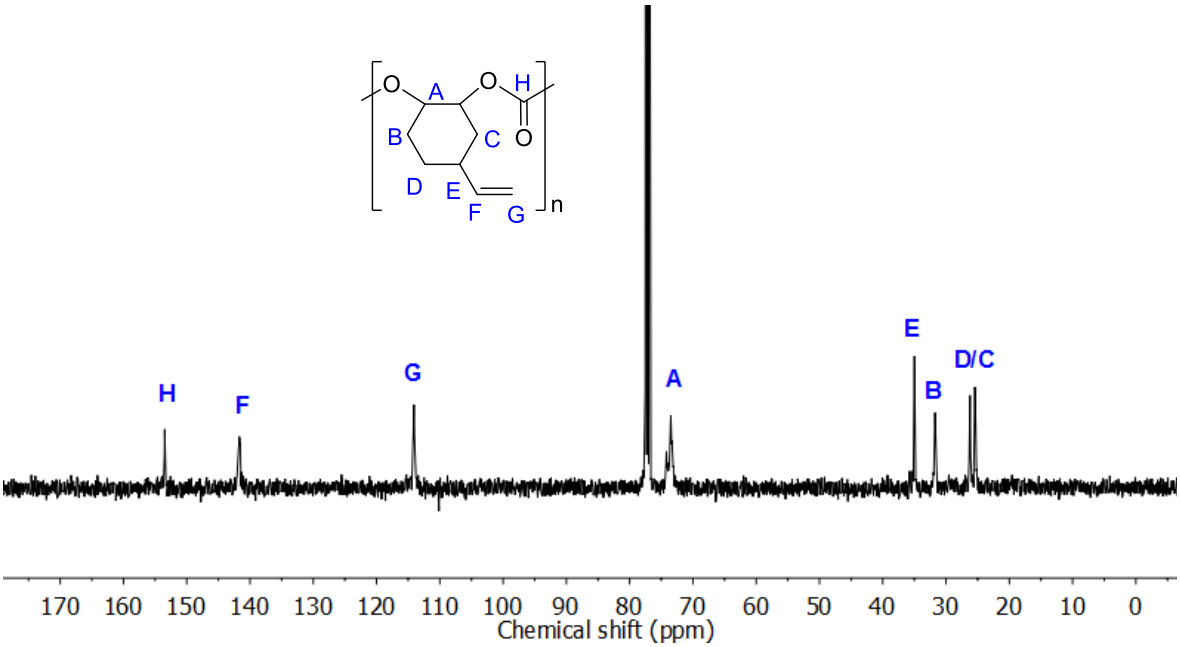


Figure 7.11 ^{13}C{^{1}H} NMR spectrum of ^{V}PC(100.7 MHz MHz, $CDCl_3$, 298 K).

7.2.2 CO_2/v-CHO copolymerisation at 1 bar of CO_2 in the presence of CTA (^{V}PC)

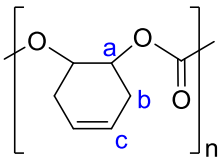
The general procedure stated above was followed, whereby multi-equivalents of CTA (CHD) were added to the reaction mixture prior to the degassing process.

Table 7.1 Relative quantities of reagents used in **Table 3.1**.

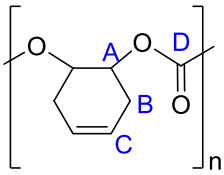
Entry	Molar ratio	Loadings			Time (h)
	[C1]/[CHD]/[v-CHO]	C1	CHD	v-CHO	
1	1/0/1000	15.0 mg	0.0 mg	2.2 mL	22
2	1/5/1000	15.0 mg	9.6 mg	2.2 mL	24
3	1/10/1000	15.0 mg	19.2 mg	2.2 mL	24

7.2.3 CO_2/CHDO copolymerisation at 20 bar of CO_2 (^{C}PC)

CHDO (6.0 mL, 64.7 mmol), [SalenCo(III)Br] (83.0 mg, 130.0 μmol), PPNCl (74.0 mg, 130.0 μmol) and ^{n}PrOH (0.1 mL, 1.6 mmol) were mixed and injected in a 20 mL high pressure Parr Reactor, at 25°C. The reactor was then pressurised to 20 bar with CO_2 and stirred at 30 °C for the given time. The polymer was purified by biphasic extraction: to a solution of ^{C}PC (4.2 g) in DCM (25.0 mL) was added excess hexanoic acid (1.0 mL). The mixture was stirred at room temperature for 3 h before all the volatiles were removed, under reduced pressure. The solid residue was dissolved in acetonitrile (30.0 mL) and washed with hexane (3 × 20.0 mL). The acetonitrile solution was then dried (anhydrous Na_2SO_4) and all the volatiles were removed *in vacuo*. The residual polymer was redissolved in DCM (5.0 mL) and precipitated twice in methanol (300.0 mL). The purified polymer was dried *in vacuo* at 40 °C for 72 h.



Labelling scheme for ^{1}H NMR assignment



Labelling scheme for ^{13}C{^{1}H} NMR assignment

^{1}H NMR ($CDCl_3$, 400 MHz) δ / ppm: 5.57 (s, 2H, H_c), 4.96 (s, 2H, H_a), 2.77-2.15 (m, 4H, H_b).

^{13}C{^{1}H} NMR ($CDCl_3$, 100.7 MHz) δ / ppm: 154.0 (C_D), 123.4(C_C), 73.7(C_A), 29.9(C_B)

^{1}H NMR and ^{13}C NMR spectra are shown in **Figure 7.12** and **Figure 7.13**.

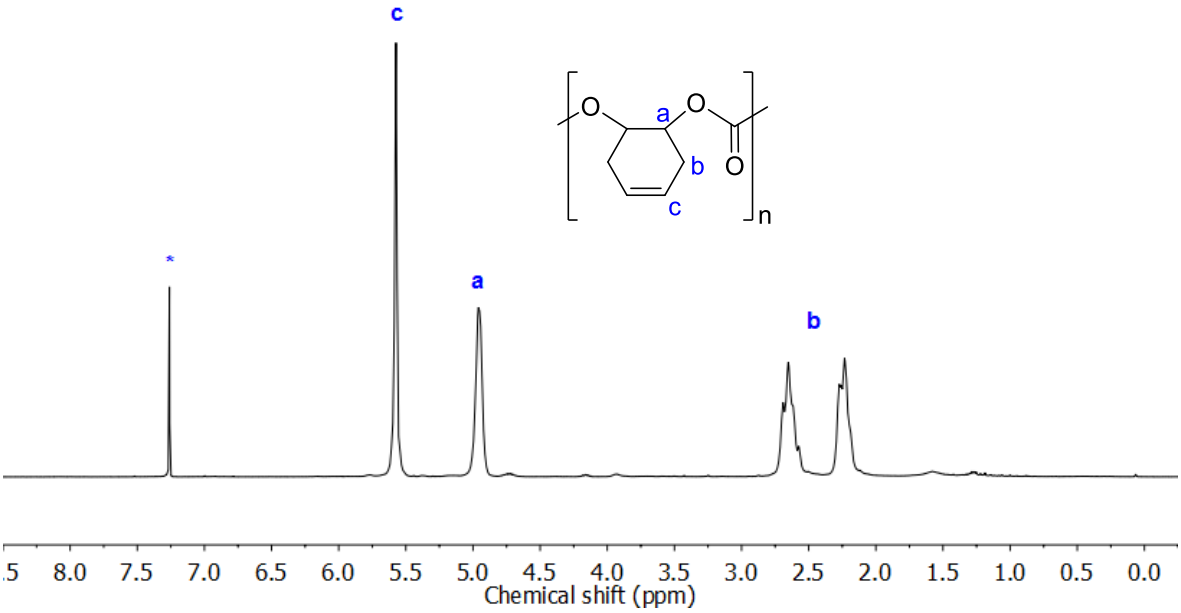


Figure 7.12 ^{1}H NMR spectrum of ^{C}PC (400.0 MHz, $CDCl_3$). The asterisk denotes the residual protio-solvent.

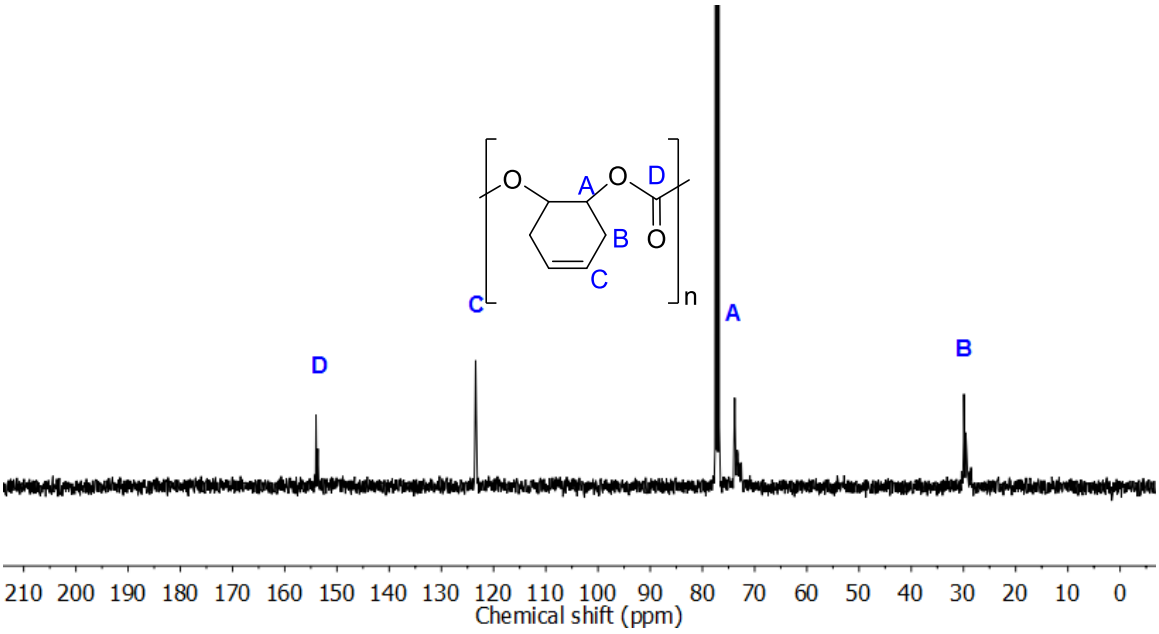


Figure 7.13 $^{13}C\{^{1}H\}$ NMR spectrum of ^{C}PC (100.7 MHz, $CDCl_3$). The asterisk denotes the residual protio-solvent.

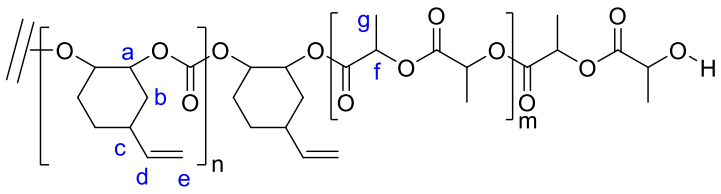
7.3 Synthesis of antibacterial poly(ester-*b*-carbonate-*b*-ester)

7.3.1 Block copolymerisation of ^{V}PC and *rac*-LA

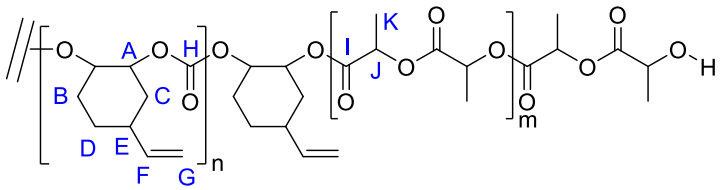
Typically, *rac*-LA (300.3 mg, 2.1 mmol) was placed in a Schlenk tube charging with a stirrer bar and dissolved in THF (5 mL) under a nitrogen atmosphere in a glovebox. In a second centrifuge tube, ^{V}PC (200.0 mg, 41.7 μmol) and TBD (11.6 mg, 83.3 μmol) were dissolved in THF. This catalyst solution was then added to the lactide solution, and the reaction mixture was allowed to stir for a pre-determined period. The polymer mixture was quenched with benzoic acid and precipitated into methanol to give a white solid. The polymer was purified by dissolving in DCM and precipitation from methanol. This process was repeated for 3 times, and the obtained white polymer was dried *in vacuo* for 48 h.

Table 7.2 Relative quantities of reagents used for preparing **P1-P6**

Polymer	Molar ratio	Loadings				Time (min)
	[^{V}PC]/[TBD]/[LA]	^{V}PC	TBD	LA	THF	
P1	1/2/50	200.0 mg	11.6 mg	300.3 mg	8.3 mL	1.0
P2	1/2/100	200.0 mg	11.6 mg	600.5 mg	16.7 mL	2.5
P3	1/2/200	200.0 mg	11.6 mg	1201.1 mg	33.3 mL	5.0
P4	1/2/300	200.0 mg	11.6 mg	1801.6 mg	50.0 mL	7.5
P5	1/2/400	200.0 mg	11.6 mg	2402.2 mg	66.8 mL	10.0
P6	1/2/150	1.5 g	87.0 mg	6.8 g	187.5 mL	3.0



Labelling scheme for ^{1}H NMR assignment



Labelling scheme for ^{13}C{^{1}H} NMR assignment

^{1}H NMR ($CDCl_3$, 400 MHz) δ / ppm: 5.76 (m, H_d), 5.25-5.10 (m, H_f), 5.03 (m, H_e), 4.89-4.77 (m, H_a), 2.43 (m, H_c), 1.90-1.40 (m, H_b), 1.57 (m, H_g).

$^{13}C\{^{1}H\}$ NMR ($CDCl_3$, 100.7 MHz) δ / ppm: 169.1 (C_I), 153.3 (C_H), 141.7 (C_F), 114.1 (C_G), 73.5 (C_A), 68.9 (C_J), 35.0 (C_E), 31.7 (C_B), 26.2 (C_D), 25.5 (C_C), 16.5 (C_K).

^{1}H NMR and ^{13}C NMR spectra are shown in **Figure 7.14** and **Figure 7.15**.

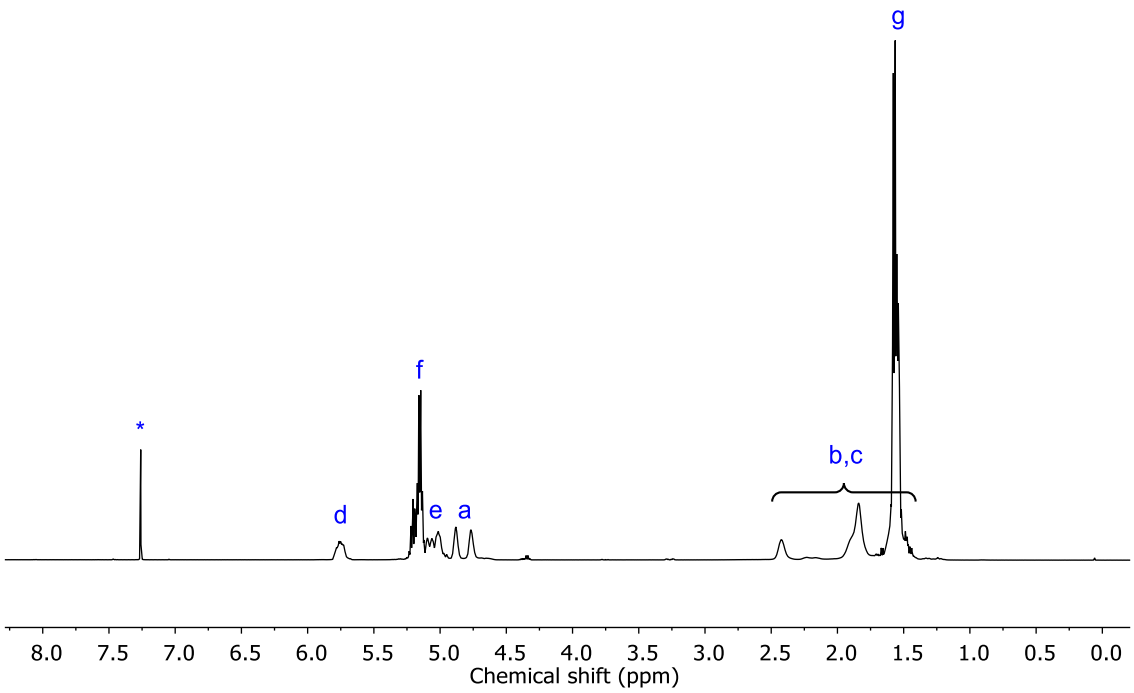


Figure 7.14 ^{1}H NMR spectrum of PLA-^{V}PC-PLA (400.0 MHz, $CDCl_3$).

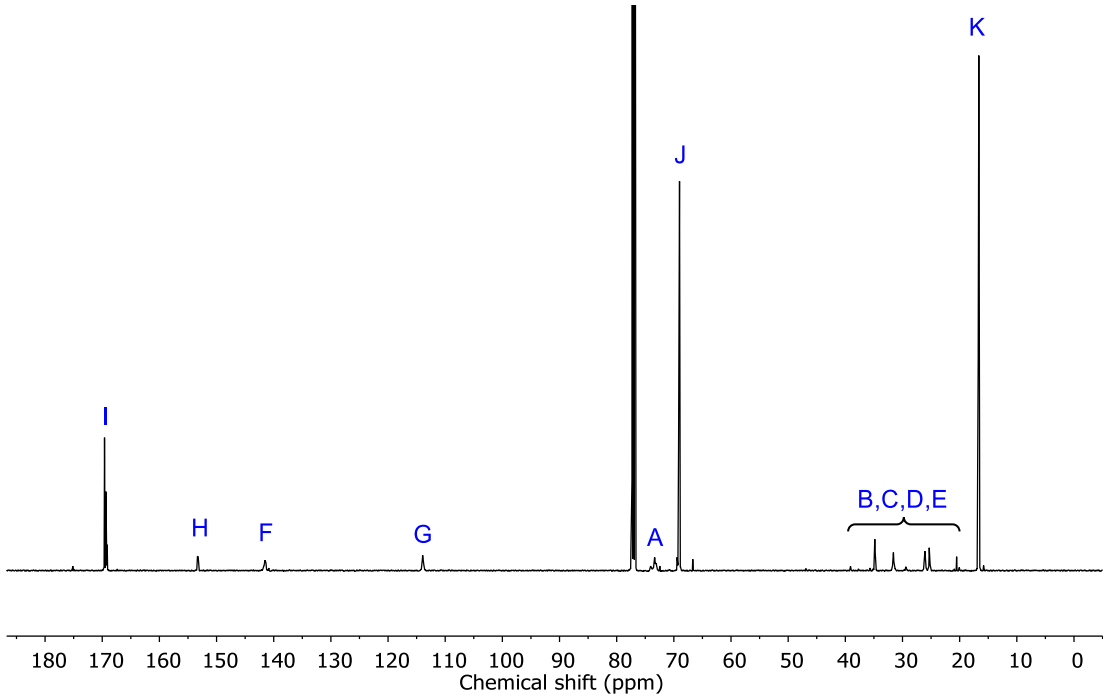
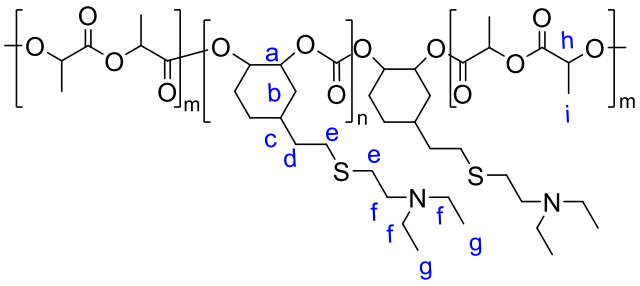
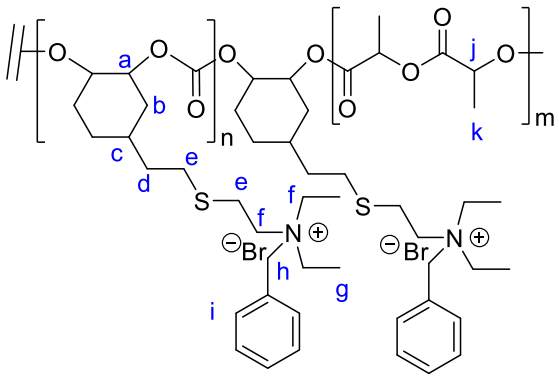


Figure 7.15 $^{13}C\{^{1}H\}$ NMR spectrum of PLA-^{V}PC-PLA (100.7 MHz, $CDCl_3$).

7.3.2 UV-mediated thiol-ene reaction between P6 and 2-(diethylamino)ethanethiol hydrochloride

P6 (1.0 g, 44.1 μmol), DMPA (181.0 mg, 0.7 mmol), 2-(diethylamino)ethanethiol hydrochloride (598.0 mg, 3.5 mmol) were dissolved in DCM (4.4 mL). The relative molar ratios of [C=C]/[Thiol]/[DMPA] were 1/2/0.4. The freeze-pump-thaw procedure was conducted for three cycles to deoxygenate the solution. Then the thiol-ene reaction was induced by UV irradiation (365 nm, 10W) for 1 h. Sodium bicarbonate aqueous solution (pH=8, 10.0 mL) was added to the reaction, and the solution mixture was extracted with DCM (3 × 25.0 mL). The organic fractions were washed with water (2 × 10.0 mL) following by brine (10.0 mL), then dried over magnesium sulfate. All volatiles were removed under reduced pressure, and the polymer was further purified by repetitive precipitation from diethyl ether (3 × 100.0 mL).


O
O
O



Labelling scheme for ^{1}H NMR assignment

^{1}H NMR ($CDCl_3$, 400 MHz) δ / ppm: 7.52 (m, H_i), 5.20 (m, H_j), 4.77-4.56 (m, H_a), 4.64 (m, H_h), 3.40 (m, H_f), 3.06-2.76 (m, H_e), 1.81 (m, H_c), 1.61 (m, H_b), 1.57 (m, H_k), 1.50 (m, H_d), 1.41 (m, H_g).

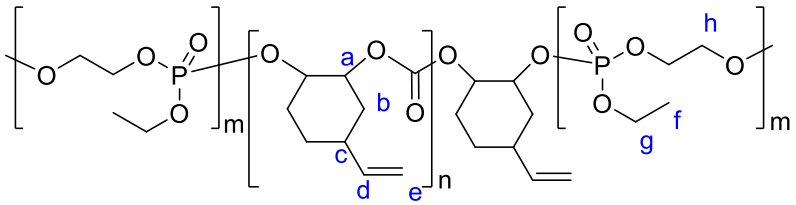
7.4 Synthesis of amphiphilic poly(phosphoester-*b*-carbonate-*b*-phosphoester)

7.4.1 Block copolymerisation of ^{V}PC and EP (PEP-^{V}PC-PEP, P7-P10)

Typically, EP (33.5 mg, 0.2 mmol) was placed in a Schlenk tube charging with a stirrer bar and dissolved in DCM under a nitrogen atmosphere in a glovebox. In a second centrifuge tube, ^{V}PC (100.0 mg, 14.7 μmol) and $Sn(Oct)_2$ (9.5 μL, 29.4 μmol) were dissolved in DCM (0.9 mL). This catalyst solution was then added to the EP solution and the reaction mixture was allowed to react for a pre-determined period. The polymer mixture was quenched by exposing to air and precipitated into cold diethyl ether (20.0 mL) to give a white gel-like solid. The polymer was purified by dissolving in DCM and precipitation from cold diethyl ether (3 × 50.0 mL). This process was repeated for 3 times, and the obtained white polymer was dried *in vacuo* for 48 h.

Table 7.4 Relative quantities of reagents used in **Table 4.1**

Polymer	Molar ratio	Loadings				Time (h)
	[^{V}PC]/[Sn(Oct)$_2$]/[EP]	^{V}PC (mg)	Sn(Oct)$_2$ (μL)	EP (mg)	DCM (mL)	
P7	1/2/15	100.0	9.5	33.5	0.9	1.0
P8	1/2/20	100.0	9.5	44.7	1.2	1.5
P9	1/2/50	100.0	9.5	111.8	3.0	3.0
P10	1/2/100	100.0	9.5	223.6	5.9	6.0



Labelling scheme for ^{1}H NMR assigment

^{1}H NMR ($CDCl_3$, 400 MHz) δ / ppm: 5.76 (m, H_d), 5.03 (m, H_e), 4.89-4.77 (m, H_a), 4.25 (m, H_h), 4.15 (m, H_g), 2.43 (m, H_c), 1.90-1.40 (m, H_b), 1.34 (m, H_f).

^{31}P{^{1}H} NMR (162.1 MHz, $CDCl_3$) δ / ppm: -1.32, -0.28 (end group).

7.5 Preparation and evaluation of PEP-^{V}PC-PEP self-assembly

7.5.1 The colloidal self-assembly protocol

Self-assemblies of PEP-^{V}PC-PEP were generally prepared according to the following protocol. The non-solvent, de-ionised (DI) water (4.0 mL) was added dropwise to the PEP-^{V}PC-PEP solution (10 mg·mL^{-1} for P7 & P8 and 0.5 mg·mL^{-1} for P9 & P10) in DMF (2.0 mL) over a period of 10 min under vigorous stirring (1400 rad·min^{-1}), Then, DI water (2.0 mL) was poured into the solution to 'quench' the self-assembled

nanostructures. The residue DMF was removed by dialysis with DI water (6 x 500 mL) over 2 days.

7.5.2 Procedure for making the calibration curve of RhB in PBS solution

A stock PBS solution (10.0 mM, pH 7.4) of RhB (500 $\mu g \cdot mL^{-1}$) was carefully diluted to a range of concentrations (1.0, 2.5, 5.0, 10.0, 25.0, 50.0 and 100.0 $ng \cdot mL^{-1}$) also using PBS solution (10.0 mM, pH 7.4). The fluorescence intensities of these samples were measured using the Fluorescence Spectrometer described in Chapter 2. The PMT (*photomultiplier* tube) voltage was set to be 570 V. 5 nm was selected as the excitation slit and 5 nm was set as the emission slit. Emission scan (500~750 nm) mode was used during the experiment and λ_{ex} was fixed to be 510 nm. The peak intensities at 591 nm were taken to prepare the calibration curve. The linear fitting of the calibration curve was conducted in Origin 8.1. The same instrument settings were used for the investigation of drug-releasing profiles.

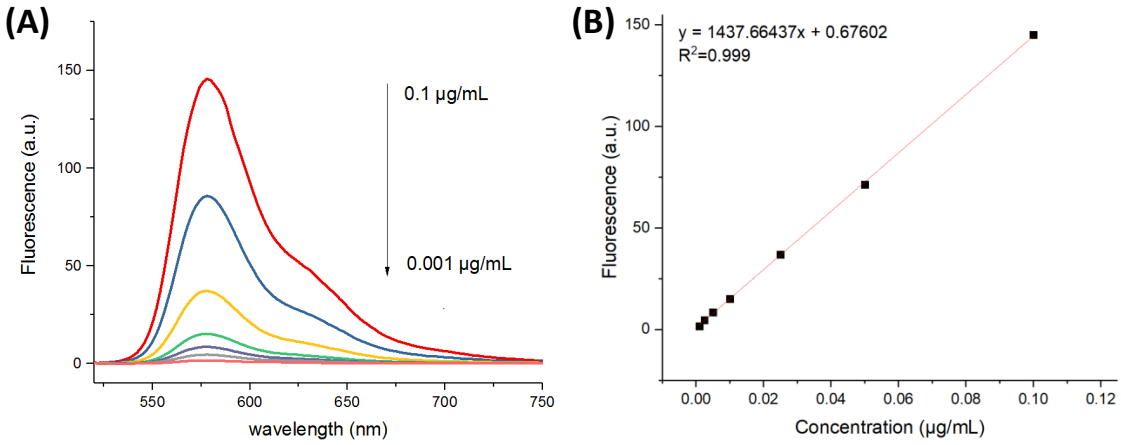


Figure 7.16 The fluorescence spectrum (A) and calibration curve (B) of Rhodamine B (RhB) in PBS solution (10.0 mM, pH 7.4). (λ_{ex}=510 nm)

7.5.3 Colloidal self-assembly drug-loading procedure and in vitro release

The loading of RhB was performed according to the following protocol. The **P10** solution (2.00 mL, 0.5 mg·mL^{-1} in DMF) was mixed with a RhB stock solution (0.50 mL, 0.4 μg·mL^{-1}). Then DI water (5.00 mL) was added, dropwise, to form **P10** vesicles. The organic solvent was removed by flushing the solution with N_2 for 2 h. The residual DMF and free RhB (not encapsulated) were removed *via* dialysis using a dialysis tube (MWCO = 14000 Da) against PBS solution (1.0 L, of a 10.0 mM solution at pH 7.4) at 25 ºC. The PBS solution was renewed 6 times every 30 min. After that, the obtained solution was weighed, and the fluorescence characterisation was conducted to determine the drug loading efficiency (DLE).

The drug loading efficiency (DLE) was calculated according to the following equation.

$$\text{DLE}\ (\%) = \frac{M_e}{M_f} \times 100\%$$

[M_e represents the weight of drug encapsulated in vesicles, M_f stands for the starting weight of drug added to the solution]

The *in vitro* drug releasing profile was conducted according to the following procedure. The RhB loaded vesicle solution (5.0 mL) was transferred immediately, to a clean dialysis tube (MWCO = 14000 Da) and dialysed against PBS solution (100.0 mL of a 10.0 mM solution at pH 7.4) at 37 ºC. Aliquots were taken for fluorescence characterisation (λ_{ex} = 510 nm) at pre-determined time intervals. In the control experiment of free RhB delivery, a PBS solution containing RhB was prepared first. The RhB concentration was adjusted to a similar value with the RhB loaded vesicle solution based on the drug loading efficiency measured by the fluorescence

spectroscopy. Then this RhB solution (5.00 mL) was transferred to a clean dialysis tube (MWCO = 14000 Da) and dialysed against PBS solution (100.00 mL of a 10.00 mM solution at pH 7.4) at 37 ^{o}C. Aliquots were taken for fluorescence characterisation (λ_{ex} = 510 nm) at pre-determined time intervals. The calibration for RhB emission has already been determined and was applied to determine the value of M_e.

7.5.4 In vitro release in the presence of enzymes

The enzyme-mediated release profiles of RhB from the vesicles were studied following the general procedures stated above. When transferring the vesicle solution, ALP (200 UmL^{-1}) or both ALP (200 UmL^{-1}) and lipase (200 UmL^{-1}) was also introduced into the tube and dialysed against PBS solution (100.0 mL of a 10.0 mM solution at pH 7.4) at 37 °C. Aliquots were taken for fluorescence characterisation (λ_{ex} = 510 nm) at pre-determined time intervals.

7.5.5 Stability of P10 vesicles

The stability of the vesicles was studied at 37 ° C in PBS (10.0 mM, pH 7.4), Tris-HCl buffer (10.0 mM, pH 8.8 or 10.0) or acetate buffer (50.0 mM, pH 5.0). After 24 h of incubation, the diameter and the polydispersity were measured using dynamic light scattering (DLS) as described in Chapter 2.

7.5.6 Enzymatic biodegradation of P10 vesicles

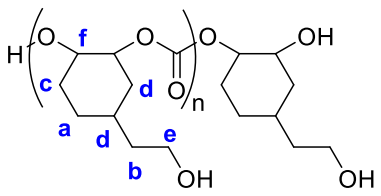
To study the effect of enzyme concentration on the biodegradation of the poly(phosphoester-carbonate) vesicles, following procedure was conducted. The polymer vesicle solution (1.0 mL of a solution of a concentration of 0.50 $mg{\cdot}mL^{-1}$) was mixed with ALP solution with pre-determined concentration. The mixtures were

then placed on a shaker (Eppendorf ThermoMixer, 600 rpm at 37 ºC) and aliquots were taken for DLS or SEC measurements at pre-determined time intervals.

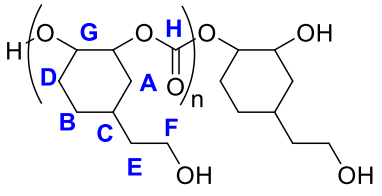
7.6 Synthesis of brush poly(carbonate-*g*-phosphoester)

7.6.1 Hydroboration-oxidation of ^{V}PC (P12)

To a solution of ^{V}PC (1.40 g, 0.26 mmol) in THF, was added a solution of 9-BBN (2.44 g, 9.99 mmol) in THF. After stirring the reaction mixture for 1.5 h at 25 ºC, 0.1 mL of pure methanol was added to react with any 9-BBN left after hydroboration. The oxidation of the hydroborated polymer was carried out in the same Schlenk tube by adding mCPBA (5.86 g, 34.0 mmol), at 0 ºC, under an inert atmosphere. After stirring the solution mixture at 25 ºC for 2 h, a methanol/water (10:1 v/v) mixture (20 mL) was added dropwise. The volatiles were removed under reduced pressure to ~ 2 mL. The product was precipitated from a 1 M $NaHCO_3$ aqueous solution (400 mL), washed with water (2 × 30 mL) and dried *in vacuo* for 72 h.



Labelling scheme for ^{1}H NMR assignment



Labelling scheme for ^{13}C{^{1}H} NMR assignment

^{1}H NMR (CD_3OD, 400 MHz) δ / ppm 4.72-4.82 (2H, m, H_f), 3.58 (2H, t, H_e), 1.81 (3H, m, H_d), 1.61 (2H, m, H_c), 1.50 (2H, m, H_b), 1.35 (2H, m, H_a).

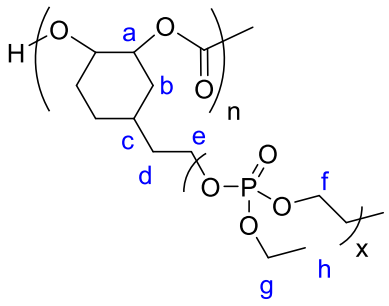
^{13}C{^{1}H} NMR (CD_3OD, 100.7 MHz) δ / ppm: 154.8 (C_H), 75.4 (C_G), 60.6 (C_F), 38.6 (C_E), 33.7 (C_D), 29.3 (C_C), 27.4 (C_B) and 26.5 (C_A).

7.6.2 Brush copolymerisation of P12 and EP (P14-P16)

EP (404.3 mg, 2.7 mmol) was placed in a Schlenk tube charging with a stirrer bar and dissolved in DMF (0.01 wt% LiBr, 3.0 mL) under a nitrogen atmosphere in a glovebox. In a second centrifuge tube, **P12** (50.0 mg, 6.6 μmol) and $Sn(Oct)_2$ (2.6 μL, 6.6 μmol) were dissolved in DMF (2.2 mL). This catalyst solution was then added to the EP solution, and the reaction mixture was allowed to react for a pre-determined period. The polymer mixture was quenched by exposing to air and precipitated into cold diethyl ether to give a white gel-like solid. The polymer was purified by dissolving in ethanol and precipitation from pentane (3 × 50.0 mL). This process was repeated for 3 times, and the obtained white polymer was dried *in vacuo* for 48 h.

Table 7.5 Relative quantities of reagents used in Table 4.5

Polymer	Molar ratio	Loadings				Time (h)
	[**P12**]/[$Sn(Oct)_2$]/[EP]	**P12** (mg)	$Sn(Oct)_2$ (μL)	EP (mg)	DMF (mL)	
P14	1/1/400	50.0	2.6	404.3	5.2	48.0
P15	1/1/400	50.0	2.6	404.3	5.2	72.0
P16	1/1/400	50.0	2.6	404.3	5.2	96.0



Labelling scheme for ^{1}H NMR assignment

^{1}H NMR (CD_3OD, 400 MHz) δ / ppm: 4.89-4.77 (m, H_a), 4.25 (m, H_f), 4.17 (m, H_g), 3.61 (m, H_e), 1.87 (m, H_c), 1.69 (m, H_b), 1.52 (m, H_d), 1.36 (m, H_h).

$^{31}P\{^{1}H\}$ NMR (162.1 MHz, $CDCl_3$) δ / ppm: -1.30, -0.28 (end group).

7.7 Synthesis and post-polymerisation modification of unsaturated polycarbonates/polyesters

7.7.1 Hydroboration-oxidation of ^{C}PC

To a solution of ^{C}PC (200.0 mg, 95.2 μmol) in THF (2.1 mL), was added a solution of 9-BBN (208.0 mg, 1.7 mmol) in THF (2.0 mL). After stirring the reaction mixture for 1.5 h at 25 ºC, 0.1 mL of pure methanol was added to react with any 9-BBN left after hydroboration. The oxidation of the hydroborated polymer was carried out in the same Schlenk tube by adding mCPBA (997.0 mg, 5.78 mmol), at 0 ºC, under an inert atmosphere. After stirring the solution mixture at 25 ºC for 2 h, a methanol/water (10/1 v/v, 5 mL) mixture was added dropwise. The volatiles were removed under reduced pressure to ~2 mL. The product was precipitated from a 1 M $NaHCO_3$ aqueous solution (100 mL), washed with water (2 × 5 mL) and dried *in vacuo* for 72 h.

7.7.2 Initial NMR reaction between ^{V}PC, ^{C}PC and 9-BBN

To a solution of ^{V}PC (20.0 mg, 4.4 μmol) and ^{C}PC (20 mg, 3.3 μmol) in THF-d_8 (0.3 mL) in an NMR tube equipped with a J. Young Teflon valve, was added a solution of 9-BBN (0.14 g, 0.58 mmol) in THF-d_8 (0.2 mL) at 25 ºC. After 16 h, all volatiles were removed *in vacuo*. The solid residue was re-dissolved in $CDCl_3$, and ^{1}H NMR spectrum was recorded. Once the reaction was monitored, the deuterated solvent was removed, and the residue was re-dissolved in THF-d_8 (0.5 mL). The solution mixture was heated at 50 ºC for 4 h, then 70 ºC for further 3 h. After which time, all volatiles were removed, and the solid was re-dissolved in $CDCl_3$ (0.3 mL). The reaction was again monitored using ^{1}H NMR spectroscopy.

7.7.3 NMR reaction between ^{V}PC, ^{C}PC and 9-BBN in the presence of an internal standard

To a solution of ^{V}PC (20.0 mg, 3.0 μmol), ^{C}PC (17.0 mg, 3.7 μmol) and mesitylene (20 μL) in $CDCl_3$ (0.35 mL) in an NMR tube equipped with a J. Young Teflon valve, was added a solution of 9-BBN (32.0 mg, 0.13 mmol) in $CDCl_3$ (0.3 mL) at 25 °C. The relative molar ratio of [C=C]/[9-BBN] was 1/1.1. The reaction was monitored for 1.5 h using ^{1}H NMR spectroscopy.

7.7.4 Ring-opening polymerisation of α-AL

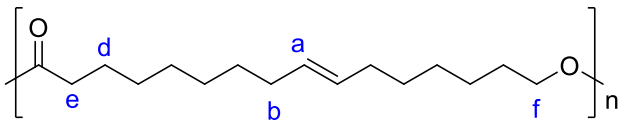
α-AL (1.3 mL, 14.8 mmol), catalyst (TBD or $Sn(Oct)_2$, 49.0 μmol), CHD (6.0 mg, 49.0 μmol) was dissolved in toluene (1.5 mL) and put into a Schlenk tube charging with a stirrer bar. The reaction mixture was heated at 120 ºC with stirring for 72 h. The polymerisation was quenched by exposing the reaction mixture to air.

7.7.5 Ring-opening polymerisation of Amb

Typically, Amb (1.3 mL, 4.9 mmol) was first put in a Schlenk tube charging with a stirred bar under a nitrogen atmosphere in a glovebox. Catalyst (TBD or $Sn(Oct)_2$, 49.0 μmol) and CHD (6.0 mg, 49.0 μmol) were added with stirring under a nitrogen atmosphere. The mixture was intensively stirred and rapidly heated to 120 °C, and then kept at this temperature for a pre-determined period. The polymerisation reaction was quenched by exposing the reaction mixture to air. The crude reaction mixture was dried *in vacuo* to remove the solvent. The remaining polymer was dissolved in DCM and precipitated into methanol (400 mL) to yield a white solid.

Table 7.6 Relative quantities of reagents used in **Table 5.1**.

Entry	Molar ratio	Loadings				Time (h)
	[cat]/[CHD]/[Amb]	CHD	$Sn(Oct)_2$	TBD	Amb	
1	1/1/100	6.0 mg	16.0 µL	0.0 mg	1.3 mL	55
2	1/1/100	6.0 mg	0.0 µL	7.0 mg	1.3 mL	55
3	1/1/100	6.0 mg	0.0 µL	7.0 mg	1.3 mL	24



Labelling scheme for ^{1}H NMR assignment

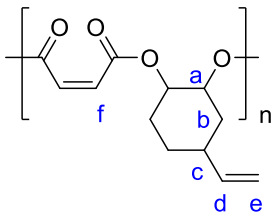
^{1}H NMR ($CDCl_3$, 400 MHz) δ / ppm: 5.38-5.36 (m, 2H, H_a), 4.06-4.03 (t, 2H, H_f), 2.30-2.26 (t, 2H, H_e), 1.96 (m, 4H, H_b), 1.63-1.57 (m, 4H, H_d), 1.34-1.29 (m, 14H, H_c)

7.7.6 Copolymerisation of v-CHO and MA (^{V,M}PE, P19)

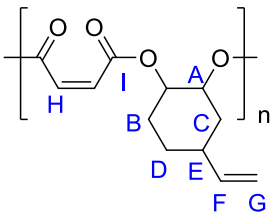
Typically, [salenCr^{III}Cl] catalyst (**C2**, 10.0 mg, 1.6 µmol), PPNCl (9.1 mg, 1.6 µmol), CHD (18.4 mg, 15.8 µmol), MA (155.1 mg, 1.6 mmol) and v-CHO (0.2 mL, 1.6 mmol) were dissolved in toluene and placed in a Schlenk tube in a glovebox. The reaction mixture was stirred at 80 ºC for 16 h. The volatiles were removed *in vacuo*. The polymer was dissolved in THF, filtered through an Amberlyst-15 plug and purified by repetitive precipitation from hexane (3 × 200 mL). The purified polymer was then dried *in vacuo* for 48 h.

Table 7.7 Relative quantities of reagents used in Table 5.2

Entry	Molar ratio	Loadings						Time (h)
	[C2]/[PPNCl]/[CHD]/ [MA]/[v-CHO]	C2 (mg)	PPNCl (mg)	CHD (mg)	MA (mg)	v-CHO (μL)	Toluene (mL)	
1	1/0/10/100/100	10.0	0.0	18.4	155.1	206.3	1.6	6
2	1/1/10/100/100	10.0	9.1	18.4	155.1	206.3	1.6	6
3	1/1/10/100/100	10.0	9.1	18.4	155.1	206.3	1.6	6
4	1/1/10/100/130	10.0	9.1	18.4	155.1	247.6	1.6	6



Labelling Scheme for ^{1}H NMR assignment



Labelling Scheme for ^{13}C{^{1}H} NMR assignment

^{1}H NMR ($CDCl_3$, 400 MHz) δ / ppm: 6.25 (m, 2H, H_f) 5.76 (m, 1H, H_d), 5.23-4.77 (m, 4H, H_a and H_e), 2.43 (m, 1H, H_c), 1.90-1.20 (m, 6H, H_b).

^{13}C{^{1}H} NMR ($CDCl_3$, 100.7 MHz) δ / ppm: 163.7 (C_I), 141.7 (C_F), 130.16 (C_H), 114.1 (C_G), 73.5 (C_A), 35.0 (C_E), 31.7 (C_B), 26.2 (C_D), 25.5 (C_C).

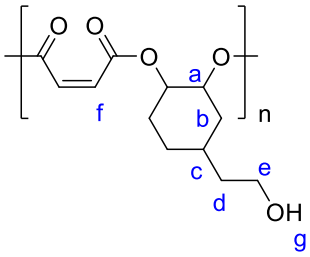
7.7.7 NMR reaction between P19 and 9-BBN

To a solution of **P19** (0.02 g, 0.008 mmol) in $CDCl_3$ (0.20 mL) in an NMR tube, equipped with a J. Young Teflon valve, was added a solution of the 9-BBN dimer (0.02 g, 0.088 mmol) in $CDCl_3$ (0.30 mL) at 25 °C. The reaction was monitored for 1.5 h using ^{1}H NMR spectroscopy with mesitylene as an internal standard.

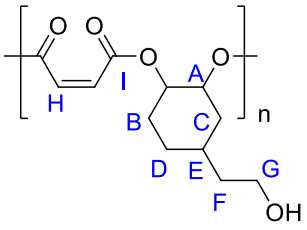
7.7.8 Hydroboration-oxidation of P19 (P20)

To a solution of **P19** (1.5 g, 0.6 mmol) in THF (17.7 mL), was added a solution of the 9-BBN dimer (2.4 g, 9.9 mmol) in THF (20.0 mL). After stirring the reaction mixture

for 1.5 h at 25 ºC, pure methanol (0.1 mL) was added to react with any 9-BBN left after hydroboration. The oxidation of the hydroborated polymer was carried out in the same Schlenk tube by adding mCPBA (11.6 g, 70.0 mmol) at 0 ºC under an inert atmosphere. The relative molar ratio of [C=C]/[9-BBN]/[mCPBA] was 1/1.5/5.1. After stirring the solution mixture at 25 ºC for 2 h, a methanol/water (10/1 v/v, 10 mL) mixture was added dropwise. The volatiles were removed under reduced pressure to ~ 2.0 mL. The product was precipitated from a 1 M $NaHCO_3$ aqueous solution (500.0 mL), washed with water and dried *in vacuo* for 72 h.



Labelling Scheme for ^{1}H NMR assignment



Labelling Scheme for ^{13}C{^{1}H} NMR assignment

^{1}H NMR (DMSO-d_6, 400 MHz) δ / ppm: 6.48 (m, 2H, H_f), 4.89 (m, 2H, H_a), 4.37 (m, 1H, H_g), 3.42 (m, 2H, H_e), 1.10-2.10 (m, 9H, H_b, H_c and H_d).

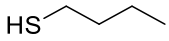
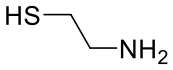
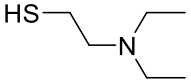
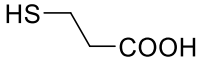
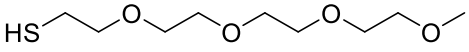
^{13}C{^{1}H} NMR (DMSO-d_6, 100.7 MHz) δ / ppm: 163.7 (C_I), 130.0 (C_H), 73.5 (C_A), 59.2 (C_G), 34.8 (C_E), 32.0 (C_B), 27.9 (C_F), 26.2 (C_D), 25.5 (C_C).

7.7.9 Thiol-ene reactions between P20 and thiols

Typically, **P20**, DMPA and thiols were dissolved in DMSO (1.7 mL), resulting in the molar ratio of [C=C]/[thiol]/[DMPA] = 1/2/0.4. The freeze-pump-thaw procedure was conducted for three cycles to deoxygenate the solution. Then, the thiol-ene reaction was induced UV irradiation (365 nm, 10 W) for 1 h. The crude reaction mixture was

dried *in vacuo* to remove the solvent. The final polymer was purified by repetitive precipitation from diethyl ether (3 × 50.0 mL).

Table 7.8 Relative quantities of reagents used in thiol-ene reactions listed in **Table 5.3**

Polymer	Thiol	Loadings		
		P20	DMPA	Thiol
P21		100.0 mg	42.0 mg	89.0 μL
P22		100.0 mg	42.0 mg	94.0 mg
P23		100.0 mg	42.0 mg	140.0 mg
P24		100.0 mg	42.0 mg	72.0 μL
P25		100.0 mg	42.0 mg	186.0 mg

7.7.10 Polyester self-assembly protocol

The polyesters (20.0 mg) were suspended into de-ionised water (2.0 mL) with vigorous stirring (1400 rad·min^{-1}) over a period of 1 h.

7.8 References

1. M. R. Kember, J. Copley, A. Buchard and C. K. Williams, *Polym. Chem.*, 2012, **3**, 1196-1201.
2. M. Winkler, C. Romain, M. A. R. Meier and C. K. Williams, *Green Chem.*, 2015, **17**, 300-306.
3. J. He, M. Zhang and P. Ni, *Soft Matter*, 2012, **8**, 6033-6038.
4. A. W. Snow and E. E. Foos, *Synthesis*, 2003, **2003**, 0509-0512.

Appendices

Appendix A – Experimental Data

A1. Chapter 3

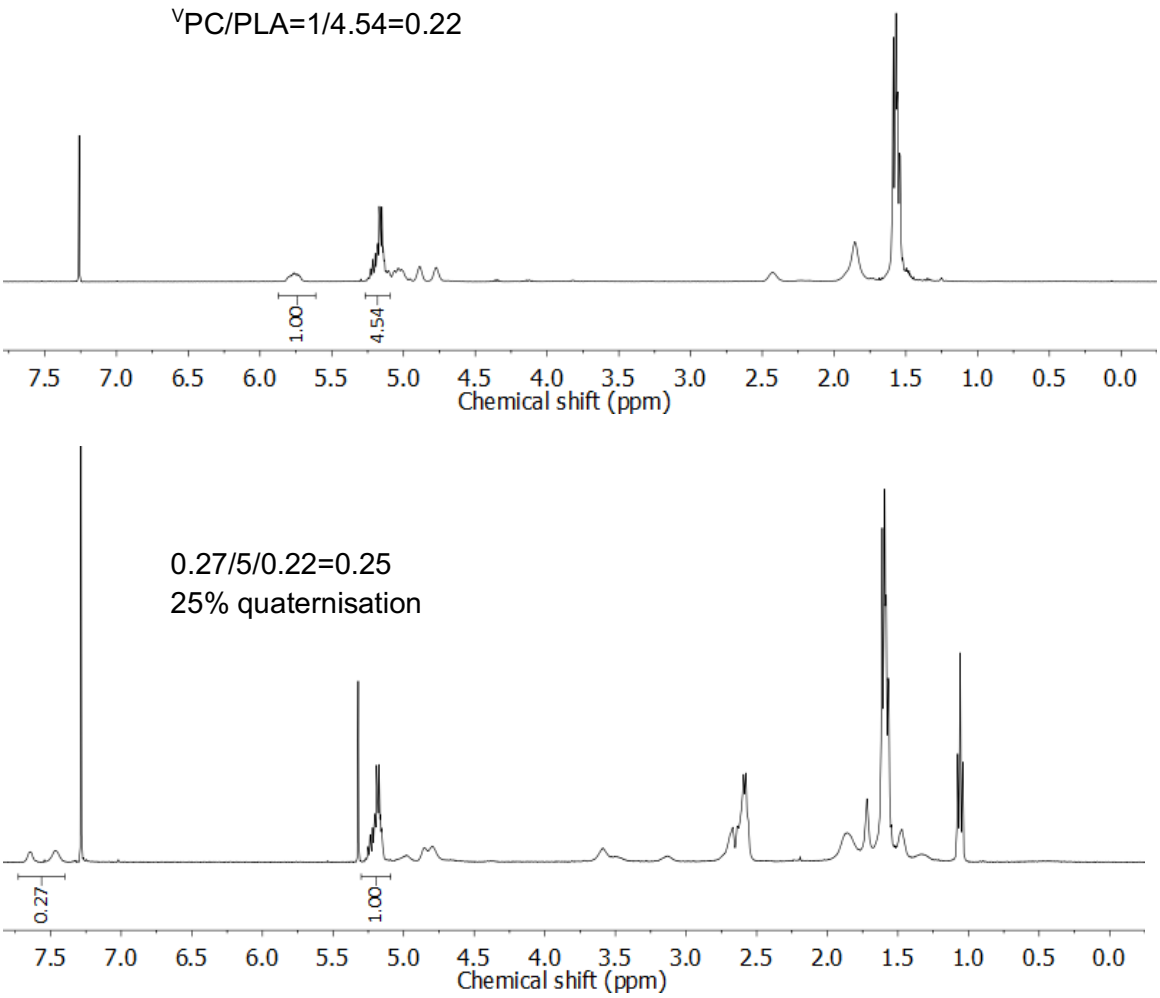


Figure A1. ^{1}H NMR spectra of P6 (25 wt% of ^{V}PC), $Q_{0.25}$P6 (400.0 MHz, $CDCl_3$, 25 ºC). The degree of quaternisation determined by ^{1}H NMR spectroscopy by comparing the integration of newly introduced aromatic proton peaks (-$N^{+}CH_2$Bn) at δ = 7.36-7.54 ppm to that of the methine protons on PLA block.

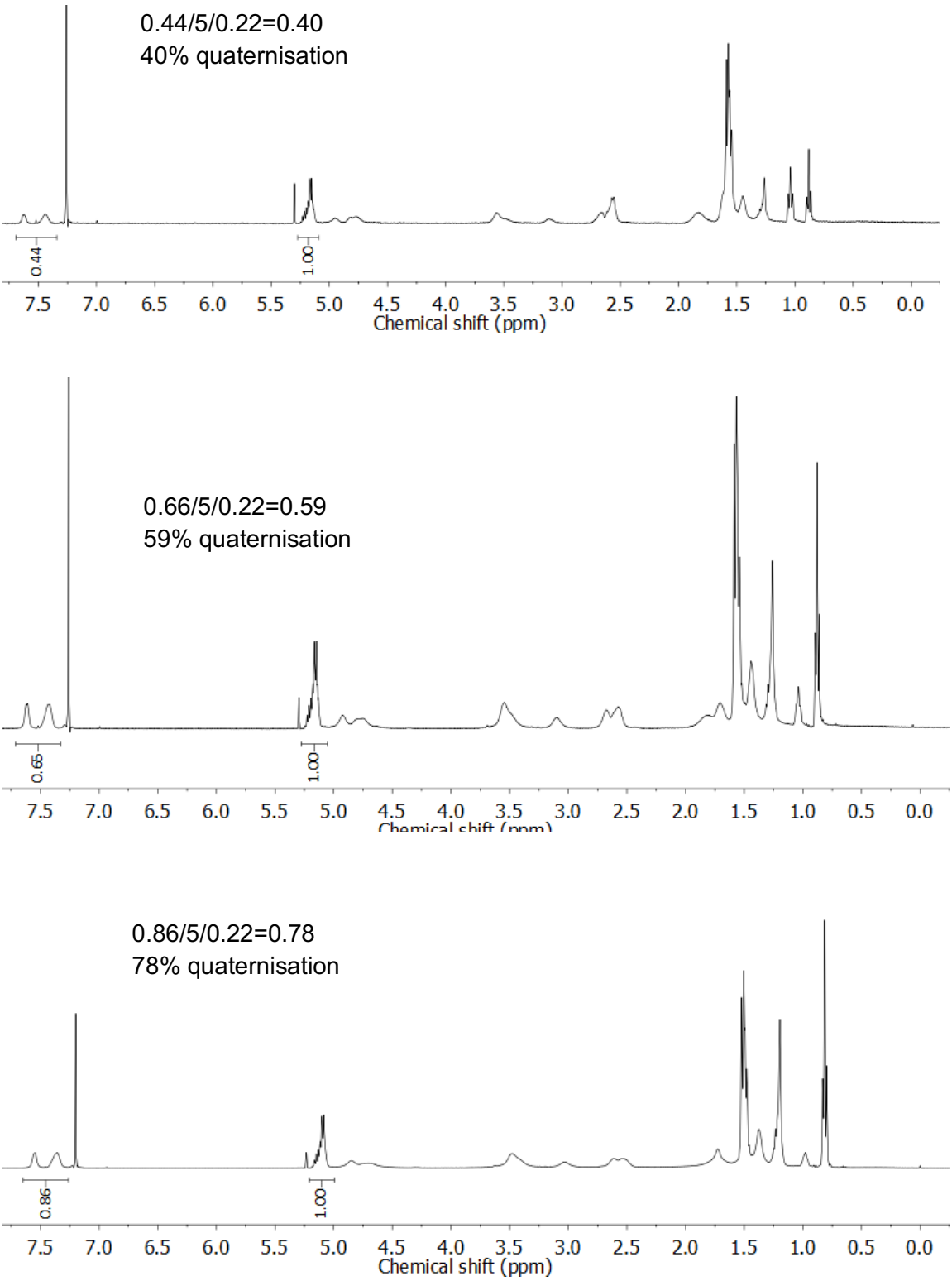


Figure A2. ^{1}H NMR spectra of $Q_{0.40}P6$, $Q_{0.59}P6$ and $Q_{0.78}P6$ (400.0 MHz, $CDCl_3$, 25 ºC).

A2. Chapter 4

Table A1. DLS analyses shown in **Table 4.2**.

	D_h (nm)			$D_{h,\,mean}$(nm)	PDI			PDI_{mean}
P7	21.5	22.4	23.2	22.3 ± 0.7	0.360	0.382	0.412	0.38 ± 0.02
P8	22.1	25.8	24.6	24.2 ± 1.5	0.164	0.177	0.172	0.17 ± 0.01
P9	299.4	301.8	314.2	305.1 ± 6.4	0.354	0.279	0.310	0.31 ± 0.03
P10	250.0	255.5	251.8	252.4 ± 2.3	0.015	0.071	0.050	0.05 ± 0.02

Table A2. TEM particle size analysis of self-assembled nanostructures formed from **P8** and **P10**.

	Number	Minimum (nm)	Maximum (nm)	Mean (nm)	Standard deviation
P8	113	11.8	29.2	18.3	3.4
P10	58	120.0	423.4	210.5	69.8

Table A3. TEM membrane thickness analysis of self-assembled nanostructures formed from **P10**.

	Number	Minimum (nm)	Maximum (nm)	Mean (nm)	Standard deviation
Thickness	20	11.2	32.4	24.8	7.7

Table A4. Zeta potential analysis of self-assembled nanostructures formed from **P10**.

	Zeta potential (mV)			Mean zeta potential (mV)
P10	-46.8	-48	-48.5	-47.8 ± 0.7

Table A5.Water contact angle measurements on polymer surfaces.

	Water contact angle (º)			Mean Water contact angle (º)
Glass	83.8	85.2	84.4	84.4 ± 0.6
^{V}PC	86.0	86.0	87.3	87.3 ± 1.8
P12	51.7	55.4	49.8	52.3 ± 2.3

A3. Chapter 5

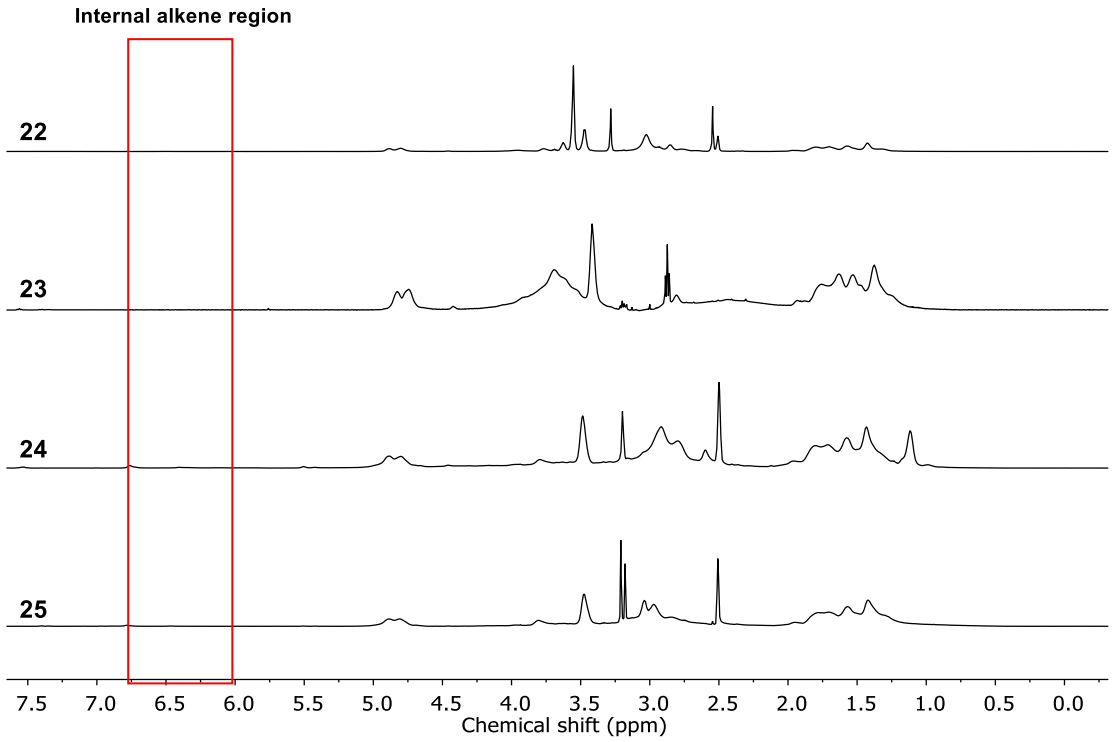


Figure A3 Overlaid ^{1}H NMR spectra of **P22**-**P25**, showing the disappearance of the internal alkene signals after the thiol-ene reactions.

Table A6.Water contact angle measurements on polymer surfaces.

	Water contact angle (º)			Mean Water contact angle (º)
P18	64.0	65.8	66.6	65.4 ± 1.1
P19	86.0	89.1	91.0	88.7 ± 2.1
P20	55.7	58.3	60.0	58.0 ± 1.8
P21	52.5	52.3	53.9	52.9 ± 0.7
P22	37.9	38.0	38.8	38.2 ± 0.5
P23	28.8	31.8	32.4	31.0 ± 1.6
P24	29.5	29.5	28.1	29.0 ± 0.7
P25	44.2	46.6	47.1	46.0 ± 1.3

Table A7. DLS analyses of self-assembled nanostructures formed from **P21.**

	D_h (nm)			$D_{h,\,mean}$(nm)	PDI			PDI_{mean}
P21	136.4	136.6	136.2	136.4 ± 0.2	0.108	0.128	0.114	0.12 ± 0.01

Table A8. Zeta potential analysis of self-assembled nanostructures formed from **P21**.

	Zeta potential (mV)			Mean zeta potential (mV)
P21	-67.9	-67.8	-66.9	-67.5 ± 0.4

Table A9. TEM particle size analysis of self-assembled nanostructures formed from **P21**.

	Number	Minimum (nm)	Maximum (nm)	Mean (nm)	Standard deviation
P21	142	15.6	32.4	25.2	5.3

Appendix B – Permissions

Figure 1.1

JOHN WILEY AND SONS LICENSE TERMS AND CONDITIONS

Jul 11, 2018

This Agreement between Ms. Ni Yi ("You") and John Wiley and Sons ("John Wiley and Sons") consists of your license details and the terms and conditions provided by John Wiley and Sons and Copyright Clearance Center.

License Number	4386101483924
License date	Jul 11, 2018
Licensed Content Publisher	John Wiley and Sons
Licensed Content Publication	Journal of Polymer Science Part A: Polymer Chemistry
Licensed Content Title	Design and synthesis of biodegradable grafted cationic polycarbonates as broad spectrum antimicrobial agents
Licensed Content Author	Zhan Yuin Ong, Daniel J. Coady, Jeremy P. K. Tan, et al
Licensed Content Date	Nov 27, 2015
Licensed Content Volume	54
Licensed Content Issue	8
Licensed Content Pages	7
Type of use	Dissertation/Thesis
Requestor type	University/Academic
Format	Electronic
Portion	Abstract
Will you be translating?	No
Title of your thesis / dissertation	Synthesis and Post-polymerisation Modification of Degradable Polymers Based on Polycarbonates/Polyesters Prepared Using Ring-opening Copolymerisation
Expected completion date	May 2018
Expected size (number of pages)	400
Requestor Location	Ms. Ni Yi 39 Oxford Castle, New Road Oxford, Oxfordshire OX1 1AY United Kingdom Attn: Ms. Ni Yi

Figure 1.2

JOHN WILEY AND SONS LICENSE TERMS AND CONDITIONS

May 20, 2018

This Agreement between University of Oxford -- Ni Yi ("You") and John Wiley and Sons ("John Wiley and Sons") consists of your license details and the terms and conditions provided by John Wiley and Sons and Copyright Clearance Center.

License Number	4353020575159
License date	May 20, 2018
Licensed Content Publisher	John Wiley and Sons
Licensed Content Publication	Macromolecular Rapid Communications
Licensed Content Title	Self-Assembled Block Copolymer Aggregates: From Micelles to Vesicles and their Biological Applications
Licensed Content Author	Adam Blanazs, Steven P. Armes, Anthony J. Ryan
Licensed Content Date	Feb 6, 2009
Licensed Content Volume	30
Licensed Content Issue	4-5
Licensed Content Pages	11
Type of use	Dissertation/Thesis
Requestor type	University/Academic
Format	Electronic
Portion	Figure/table
Number of figures/tables	1
Original Wiley figure/table number(s)	Figure 1
Will you be translating?	No
Title of your thesis / dissertation	Synthesis and Post-polymerisation Modification of Degradable Polymers Based on Polycarbonates/Polyesters Prepared Using Ring-opening Copolymerisation
Expected completion date	May 2018
Expected size (number of pages)	400
Requestor Location	University of Oxford 39 Oxford Castle, New Road Oxford OX1 (Oxfordshire), Oxfordshire OX1 1AY United Kingdom Attn: Ni Yi
Publisher Tax ID	EU826007151
Total	0.00 GBP
Terms and Conditions	

Figure 1.6

JOHN WILEY AND SONS LICENSE TERMS AND CONDITIONS

Apr 04, 2018

This Agreement between Ms. Ni Yi ("You") and John Wiley and Sons ("John Wiley and Sons") consists of your license details and the terms and conditions provided by John Wiley and Sons and Copyright Clearance Center.

License Number	4321980003777
License date	Apr 04, 2018
Licensed Content Publisher	John Wiley and Sons
Licensed Content Publication	Macromolecular Chemistry and Physics
Licensed Content Title	CO2-Based Non-ionic Surfactants: Solvent-Free Synthesis of Poly(ethylene glycol)-block-Poly(propylene carbonate) Block Copolymers
Licensed Content Author	Jeannette Hilf, Patricia Schulze, Holger Frey
Licensed Content Date	Oct 25, 2013
Licensed Content Volume	214
Licensed Content Issue	24
Licensed Content Pages	8
Type of use	Dissertation/Thesis
Requestor type	University/Academic
Format	Electronic
Portion	Figure/table
Number of figures/tables	1
Original Wiley figure/table number(s)	TOC
Will you be translating?	No
Title of your thesis / dissertation	Synthesis and Post-polymerisation Modification of Degradable Polymers Based on Polycarbonates/Polyesters Prepared Using Ring-opening Copolymerisation
Expected completion date	May 2018
Expected size (number of pages)	400
Requestor Location	Ms. Ni Yi 39 Oxford Castle, New Road Oxford, Oxfordshire OX1 1AY United Kingdom Attn: Ms. Ni Yi
Publisher Tax ID	EU826007151
Total	0.00 GBP
Terms and Conditions	

Figure 1.7

SPRINGER NATURE LICENSE
TERMS AND CONDITIONS

May 20, 2018

This Agreement between University of Oxford -- Ni Yi ("You") and Springer Nature ("Springer Nature") consists of your license details and the terms and conditions provided by Springer Nature and Copyright Clearance Center.

License Number	4353021249575
License date	May 20, 2018
Licensed Content Publisher	Springer Nature
Licensed Content Publication	Nature Chemistry
Licensed Content Title	Biodegradable nanostructures with selective lysis of microbial membranes
Licensed Content Author	Fredrik Nederberg, Ying Zhang, Jeremy P. K. Tan, Kaijin Xu, Huaying Wang et al.
Licensed Content Date	Apr 3, 2011
Licensed Content Volume	3
Licensed Content Issue	5
Type of Use	Thesis/Dissertation
Requestor type	academic/university or research institute
Format	electronic
Portion	figures/tables/illustrations
Number of figures/tables/illustrations	1
High-res required	no
Will you be translating?	no
Circulation/distribution	501 to 1000
Author of this Springer Nature content	no
Title	Synthesis and Post-polymerisation Modification of Degradable Polymers Based on Polycarbonates/Polyesters Prepared Using Ring-opening Copolymerisation
Instructor name	n/a
Institution name	n/a
Expected presentation date	May 2018
Portions	Figure 1
Requestor Location	University of Oxford 39 Oxford Castle, New Road Oxford OX1 (Oxfordshire), Oxfordshire OX1 1AY United Kingdom Attn: Ni Yi

Figure 1.8

JOHN WILEY AND SONS LICENSE TERMS AND CONDITIONS

May 20, 2018

This Agreement between University of Oxford -- Ni Yi ("You") and John Wiley and Sons ("John Wiley and Sons") consists of your license details and the terms and conditions provided by John Wiley and Sons and Copyright Clearance Center.

License Number	4353021438882
License date	May 20, 2018
Licensed Content Publisher	John Wiley and Sons
Licensed Content Publication	Advanced Materials
Licensed Content Title	Antimicrobial and Antifouling Hydrogels Formed In Situ from Polycarbonate and Poly(ethylene glycol) via Michael Addition
Licensed Content Author	Shao Qiong Liu, Chuan Yang, Yuan Huang, et al
Licensed Content Date	Sep 27, 2012
Licensed Content Volume	24
Licensed Content Issue	48
Licensed Content Pages	6
Type of use	Dissertation/Thesis
Requestor type	University/Academic
Format	Electronic
Portion	Figure/table
Number of figures/tables	1
Original Wiley figure/table number(s)	Scheme 1
Will you be translating?	No
Title of your thesis / dissertation	Synthesis and Post-polymerisation Modification of Degradable Polymers Based on Polycarbonates/Polyesters Prepared Using Ring-opening Copolymerisation
Expected completion date	May 2018
Expected size (number of pages)	400
Requestor Location	University of Oxford 39 Oxford Castle, New Road Oxford OX1 (Oxfordshire), Oxfordshire OX1 1AY United Kingdom Attn: Ni Yi
Publisher Tax ID	EU826007151
Total	0.00 USD

Figure 1.9





Title:	Bio-based polycarbonate as synthetic toolbox
Author:	O. Hauenstein, S. Agarwal, A. Greiner
Publication:	Nature Communications
Publisher:	Springer Nature
Date:	Jun 15, 2016

Copyright © 2016, Springer Nature

Creative Commons

This is an open access article distributed under the terms of the Creative Commons CC BY license, which permits unrestricted use, distribution, and reproduction in any medium, provided the original work is properly cited.

You are not required to obtain permission to reuse this article.

Figure 1.10

JOHN WILEY AND SONS LICENSE TERMS AND CONDITIONS

May 20, 2018

This Agreement between University of Oxford -- Ni Yi ("You") and John Wiley and Sons ("John Wiley and Sons") consists of your license details and the terms and conditions provided by John Wiley and Sons and Copyright Clearance Center.

License Number	4353030335621
License date	May 20, 2018
Licensed Content Publisher	John Wiley and Sons
Licensed Content Publication	Journal of Polymer Science Part A: Polymer Chemistry
Licensed Content Title	Novel aliphatic poly(ester-carbonate) with pendant allyl ester groups and its folic acid functionalization
Licensed Content Author	Xiuli Hu, Xuesi Chen, Shi Liu, et al
Licensed Content Date	Jan 25, 2008
Licensed Content Volume	46
Licensed Content Issue	5
Licensed Content Pages	10
Type of use	Dissertation/Thesis
Requestor type	University/Academic
Format	Electronic
Portion	Figure/table
Number of figures/tables	1
Original Wiley figure/table number(s)	Figure 8
Will you be translating?	No
Title of your thesis / dissertation	Synthesis and Post-polymerisation Modification of Degradable Polymers Based on Polycarbonates/Polyesters Prepared Using Ring-opening Copolymerisation
Expected completion date	May 2018
Expected size (number of pages)	400
Requestor Location	University of Oxford 39 Oxford Castle, New Road Oxford OX1 (Oxfordshire), Oxfordshire OX1 1AY United Kingdom Attn: Ni Yi
Publisher Tax ID	EU826007151
Total	0.00 USD
Terms and Conditions	